Scalar Sector Extension and Physics Beyond Standard Model

Yoshihiko Abe

*Department of physics of Kyoto University,
Kyoto 606-8502, Japan*

Abstract

The Standard Model of particles physics is an experimentally well-tested theory and has succeeded in explaining many experimental data with a very high accuracy. However, there have been reported results of experiments and observations that cannot be explained by the Standard Model alone, such as the existence of dark matter, the origin of the baryon asymmetry and so on, which suggests the existence of physics beyond the Standard Model. In addition, in recent years, the importance of the consistency between phenomenology and quantum gravity theory has become well appreciated. Revealing the connection between physics beyond the Standard Model and the ultimate theory is one of the most important and fundamental problems left in particle physics.

One attractive and powerful direction for investigating models of physics beyond the Standard Model is to extend the scalar sector. Such extensions occur naturally in models beyond the Standard Model, and it is important to clarify how the new scalar interactions, their scalar potentials, and vacuum expectation values are determined in order to give a constraint on the model from experiments and observations. In particular, a (pseudo-) Nambu-Goldstone boson is a particle that appears universally in various models, reflecting the symmetry of the theory. It plays an important role not only in understanding the theoretical aspects but also in studying phenomenology. This new scalar field could also be an attractive candidate for dark matter that naturally escapes the severe constraints of current experiments. In addition to new particle contents, non-perturbative objects in field theories, such as topological solitons, can also appear in the model of the beyond Standard Model, which brings richer physics not only to particle physics but also to cosmology.

In this thesis, we consider a scalar sector extension based on the singlet scalar and study the physics beyond the Standard Model that results from it, focusing on the dynamics of pseudo-Nambu-Goldstone bosons. First, we consider the case where the scalar sector extension produces a pseudo-Nambu-Goldstone boson dark matter, which can be a natural scalar dark matter candidate consistent with the current experiments. We investigate its ultraviolet completion, the relation between this model and inflation, neutrino oscillations, and other related physics. In proposing of the ultraviolet completed model, we take into account the conditions obtained from the consistency with quantum gravity theory, and study the effects on the dark matter physics and the relationship with the grand unification. For the case of a singlet scalar having a very large vacuum expectation value. We study the production mechanism of the pseudo-Nambu-Goldstone dark matter, and discuss the possibility of compatibility with inflation and neutrino oscillations. Lastly, we investigate the case where the additional scalar field becomes an axion, and construct an axion string solution with a novel structure. This string is different from the known axion string, and we discuss its implications to cosmology.

Contents

Chapter 1

Introduction

The Standard Model (SM) of particle physics is a well-tested theory. It is formulated as a chiral gauge theory based on the SM gauge group

$$G_{\text{SM}} := SU(3)_C \times SU(2)_L \times U(1)_Y,$$

and the Higgs mechanism via a Higgs doublet, which was observed in the ATLAS [A$^+$12] and CMS [C$^+$12] experiments at the Large Hadron Collider (LHC). All the chiral fermions, quarks and leptons, and the massive vector bosons acquire their mass from the vacuum expectation value (VEV) of the Higgs boson. The SM have achieved a successful outcome to explain experimental and observational facts.

However, the SM is not ultimate theory of our universe from the following theoretical and observational reasons, and it may be a low-energy effective field theory of an ultraviolet (UV) completed theory such as quantum gravity theory/string theory. In the theoretical aspects, for example, the following puzzles have been left in the SM:

- The absence of the quantum theory of the gravity and the the selection rule of our universe being unknown
- The initial value problems of our universe
- The origin of the SM gauge group G_{SM}
- Why there is a hierarchy between the electroweak scale and the Planck scale
- The origin of the three generations of quarks and leptons
- The hierarchical structure among Yukawa couplings
- The reason why the charge of the matter field is quantized

In addition to these theoretical mysteries, the following observational results imply the physics beyond the Standard Model (BSM):

- The source of matter-antimatter asymmetry [A$^+$20a]
- The origin of the neutrino masses and neutrino oscillations
- The θ-parameter in $SU(3)_C$ sector being highly suppressed [Bor00, B$^+$06] (Strong CP problem)
- Unidentified dark sector: 26.8 % and 68.3 % of the total energy density of our universe being dark matter and dark energy, respectively [A$^+$20a]

- The anomalies between the SM predictions and experimental results such as the muon $g-2$ [A$^+$21], and flavor anomalies

The construction of a UV completed theory from the SM solving these theoretical and experimental problems and describing the phenomenology of the BSM is the most important task left for particle physics. This task is important not only for the phenomenology but also for the construction of quantum gravity theory and the revelation of the selection rule of the vacuum in quantum gravity theory as pointed out in Ref. [Vaf05], where the consistency conditions of quantum gravity theory gives constraints on the low-energy effective theory. The classification of the constraints is discussed in the context of the Swampland Programs. This may bridge the phenomenology to the theory of everything.

In addition to the collider physics, the cosmology and astrophysics give us new hints to both the bottom-up and top-down approaches. In particular, dark matter is one of big probes to investigate the BSM. The existence of dark matter has been confirmed by several astronomical observations such as spiral galaxies [CS00, SR01], gravitational lensing [MKR10], cosmic microwave background [A$^+$20b], and collision of bullet cluster [RMC$^+$08]. However, the nature of dark matter is still unknown and any standard model particles cannot play a role of dark matter. Then, identification of dark matter is important not only for cosmology but also for particle physics. One of the prominent candidate is so-called Weakly Interacting Massive Particle (WIMP). The attractive feature of WIMPs is that the relic abundance is thermally determined through the interactions with the SM thermal bath in the early universe. The WIMP mass whose interaction is close the electroweak interaction is predicted in the range of 10 GeV – 100 TeV. Such WIMPs are basically detectable through non-gravitational interactions. Although WIMPs are being searched through direct detection, indirect detection and collider production, no clear signals of WIMPs have been confirmed yet. In particular, recent direct detection experiments provide a strong upper bound on the elastic scattering cross section between dark matter and nucleon [A$^+$17a, C$^+$17, A$^+$18, A$^+$20d].

One of powerful approaches investigating the BSM theory is the extension of the scalar sector. Depending on the charges of additional scalar fields, the dynamics of these scalars can describe the phenomenology of the BSM and give us interesting probes. In particular, the Nambu-Goldstone boson (NGB) can generally appear in the low energy region, reflecting the symmetry of the theory. However, since the existence of the massless scalar field is constrained by experiments and observations such as the fifth force bound and a massive particle is desirable, we are interested in a pseudo-Nambu-Goldstone boson (pNGB)[1], which is stabilized and has non-vanishing mass by introducing an explicit breaking term, background fluxes or non-perturbative effects such as the instanton effects.[2] As we dis-

---

[1]This kind of scalar also appears in the higher dimensional theory with a higher form field, such as string theory [ADD$^+$10, CGR12]. The extra dimensional components of the higher form fields plays the role of the NGB-like scalar via compactification and the Chern-Simons term between the higher form field and the gauge field strength leads the axion interaction in four dimension.

[2]It is known that a lot of scalar fields appear in the low energy effective field theory through the com-

cuss in the following chapters, this kind of pNGB can be a natural candidate of WIMPs escaping the constraints by the direct detections via the nature of its interaction. The additional scalar field not only provides candidates for new particles such as dark matter, but also can be a new source of non-perturbative objects in field theories such as topological solitons. The existence and dynamics of these solitons and the interactions between the solitons or those between the solitons and the elementary particles can have new effects on the cosmological observations and they can make the BSM model detectable by the current or future experiments.

In this thesis, We consider a scalar sector extension by a SM singlet scalar field, which can carry other charges such as $U(1)_{B-L}$ or $U(1)_L$. We study the dynamics and phenomenology of pNGB arising from the spontaneous symmetry breaking of the scalar potential. First, we investigate the possibilities that this pNGB can be a natural candidate of dark matter and propose a UV completed model from the viewpoint of the consistency with quantum gravity theory. We also study the related topics depending on the symmetry associated with this new scalar field, for example inflationary scenario in the scalar extension model and the neutrino oscillations. Then, the construction and the phenomenology of the topological solition, which is a new type of axion string dressed by the SM gauge flux, is discussed by introducing an SM singlet scalar field and the second Higgs doublet to the SM.

Organization of the thesis

The main part of this thesis is based on my five papers [ATT20, ATTY21, ATY21, AHO⁺20, AHY21]. The rest parts are organized as follows.

We propose the UV completion of the simple pNGB dark matter model based on a gauged $U(1)_{B-L}$ symmetry in Chapter 2. This model is motivated by the consistency of quantum gravity theory and the symmetry of that model is realized as a discrete gauge symmetry. The pNGB is stabilized by the cubic coupling to another SM singlet scalar field spontaneously breaking the $U(1)_{B-L}$ symmetry. In return for this UV completion motivated by the swampland conditions, the pNGB dark matter candidate is not stable due to the new interactions with the $B-L$ gauge boson and the scalar mass mixing, while the original simple pNGB dark matter is stabilized by the $\mathbb{Z}_2$ sign flip symmetry associated with the CP-symmetry of the scalar sector. This result means that this pNGB is the decaying dark matter and the long-livednes gives a strong constraint on the model through the $U(1)_{B-L}$ breaking scale. We evaluate the life-time of the dark matter candidate and show the parameter space realizing the current dark matter relic as a thermal relic avoiding the several experimental constraints.

---

pactification, which is so called moduli fields. In general, these scalars have a flat direction corresponding to the continum deformation of the background. In order to stabilize them, higher form background fluxes [DK07] or non-perturbative effects play the important role to generate the scalar potential.

In Chapter 3, we further advance the possibility of a connection between the pNGB dark matter and UV physics that we considered in the previous chapter, and investigate whether the existence of dark matter and the swampland conjecture imply a grand unification. If the pNGB dark matter model based on the gauged $U(1)_{B-L}$ symmetry is embedded to the grand unified theory (GUT) with $SO(10)$ gauge group, it is found that the symmetry breaking pattern via the Pati-Salam gauge group is favored. Some free parameters in the previous model, $U(1)_{B-L}$ gauge coupling, the gauge kinetic mixing between $U(1)_Y$ and $U(1)_{B-L}$ and the intermediate scale at the $U(1)_{B-L}$ being broken, are fixed by the unification condition. We discuss that this determined intermediate scale predicts the pNGB dark matter mass less than $\mathcal{O}(100)$ GeV.

In Chapter 4, we study another possibility to the WIMP pNGB dark matter model in the previous chapters, where the VEV of the symmetry breaking is much larger than the electroweak scale. In this situation, the interaction of the pNGB is highly suppressed by the huge VEV due to its derivative coupling, and the pNGB does not realize the dark matter relic by the freeze-out mechanism. However, it can be a dark matter candidate by the freeze-in production through the VEV suppressed interaction and we show that the pNGB with the huge VEV can be a typical candidate of the Feebly Interacting Massive Paricle (FIMP). In addition to this, we also investigate the possibility that the symmetry breaking scalar field which mediates the interactions between the pNGB and SM particles plays the role of the inflaton via using the non-minimal coupling. We discuss the dark matter relic by taking the direct production from the inflaton decay to the pNGB and the ordinary freeze-in production into account.

We consider a special type of the pNGB, called Majoron which arises from the spontaneous symmetry breaking of the lepton number, and study whether Majoron with TeV-scale soft breaking mass can be the dark matter candidate in Chapter 5. The VEV of the SM singlet scalar of the TeV-scale Majoron is highly constrained by the life-time of the Majoron decaying to two left-handed neutrinos. In addition to this, the Yukawa coupling between the right-handed neutrinos and this scalar is also restricted by the cosmic-ray observations via the Majoron decay channel to top quarks. These results show the interactions in the right-handed neutrino sector of the TeV-scale Majoron dark matter scenario is very feeble and the production of this dark matter candidate seems hard. We discuss three possible scenarios for the creation of the TeV-scale Majoron dark matter. This analysis is related to the FIMP pNGB dark matter scenario in Chapter 4.

In Chapter 6, we consider another interesting pNGB appearing in the scalar sector extension, which is the QCD axion solving the strong CP problem by the Peccei-Quinn mechanism. We study the topological string in the DFSZ axion model [Zhi80, DFS81] and construct a new type of soliton solution which has a thin axion string core and the SM gauge flux surrounds this. Then we also find that the electromagnetic symmetry can be broken around the string core, and the axion string can be superconducting in some parameter space. If the axion string becomes superconducting string, the zero mode

current associated with the breaking of the electromagnetic gauge symmetry travels along this string. It can be the source of a long-range attractive force between the strings while the axion exchange force is repulsive. This new attractive force can lead to a string bound state called Y-shaped junction, and we discuss the possibility of the formation of this Y-junction in the DFSZ axion model and its cosmological impacts.

Chapter 7 is devoted to the conclusion of this thesis. We summarize our notation and convention in Appendix A. In Appendix B, we give a brief review of (scalar-) weak gravity conjecture, which is one of the swampland conjectures. We consider the application to the anomalous quiver gauge theories and discuss the constraints on the gauge groups. In Appendix C, we discuss the lepton asymmetry production via the right-handed neutrino decay with a light flavored scalar. This is a complementary study to the Majoron dark matter creation in Chapter 5.

Chapter 2

Pseudo-Nambu-Goldstone dark matter from gauged $U(1)_{B-L}$ model

2.1 Pseudo-Nambu-Goldstone dark matter model and UV completion

The direct detection experiments [A+17a, C+17, A+18, A+20d] give the strong constraint on the mass and interactins of WIMPs. In order to pursue WIMPs further in the current situation, we have to consider mechanisms to avoid this severe constraint from the direct detection experiments. One option is to consider a pseudo-Nambu-Goldstone boson (pNGB) as dark matter [BMS10, GLT17]. Since all the interactions are written by derivative couplings in non-linear representation, the scattering amplitude for direct detection vanishes in non-relativistic limit.[1] The leading contribution comes from one-loop level, and the order of the elastic cross section has been evaluated as $\mathcal{O}(10^{-48})$ cm^2 at most [ADG+19, IT18]. Since this magnitude of the elastic cross section is considerably small, probing pNGB dark matter by future direct detection experiments may be difficult. However, indirect detection and collider searches are more promising, and there are some works in this direction [HKL+19, CT19]. In addition, global fitting of the pNGB dark matter with comprehensive analysis has been done in Ref. [ABD+20].

A pNGB dark matter is an attractive candidate of WIMP, but there are some questions, such as the origin of the soft breaking mass or the stabilization of this scalar and the UV completion of this model. From the point of view of consistency with quantum gravity theory, gauge symmetries are motivated by the conjecture that there is no global symmetry in quantum gravity [BD88, BS11]. This conjecture implies that the discrete symmetry $\mathbb{Z}_2$ of the pNGB dark matter model should be realized as the gauged discrete symmetry.

---

[1] A pNGB dark matter also appears in the composite Higgs models. In this context, the suppression of the elastic scattering amplitude has been studied in Refs. [FZFLLH15, BGM+16, BBD+17, BRSW17, BRSW18, RSW20, Ram20].

In this chapter, we propose a model of the pNGB dark matter from a *gauged* $U(1)_{B-L}$ symmetry, which is motivated by the quantum gravity consistency. We introduce two complex scalars with $Q_{B-L} = +1$ and $+2$, and three right-handed neutrinos for gauge anomaly cancellation. The pNGB dark matter scenario in Ref. [GLT17] is realized in the decoupling limit, where the $U(1)_{B-L}$ symmetry breaking scale is taken to be infinity. In contrast to the original pNGB dark matter scenario, the pNGB decays due to the new interactions through the heavy particles. This is a result with a scalar sector with a discrete gauge symmetry. The stability of the pNGB is determined by the breaking scale of the $U(1)_{B-L}$ symmetry. We show that the pNGB can be long-lived over the current upper bound of the lifetime from the cosmic-ray observations. We also study the consistencies with the relic abundance of dark matter, and low energy phenomenology.

The rest of this chapter is organized as follows. We give a brief review of the simple pNGB dark matter model and show the suppression mechanism of the scattering amplitude in Section 2.2. In Section 2.3, a pNGB is introduced from the $U(1)_{B-L}$ symmetry breaking. In Section 2.4, the longevity of the pNGB as dark matter is investigated. We also study the relevant constraints on our pNGB dark matter such as the relic abundance of dark matter, the perturbative unitarity, and the Higgs invisible decay and signal strength. Section 2.5 is devoted to our summary.

2.2   Brief review of simple pNGB dark matter model

The simple pNGB dark matter model is given by the SM singlet complex scalar extension [GLT17]. The scalar potential is given by

$$
\mathcal{V}(H, S) = -\frac{\mu_H^2}{2}|H|^2 - \frac{\mu_S^2}{2}|S|^2 + \frac{\lambda_H}{2}|H|^4 + \frac{\lambda_S}{2}|S|^4 + \lambda_{HS}|H|^2|S|^2
$$
$$
- \frac{m^2}{4}\big(S^2 + S^{*2}\big), \tag{2.2.1}
$$

where the second line is the soft breaking mass term, which is introduced so that the pNGB is stabilized as shown in the following part. This soft term breaks explicitly the $U(1)_S$ phase rotational symmetry of S to $\mathbb{Z}_2$ associated with the sign flip of S: $\mathbb{Z}_2 : S \mapsto -S$. These scalars are parametrized by

$$
H = \frac{1}{\sqrt{2}}\begin{pmatrix} 0 \\ v+h \end{pmatrix}, \qquad S = \frac{v_s + s + i\chi}{\sqrt{2}}, \tag{2.2.2}
$$

and the following stationary conditions are satisfied:

$$
\mu_H^2 = \lambda_H v^2 + \lambda_{HS} v_s^2, \qquad \mu_S^2 + m^2 = \lambda_S v_s^2 + \lambda_{HS} v^2. \tag{2.2.3}
$$

Using these equations, the mass matrix of the CP-even scalars is given by

$$
M_e^2 = \begin{pmatrix} \lambda_H v^2 & \lambda_{HS} v v_s \\ \lambda_{HS} v v_s & \lambda_S v_s^2 \end{pmatrix}, \tag{2.2.4}
$$

7

and the CP-odd scalar, which is the pNGB, obtains the mass $m_\chi^2 = m^2$. The mass eigenstates of the CP-even scalars (h_1, h_2) are introduced by

$$\begin{pmatrix} h \\ s \end{pmatrix} = \begin{pmatrix} \cos\theta & \sin\theta \\ -\sin\theta & \cos\theta \end{pmatrix} \begin{pmatrix} h_1 \\ h_2 \end{pmatrix}, \tag{2.2.5}$$

and the mixing angle is given by

$$\tan 2\theta = \frac{2\lambda_{HS} v v_s}{\lambda_S v_s^2 - \lambda_H v^2}. \tag{2.2.6}$$

The mass eigenvalues are given by

$$m_{h_1}^2 = \frac{1}{2}\left[\lambda_H v^2 + \lambda_S v_s^2 - \sqrt{(\lambda_S v_s^2 - \lambda_H v^2)^2 + 4\lambda_{HS} v^2 v_s^2}\right], \tag{2.2.7}$$

$$m_{h_2}^2 = \frac{1}{2}\left[\lambda_H v^2 + \lambda_S v_s^2 + \sqrt{(\lambda_S v_s^2 - \lambda_H v^2)^2 + 4\lambda_{HS} v^2 v_s^2}\right]. \tag{2.2.8}$$

Using these physical parameters, mass eigenvalues and mixing angle, the scalar quartic couplings are written as

$$\lambda_H = \frac{\cos^2\theta m_{h_1}^2 + \sin^2\theta m_{h_2}^2}{v^2}, \quad \lambda_{HS} = \frac{\sin\theta\cos\theta(m_{h_2}^2 - m_{h_1}^2)}{v v_s}, \quad \lambda_S = \frac{\sin^2\theta m_{h_1}^2 + \cos^2\theta m_{h_2}^2}{v_s^2}. \tag{2.2.9}$$

Let us consider the interaction Lagrangian. The χ-χ-h_i interactions dominant to the dark matter-SM particle scattering are given by

$$\mathcal{L} \ni \frac{1}{2}\sum_{i=1,2} \kappa_{\chi\chi h_i}\chi^2 h_i, \tag{2.2.10}$$

$$\kappa_{\chi\chi h_1} = -\frac{m_{h_1}^2 \sin\theta}{v_s}, \quad \kappa_{\chi\chi h_2} = \frac{m_{h_2}^2 \cos\theta}{v_s}. \tag{2.2.11}$$

The interactions among CP-even scalars are given by [AT21]

$$\kappa_{111} = 3m_{h_1}^2\left(-\frac{\sin^3\theta}{v_s} + \frac{\cos^3\theta}{v}\right), \tag{2.2.12}$$

$$\kappa_{112} = (2m_{h_1}^2 + m_{h_2}^2)\sin\theta\cos\theta\left(\frac{\sin\theta}{v_s} + \frac{\cos\theta}{v}\right), \tag{2.2.13}$$

$$\kappa_{122} = (m_{h_1}^2 + 2m_{h_2}^2)\sin\theta\cos\theta\left(-\frac{\cos\theta}{v_s} + \frac{\sin\theta}{v}\right), \tag{2.2.14}$$

$$\kappa_{222} = 3m_{h_2}^2\left(\frac{\cos^3\theta}{v_s} + \frac{\sin^3\theta}{v}\right), \tag{2.2.15}$$

with the convention

$$-\mathcal{L} \ni \mathcal{V} \ni \frac{\kappa_{111}}{3!}h_1^3 + \frac{\kappa_{112}}{2!}h_1^2 h_2 + \frac{\kappa_{122}}{2!}h_1 h_2^2 + \frac{\kappa_{222}}{3!}h_2^3. \tag{2.2.16}$$
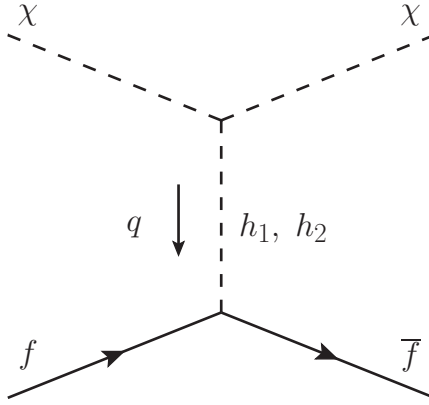
Figure 2.1: Feynman diagram for the tree-level dark matter scattering with the SM matter.

The interactions among the CP-even scalars and SM fermions become

$$\mathcal{L} \ni -\sum_f \frac{m_f}{v} h \bar{f} f = -(h_1 \cos\theta + h_2 \sin\theta) \sum_f \frac{m_f}{v} \bar{f} f. \qquad (2.2.17)$$

Fig. 2.1 shows the scattering process between the pNGB dark matter χ and SM fermions f, with the momentum transfer q. Using Eqs. (2.2.11) and (2.2.17), the scattering amplitude of this process is given by

$$i\mathcal{M} \propto \sin\theta\cos\theta\left(\frac{m_{h_2}^2}{t - m_{h_2}^2} - \frac{m_{h_1}^2}{t - m_{h_1}^2}\right) \approx \sin\theta\cos\theta\frac{t(m_{h_2}^2 - m_{h_1}^2)}{m_{h_1}^2 m_{h_2}^2} \xrightarrow[t\to 0]{} 0, \qquad (2.2.18)$$

where the Mandelstam variable is defined by $t = q^2$. Due to the momentum dependence of the amplitude, the pNGB dark matter escape the severe direct detection constraint.[2] This behavior can be understood by the soft pion theorem, which implies the NGB becomes free particle in the infrared (IR) limit due to the derivative couplings.

The scatterin amplitude (2.2.18) is proportional to $t(m_{h_2}^2 - m_{h_1}^2)$, which is character of the introduction quadratic breaking term. Let me put it another way, the soft breaking mass term does not change the interactions of the pNGB. If one introduce another type of breaking term, the amplitude includes the additional term proportional to the breaking term and it is not possible to say in general that the amplitude vanishs in $t \to 0$ limit.

The authors of Ref. [GLT17] show the parameter space where the current dark matter relic is realized as the thermal relic via the freeze-out mechanism.

	Q_L	u_R^c	d_R^c	L	e_R^C	H	ν_R^C	S	Φ
$SU(3)_C$	**3**	$\bar{\mathbf{3}}$	$\bar{\mathbf{3}}$	**1**	**1**	**1**	**1**	**1**	**1**
$SU(2)_L$	**2**	**1**	**1**	**2**	**1**	**2**	**1**	**1**	**1**
$U(1)_Y$	$+1/6$	$-2/3$	$+1/3$	$-1/2$	$+1$	$+1/2$	0	0	0
$U(1)_{B-L}$	$+1/3$	$-1/3$	$-1/3$	-1	$+1$	0	$+1$	$+1$	$+2$

Table 2.1: Particle contents and quantum charges.

2.3 Model

The particle contents and the charge assignments under the gauge group $G_{\mathrm{SM}} \times U(1)_{B-L}$ are shown in Table 2.1. We note that the model is consist of particles in the ordinary $U(1)_{B-L}$ model and an additional scalar singlet S with $Q_{B-L} = +1$. The gauge kinetic terms of the new particles charged under $U(1)_{B-L}$ are written as

$$\mathcal{L}_K = (D_\mu S)^\dagger (D^\mu S) + (D_\mu \Phi)^\dagger (D^\mu \Phi) + \overline{\nu_R} i \slashed{D} \nu_R - \frac{1}{4} X_{\mu\nu} X^{\mu\nu} - \frac{\sin \epsilon}{2} X_{\mu\nu} B^{\mu\nu} \quad (2.3.1)$$

where $D_\mu = \partial_\mu + i g_{B-L} Q_{B-L} X_\mu$ is the covariant derivative with the new gauge boson X_μ associated with the $U(1)_{B-L}$ symmetry. The field strengths for $U(1)_{B-L}$ and $U(1)_Y$ are denoted by $X_{\mu\nu}$ and $B_{\mu\nu}$, respectively. The last term is the gauge kinetic mixing between X_μ and B_μ. An extra mass eigenstate Z' of neutral gauge bosons is mainly composed by the new gauge boson X_μ. The detailed calculations of diagonalization of the kinetic mixing and mass matrix is summarized in Appendix 2.A.

The scalar potential is written as

$$V(H, S, \Phi) = -\frac{\mu_H^2}{2}|H|^2 - \frac{\mu_S^2}{2}|S|^2 - \frac{\mu_\Phi^2}{2}|\Phi|^2 + \frac{\lambda_H}{2}|H|^4 + \frac{\lambda_S}{2}|S|^4 + \frac{\lambda_\Phi}{2}|\Phi|^4$$
$$+ \lambda_{HS}|H|^2|S|^2 + \lambda_{H\Phi}|H|^2|\Phi|^2 + \lambda_{S\Phi}|S|^2|\Phi|^2 - \left(\frac{\mu_{\mathrm{c}}}{\sqrt{2}} \Phi^* S^2 + \text{c.c.} \right) \quad (2.3.2)$$

The CP phase of the cubic term is eliminated by the field redefinition of Φ. All the scalar fields develop VEVs, and they are parametrized by

$$H = \begin{pmatrix} 0 \\ (v+h)/\sqrt{2} \end{pmatrix}, \qquad S = \frac{v_s + s + i\eta_s}{\sqrt{2}}, \qquad \Phi = \frac{v_\phi + \phi + i\eta_\phi}{\sqrt{2}} \quad (2.3.3)$$

In the limit $\mu_{\mathrm{c}} \to 0$, the scalar potential has two independent global $U(1)$ symmetries associated with the phase rotation of S and Φ, respectively. When $\mu_{\mathrm{c}} \neq 0$, these $U(1)$

---

[2]Another way is to consider a fermionic dark matter with pseudo-scalar interactions [FL11]. In this case, since the scattering amplitude at tree level is suppressed by the momentum transfer in non-relativistic limit due to the spin structure, the leading contribution to the amplitude appears at loop level [IMN14, ALQ$^+$18, BBS18, AFH19, AFHS20]. This behavior of the amplitude is similar to the pion exchange potential.

symmetries are merged to the $U(1)_{B-L}$ symmetry. Therefore, one of NGBs is absorbed by X_μ, while the other appears as a physical pNGB with the mass proportional to μ_c. We note that μ_c is naturally small in 't Hooft sense because of the enhanced symmetry argument. One can intuitively understand that if the scalar Φ gets the VEV v_ϕ, the last term gives effective mass term $\mu_c v_\phi S^2/2$ for the pNGB.

By solving stationary conditions for $\mu_H^2, \mu_S^2, \mu_\Phi^2$, the mass matrix for the CP-even scalars in the (h, s, ϕ) basis is

$$
M_{\text{even}}^2 = \begin{pmatrix} \lambda_H v^2 & \lambda_{HS} v v_s & \lambda_{H\Phi} v v_\phi \\ \lambda_{HS} v v_s & \lambda_S v_s^2 & \lambda_{S\Phi} v_s v_\phi - \mu_c v_s \\ \lambda_{H\Phi} v v_\phi & \lambda_{S\Phi} v_s v_\phi - \mu_c v_s & \lambda_\Phi v_\phi^2 + \frac{\mu_c v_s^2}{2 v_\phi} \end{pmatrix} \tag{2.3.4}
$$

This mass matrix is approximately diagonalized by the matrix

$$
U \approx \begin{pmatrix} 1 & 0 & \frac{\lambda_{H\Phi} v}{\lambda_\Phi v_\phi} \\ 0 & 1 & \frac{\lambda_{S\Phi} v_s}{\lambda_\Phi v_\phi} \\ -\frac{\lambda_{H\Phi} v}{\lambda_\Phi v_\phi} & -\frac{\lambda_{S\Phi} v_s}{\lambda_\Phi v_\phi} & 1 \end{pmatrix} \begin{pmatrix} \cos\theta & \sin\theta & 0 \\ -\sin\theta & \cos\theta & 0 \\ 0 & 0 & 1 \end{pmatrix} \tag{2.3.5}
$$

where $U(1)_{B-L}$ symmetry breaking is assumed mainly by v_ϕ. The gauge eigenstates (h, s, ϕ) are expressed by the mass eigenstates (h_1, h_2, h_3) as

$$
\begin{pmatrix} h \\ s \\ \phi \end{pmatrix} = U \begin{pmatrix} h_1 \\ h_2 \\ h_3 \end{pmatrix} \tag{2.3.6}
$$

where the mixing angle θ is given by

$$
\tan\theta \approx \frac{2 v v_s (\lambda_{HS} \lambda_\Phi - \lambda_{H\Phi} \lambda_{S\Phi})}{v^2 (\lambda_{H\Phi}^2 - \lambda_H \lambda_\Phi) - v_s^2 (\lambda_{S\Phi}^2 - \lambda_S \lambda_\Phi)}. \tag{2.3.7}
$$

The corresponding mass eigenvalues for h_i are approximately evaluated as

$$
m_{h_1}^2 \approx \lambda_H v^2 - \frac{\lambda_{H\Phi} \lambda_S - 2\lambda_{HS} \lambda_{H\Phi} \lambda_{S\Phi} + \lambda_\Phi \lambda_{HS}^2}{\lambda_S \lambda_\Phi - \lambda_{S\Phi}^2} v^2, \tag{2.3.8}
$$

$$
m_{h_2}^2 \approx \frac{\lambda_S \lambda_\Phi - \lambda_{S\Phi}^2}{\lambda_\Phi} v_s^2 + \frac{(\lambda_\Phi \lambda_{HS} - \lambda_{H\Phi} \lambda_{S\Phi})^2}{\lambda_\Phi (\lambda_S \lambda_\Phi - \lambda_{S\Phi}^2)} v^2, \tag{2.3.9}
$$

$$
m_{h_3}^2 \approx \lambda_\Phi v_\phi^2. \tag{2.3.10}
$$

We identify h_1 as the SM-like Higgs boson with the mass $m_{h_1} = 125$ GeV.

The mass matrix of the CP-odd scalars in the gauge eigenstates (η_s, η_ϕ) is written as

$$
M_{\text{odd}}^2 = \frac{\mu_c}{2 v_\phi} \begin{pmatrix} 4 v_\phi^2 & -2 v_s v_\phi \\ -2 v_s v_\phi & v_s^2 \end{pmatrix} \tag{2.3.11}
$$

This mass matrix can be diagonalized as

$$
{}^t V M_{\text{odd}}^2 V = \begin{pmatrix} m_\chi^2 & 0 \\ 0 & 0 \end{pmatrix}, \quad m_\chi^2 = \frac{\mu_{\text{c}}(v_s^2 + 4v_\phi^2)}{4v_\phi} \tag{2.3.12}
$$

where the unitary matrix V is given by

$$
V = \frac{1}{\sqrt{v_s^2 + 4v_\phi^2}} \begin{pmatrix} 2v_\phi & v_s \\ -v_s & 2v_\phi \end{pmatrix}. \tag{2.3.13}
$$

The gauge eigenstates (η_s, η_ϕ) are rewritten by the mass eigenstates $(\chi, \tilde{\chi})$ as

$$
\begin{pmatrix} \eta_s \\ \eta_\phi \end{pmatrix} = \frac{1}{\sqrt{v_s^2 + 4v_\phi^2}} \begin{pmatrix} 2v_\phi & v_s \\ -v_s & 2v_\phi \end{pmatrix} \begin{pmatrix} \chi \\ \tilde{\chi} \end{pmatrix}. \tag{2.3.14}
$$

where $\tilde{\chi}$ is the NGB absorbed by X_μ, and χ corresponds to the pNGB which will be identified as dark matter.

The following Yukawa interactions are also invariant under the imposed symmetry

$$
\mathcal{L}_Y = -y_{ij}^\nu \overline{\nu_{Ri}} \tilde{H}^\dagger L_j - \frac{y_{ij}^\Phi}{2} \Phi \overline{\nu_{Ri}^C} \nu_{Rj} + \text{h.c.,} \tag{2.3.15}
$$

where $\tilde{H} := i\sigma^2 H^*$ with the second component of the Pauli matrices σ^2. After the $U(1)_{B-L}$ symmetry breaking, the right-handed neutrinos obtain the Majorana mass $M_N := y_\Phi v_\phi/\sqrt{2}$. Thus, the small masses for active neutrinos are generated by the type-I seesaw mechanism as $m_\nu \approx -m_D M_N^{-1}\,{}^t m_D$ with the Dirac mass $m_D := y_\nu v/\sqrt{2}$. Since the heaviest neutrino mass is roughly fixed by the neutrino oscillation data as $m_\nu \sim 0.1$ eV, the required scale of the VEV v_ϕ is estimated as

$$
m_\nu \sim \frac{y^{\nu 2} v^2}{\sqrt{2} y^\Phi v_\phi} \sim 0.1 \text{ eV} \quad \rightarrow \quad v_\phi \sim 4.3 \times 10^{14} \text{ eV} \left(\frac{y^{\nu 2}}{y^\Phi} \right) \tag{2.3.16}
$$

The scale v_ϕ is large enough as compared to the electroweak scale unless the Dirac Yukawa coupling y^ν is considerably small.

2.4 Long-lived dark matter

First of all, we check the cancellation of the scattering amplitude for direct detection in this model. When v_ϕ is much larger than v and v_s, the three-point interactions among the pNGB and CP-even scalars are expressed as

$$
\mathcal{L}_{\chi\chi h_i} = -\sum_{i=1,2,3} \frac{\kappa_{\chi\chi h_i}}{2} \chi^2 h_i \tag{2.4.1}
$$

where each coupling coefficient $\kappa_{\chi\chi h_i}$ is given by

$$\kappa_{\chi\chi h_1} \approx -\frac{m_{h_1}^2 \sin\theta}{v_s}, \quad \kappa_{\chi\chi h_2} \approx +\frac{m_{h_2}^2 \cos\theta}{v_s}, \quad \kappa_{\chi\chi h_3} \approx +\frac{m_{h_3}^2}{v_s}\frac{\lambda_{S\Phi}v_s}{\lambda_\Phi v_\phi} \qquad (2.4.2)$$

We note that these couplings are proportional to the corresponding scalar masses. The CP-even scalar exchanging scattering amplitudes of the pNGB and SM particles are expressed as

$$i\mathcal{M} \propto \frac{\sin\theta\cos\theta}{v_s}\left(-\frac{m_{h_1}^2}{q^2 - m_{h_1}^2} + \frac{m_{h_2}^2}{q^2 - m_{h_2}^2}\right) + \mathcal{O}(1/v_\phi), \qquad (2.4.3)$$

where q is the momentum transfer. Due to this structure, the elastic scattering cross section of dark matter and nucleon is suppressed in the non-relativistic limit. This is nothing less than the same cancellation mechanism of the pNGB dark matter for the direct detection [GLT17].[3] Therefore, the pNGB derived from the gauged $U(1)_{B-L}$ model can be a good candidate for dark matter.

It is necessary to examine the longevity of the pNGB to be dark matter, because our pNGB is unstable. The SM particles are produced by the decays of the pNGB dark matter candidate, and these particles further decay into the stable particles such as $e^\pm$, γ, ν, p, $\bar{p}$. These cosmic-rays can be signals of dark matter or constrained by observations. In this paper, following the analysis of gamma rays coming from dwarf spheroidal galaxies using Fermi-LAT data [BGQS16], we study constraints of our model from a conservative limit of the dark matter lifetime $\tau_{\rm DM} \gtrsim 10^{27}$ s, or equivalently $\Gamma_{\rm DM} \lesssim 6.6 \times 10^{-52}$ GeV in terms of decay width.

One of possible two body decay channels is $\chi \to \nu\nu$ through the scalar mixing and the neutrino heavy-light mixing. The partial decay width is roughly estimated as $\Gamma_{\chi\to\nu\nu} \lesssim 10^{-67}$ GeV. This is small enough to guarantee the dark matter (meta-)stability thanks to the strong suppression by the small neutrino masses. In addition, the current experimental upper bound for this channel is much weaker than our estimate, since the observation of the produced neutrino cosmic-rays is much more difficult than those of charged particles such as $e^\pm$, p, $\bar{p}$. Thus, this decay channel can be safely ignored.

Another two body decay mode $\chi \to h_i Z$, depicted in the left panel of Fig. 2.2, becomes important if it is kinematically allowed for $m_\chi > m_{h_i} + m_Z$. The total decay width for this channel is computed as

$$\Gamma_{\text{2-body}} = \sum_i \Gamma_{\chi\to h_i Z} \approx \frac{g_{B-L}^2}{16\pi m_{Z'}^4}m_Z^2 m_\chi^2 \sin^2\theta_W \sin^2\epsilon$$

$$= 5.8 \times 10^{-52} \text{ GeV}\left(\frac{m_\chi}{0.5 \text{ TeV}}\right)^3\left(\frac{10^{15} \text{ GeV}}{m_{Z'}}\right)^2\left(\frac{10^{15} \text{ GeV}}{v_\phi}\right)^2\left(\frac{\sin\epsilon}{1/\sqrt{2}}\right)^2 \qquad (2.4.4)$$

where the mass hierarchy $m_{h_1}, m_{h_2}, m_Z \ll m_\chi \ll m_{h_3}, m_{Z'}$ is applied for this approximated formula. This two body decay becomes important if there is a large gauge kinetic

---

[3]This cancellation mechanism works if and only if the $U(1)_{B-L}$ charge of S is unity.
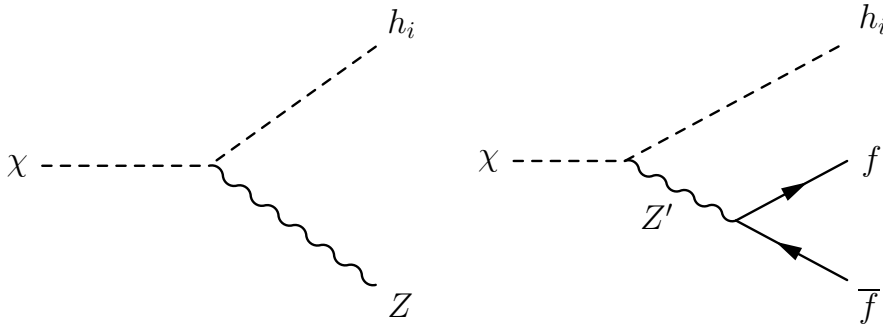
Figure 2.2: Feynman diagrams of the dark matter decay [ATT20].

mixing $\sin \epsilon$,[4] and is irrelevant for the vanishing gauge-kinetic mixing. Since χ is η_s-like, the main contribution to this decay channel comes from $\chi \to h_2 Z$ where h_2 is s-like. Further suppression due to the scalar mixing is expected for other decay channels, e.g., $\chi \to h_1 Z$. A decay process emitting a photon such as $\chi \to h_i \gamma$ is forbidden due to the helicity conservation.

One can naively expect that three body decay processes are subdominant if the above two body decay processes are kinematically allowed. However, three body decays could be dominant depending on parameters, in particular when the gauge kinetic mixing is small. There are two possible three body decay processes $\chi \to Z f \bar{f}$ and $\chi \to h_i f \bar{f}$. The former is mediated by the heavy CP-even scalar h_3, and is possible only when the gauge kinetic mixing is non-zero as same as the above two body decay process. The decay width is extremely suppressed by the heavy h_3 mass and small scalar mixing, thus this is ignored. The latter process is mediated by the heavy Z' gauge boson as depicted in the right panel of Fig. 3.3. In the case that $m_f \ll m_{h_i}, m_\chi \ll m_{Z'}$, the decay width is computed as

$$\Gamma_{\chi \to h_i f \bar{f}} = \frac{g_{B-L}^2 U_{si}^2 m_\chi^5}{768 \pi^3 m_{Z'}^4} \frac{\cos^2 \zeta}{\cos^2 \epsilon} \left(g_V^{f\,2} + g_A^{f\,2} \right) \left[1 - 8\xi_i + 8\xi_i^3 - \xi_i^4 - 12\xi_i^2 \log \xi_i \right] \quad (2.4.5)$$

where $\xi_i := m_{h_i}^2 / m_\chi^2$ and U_{si} ($i = 1, 2$) is the element of the CP-even scalar mixing matrix in Eq. (2.3.5). The mixing matrix elements are explicitly given by $U_{s1} \approx -\sin \theta$, $U_{s2} \approx \cos \theta$. The coefficients $g_{V/A}^f$ are the coupling constants between the heavy gauge boson Z' and vector or axial vector current, which are defined by

$$\mathcal{L}_{Z' \bar{f} f} = -Z'_\mu \bar{f} \gamma^\mu \left[g_V^f + g_A^f \gamma_5 \right] f. \quad (2.4.6)$$

Their expressions in $m_Z \ll m_{Z'}$ limit are given by

$$g_V^f \approx -g_1 \left(Q_{EM}^f - T_3^f \right) \tan \epsilon + \frac{g_{B-L}}{\cos \epsilon} Q_{B-L}^f, \quad (2.4.7)$$

---

[4] A bound on the kinetic mixing $\sin \epsilon$ is obtained from the perturbative unitarity if the new gauge boson mass is lighter than TeV scale [BBDR18]. However this bound is irrelevant to our case since the new gauge mass is assumed to be much heavier than TeV scale.

$$g_A^f \approx 0, \tag{2.4.8}$$

where Q_{EM}^f, T_3^f and Q_{B-L}^f corresponds to the electromagnetic charge, the third component of weak isospin and $B - L$ charge of the fermion f, respectively. The mixing angle ζ is introduced to diagonalize the gauge boson mass matrix as summarized in Appendix 2.A.

It is useful to take some specific values of the parameters to understand the behavior of the three body decay width. Here, we consider the two cases, $\sin \epsilon = 0$ and $1/\sqrt{2}$. First, when there is vanishing gauge kinetic mixing ($\sin \epsilon = 0$), the total three body decay width can simply be computed as

$$
\begin{aligned}
\Gamma_{\text{3-body}}\Big|_{\sin \epsilon \to 0} = \sum_i \sum_f \Gamma_{\chi \to f \bar{f}} &\approx \frac{13}{16} \frac{g_{B-L}^4}{1536 \pi^3} \frac{m_\chi^5}{m_{Z'}^4} \\
&= 5.3 \times 10^{-52} \ \text{GeV} \left(\frac{m_\chi}{0.5 \ \text{TeV}} \right)^5 \left(\frac{10^{15} \ \text{GeV}}{v_\phi} \right)^4
\end{aligned} \tag{2.4.9}
$$

where we used the relation $m_{Z'}^2 \approx 4 g_{B-L}^2 v_\phi^2$.

The second case is a typical value of non-zero gauge kinetic mixing ($\sin \epsilon = 1/\sqrt{2}$). Then, the total decay width can be evaluated as

$$
\begin{aligned}
\Gamma_{\text{3-body}}\Big|_{\sin \epsilon \to 1/\sqrt{2}} = \sum_i \sum_f \Gamma_{\chi \to h_i f \bar{f}} &\approx \frac{g_{B-L}^2}{768 \pi^3} \frac{m_\chi^5}{m_{Z'}^4} \left(10 g_1^2 - 8\sqrt{2} g_1 g_{B-L} + 26 g_{B-L}^2 \right) \\
&= 4.1 \times 10^{-52} \ \text{GeV} \left(\frac{m_\chi}{0.5 \ \text{TeV}} \right)^5 \left(\frac{10^{15} \ \text{GeV}}{m_{Z'}} \right)^2 \left(\frac{10^{15} \ \text{GeV}}{v_\phi} \right)^2 \\
&\quad \times \left[1 - \frac{2\sqrt{2}}{5} \frac{m_{Z'}}{g_1 v_\phi} + \frac{13}{20} \frac{m_{Z'}^2}{g_1^2 v_\phi^2} \right]
\end{aligned} \tag{2.4.10}
$$

From the above calculations, one can find that the two body decay width in Eq. (2.4.4) is proportional to m_χ^3, while the three body decay widths in Eq. (2.4.9), (2.4.10) are proportional to m_χ^5. Therefore the three body decay width tends to be dominant when the dark matter mass m_χ is large. Another important point is that the two body decay width vanishes when there is no gauge kinetic mixing while the three body decay occurs even in the case.

In our model, there are 10 independent parameters in total, which are relevant to the decaying pNGB dark matter. These may be chosen to as $m_\chi, m_{h_2}, m_{h_3}, m_{Z'}, \sin \theta, v_s, v_\phi$, $\lambda_{H\Phi}, \lambda_{S\Phi}$ and $\sin \epsilon$. The Yukawa couplings y_ν and y_Φ are irrelevant for the pNGB sector, and one can always take appropriate Yukawa couplings and right-handed neutrino masses consistently with the neutrino oscillation data. Only 4 parameters ($m_\chi, \sin \theta, v_s, m_{h_2}$) are important for the phenomena of the stable dark matter, which are used in the discussion in the next section. The other parameters are relevant to the dark matter decay. In our numerical calculations, we choose the following parameter sets as examples:

$$m_{h_2} = 300 \text{ or } 1000 \ \text{GeV}, \quad m_{h_3} = 10^{13} \ \text{GeV}, \quad m_{Z'} = 10^{14} \text{ or } 10^{15} \ \text{GeV},$$

Figure 2.3: Allowed regions in the (m_χ, v_ϕ) plane [ATT20]. The scalar mass is fixed as $m_{h_2} = 300$ GeV for the left panels and $m_{h_2} = 1000$ GeV for the right panels. The new gauge boson mass is fixed as $m_{Z'} = 10^{14}$ GeV in the upper panels and $m_{Z'} = 10^{15}$ GeV in the lower panels. The orange regions are excluded by the conservative bound of the dark matter lifetime ($\tau_{\mathrm{DM}} \gtrsim 10^{27}$ s). The gray region is disfavored by the perturbative unitarity bound of the gauge coupling g_{B-L}. The upper light blue region denotes the parameter space that the VEV v_ϕ becomes larger than the Planck mass M_P.

$$\sin\theta = 0.1, \quad \lambda_{H\Phi} = \lambda_{S\Phi} = 10^{-6}, \quad \sin\epsilon = 0 \text{ or } \frac{1}{\sqrt{2}}. \tag{2.4.11}$$

The gauge coupling g_{B-L} and the quartic coupling λ_Φ are fixed by $g_{B-L} \approx m_{Z'}^2/(4v_\phi^2)$ and $\lambda_\phi \approx m_{h_3}^2/v_\phi^2$ for a given VEV v_ϕ. The mixing angle $\sin\theta$ is constrained as $\sin\theta \lesssim 0.3$ for $m_{h_2} \gtrsim 100$ GeV by the electroweak precision measurements and the direct search of the second Higgs boson [MLMP15, FGL15]. This constraint can also be applied for our model. The quartic couplings $\lambda_{H\Phi}$ and $\lambda_{S\Phi}$ are taken small such that the approximate formulae Eq. (2.3.8) and (2.3.9) are valid. If these couplings are large, the negative contributions to the CP-even scalar masses in Eq. (2.3.8) and (2.3.9) become significant and make them tachyonic. Note that one can take these quartic couplings larger than Eq. (2.4.11) for smaller VEV v_ϕ. However, we choose as Eq. (2.4.11) for simplicity so that the quartic couplings retain constant in our numerical calculations.

16

In Fig. 2.3, we show the allowed parameter region from the (meta-)stability constraint of dark matter in the plane (m_χ, v_ϕ). The orange region is ruled out by the cosmic-ray observation. The perturbative unitarity bound of the $U(1)_{B-L}$ gauge coupling exclude the lower gray region. The VEV v_ϕ becomes larger than the Planck scale $M_P = 1.2 \times 10^{19}$ GeV in the upper light blue region.[5] One can find from the plots that when the dark matter mass m_χ becomes larger than the threshold of the decay channel $\chi \to h_2 f \bar{f}$ $(m_\chi \gtrsim m_{h_2})$, the total decay width is enhanced and the bound of the cosmic-ray observations becomes stronger. The scaling behavior of the orange region is observed as $v_\phi \propto m_\chi^{5/4}$ for no kinetic mixing and $v_\phi \propto m_\chi^{5/2}$ for a large kinetic mixing in heavier dark matter mass region. This follows from the analytic formulae of the total three body decay width in Eqs. (2.4.9) and (2.4.10). Characteristic threshold behaviors are also seen at $m_\chi \sim m_{h_2} + m_Z$, where $m_{h_2} = 300$ (1000) GeV is taken in the left (right) panels.

We here comment on the possible four body decay channel. If the dark matter mass is too small to decay through the above two or three body decay process, the four body decay process $\chi \to h_i^* Z^* \to f\bar{f}f'\bar{f}'$ would be the main decay channel of dark matter. However, the decay width is too small to be constrained or be signals of dark matter at present.

Finally, we confirm the consistency of our model with the observed dark matter relic abundance. For calculations of the dark matter relic abundance, the model is implemented in `CalcHEP` [BCP13] by using `LanHEP` [Sem16]. The physical quantities relevant to dark matter such as thermal relic abundance, all the decay widths, spin-independent cross section for direct detection are computed by using `MicrOMEGAs` [BBG+18a]. In Fig. 2.4, we show the consistency of our pNGB dark matter model with the observed relic abundance in the plane $(m_\chi, v/v_s)$. The red line represents the parameter space reproducing the observed thermal relic abundance within 3σ range of the PLANCK data $\Omega_{\mathrm{DM}} h^2 = 0.120 \pm 0.001$ [A+20b]. One can see the two resonances in Fig. 2.4 due to the two Higgs bosons h_1 and h_2. The purple region is excluded by the measurements of the Higgs invisible decay [S+19, A+19a] and the signal strength [A+16] and the upper gray region is ruled out by the perturbative unitarity bound of the quartic coupling $\lambda_S < 8\pi/3$ [CDL15]. The green region is excluded by the gamma-ray observation coming from dwarf spheroidal galaxies where the effective annihilation cross section into $b\bar{b}$ defined by $\langle \sigma_{\mathrm{eff}} v_{\mathrm{rel}} \rangle := \langle \sigma_{b\bar{b}} v_{\mathrm{rel}} \rangle (\Omega_{\mathrm{DM}} h^2/0.120)^2$ with the dark matter relative velocity v_{rel} becomes larger than the current upper bound given by Fermi-LAT [A+17b].[6]

---

[5]If we consider a cosmic string creation after the inflation, the VEV breaking $U(1)_{B-L}$ symmetry is restricted as $v_\phi < 4 \times 10^{15}$ GeV from the CMB observation, which is discussed in Ref. [CACM16].

[6]Note that the parameter space excluded by the gamma-ray observation shown in Fig. 2.4 is different from the previous work [HKL+19]. This is because in the previous work the dark matter abundance in our galaxy has been assumed to be the observed value $(\Omega_{\mathrm{DM}} h^2 \approx 0.120)$ regardless of the thermal abundance computed at each parameter space. This can occur after thermal production of dark matter via additional non-thermal dark matter production or entropy production, for instance. On the other hand in our case, thermal dark matter production is only assumed.
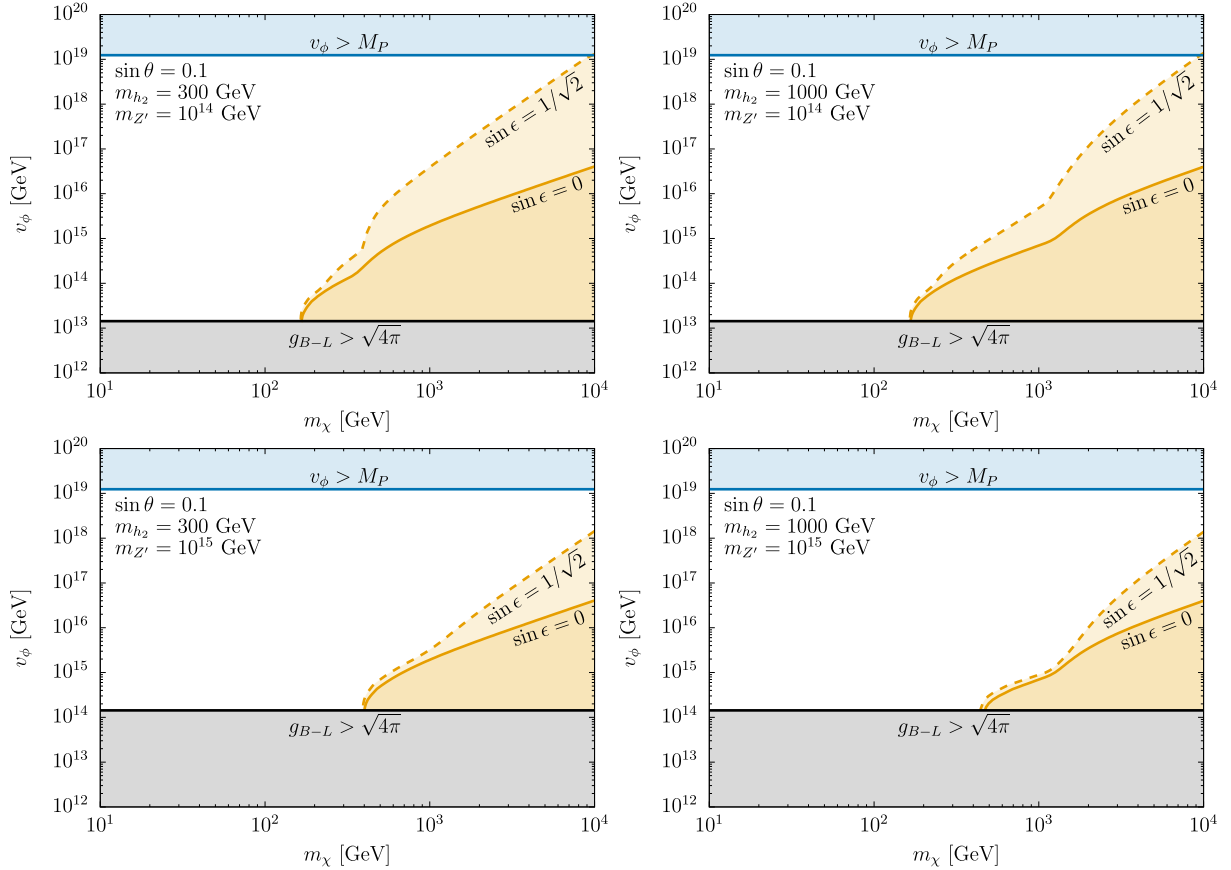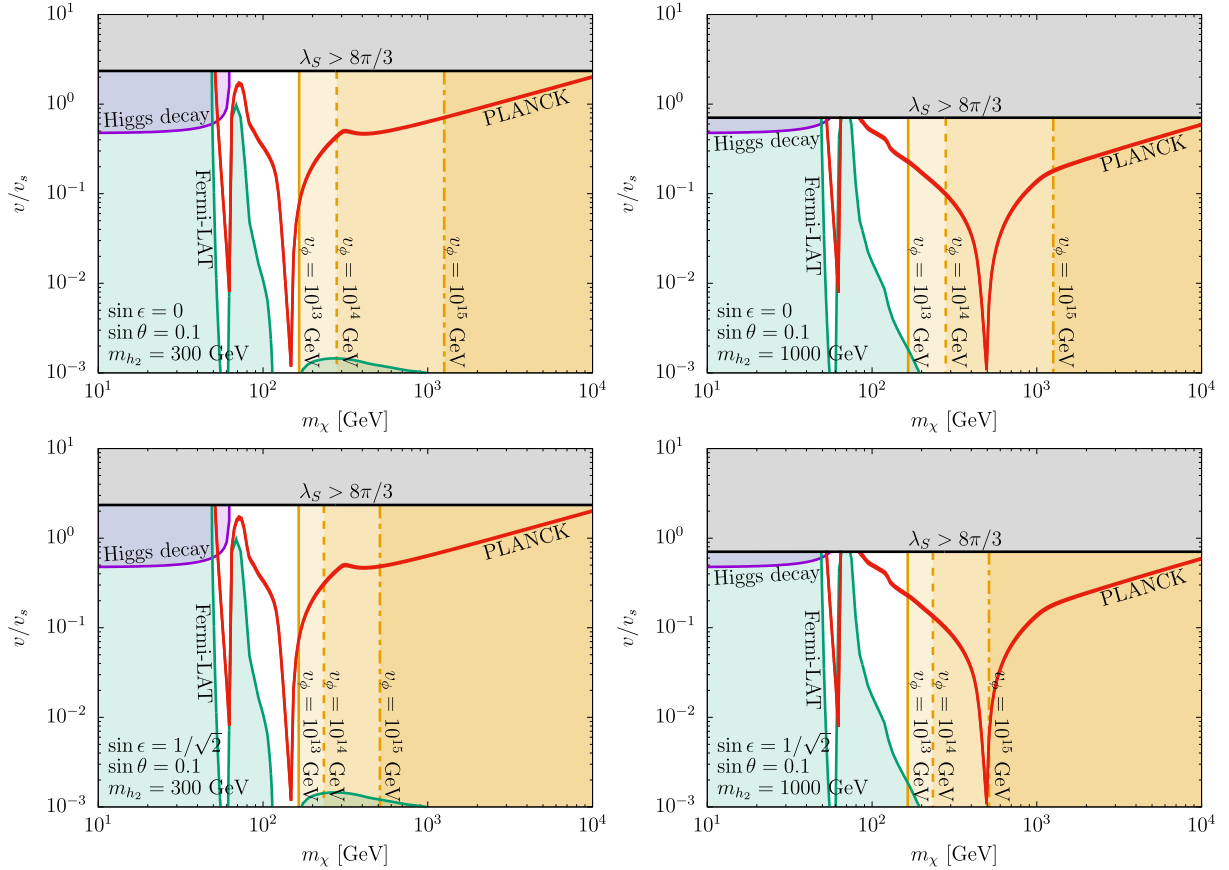
Figure 2.4: Allowed regions in the $(m_\chi, v/v_s)$ plane [ATT20]. The scalar mass is fixed as $m_{h_2} = 300$ GeV for the left panels and $m_{h_2} = 1000$ GeV for the right panels. The gauge kinetic mixing is chosen as $\sin \epsilon = 0$ (no kinetic mixing) in the upper panels and $\sin \epsilon = 1/\sqrt{2}$ (maximal mixing) in the lower panels. The red line corresponds to the thermal dark matter relic abundance consistent with the PLANCK Collaboration [A+20b]. The purple, gray, orange and green regions are excluded by the constraints of the Higgs invisible decays [S+19, A+19a] and the Higgs signal strength [A+16], the perturbative unitarity bound on λ_S [CDL15], the cosmic-ray constraint ($\tau_{DM} \gtrsim 10^{27}$ s) [BGQS16] and the gamma-ray observation [A+17b], respectively.

These behavior is basically same with the previous work as expected [GLT17]. The orange region is excluded by the upper bound on the dark matter lifetime $\tau_{DM} \gtrsim 10^{27}$ s where the VEV is fixed as $v_\phi = 10^{13}$ GeV, 10^{14} GeV, 10^{15} GeV. One can observe from the plots that the bound becomes stronger for small v_ϕ and non-zero gauge kinetic mixing $\sin \epsilon$.

18

2.5 Summary

We have studied the pNGB dark matter scenario derived from the gauged $U(1)_{B-L}$ symmetry. The model is consist of particles in the ordinary $U(1)_{B-L}$ model with an additional scalar singlet with $Q_{B-L} = +1$. The small neutrino masses have also been generated via type-I seesaw mechanism as usual. In this model, the pNGB associated with $U(1)_{B-L}$ symmetry breaking is identified as a dark matter candidate. The interactions of the new $U(1)_{B-L}$ gauge boson and the scalar mixing have led the decays of the pNGB. We have shown that the lifetime of the pNGB is long enough to be dark matter. We have also found the parameter space, which are consistent with the relevant constraints such as observed relic abundance of dark matter, Higgs invisible decay, Higgs signal strength, and perturbative unitarity bound of the couplings.

For future prospects, the planned gamma-ray observations such as Cherenkov Telescope Array (CTA) [C+16] and Large High Altitude Air Shower Observatory (LHAASO) [B+19] can explore the dark matter mass over 100 GeV. In particular, the LHAASO experiment is already being operated, and can search the dark matter mass region between 1 TeV and 100 TeV. The upper bound on the dark matter lifetime is expected to be updated by one order of magnitude as discussed in Ref. [HBL+20]. These upcoming experiments will be able to explore full parameter space of our gauged $U(1)_{B-L}$ pNGB dark matter.

Appendix 2.A   Gauge kinetic mixing

When the kinetic terms of the $U(1)_Y$ and $U(1)_{B-L}$ gauge fields are given by

$$\mathcal{L}_{GK} = -\frac{1}{4} B_{\mu\nu} B^{\mu\nu} - \frac{1}{4} X_{\mu\nu} X^{\mu\nu} - \frac{\sin\epsilon}{2} B_{\mu\nu} X^{\mu\nu}, \tag{2.A.1}$$

these can be diagonalized as

$$\mathcal{L}_{GK} = -\frac{1}{4} \hat{B}_{\mu\nu} \hat{B}^{\mu\nu} - \frac{1}{4} \hat{X}_{\mu\nu} \hat{X}^{\mu\nu}, \tag{2.A.2}$$

by the linear transformation

$$\begin{pmatrix} B_{\mu\nu} \\ X_{\mu\nu} \end{pmatrix} = \begin{pmatrix} 1 & -\tan\epsilon \\ 0 & 1/\cos\epsilon \end{pmatrix} \begin{pmatrix} \hat{B}_{\mu\nu} \\ \hat{X}_{\mu\nu} \end{pmatrix} =: V_{GK} \begin{pmatrix} \hat{B}_{\mu\nu} \\ \hat{X}_{\mu\nu} \end{pmatrix}. \tag{2.A.3}$$

On the other hand, the mass matrix of the neutral gauge bosons is given by

$$\mathcal{L}_M = \frac{1}{2} \begin{pmatrix} B_\mu & W_\mu^3 & X_\mu \end{pmatrix} \begin{pmatrix} \sin^2\theta_W m_{\tilde{Z}}^2 & -\sin\theta_W \cos\theta_W m_{\tilde{Z}}^2 & 0 \\ -\sin\theta_W \cos\theta_W m_{\tilde{Z}}^2 & \cos^2\theta_W m_{\tilde{Z}}^2 & 0 \\ 0 & 0 & m_X^2 \end{pmatrix} \begin{pmatrix} B^\mu \\ W^{3\mu} \\ X^\mu \end{pmatrix}, \tag{2.A.4}$$

where the following parameters are defined:

$$\sin\theta_W := \frac{g_1}{\sqrt{g_1^2 + g_2^2}}, \quad \cos\theta_W := \frac{g_2}{\sqrt{g_1^2 + g_2^2}}, \tag{2.A.5}$$

$$m_{\tilde{Z}}^2 := \frac{g_1^2 + g_2^2}{4}v^2, \quad m_X^2 := g_{B-L}^2(v_s^2 + 4v_\phi^2). \tag{2.A.6}$$

In the kinetic term diagonalized base, the mass matrix of the neutral gauge boson $\hat{M}_G^2$ is written as

$$\hat{M}_G^2 = {}^t\tilde{V}_{GK}\begin{pmatrix} \sin^2\theta_W m_{\tilde{Z}}^2 & -\sin\theta_W\cos\theta_W m_{\tilde{Z}}^2 & 0 \\ -\sin\theta_W\cos\theta_W m_{\tilde{Z}}^2 & \cos^2\theta_W m_{\tilde{Z}}^2 & 0 \\ 0 & 0 & m_X^2 \end{pmatrix}\tilde{V}_{GK}, \tag{2.A.7}$$

where $\tilde{V}_{GK}$ is given by

$$\tilde{V}_{GK} = \begin{pmatrix} 1 & 0 & -\tan\epsilon \\ 0 & 1 & 0 \\ 0 & 0 & 1/\cos\epsilon \end{pmatrix}. \tag{2.A.8}$$

The mass matrix $\hat{M}_G^2$ can be diagonalized by the unitary matrix

$$U_G = \begin{pmatrix} \cos\theta_W & -\sin\theta_W & 0 \\ \sin\theta_W & \cos\theta_W & 0 \\ 0 & 0 & 1 \end{pmatrix}\begin{pmatrix} 1 & 0 & 0 \\ 0 & \cos\zeta & -\sin\zeta \\ 0 & \sin\zeta & \cos\zeta \end{pmatrix}, \tag{2.A.9}$$

where the mixing angle ζ is expressed by

$$\tan 2\zeta = \frac{-m_{\tilde{Z}}^2\sin\theta_W\sin 2\epsilon}{m_X^2 - m_{\tilde{Z}}^2(\cos^2\epsilon - \sin^2\theta_W\sin^2\epsilon)}. \tag{2.A.10}$$

In the limit of $m_{\tilde{Z}}^2 \ll m_X^2$ as in our case, we can find that $\tan 2\zeta \approx -\frac{m_{\tilde{Z}}^2}{m_{Z'}^2}\sin\theta_W\sin 2\epsilon \ll 1$. As a result, the gauge eigenstates can be written in terms of the mass eigenstates (A_μ, Z_μ, Z'_μ) as

$$\begin{pmatrix} B_\mu \\ W_\mu^3 \\ X_\mu \end{pmatrix} = \tilde{V}_{GK}U_G\begin{pmatrix} A_\mu \\ Z_\mu \\ Z'_\mu \end{pmatrix}, \tag{2.A.11}$$

where the gauge bosons A_μ, Z_μ and Z'_μ correspond to the photon, the SM-like Z boson and the new massive gauge boson. The mass eigenvalues are given by

$$m_Z^2 = \frac{1}{2}\left[\overline{M}^2 - \sqrt{\overline{M}^4 - \frac{4m_{\tilde{Z}}^2 m_X^2}{\cos^2\epsilon}}\right], \quad m_{Z'}^2 = \frac{1}{2}\left[\overline{M}^2 + \sqrt{\overline{M}^4 - \frac{4m_{\tilde{Z}}^2 m_X^2}{\cos^2\epsilon}}\right], \tag{2.A.12}$$

where $\overline{M}^2$ is defined by $\overline{M}^2 := m_{\tilde{Z}}^2(1 + \sin^2\theta_W \tan^2\epsilon) + m_X^2/\cos^2\epsilon$. In the limit $\epsilon \to 0$, these mass eigenvalues are reduced to the usual expressions

$$m_Z^2 \to m_{\tilde{Z}}^2 = \frac{g_1^2 + g_2^2}{4}v^2, \quad m_{Z'}^2 \to m_X^2 = g_{B-L}^2(v_s^2 + 4v_\phi^2). \tag{2.A.13}$$

One can see that Eq. (2.A.13) corresponds to the SM Z boson mass.

Finally, we will derive the interactions of these gauge bosons, which are used to evaluate the decay widths of the pNGB dark matter. The interactions with the dark matter come from the covariant derivative of S, and its expressions are given by

$$\mathcal{L}_{Zh_i\chi} = \sum_i g_{B-L}\frac{\sin\zeta}{\cos\epsilon}\frac{U_{si}}{\sqrt{1 + \frac{v_s^2}{4v_\phi^2}}}Z_\mu(h_i\partial^\mu\chi - \chi\partial^\mu h_i), \tag{2.A.14}$$

$$\mathcal{L}_{Z'h_i\chi} = \sum_i g_{B-L}\frac{\cos\zeta}{\cos\epsilon}\frac{U_{si}}{\sqrt{1 + \frac{v_s^2}{4v_\phi^2}}}Z'_\mu(h_i\partial^\mu\chi - \chi\partial^\mu h_i). \tag{2.A.15}$$

The couplings between the heavy gauge boson Z' and the (axial) vector currents of the SM fermion f is defined by

$$\mathcal{L}_{Z'\bar{f}f} = -Z'_\mu\bar{f}\gamma^\mu\left[g_V^f + g_A^f\gamma_5\right]f, \tag{2.A.16}$$

and the explicit expression of the coefficients are given by

$$g_V^f = -\frac{g_2}{2}T_3^f\sin\zeta\cos\theta_W + g_1(Q_{\rm em}^f - T_3^f)(\sin\zeta\sin\theta_W - \cos\zeta\tan\epsilon)$$

$$+ g_{B-L}Q_{B-L}^f\frac{\cos\zeta}{\cos\epsilon}, \tag{2.A.17}$$

$$g_A^f = \frac{g_2}{2}T_3^f\sin\zeta\cos\theta_W. \tag{2.A.18}$$

Appendix 2.B   Discrete gauge symmetry

In this appendix, we will give a brief summary of the discrete gauge symmetry. For simplicity, we use the differential forms for the p-form field. The notation is summarized in Appendix A.3 and the asymmetric tensor is normalized as $\epsilon^{0123} = +1$.

2.B.1 $\mathbb{Z}_k$ gauge theory

The $\mathbb{Z}_k$ discrete gauge theory is realized by restricting the gauge configuration as

$$A_1 = \frac{1}{k}db, \tag{2.B.1}$$

with a compact scalar field $b \sim b + 2\pi$ satisfying

$$\int_C db \in 2\pi\mathbb{Z}. \tag{2.B.2}$$

In this configuration, the Wilson loop is given by

$$w(C) = \exp\left(i \int_C A_1\right) = \exp\left(i \int_{D=\partial C} F_2\right) = \exp\left(i\frac{1}{k} \int_C db\right) = \exp\left(\frac{2\pi i n}{k}\right), \quad \text{(2.B.3)}$$

where $n := \int_C \frac{db}{2\pi} \in \mathbb{Z}$. This equation shows $w(C)$ becomes the unitary representation of $\mathbb{Z}_k$. Then $\mathbb{Z}_k$ gauge theory is given by the set of the gauge field and the compact scalar satisfying Eq. (2.B.1).[7] Eq. (2.B.1) is invariant under the gauge transformation

$$A_1 \mapsto A_1 + d\theta, \qquad b \mapsto b + k\theta. \quad \text{(2.B.4)}$$

The action describing the above system is given by

$$S = \int \frac{t^2}{2}(db - kA_1) \wedge *_4(db - kA_1), \quad \text{(2.B.5)}$$

which is invariant under the gauge transformation (2.B.4). This is nothing but the Stückerlberg action of A_1 and b.[8]

2.B.2 Dual picture

In this subsection, we give the dual picture of the $\mathbb{Z}_k$ gauge theory by using a higher form field. Let us consider the following 4D action:

$$S = \int \left[\frac{1}{2t^2}H_3 \wedge *_4 H_3 + \frac{s}{2}F_2 \wedge *_4 F_2 + kB_2 \wedge F_2\right]. \quad \text{(2.B.7)}$$

where the field strengths are given by $F_2 = dA_1$, $H_3 = dB_2$. The last term of this action is called as BF coupling and the coefficient is k. The EOMs are obtained as

$$\frac{1}{t^2}d *_4 H_3 = qF_2, \quad sd *_4 F_2 = -qH_3, \quad dH_3 = dF_2 = 0. \quad \text{(2.B.8)}$$

On the other hand, the following action with *arbitrary* 3-form field h_3 and Lagrange multiplier b are considered:

$$S = \int \left[\frac{1}{2t^2}h_3 \wedge *_4 h_3 + \frac{s}{2}F_2 \wedge *_4 F_2 + h_3 \wedge (db - kA_1)\right]. \quad \text{(2.B.9)}$$

---

[7] The existence of a particle of the unit charge is assumed so that k is not absorbed in the redefinition of the coupling.

[8] In the field theory context, this kind of action is realized by the higgsing in the abelian-Higgs model via $U(1)$ gauge charge k:

$$|(\partial_\mu - ikA_\mu)\Phi|^2 \quad \rightarrow \quad \frac{v^2}{2}(\partial_\mu b - kA_\mu)^2, \quad \text{(2.B.6)}$$

where $\Phi = \frac{v}{\sqrt{2}}e^{ib}$ is assumed. This is regarde as the decaoupling limit of the massive scalar field, which arises from the radial direction of Φ.

The EOMs of this action are given by

$$\frac{1}{t^2} *_4 h_3 = -(db - qA_1) \quad \Rightarrow \quad \frac{1}{t^2} d *_4 h_3 = qF_2, \tag{2.B.10}$$

$$sd *_4 F_2 = -qh_3, \tag{2.B.11}$$

$$dh_3 = 0 \quad \Rightarrow \quad h_3 = dB_2 \tag{2.B.12}$$

From the EOM of ϕ, h_3 is given as $h_3 = dB_2 = H_3$ by introducing the 2-form field B_2 and the action becomes

$$S = \int \left[\frac{1}{2t^2} H_3 \wedge *_4 H_3 + \frac{s}{2} F_2 \wedge *F_2 + kB_2 \wedge F_2 \right], \tag{2.B.13}$$

which implies the two actions are equivalent. By using the EOM of h_3, $*_4 h_3 = -t^2(db - kA_1)$, we can integrate out h_3 and the action reduces to

$$S = \int \left[\frac{t^2}{2}(db - kA_1) \wedge *_4(db - kA_1) + \frac{s}{2} F_2 \wedge *_4 F_2 \right]. \tag{2.B.14}$$

From these equations, we can find that the string object characterized by the holonomy (2.B.3), so called Aharonov-Bohm string, couples electrically to B_2 as $\int_\Sigma B_2$ with the string world-sheet Σ.

23

Chapter 3

Pseudo-Nambu-Goldstone dark matter model inspired by grand unification

3.1 Gauged $U(1)_{B-L}$ pNGB dark matter model and $SO(10)$ grand unification

In Chapter 2, a pNGB dark matter model is proposed based on $G_{\mathrm{SM}} \times U(1)_{B-L}$ gauge groups. Two complex scalars with $Q_{B-L} = +1$ and $+2$, denoted as S and Φ, and three right-handed neutrinos due to the gauge anomaly cancellation are introduced. The gauge symmetry is spontaneously broken via the non-vanishing VEV of the scalar fields S, Φ and the SM Higgs boson as

$$G_{\mathrm{SM}} \times U(1)_{B-L} \longrightarrow G_{\mathrm{SM}} \longrightarrow SU(3)_C \times U(1)_{\mathrm{EM}}. \qquad (3.1.1)$$

The dark matter direct detection cross section is naturally suppressed as the same as other pNGB dark matter models. The pNGB can decay through the new high scale suppressed operators, but the pNGB has a lifetime long enough to be a dark matter in the wide range of the parameter space of the model. The thermal relic abundance of pNGB dark matter can be fit with the observed value against the constraints on the dark matter decays from the cosmic-ray observations.

From other viewpoints, the charge quantization of $U(1)_Y$, the gauge anomaly cancellation of G_{SM}, and the almost SM gauge coupling unification even in non-supersymmetric SM seem to imply the existence of grand unification [GG74]. The unification scale is expected to be $\mathcal{O}(10^{15} - 10^{18})\,\mathrm{GeV}$, where the lower bound comes from the current non-observation of the nucleon decay [HT20] and the upper bound comes from the Planck scale. Also, the tiny neutrino masses from the neutrino oscillation data seem to suggest an intermediate scale $\mathcal{O}(10^{10}\text{--}10^{14})\,\mathrm{GeV}$ through a see-saw mechanism [Min77].

	A_μ	$\Psi_{\mathbf{16}}$	$\Phi_{\mathbf{10}}$	$\Phi_{\mathbf{16}}$	$\Phi_{\overline{\mathbf{126}}}$	$\Phi_{\mathbf{210}}$
$SO(10)$	**45**	**16**	**10**	**16**	$\overline{\mathbf{126}}$	**210**
$SL(2,\mathbb{C})$	$(1/2,1/2)$	$(1/2,0)$	$(0,0)$	$(0,0)$	$(0,0)$	$(0,0)$

Table 3.1: The matter content in the $SO(10)$ model is shown.

In this chapter, we propose an $SO(10)$ pNGB dark matter model in the framework of grand unified theories (GUTs). Each Weyl fermion in **16** of $SO(10)$ contains one generation of quarks and leptons, which includes a right-handed neutrino [FM75]. The SM Higgs and two complex scalar fields S and Φ in Refs. [ATT20, ORS21] are assigned to a scalar field in **10**, **16**, and $\overline{\mathbf{126}}$ of $SO(10)$, respectively. There are several symmetry breaking patterns of $SO(10)$ to $G_{\mathrm{SM}} \times U(1)_{B-L}$ as below,

$$SO(10) \longrightarrow G_I \longrightarrow G_{\mathrm{SM}} \times U(1)_{B-L}. \tag{3.1.2}$$

where G_I stands for the intermediate gauge group such as the Pati-Salam gauge group $G_{\mathrm{PS}} := SU(4)_C \times SU(2)_L \times SU(2)_R$ [PS74] and a left-right gauge group $G_{\mathrm{LR}} := SU(3)_C \times SU(2)_L \times SU(2)_R \times U(1)_{B-L}$ [PSS75, MS78]. We mainly focus on the case of $G_I = G_{\mathrm{PS}}$, but we also consider the possibility for such as $G_I = G_{\mathrm{LR}}$, where the cases are not favored for a pNGB DM model under our assumption and experimental constraints. (For more information about GUT model building in general, see, e.g., Refs. [Sla81, Yam15].)

We discuss the following three things. First, the value of the gauge kinetic mixing between $U(1)_Y$ and $U(1)_{B-L}$ is a free parameter in e.g., the non-GUT pNGB DM models [ATT20, ORS21], while that is determined mainly by the GUT gauge group in $SO(10)$ models. Second, gauge coupling unification can be achieved due to the contribution from the additional scalar fields that contain a DM candidate. Then the intermediate scale M_I, the unification scale M_U, and the gauge coupling constant of $U(1)_{B-L}$ are fixed by using the renormalization group equations (RGEs) for gauge coupling constants. Third, the mass of the pNGB in the $SO(10)$ pNGB DM model is limited to be $\mathcal{O}(10-100)\,\mathrm{GeV}$ from experimental constraints.

This chapter is organized as follows. In Section 3.2, we introduce the $SO(10)$ pNGB DM model. In Section 3.3, we find gauge coupling unification determines mass scales and gauge coupling constants of the model. In Section 3.4, the constraints from experiments are discussed. Section 3.5 is devoted to summary and discussions.

3.2 The model

The model consists of an $SO(10)$ gauge field A_μ, fermions in **16** of $SO(10)$, a real scalar field in **210** of $SO(10)$, and complex scalar fields in **10**, **16** and $\overline{\mathbf{126}}$ of $SO(10)$. The $SO(10)$ gauge field contains G_{SM} and $U(1)_{B-L}$ gauge fields. Each fermion in **16** of $SO(10)$ corresponds to quarks and leptons. Scalar fields in **10**, **16**, and $\overline{\mathbf{126}}$ of $SO(10)$

	Ψ_{16}					
$SO(10)$	**16**					
	$\psi_{(\mathbf{4},\mathbf{2},\mathbf{1})}$		$\psi_{(\overline{\mathbf{4}},\mathbf{1},\mathbf{2})}$			
G_{PS}	$(\mathbf{4},\mathbf{2},\mathbf{1})$		$(\overline{\mathbf{4}},\mathbf{1},\mathbf{2})$			
	Q_L	L	u_R^C	d_R^C	e_R^C	ν_R^C
$SU(3)_C$	**3**	**1**	$\overline{\mathbf{3}}$	$\overline{\mathbf{3}}$	**1**	**1**
$SU(2)_L$	**2**	**2**	**1**	**1**	**1**	**1**
$U(1)_Y$	$+1/6$	$-1/2$	$-2/3$	$+1/3$	$+1$	0
$U(1)_{B-L}$	$+1/3$	-1	$-1/3$	$-1/3$	$+1$	$+1$

Table 3.2: The content of the fermions in the $SO(10)$ model is shown in the $G_{\mathrm{PS}} = SU(4)_C \times SU(2)_L \times SU(2)_R$ basis, where the fermions belong to $(1/2, 0)$ under $SL(2,\mathbb{C})$. The $U(1)_{B-L}$ charge Q_{B-L} is given by $U(1)(\supset SU(4)/SU(3))$ [Yam15].

include the Higgs H, S and Φ, respectively. A scalar field in **210** of $SO(10)$ is responsible for breaking the $SO(10)$ symmetry to G_{PS}. The matter content in the $SO(10)$ model is summarized in Table 3.1.[1]

The Lagrangian is given by

$$\mathcal{L} = \sum_{\mathbf{y}=\mathbf{10},\mathbf{16},\overline{\mathbf{126}}} (\mathsf{D}_\mu \Phi_{\mathbf{y}})^\dagger (\mathsf{D}^\mu \Phi_{\mathbf{y}}) + \frac{1}{2}\,{}^{\mathrm{t}}(\mathsf{D}_\mu \Phi_{\mathbf{210}})(\mathsf{D}^\mu \Phi_{\mathbf{210}}) + \sum_{a=1}^{3} \overline{\Psi_{\mathbf{16}}^{(a)}} i \slashed{\mathsf{D}} \Psi_{\mathbf{16}}^{(a)} - \frac{1}{2}\,\mathrm{tr}[\mathsf{F}_{\mu\nu}\mathsf{F}^{\mu\nu}]$$

$$- \left(\sum_{\mathbf{y}=\mathbf{10},\overline{\mathbf{126}}} \sum_{a,b} \mathsf{y}_{\mathbf{y}}^{(ab)} \Phi_{\overline{\mathbf{y}}} \left(\Psi_{\mathbf{16}}^{(a)} \Psi_{\mathbf{16}}^{(b)} \right)_{\mathbf{y}} + \mathrm{h.c.} \right) - V(\{\Phi_{\mathbf{x}}\}) \tag{3.2.1}$$

where $\mathsf{D}_\mu := \partial_\mu + i\mathsf{g}\mathsf{A}_\mu$, $\mathsf{F}_{\mu\nu} = \partial_\mu \mathsf{A}_\mu - \partial_\nu \mathsf{A}_\nu + i\mathsf{g}[\mathsf{A}_\mu, \mathsf{A}_\nu]$. The scalar potential $V(\{\Phi_{\mathbf{x}}\})$ contains quadratic, cubic, and quartic coupling terms, where $\mathbf{x} = \mathbf{10}, \mathbf{16}, \overline{\mathbf{126}}, \mathbf{210}$.

We consider the following symmetry breaking patterns of $SO(10)$ broken to G_{PS} at the unification scale M_U by the non-vanishing VEV of the scalar field in **210** in $SO(10)$, further to G_{SM} at the intermediate scale M_I by the VEV of the scalar field in $\overline{\mathbf{126}}$ in $SO(10)$, where the M_U and M_I will be determined by gauge coupling unification using the renormalization group equations (RGEs) for the gauge coupling constants in the next section.

$$SO(10) \xrightarrow{\langle\Phi_{\mathbf{210}}\rangle\neq 0} G_{\mathrm{PS}} (\supset G_{\mathrm{SM}} \times U(1)_{B-L}) \xrightarrow{\langle\Phi_{\overline{\mathbf{126}}}\rangle\neq 0} G_{\mathrm{SM}} \xrightarrow{\langle\Phi_{\mathbf{10}}\rangle\neq 0} SU(3)_C \times U(1)_{\mathrm{EM}},$$

$$\tag{3.2.2}$$

where the dominant contribution for the symmetry breaking from the VEVs are shown. The type of symmetry breaking has been already discussed in e.g., Refs. [FM75, AM83,

---

[1]In this paper, we introduced a scalar in **10** of $SO(10)$ as a complex scalar. To reproduce the observed mass spectra of quarks and leptons, it is discussed in e.g., Ref. [BMSV06] that only the real scalar in **10** of $SO(10)$ has some tensions.

	$\Phi_{\mathbf{10}}$	$\Phi_{\mathbf{16}}$	$\Phi_{\overline{\mathbf{126}}}$
$SO(10)$	$\mathbf{10}$	$\mathbf{16}$	$\overline{\mathbf{126}}$
	$\phi_{(\mathbf{1,2,2})}$	$\phi_{(\overline{\mathbf{4}},\mathbf{1,2})}$	$\phi'_{(\overline{\mathbf{10}},\mathbf{1,3})}$
G_{PS}	$(\mathbf{1,2,2})$	$(\overline{\mathbf{4}},\mathbf{1,2})$	$(\overline{\mathbf{10}},\mathbf{1,3})$
	H	S	Φ
$SU(3)_C$	$\mathbf{1}$	$\mathbf{1}$	$\mathbf{1}$
$SU(2)_L$	$\mathbf{2}$	$\mathbf{1}$	$\mathbf{1}$
$U(1)_Y$	$+1/2$	0	0
$U(1)_{B-L}$	0	$+1$	$+2$

Table 3.3: The content of scalar fields in the $SO(10)$ model is shown, where the scalars belong to $(0,0)$ under $SL(2,\mathbb{C})$; $\Phi_{\mathbf{10}}$, $\Phi_{\mathbf{16}}$ and $\Phi_{\overline{\mathbf{126}}}$ are complex scalar fields. Here we assume all unlisted components of G_{PS} have $\mathcal{O}(M_U)$ masses adn also all unlisted components of $G_{\mathrm{SM}} \times U(1)_{B-L}$ have $\mathcal{O}(M_I)$ and $\mathcal{O}(M_U)$ masses, respectively. Other information is the same as in Table 3.2.

	A$_\mu$		
$SO(10)$	$\mathbf{45}$		
	G'_μ	W_μ	W'_μ
G_{PS}	$(\mathbf{15,1,1})$	$(\mathbf{1,3,1})$	$(\mathbf{1,1,3})$
	G_μ	C_μ	W_μ	Z'_μ
$SU(3)_C$	$\mathbf{8}$	$\mathbf{1}$	$\mathbf{1}$	$\mathbf{1}$
$SU(2)_L$	$\mathbf{1}$	$\mathbf{1}$	$\mathbf{3}$	$\mathbf{1}$
$U(1)_Y$	0	0	0	0
$U(1)_{B-L}$	0	0	0	0

Table 3.4: The content of gauge fields in the $SO(10)$ model is shown, where the gauge fields belong to $(1/2, 1/2)$ under $SL(2,\mathbb{C})$; Other information is the same as in Tables 3.2 and 3.3.

BM93, ABM$^+$04, BMSV06, FIK$^+$05, BDLM09, AM13, Fuk13, MNO$^+$15, EGKO18, FHHT19, CMK19, CPS20]. The field content of fermion, scalar, and gauge bosons are shown in Tables 3.2, 3.3, and 3.4. (The potential analysis of $\mathbf{210}$ in $SO(10)$ has already discussed in e.g., Ref. [CK86]; $SO(10)$ is broken to G_{PS} for appropriate parameter sets.)

3.2.1 Scalar sector

Here we focus on the scalar potential of SM Higgs and pNGB relevant part that contains scalar fields H, S, Φ belonging to $\mathbf{10}$, $\mathbf{16}$, and $\overline{\mathbf{126}}$ of $SO(10)$, respectively.

We assume that the other components of $\Phi_{\mathbf{10}}$, $\Phi_{\mathbf{16}}$ and $\Phi_{\overline{\mathbf{126}}}$ shown in Table 3.3 have the intermediate scale or larger masses and they do not contribute $SU(2)_L \times U(1)_Y$ and $U(1)_{B-L}$ breakings.

From the scalar potential $V(\{\Phi_{\mathbf{x}}\})$ in Eq. (3.2.1), we extract the terms that contain only H, S, Φ:

$$V(H, S, \Phi) = -\frac{\mu_H^2}{2}|H|^2 - \frac{\mu_S^2}{2}|S|^2 - \frac{\mu_\Phi^2}{2}|\Phi|^2 + \frac{\lambda_H}{2}|H|^4 + \frac{\lambda_S}{2}|S|^4 + \frac{\lambda_\Phi}{2}|\Phi|^4$$
$$+ \lambda_{HS}|H|^2|S|^2 + \lambda_{H\Phi}|H|^2|\Phi|^2 + \lambda_{S\Phi}|S|^2|\Phi|^2 - \left(\frac{\mu_c}{\sqrt{2}}\Phi^*S^2 + \text{c.c.}\right). \quad (3.2.3)$$

The quadratic terms $|H|^2$, $|S|^2$, and $|\Phi|^2$ come from $(\Phi_{\mathbf{10}}\Phi_{\mathbf{10}})_{\mathbf{1}}$, $(\Phi_{\mathbf{16}}\Phi_{\mathbf{16}}^*)_{\mathbf{1}}$, and $(\Phi_{\overline{\mathbf{126}}}\Phi_{\overline{\mathbf{126}}}^*)_{\mathbf{1}}$, respectively; the quartic terms $|H|^4$, $|S|^4$, and $|\Phi|^4$ come from $((\Phi_{\mathbf{10}}\Phi_{\mathbf{10}})_{\mathbf{1}})^2$ and $|(\Phi_{\mathbf{10}}\Phi_{\mathbf{10}})_{\mathbf{54}}|^2$ $|(\Phi_{\mathbf{16}}\Phi_{\mathbf{16}})_{\overline{\mathbf{126}}}|^2$, and $|(\Phi_{\overline{\mathbf{126}}}\Phi_{\overline{\mathbf{126}}})_{\overline{\mathbf{2772}}}|^2$, respectively; the quartic terms $|H|^2|S|^2$, $|H|^2|\Phi|^2$, and $|S|^2|\Phi|^2$ come from $(\Phi_{\mathbf{10}}\Phi_{\mathbf{10}})_{\mathbf{1}}(\Phi_{\mathbf{16}}\Phi_{\mathbf{16}}^*)_{\mathbf{1}}$, $(\Phi_{\mathbf{10}}\Phi_{\mathbf{10}})_{\mathbf{1}}(\Phi_{\overline{\mathbf{126}}}\Phi_{\overline{\mathbf{126}}}^*)_{\mathbf{1}}$, and $(\Phi_{\mathbf{16}}\Phi_{\mathbf{16}}^*)_{\mathbf{1}}(\Phi_{\overline{\mathbf{126}}}\Phi_{\overline{\mathbf{126}}}^*)_{\mathbf{1}}$, respectively; the cubic term Φ^*S^2 comes from $\Phi_{\overline{\mathbf{126}}}^*(\Phi_{\mathbf{16}}\Phi_{\mathbf{16}})_{\overline{\mathbf{126}}}$, [2] where the above sub-script such as $\mathbf{1}$ and $\mathbf{54}$ stands for the product representation of $SO(10)$. This potential is exactly the same as that in Refs. [ATT20, ORS21]. See Appendix 3.A for details.

We assume that the scalar fields H, S, and Φ develop the VEVs, which are parameterized by

$$H = \begin{pmatrix} 0 \\ \frac{v+h}{\sqrt{2}} \end{pmatrix}, \qquad S = \frac{v_s + s + i\eta_s}{\sqrt{2}}, \qquad \Phi = \frac{v_\phi + \phi + i\eta_\phi}{\sqrt{2}}, \qquad (3.2.4)$$

where h, s, and ϕ are CP-even modes, η_s and η_ϕ are CP-odd modes, and v, v_s, and v_ϕ are the VEVs of H, S, and Φ, respectively. The CP phase of the cubic term Φ^*S^2 is eliminated by the field redefinition of Φ. In the limit $\mu_c \to 0$, there are two independent global $U(1)$ symmetries associated with the phase rotation of S and Φ. For $\mu_c \neq 0$, the $U(1)$ symmetries are merged to the $U(1)_{B-L}$ (or $U(1)_X$) symmetry. Once $U(1)_{B-L}$ is broken, one of two CP-odd modes is absorbed by the $U(1)_{B-L}$ gauge field denoted as C_μ, while the other appears as a physical pNGB whose mass is proportional to μ_c.

The scalar fields H, S, Φ have five modes; three of them are CP-even scalar modes and the other two are CP-odd modes. The mass matrix for the CP-even scalars in the (h, s, ϕ) basis is given by

$$M_{\text{even}}^2 = \begin{pmatrix} \lambda_H v^2 & \lambda_{HS}vv_s & \lambda_{H\Phi}vv_\phi \\ \lambda_{HS}vv_s & \lambda_S v_s^2 & \lambda_{S\Phi}v_s v_\phi - \mu_c v_s \\ \lambda_{H\Phi}vv_\phi & \lambda_{S\Phi}v_s v_\phi - \mu_c v_s & \lambda_\Phi v_\phi^2 + \frac{\mu_c v_s^2}{2v_\phi} \end{pmatrix}. \qquad (3.2.5)$$

---

[2] When we take into account the nonvanishing VEV of $\Phi_{\mathbf{210}}$, quadratic terms $|H|^2$, $|S|^2$, and $|\Phi|^2$ and the cubic term Φ^*S^2 also come from $(\Phi_{\mathbf{10}}\Phi_{\mathbf{10}})_{\mathbf{1}}(\Phi_{\mathbf{210}}\Phi_{\mathbf{210}})_{\mathbf{1}}$, $(\Phi_{\mathbf{16}}\Phi_{\mathbf{16}}^*)_{\mathbf{1}}(\Phi_{\mathbf{210}}\Phi_{\mathbf{210}})_{\mathbf{1}}$, $(\Phi_{\overline{\mathbf{126}}}\Phi_{\overline{\mathbf{126}}}^*)_{\mathbf{1}}(\Phi_{\mathbf{210}}\Phi_{\mathbf{210}})_{\mathbf{1}}$, $\Phi_{\mathbf{16}}\Phi_{\mathbf{16}}\Phi_{\overline{\mathbf{126}}}\Phi_{\mathbf{210}}$, respectively. Therefore, each coefficient such as μ_c in Eq. (3.2.3) should be regarded as the total value including all the corresponding terms such as $\Phi_{\mathbf{16}}\Phi_{\mathbf{16}}\Phi_{\overline{\mathbf{126}}}$ and $\Phi_{\mathbf{16}}\Phi_{\mathbf{16}}\Phi_{\overline{\mathbf{126}}}\Phi_{\mathbf{210}}$.

Since the matrix is real and symmetric, it can be diagonalized by a real orthogonal matrix. As discussed in Chapter 2, the gauge eigenstates (h, s, ϕ) are related with the mass eigenstates (h_1, h_2, h_3) as

$$\begin{pmatrix} h \\ s \\ \phi \end{pmatrix} = U_e \begin{pmatrix} h_1 \\ h_2 \\ h_3 \end{pmatrix}, \tag{3.2.6}$$

where the approximate form of the real orthogonal matrix and its mixing angle are given by

$$U_e \approx \begin{pmatrix} 1 & 0 & \frac{\lambda_{H\Phi}v}{\lambda_\Phi v_\phi} \\ 0 & 1 & \frac{\lambda_{S\Phi}v}{\lambda_\Phi v_\phi} \\ -\frac{\lambda_{H\Phi}v}{\lambda_\Phi v_\phi} & -\frac{\lambda_{S\Phi}v}{\lambda_\Phi v_\phi} & 1 \end{pmatrix} \begin{pmatrix} \cos\theta & \sin\theta & 0 \\ -\sin\theta & \cos\theta & 0 \\ 0 & 0 & 1 \end{pmatrix}, \tag{3.2.7}$$

$$\tan 2\theta \approx \frac{2vv_s(\lambda_{HS}\lambda_\Phi - \lambda_{H\Phi}\lambda_{S\Phi})}{v^2(\lambda_{H\Phi}^2 - \lambda_H\lambda_\Phi) - v_s^2(\lambda_{S\Phi}^2 - \lambda_S\lambda_\Phi)}. \tag{3.2.8}$$

The masses of (h_1, h_2, h_3) are given by

$$m_{h_1}^2 \approx \lambda_H v^2 - \frac{\lambda_{H\Phi}^2\lambda_S - 2\lambda_{HS}\lambda_{H\Phi}\lambda_{S\Phi} + \lambda_\Phi\lambda_{HS}^2}{\lambda_S\lambda_\Phi - \lambda_{S\Phi}^2}v^2, \tag{3.2.9}$$

$$m_{h_2}^2 \approx \frac{\lambda_S\lambda_\Phi - \lambda_{S\Phi}^2}{\lambda_\Phi}v_s^2 + \frac{(\lambda_\Phi\lambda_{HS} - \lambda_{H\Phi}\lambda_{S\Phi})^2}{\lambda_\Phi(\lambda_S\lambda_\Phi - \lambda_{S\Phi}^2)}v^2, \tag{3.2.10}$$

$$m_{h_3}^2 \approx \lambda_\Phi v_\phi^2. \tag{3.2.11}$$

The mass eigenstate h_1 is identified as the SM-like Higgs boson with the mass $m_{h_1} \approx 125\,\text{GeV}$, h_2 is a light CP-even scalar, and h_3 is a heavy CP-even scalar.

The mass matrix of the CP-odd scalars in the gauge eigenstates (η_s, η_ϕ) is given by

$$M_{\text{odd}}^2 = \frac{\mu_c}{2v_\phi} \begin{pmatrix} 4v_\phi^2 & -2v_s v_\phi \\ -2v_s v_\phi & v_s^2 \end{pmatrix}. \tag{3.2.12}$$

The gauge eigenstates (η_s, η_ϕ) are related with the mass eigenstates $(\chi, \tilde{\chi})$ as

$$\begin{pmatrix} \eta_s \\ \eta_\phi \end{pmatrix} = U_o \begin{pmatrix} \chi \\ \tilde{\chi} \end{pmatrix}, \tag{3.2.13}$$

where the real orthogonal matrix is given by

$$U_o = \frac{1}{\sqrt{v_s^2 + 4v_\phi^2}} \begin{pmatrix} 2v_\phi & v_s \\ -v_s & 2v_\phi \end{pmatrix}. \tag{3.2.14}$$

By using the 2×2 real orthogonal matrix U_o, the mass eigenvalues of $(\chi, \tilde{\chi})$ are given by

$$m_\chi^2 = \frac{(v_s^2 + 4v_\phi^2)\mu_c}{4v_\phi}, \tag{3.2.15}$$

$$m_{\tilde{\chi}}^2 = 0. \tag{3.2.16}$$

The $\tilde{\chi}$ is the NGB absorbed by the $U(1)_{B-L}$ gauge boson C_μ, and χ is the pNGB identified as dark matter in the paper.

3.2.2 Gauge sector

The gauge kinetic term of the $SO(10)$ can be canonically normalized at the unification scale M_U as in Eq. (3.2.1). In general, the kinetic-mixing term of multiple $U(1)$ symmetries are allowed for the case of at least two abelian groups because a field strength itself is gauge-invariant for abelian groups, while that is not gauge-invariant for non-abelian groups. So, in the energy scale $M_I < \mu < M_U$, there is the gauge kinetic mixing of G_{PS}. At the scale $\mu = M_I$, there are two $U(1)$s, i.e. $U(1)_Y$ and $U(1)_{B-L}$ although one of the $U(1)$s, which is the $U(1)_{B-L}$, is broken at the scale. It is generated by threshold corrections or via RGE flows. In $SO(10)$ models, $SO(10)/(SU(3)_C \times SU(2)_L)$ contains $U(1)_Y$ and $U(1)_{B-L}$ as two independent $U(1)$s, while they are not orthogonal. In fact, $U(1)_Y$ is orthogonal to $U(1)_X (\subset SO(10)/SU(5))$; $U(1)_{B-L}$ is orthogonal to $U(1)_R (\subset SU(2)_R)$. Therefore, it is expected that the kinetic mixing parameter between $U(1)_Y$ and $U(1)_{B-L}$ denoted as ϵ is non-zero at classical level.

To determine the value of the kinetic mixing parameter between $U(1)_Y$ and $U(1)_{B-L}$, we focus on the kinetic terms of the gauge fields. First, from Eq. (3.2.1), the gauge kinetic term of $SO(10)$ is given by

$$\mathcal{L}_{\text{gauge}} = -\frac{1}{2}\,\text{tr}\left[\mathsf{F}_{\mu\nu}\mathsf{F}^{\mu\nu}\right]. \tag{3.2.17}$$

Next, the gauge kinetic terms of G_{PS} are given by

$$\mathcal{L}_{\text{gauge}} \ni -\frac{1}{2}\text{tr}\left[G'_{\mu\nu}G'^{\mu\nu}\right] - \frac{1}{4}W^a_{\mu\nu}W^{a\mu\nu} - \frac{1}{4}W'^a_{\mu\nu}W'^{a\mu\nu}, \tag{3.2.18}$$

where $G'_{\mu\nu}$, $W^a_{\mu\nu}$, and $W'^a_{\mu\nu}$ stand for the field strengths of $SU(4)_C$, $SU(2)_L$, and $SU(2)_R$, respectively; the gauge kinetic terms and mass terms of $SO(10)/G_{\mathrm{PS}}$ are omitted at M_U. The gauge coupling constants are running from M_U to M_I. Third, the $SU(3)_C \times SU(2)_L \times U(1)_R \times U(1)_{B-L}$ are given by

$$\mathcal{L}_{\text{gauge}} \ni -\frac{1}{2}\,\text{tr}\left[G_{\mu\nu}G^{\mu\nu}\right] - \frac{1}{4}W^a_{\mu\nu}W^{a\mu\nu} - \frac{1}{4}B'_{\mu\nu}B'^{\mu\nu} - \frac{1}{4}C'_{\mu\nu}C'^{\mu\nu}, \tag{3.2.19}$$

where $G_{\mu\nu}$, $B'_{\mu\nu}$ and $C'_{\mu\nu}$ stand for the field strength of $SU(3)_C (\subset SU(4)_C)$, $U(1)_R (\subset SU(2)_R)$, and $U(1)_{B-L} (\subset SU(4)_C/SU(3)_C)$, respectively; the gauge kinetic terms and mass terms of $SU(4)_C/(SU(3)_C \times U(1)_{B-L})$ and $SU(2)_R/U(1)_R$ are omitted at M_I. Further, by using the following $GL(2, \mathbb{R})$ transformation

$$\begin{matrix} U(1)_Y \\ U(1)_{B-L} \end{matrix} : \begin{pmatrix} B_\mu \\ C_\mu \end{pmatrix} = \begin{pmatrix} 1 & -\tan\epsilon \\ 0 & \frac{1}{\cos\epsilon} \end{pmatrix} \begin{pmatrix} B'_\mu \\ C'_\mu \end{pmatrix} =: U_{GK} \begin{pmatrix} B'_\mu \\ C'_\mu \end{pmatrix} : \begin{matrix} U(1)_R \\ U(1)_{B-L} \end{matrix}, \tag{3.2.20}$$

we can change the basis of $U(1)$s from $U(1)_R \times U(1)_{B-L}$ to $U(1)_Y \times U(1)_{B-L}$;

$$-\frac{1}{4}B'_{\mu\nu}B'^{\mu\nu} - \frac{1}{4}C'_{\mu\nu}C'^{\mu\nu} = -\frac{1}{4}B_{\mu\nu}B^{\mu\nu} - \frac{1}{4}C_{\mu\nu}C^{\mu\nu} - \frac{\sin\epsilon}{2}C_{\mu\nu}B^{\mu\nu}, \tag{3.2.21}$$

where $B_{\mu\nu}$ and $C_{\mu\nu}$ stand for the field strength of $U(1)_Y$ and $U(1)_{B-L}$, respectively; ϵ is the kinetic mixing parameter between $U(1)_Y$ and $U(1)_{B-L}$. In the case, since the $U(1)_Y$ generator is given by the following linear combination of $U(1)_R$ and $U(1)_{B-L}$

$$I_Y = \sqrt{\frac{3}{5}} I_{3R} + \sqrt{\frac{2}{5}} I_{B-L}. \tag{3.2.22}$$

Due to the orthogonality, the kinetic mixing parameter ϵ at $\mu = M_I$ is given by

$$\epsilon = -\tan^{-1} \sqrt{\frac{2}{3}}. \tag{3.2.23}$$

The Lagrangian for the electro-magnetic neutral part of the $SU(2)_L \times U(1)_Y \times U(1)_{B-L}$ gauge fields including mass terms generated by the VEVs of the spontaneous $SU(2)_L \times U(1)_Y$ and $U(1)_{B-L}$ breaking scalar fields is given by

$$\begin{aligned}
\mathcal{L} = &-\frac{1}{4} B_{\mu\nu} B^{\mu\nu} - \frac{1}{4} W^3_{\mu\nu} W^{3\mu\nu} + \frac{1}{2} m^2_{\tilde{Z}} Z_\mu Z^\mu \\
&-\frac{1}{4} C_{\mu\nu} C^{\mu\nu} + \frac{1}{2} m^2_C C_\mu C^\mu - \frac{\sin\epsilon}{2} C_{\mu\nu} B^{\mu\nu},
\end{aligned} \tag{3.2.24}$$

where $Z_\mu = \cos\theta_W W^3_\mu - \sin\theta_W B_\mu$ is the usual Z boson, θ_W is the Weinberg angle $\tan\theta_W := g_1/g_2$; g_1 and g_2 stand for the $U(1)_Y$ and $SU(2)_L$ coupling constants, respectively. The mass parameters are given by

$$m^2_{\tilde{Z}} = \frac{g^2_1 + g^2_2}{4} v^2, \quad m^2_C = g^2_{B-L}(v^2_s + 4v^2_\phi), \tag{3.2.25}$$

where g_{B-L} is the gauge coupling constant of $U(1)_{B-L}$.

To discuss the physical implications of $U(1)_{B-L}$ gauge boson, we requires both diagonalizing the field strength terms and the mass terms. The following discussion is done in the same manner as Section 2.A. First, we diagonalize the kinetic term in Eq. (3.2.24) by using the following $GL(2, \mathbb{R})$ transformation:

$$\begin{array}{cc}
U(1)_Y \\
U(1)_{B-L}
\end{array} : \begin{pmatrix} B_\mu \\ C_\mu \end{pmatrix} = \begin{pmatrix} 1 & -\tan\epsilon \\ 0 & \frac{1}{\cos\epsilon} \end{pmatrix} \begin{pmatrix} \hat{B}_\mu \\ \hat{C}_\mu \end{pmatrix} = U_{GK} \begin{pmatrix} \hat{B}_\mu \\ \hat{C}_\mu \end{pmatrix}, \tag{3.2.26}$$

where $\hat{B}_\mu$ and $\hat{C}_\mu$ stand for the gauge fields of the $U(1)_Y$ and "$U(1)_{B-L}$" in the physical basis. The transformation is exactly the same as that in Eq. (3.2.20). That is, "$U(1)_{B-L}$" can be identified as $U(1)_X (\subset SO(10)/SU(5))$. Then, the gauge kinetic terms in Eq. (3.2.24) become

$$\mathcal{L}_{\text{GK}} = -\frac{1}{4} \hat{B}_{\mu\nu} \hat{B}^{\mu\nu} - \frac{1}{4} \hat{W}^3_{\mu\nu} \hat{W}^{3\mu\nu} - \frac{1}{4} \hat{C}_{\mu\nu} \hat{C}^{\mu\nu}. \tag{3.2.27}$$

Next, we consider the physical eigenstate via an $O(3)$ rotation by diagonalizing the mass terms that arise after both $U(1)_{B-L}$ and $SU(2)_L \times U(1)_Y$ breaking. One mass eigenstate

is massless corresponding to the photon A_μ, while the other two denoted Z and Z' receive masses. The mass terms of the neutral gauge boson in terms of (B_μ, W_μ^3, C_μ) is given by

$$
\mathcal{L}_{\text{mass}} = \frac{1}{2} \begin{pmatrix} B_\mu & W_\mu^3 & C_\mu \end{pmatrix} \begin{pmatrix} \sin^2 \theta_W m_{\tilde{Z}}^2 & -\sin \theta_W \cos \theta_W m_{\tilde{Z}}^2 & 0 \\ -\sin \theta_W \cos \theta_W m_{\tilde{Z}}^2 & \cos^2 \theta_W m_{\tilde{Z}}^2 & 0 \\ 0 & 0 & M_C^2 \end{pmatrix} \begin{pmatrix} B^\mu \\ W^{3\mu} \\ C^\mu \end{pmatrix}.
$$

(3.2.28)

By using $GL(2, \mathbb{R})$ transformation in Eq. (3.2.26), we change the basis whose kinetic term is diagonalized as below:

$$
\mathcal{L}_{\text{mass}} = \frac{1}{2} \begin{pmatrix} \hat{B}_\mu & W_\mu^3 & \hat{C}_\mu \end{pmatrix} {}^t\tilde{U}_{GK} \begin{pmatrix} \sin^2 \theta_W m_{\tilde{Z}}^2 & -\sin \theta_W \cos \theta_W m_{\tilde{Z}}^2 & 0 \\ -\sin \theta_W \cos \theta_W m_{\tilde{Z}}^2 & \cos^2 \theta_W m_{\tilde{Z}}^2 & 0 \\ 0 & 0 & M_C^2 \end{pmatrix}
$$
$$
\times \tilde{U}_{GK} \begin{pmatrix} \hat{B}^\mu \\ W^{3\mu} \\ \hat{C}^\mu \end{pmatrix},
$$

(3.2.29)

where

$$
\tilde{U}_{GK} := \begin{pmatrix} 1 & 0 & -\tan \epsilon \\ 0 & 1 & 0 \\ 0 & 0 & \frac{1}{\cos \epsilon} \end{pmatrix}.
$$

(3.2.30)

The above mass matrix is a real symmetric matrix. In fact, it can be diagonalized by using a real orthogonal matrix:

$$
U_G = \begin{pmatrix} \cos \theta_W & -\sin \theta_W & 0 \\ \sin \theta_W & \cos \theta_W & 0 \\ 0 & 0 & 1 \end{pmatrix} \begin{pmatrix} 1 & 0 & 0 \\ 0 & \cos \zeta & -\sin \zeta \\ 0 & \sin \zeta & \cos \zeta \end{pmatrix},
$$

(3.2.31)

where the mixing angle ζ is given by

$$
\tan 2\zeta = \frac{-2m_{\tilde{Z}}^2 \sin \theta_W \sin \epsilon \cos \epsilon}{m_C^2 - m_{\tilde{Z}}^2 (\cos^2 \epsilon - \sin^2 \theta_W \sin^2 \epsilon)}.
$$

(3.2.32)

From the above, we find the masses of A_μ, Z_μ, and Z'_μ as

$$
m_A^2 = 0,
$$

(3.2.33)

$$
m_Z^2 = \frac{1}{2} \left[\overline{M}^2 - \sqrt{\overline{M}^4 - \frac{4m_{\tilde{Z}}^2 m_C^2}{\cos^2 \epsilon}} \right],
$$

(3.2.34)

$$
m_{Z'}^2 = \frac{1}{2} \left[\overline{M}^2 + \sqrt{\overline{M}^4 - \frac{4m_{\tilde{Z}}^2 m_C^2}{\cos^2 \epsilon}} \right],
$$

(3.2.35)

where $\overline{M}^2$ is given by

$$\overline{M}^2 := m_Z^2 \left(1 + \sin\theta_W \tan^2\epsilon\right) + \frac{m_C^2}{\cos^2\epsilon}. \tag{3.2.36}$$

In this section, we find that the gauge kinetic mixing ϵ in Refs. [ATT20, ORS21] is regarded as the mixing angle. In Appendix 3.B, we will show this more explicitly.

3.3 Gauge coupling constants

To determine such as the $U(1)_{B-L}$ breaking scale, i.e., intermediate scale M_I, and magnitude of the gauge coupling constant of the $U(1)_{B-L}$, we discuss the RGEs for gauge coupling constants running among the electroweak scale m_Z, the intermediate scale M_I, and the unification scale M_U.

The RGE for the gauge coupling constant $\alpha_i(\mu) := g_i^2(\mu)/4\pi$ at one-loop level is given in e.g., Refs. [Sla81, Yam15] by

$$\frac{d}{d\log(\mu)}\alpha_i^{-1}(\mu) = -\frac{b_i}{2\pi}, \tag{3.3.1}$$

where i stands for a gauge group G; e.g., $4C$ stands for the gauge coupling constant of $SU(4)_C$, and the beta function coefficient is given by

$$b_i = -\frac{11}{3}\sum_{\text{Vector}} T(R_V) + \frac{2}{3}\sum_{\text{Weyl}} T(R_F) + \frac{1}{6}\sum_{\text{Real}} T(R_S), \tag{3.3.2}$$

where Vector, Weyl, and Real stand for real vector, Weyl fermion, and real scalar fields, respectively. Since the vector bosons are gauge bosons, they belong to the adjoint representation of the Lie group G: $T(R_V) = C_2(G)$. $C_2(G)$ is the quadratic Casimir invariant of the adjoint representation of G, and $T(R_i)$ is a Dynkin index of the irreducible representation R_i of G. Note that when the Lie group G is spontaneously broken into its Lie subgroup G', it is convenient to use the irreducible representations of G'. (For the Dynkin index and the branching rules, see e.g., Refs. [Yam15, MP81] or calculated by using appropriate computer programs such as Susyno [Fon12], LieART [FK15, FKS20], and GroupMath [Fon21]. For the RGEs at the two-loop level, see, e.g., Refs. [MV83, MV84, MV85].)

Let us consider the RGEs for gauge coupling constants in the pNGB dark matter model shown in Tables 3.2, 3.3, and 3.4. For the energy scale between $M_Z < \mu < M_I$ and $M_I < \mu < M_U$, we use the RGEs for the gauge coupling constants of G_{SM} and G_{PS}, respectively. In the following calculation, we assume that there is only one intermediate scale M_I and one unification scale M_U, which should be recognized as effective scales.

We can obtain the beta function coefficients of the gauge coupling constants of G_{SM} and G_{PS} by using the generic RGE in Eq. (3.3.2) and the matter content of the model

given in Tables 3.2, 3.3, and 3.4. The beta function coefficients of $G_{\rm SM}$ in $M_Z < \mu < M_I$ are given by

$$\begin{pmatrix} b_{3C} \\ b_{2L} \\ b_{1Y} \end{pmatrix} = \begin{pmatrix} -7 \\ -19/6 \\ +41/10 \end{pmatrix}, \tag{3.3.3}$$

where $i = 3C, 2L, 1Y$ stand for $SU(3)_C$, $SU(2)_L$, $U(1)_Y$, respectively, and we took the $SU(5)$ normalization for $U(1)_Y$. (The values of b_i are the same as the ordinary SM.) The beta function coefficients of $G_{\rm PS}$ in $M_I < \mu < M_U$ are given by

$$\begin{pmatrix} b_{4C} \\ b'_{2L} \\ b_{2R} \end{pmatrix} = \begin{pmatrix} -22/3 \\ -3 \\ +13/3 \end{pmatrix}, \tag{3.3.4}$$

where $i = 4C, 2L, 2R$ stand for $SU(4)_C$, $SU(2)_L$, $SU(2)_R$, respectively. To distinguish the beta function coefficient of the $SU(2)_L$ in $G_{\rm SM}$ and that in $G_{\rm PS}$, we use unprimed and primed, and the same notation is used below.

To solve the above RGEs, we need to set the initial conditions at $\mu = m_Z$. The gauge coupling constants must satisfy the matching conditions between $G_{\rm SM}$ and $G_{\rm PS}$ at $\mu = M_I$ and also the matching condition between $G_{\rm PS}$ and $SO(10)$ at $\mu = M_U$. They are listed below.

- The input parameters for the three SM gauge coupling constants at $\mu = m_Z = 91.1876 \pm 0.0021\,{\rm GeV}$ are given in Ref. [Z$^+$20]:

$$\alpha_{3C}(m_Z) = 0.1181 \pm 0.0011, \quad \alpha_{2L}(m_Z) = \frac{\alpha_{\rm EM}(M_Z)}{\sin^2\theta_W(m_Z)}, \quad \alpha_{1Y}(m_Z) = \frac{5\alpha_{\rm EM}(M_Z)}{3\cos^2\theta_W(m_Z)}, \tag{3.3.5}$$

where the experimental values of the EM gauge coupling constant $\alpha_{\rm EM}$ and the Weinberg angle are given as

$$\alpha_{\rm EM}^{-1}(M_Z) = 127.955 \pm 0.010, \quad \sin^2\theta_W(m_Z) = 0.23122 \pm 0.00003. \tag{3.3.6}$$

- The matching conditions between $G_{\rm SM}$ and $G_{\rm PS}$ at $\mu = M_I$ are given by

$$\alpha_{3C}(M_I) = \alpha_{4C}(M_I), \quad \alpha_{2L}(M_I) = \alpha'_{2L}(M_I), \quad \alpha_{1Y}^{-1}(M_I) = \frac{3}{5}\alpha_{2R}^{-1}(M_I) + \frac{2}{5}\alpha_{4C}^{-1}(M_I), \tag{3.3.7}$$

where they are determined by the normalization conditions of the generators of $G_{\rm PS}$ and $G_{\rm SM}$. (See e.g., Ref. [Moh02] at one-loop level; Refs. [DKP93a, DKP93b] at two-loop level.)

- The matching condition at the unification scale M_U is given by

$$\alpha_{4C}(M_U) = \alpha'_{2L}(M_U) = \alpha_{2R}(M_U). \tag{3.3.8}$$

By using the RGEs of G_{SM} and G_{PS} and the matching conditions at $\mu = M_I$ and M_U, we can obtain M_I and M_U as

$$M_I = m_Z \, \exp\left[\frac{A_1 B_3 - A_3 B_1}{A_2 B_3 - A_3 B_2}\right],$$

$$M_U = m_Z \, \exp\left[\left(\frac{A_1 B_3 - A_3 B_1}{A_2 B_3 - A_3 B_2}\right) + \left(\frac{A_1 B_2 - A_2 B_1}{A_3 B_2 - A_2 B_3}\right)\right], \tag{3.3.9}$$

where

$$A_1 = \alpha_{3C}^{-1}(m_Z) - \alpha_{2L}^{-1}(m_Z), \quad A_2 = \frac{b_{3C} - b_{2L}}{2\pi}, \quad A_3 = \frac{b_{4C} - b'_{2L}}{2\pi},$$

$$B_1 = \frac{5}{3}\left(\alpha_{3C}^{-1}(m_Z) - \alpha_{1Y}^{-1}(m_Z)\right), \quad B_2 = \frac{5}{3}\frac{b_{3C} - b_{1Y}}{2\pi}, \quad B_3 = \frac{b_{4C} - b_{2R}}{2\pi}. \tag{3.3.10}$$

The gauge coupling constants such as $\alpha_{4C}(M_U)$ and $\alpha'_{2L}(M_U)$ are also expressed by the Z boson mass m_Z, the gauge coupling constants at $\mu = m_Z$ and the beta function coefficients of G_{SM} and G_{PS} b_is. (The detail analysis is given in Appendix 3.C.)

By substituting b_i in Eqs. (3.3.3) and (3.3.4) and the parameters at $\mu = m_Z$ in Eqs. (3.3.5) and (3.3.6) into the expressions of M_I and M_U in Eq. (3.3.9), we find the values of the M_I and M_U as

$$M_I = (1.261 \pm 0.242) \times 10^{11}\,\mathrm{GeV}, \quad M_U = (2.057 \pm 0.688) \times 10^{16}\,\mathrm{GeV}. \tag{3.3.11}$$

Note that we ignore such as mass splitting at the intermediate and unification scales, so the uncertainty must be larger. The values of the model parameters at $\mu = M_I$ are given by

$$\alpha_{4C}^{-1}(M_I) = 31.92 \pm 0.23, \quad \alpha'^{-1}_{2L}(M_I) = 40.19 \pm 0.10, \quad \alpha_{2R}^{-1}(M_I) = 54.20 \pm 0.26. \tag{3.3.12}$$

We also find the gauge coupling constants of $U(1)_{B-L}$ and $U(1)_R$ at $\mu = M_I$

$$g_{B-L}(M_I) = 0.3843 \pm 0.0009, \quad g_R(M_I) = 0.4815 \pm 0.0011, \tag{3.3.13}$$

by using $g_{B-L}(M_I) = \sqrt{\frac{3\pi}{2}\alpha_{4C}(M_I)}$ and $g_R(M_I) = \sqrt{4\pi\alpha_{2R}(M_I)}$. Since the standard normalization of $U(1)_{B-L}$ is not the same as that of "$U(1)_{B-L}$"($\subset SU(4)_C/SU(3)_C$), the modified normalization factor is used. The unified gauge coupling constants at $\mu = M_U$ is given by

$$\alpha_U^{-1} = 45.92 \pm 0.50. \tag{3.3.14}$$

The energy dependence of the gauge coupling constants $\alpha_i(\mu)$ in the $SO(10)$ pNGB model is plotted in Fig. 3.1.
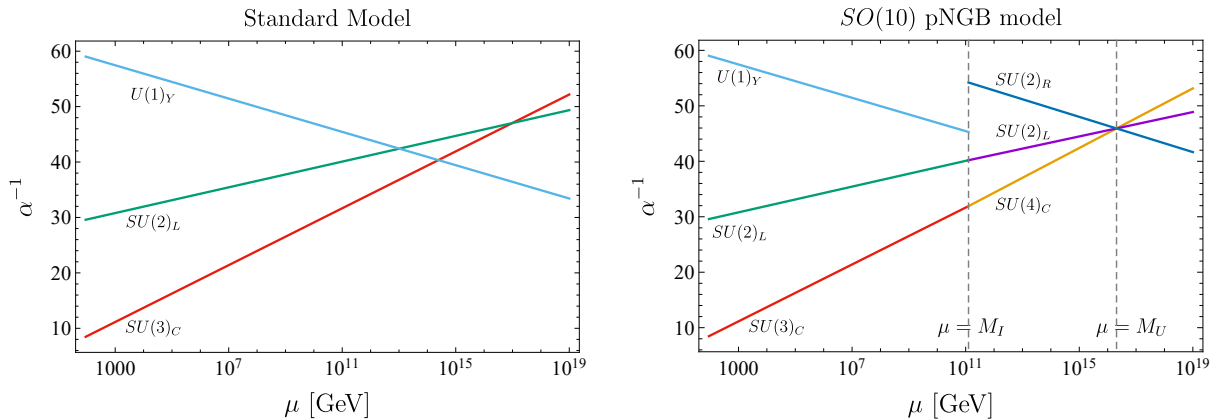
Figure 3.1: The gauge coupling constants α_i vs the energy scale μ for the SM (the left figure) and the $SO(10)$ pNGB model (the right figure) are shown [ATTY21]. The left figure shows the energy dependence of three gauge coupling constants of $SU(3)_C$, $SU(2)_L$, and $U(1)_Y$, α_{3C}, α_{2L}, and α_{1Y} in all the energy ranges $\mu = [m_Z, M_H]$, where $M_H = 10^{19}$ GeV. The right figure shows α_{3C}, α_{2L}, and α_{1Y} in the energy ranges $\mu = [m_Z, M_I]$; α_{4C}, α_{2L}, α_{2R} in the energy ranges $\mu = [M_I, M_H]$, where the value of α_{3C} is fixed as the central value $\alpha_{3C}(m_Z) = 0.1181$ [Z+20].

As the same as the usual GUT models, nucleon can decay via the so-called lepto-quark gauge bosons. The proton lifetime via the gauge bosons is roughly estimated as $\tau \approx M_U^4 / \alpha_U^2 m_p^5$ [NFP07, Moh02, Z+20], where m_p is the proton mass and the gauge boson masses are assumed to be M_U. From the values of M_U and α_U given in Eqs. (3.3.11) and (3.3.14), the proton lifetime $\tau \approx 1.1 \times 10^{37}$ years is predicted. It is far from the current constraint $\tau(p \to e^+\pi^0) > 2.4 \times 10^{34}$ years at 90% CL [T+20]; $M_U > (4.3 - 4.8) \times 10^{15}$ GeV for $40 \lesssim \alpha_U^{-1} \lesssim 50$. There is contribution for the proton decay modes via colored scalar fields shown in Table 3.3. The color triplet component of $\Phi_{\mathbf{10}}$ has assumed to have $\mathcal{O}(M_U)$, so the contribution for the proton decay via the Yukawa coupling constant $\mathsf{y}_{\mathbf{10}}^{(ab)}$ of the term $\Phi_{\mathbf{10}} \left(\Psi_{\mathbf{16}}^{(a)} \Psi_{\mathbf{16}}^{(b)} \right)_{\mathbf{10}}$ in Eq. (3.2.1) is small. Color non-singlet components of $\Phi_{\overline{\mathbf{126}}}$ have assumed to $\mathcal{O}(M_I)$, so the contribution for the proton decay via the Yukawa coupling constant $\mathsf{y}_{\overline{\mathbf{126}}}^{(ab)}$ of the term $\Phi_{\overline{\mathbf{126}}}^* \left(\Psi_{\mathbf{16}}^{(a)} \Psi_{\mathbf{16}}^{(b)} \right)_{\overline{\mathbf{126}}}$ in Eq. (3.2.1) can be larger than the current experimental bounds. This leads to an upper bound of the values of $\mathsf{y}_{\overline{\mathbf{126}}}^{(ab)}$ in the model.

We comment on proton decay via a colored Higgs scalar or lepto-quark scalar denoted as S_1 in Ref. [DFG+16], which belongs to $(\mathbf{3}, \mathbf{1}, 1/3)$ under G_{SM}. In the following, we omit Clebsch-Gordan coefficients for simplicity. When the lepto-quark scalar S_1 has di-quark and quark-lepton couplings, there are proton decay modes such as $p \to e^+\pi^0$, and the proton lifetime is roughly estimated as $\tau \approx m_{LQ}^4 / (|y|^2 |z|^2 m_p^5)$, where m_{LQ} is a lepto-quark mass, y and z represent generic values of relevant Yukawa coupling constants of the lepto-quark with the quark-lepton and quark-quark pairs, respectively. For example, for the lepto-quark with the intermediate scale mass $m_{LQ} = M_I$ and the universal Yukawa

Group G_I	Scalars at $\mu = M_I$	b_j	$\dfrac{\log_{10}(M/1[\text{GeV}])}{M_I \qquad M_U}$		α_U^{-1}
G_{PS}	$(\mathbf{1},\mathbf{2},\mathbf{2})_{\mathbf{10}}$ $(\overline{\mathbf{4}},\mathbf{1},\mathbf{2})_{\mathbf{16}}$ $(\overline{\mathbf{10}},\mathbf{1},\mathbf{3})_{\overline{\mathbf{126}}}$	$\begin{pmatrix} b_{4C} \\ b'_{2L} \\ b_{2R} \end{pmatrix} = \begin{pmatrix} -\frac{22}{3} \\ -3 \\ +\frac{13}{3} \end{pmatrix}$	11.10 ± 0.08	16.31 ± 0.15	45.92 ± 0.50
$G_{\mathrm{PS}} \times D$	$(\mathbf{1},\mathbf{2},\mathbf{2})_{\mathbf{10}}$ $(\mathbf{4},\mathbf{2},\mathbf{1})_{\mathbf{16}}$ $(\overline{\mathbf{4}},\mathbf{1},\mathbf{2})_{\mathbf{16}}$ $(\overline{\mathbf{10}},\mathbf{1},\mathbf{3})_{\overline{\mathbf{126}}}$ $(\mathbf{10},\mathbf{3},\mathbf{1})_{\overline{\mathbf{126}}}$	$\begin{pmatrix} b_{4C} \\ b'_{2L} \\ b_{2R} \end{pmatrix} = \begin{pmatrix} -4 \\ +\frac{13}{3} \\ +\frac{13}{3} \end{pmatrix}$	13.71 ± 0.03	15.22 ± 0.04	40.82 ± 0.13
G_{LR}	$(\mathbf{1},\mathbf{2},\mathbf{2},0)_{\mathbf{10}}$ $(\mathbf{1},\mathbf{1},\mathbf{2},1)_{\mathbf{16}}$ $(\mathbf{1},\mathbf{1},\mathbf{3},2)_{\overline{\mathbf{126}}}$	$\begin{pmatrix} b'_{3C} \\ b'_{2L} \\ b_{2R} \\ b_{B-L} \end{pmatrix} = \begin{pmatrix} -7 \\ -3 \\ -\frac{13}{6} \\ +\frac{23}{4} \end{pmatrix}$	8.57 ± 0.06	16.64 ± 0.13	46.13 ± 0.41
$G_{\mathrm{LR}} \times D$	$(\mathbf{1},\mathbf{2},\mathbf{2},0)_{\mathbf{10}}$ $(\mathbf{1},\mathbf{1},\mathbf{2},1)_{\mathbf{16}}$ $(\mathbf{1},\mathbf{2},\mathbf{1},1)_{\mathbf{16}}$ $(\mathbf{1},\mathbf{1},\mathbf{3},2)_{\overline{\mathbf{126}}}$ $(\mathbf{1},\mathbf{3},\mathbf{1},-2)_{\overline{\mathbf{126}}}$	$\begin{pmatrix} b'_{3C} \\ b'_{2L} \\ b_{2R} \\ b_{B-L} \end{pmatrix} = \begin{pmatrix} -7 \\ -\frac{13}{6} \\ -\frac{13}{6} \\ +\frac{15}{2} \end{pmatrix}$	10.11 ± 0.04	15.57 ± 0.09	43.38 ± 0.30

Table 3.5: The values of M_I, M_U, and α_U^{-1} for several matter contents and symmetry breaking patterns are summarized. The top of the table corresponds to the present $SO(10)$ pNGB model. The first, second, and third columns represent the intermediate scale group G_I, the matter content for scalar sector at $\mu = M_I$, the beta function coefficients b_j of G_I, respectively. The fourth and fifth columns show the values of M_I, M_U, and α_U^{-1}. The subscript in the second column stands for each $SO(10)$ representation.

coupling constants $|y| = |z|$, we obtain a constraint for the Yukawa coupling constants $|y| = |z| \lesssim 4.2 \times 10^{-6}$ from the current constraint $\tau(p \to e^+\pi^0) > 2.4 \times 10^{34}$ years at 90% CL. To apply this for the current model, for the scalar field S_1 in $\mathbf{10}$ of $SO(10)$, which belongs to $(\mathbf{6},\mathbf{1},\mathbf{1})$ under G_{PS}, the mass of the lepto-quark scalar is the unification scale mass $m_{LQ} = M_U$ and the Yukawa coupling constants are roughly expected as $|y| = |z| \approx |y_{\mathbf{10}}^{(11)}|$. The current constraint $\tau(p \to e^+\pi^0) > 2.4 \times 10^{34}$ years at 90% CL leads to $|y_{\mathbf{10}}^{(11)}| \lesssim 0.68$. To realize the mass of up quark, $y_{\mathbf{10}}^{(11)}$ is roughly $\mathcal{O}(10^{-5})$, so it is consistent with the current constraint, where the actual values of the Yukawa coupling constants depend on how to realized the observed quark and lepton masses. Next, for the scalar fields $S_{1(\overline{\mathbf{10}},\mathbf{1},\mathbf{3})}$ and $S_{1(\mathbf{1},\mathbf{1},\mathbf{3})}$ in $\overline{\mathbf{126}}$ of $SO(10)$, which belongs to $(\overline{\mathbf{10}},\mathbf{1},\mathbf{3})$ and $(\mathbf{6},\mathbf{1},\mathbf{1})$ under G_{PS}. The lepto-quark scalar $S_{1(\overline{\mathbf{10}},\mathbf{1},\mathbf{3})}$ and $S_{1(\mathbf{6},\mathbf{1},\mathbf{1})}$ have the intermediate scale mass M_I and the unification scale mass M_U, respectively. For $S_{1(\overline{\mathbf{10}},\mathbf{1},\mathbf{3})}$, the Yukawa coupling couplings are given by $|y| = 0$ and $|z| \approx |y_{\overline{\mathbf{126}}}|$, so the proton decay mediated by $S_{1(\overline{\mathbf{10}},\mathbf{1},\mathbf{3})}$ does not occur. Therefore, this does not lead to any constraint for $y_{\overline{\mathbf{126}}}^{(ab)}$. For $S_{1(\mathbf{6},\mathbf{1},\mathbf{1})}$, the Yukawa coupling couplings are given by $|y| = |z| \approx |y_{\overline{\mathbf{126}}}|$. the current constraint $\tau(p \to e^+\pi^0) > 2.4 \times 10^{34}$ years at 90% CL leads to $|y_{\overline{\mathbf{126}}}^{(11)}| \lesssim 0.68$ as the same as S_1 in

10 of $SO(10)$. In the above discussion, we assumed $S_{1(\overline{\mathbf{10}},\mathbf{1},\mathbf{3})}$ does not mix with $S_{1(\mathbf{6},\mathbf{1},\mathbf{1})}$, but they have the same quantum numbers, so it depends on the structure of the scalar potential, they can be mixed in general. Even when the mixing parameter denoted as ε between $S_{1(\overline{\mathbf{10}},\mathbf{1},\mathbf{3})}$ and $S_{1(\mathbf{6},\mathbf{1},\mathbf{1})}$ is about the ratio of the masses $\varepsilon \approx M_I/M_U \approx 6.1 \times 10^{-6}$, the current constraint $\tau(p \to e^+\pi^0) > 2.4 \times 10^{34}$ years at 90% CL leads to the constraint for the first generation Yukawa coupling constant $|y_{\overline{\mathbf{126}}}^{(11)}| \lesssim 1.7 \times 10^{-3}$. (For $\varepsilon = 1$, $|y_{\overline{\mathbf{126}}}^{(11)}| \lesssim 4.2 \times 10^{-6}$.)

Further, we comment on the relation between neutrino masses and the Yukawa coupling constants $y_{\overline{\mathbf{126}}}^{(ab)}$ of the cubic term $\Phi_{\mathbf{16}}\Phi_{\mathbf{16}}\Phi_{\overline{\mathbf{126}}}$. Since the right-handed neutrino masses are given by $M_N^{(ab)} = y_{\overline{\mathbf{126}}}^{(ab)}v_\phi$, we obtain $2.1 \times 10^8\,\text{GeV} \lesssim M_N^{(11)} = y_{\overline{\mathbf{126}}}^{(11)}v_\phi \lesssim 1.4 \times 10^{11}\,\text{GeV}$ for $1.7 \times 10^{-3} \lesssim y_{\overline{\mathbf{126}}}^{(11)} \lesssim 0.68$ and $v_\phi = M_I$. From the Type-I see-saw mechanism, the light neutrino mass is roughly $m_\nu^{(11)} \approx |y_{\mathbf{10}}^{(11)}v|^2/M_N^{(11)}$ when we ignore the off-diagonal part of $M_N^{(ab)}$. Therefore, $4.4 \times 10^{-8}\,\text{eV} \lesssim m_\nu^{(11)} \lesssim 2.9 \times 10^{-5}\,\text{eV}$ for $1.7 \times 10^{-3} \lesssim y_{\overline{\mathbf{126}}}^{(11)} \lesssim 0.68$, $|y_{\mathbf{10}}^{(11)}| \approx 10^{-5}$ and $v \approx 246\,\text{GeV}$. The proton decay constraints only a part of the Yukawa coupling constants $y_{\overline{\mathbf{126}}}^{(ab)}$, so it is expected that the observed neutrino masses can be reproduced, but to perform it properly, we need to investigate how to reproduce the observed quark and charged lepton masses. We leave it for a future study.

Up to this point, we only consider the specific symmetry breaking pattern, $SO(10)$ broken to $G_I = G_{\text{PS}}$ at $\mu = M_U$ in Eq. (3.1.2). We comment on other cases $G_I = G_{\text{PS}} \times D$, G_{LR}, $G_{\text{LR}} \times D$ discussed in e.g., Refs. [DKP93a, DKP93b, BK15, FHHT19], where D stands for a discrete Z_2 left-right exchange symmetry [CMP84b, CMP84a]. (Note that the same analysis in $SO(10)$ GUT models whose matter content is slightly different from the present model has been already discussed in e.g., Refs. [DKP93a, DKP93b] by using two-loop RGEs [Jon82] and the corresponding matching condition [Hal81, CMG+85].) To realize the appropriate symmetry breaking patterns, we need different $SO(10)$ breaking Higgs fields; each $G_I = G_{\text{PS}}, G_{\text{PS}} \times D, G_{\text{LR}}, G_{\text{LR}} \times D$ is realized by the VEV of a scalar field in e.g., **210**, **54**, **45**, **210** of $SO(10)$, respectively.

The values of M_I, M_U, and α_U^{-1} for several matter contents and symmetry breaking patterns are summarized in Table 3.5, which are estimated by using each analytical solution shown in Appendix 3.C. Substituting the values of M_U and α_U^{-1} for the $G_{\text{PS}} \times D$ and $G_{\text{LR}} \times D$ cases into $\tau \approx M_U^4/\alpha_U^2 m_p^5$, rapid proton decay is expected. For the G_{LR} case, the proton decay via lept-quark gauge bosons is consistent with the current experimental constraints, but the pNGB cannot be identified as dark matter because pNGB decays too rapidly or the observed relic abundance cannot be reproduced.

3.4 Long-lived pNGB as dark matter candidate

The dark matter lifetime should be longer than the age of the universe, 10^{17} s at least. The bound on dark matter lifetime becomes stronger depending on dark matter decay channels due to the constraint of cosmic-ray observations. In particular, the bound from gamma-ray observations is strong as roughly $\tau_\chi \gtrsim 10^{27}$ s for two body decays [BGQS16]. Since the dark matter lifetime is proportional to the power of the VEV v_ϕ, it becomes longer for larger v_ϕ. The evaluation of dark matter lifetime without GUT has been studied in Refs. [ATT20, ORS21], and it has turned out that the VEV should roughly be $v_\phi \gtrsim 10^{13}$ GeV in order to be consistent with the gamma-ray observations if three body decays $\chi \to h_i f\overline{f}$ and $Zf\overline{f}$ can occur. Since in the current GUT pNGB model the kinetic mixing $\sin \epsilon$ and the VEV v_ϕ are fixed to be $\sin \epsilon = -\sqrt{2/5}$ and $v_\phi \approx 10^{11}$ GeV by the requirement of the gauge coupling unification, the three body decays should kinematically be forbidden. Therefore we consider the mass region $m_\chi \lesssim \mathcal{O}(100)$ GeV and estimate dominant four body decay channels.

Before proceeding to four body decays, we comment on the two body decay channel $\chi \to \nu\nu$, which is possible even in the case $m_\chi \lesssim \mathcal{O}(100)$ GeV. Similarly to the $U(1)_{B-L}$ model in the previous paper [ATT20], this process occurs via the scalar mixing given by Eq. (3.2.14) and the mixing between the left-handed and right-handed neutrinos after the electroweak symmetry breaking. The decay width for this channel is calculated as

$$
\Gamma_{\nu\nu} = \frac{m_\chi}{64\pi} \frac{v_s^2}{v_\phi^4} \sum_i m_{\nu_i}^2
$$

$$
= 5 \times 10^{-59} \,\text{GeV} \left(\frac{m_\chi}{100 \,\text{GeV}} \right) \left(\frac{v_s}{1 \,\text{TeV}} \right)^2 \left(\frac{10^{11} \,\text{GeV}}{v_\phi} \right)^4 \sum_i \left(\frac{m_{\nu_i}}{0.1 \,\text{eV}} \right)^2, \qquad (3.4.1)
$$

where m_{ν_i} is the small neutrino mass eigenvalues. Eq. (3.4.1) roughly corresponds to the lifetime $\tau_{\nu\nu} = \mathcal{O}(10^{34})$ s, which is too small to be observed in neutrino cosmic-rays [PR08, CGIT10] because of the suppression by the small neutrino mass squared $m_{\nu_i}^2$. Note that since the scale of the VEV in the GUT pNGB model is $v_\phi \approx 10^{11}$ GeV which is much smaller than the previous analysis [ATT20], the order of the lifetime for this channel is much shorter. However it is still too long to be detectable by experiments and observations.

The four body decay processes $\chi \to f\overline{f}f'\overline{f'}$ mediated by h_i, Z, Z' can occur as shown in Fig. 3.2. Note that if f and f' are identical particles, additional diagrams exist due to interference. We numerically evaluated the decay width for all the four body decay processes using `CalcHEP` [BCP13], and furthermore we took into account three body decay processes when these are kinematically possible. The results are shown in Fig. 3.3 in (m_χ, v_ϕ) plane where the second Higgs mass is fixed to be $m_{h_2} = 70$ GeV (left) and 130 GeV (right). The orange region below the solid, dashed and dot-dashed lines are the region where the dark matter lifetime is shorter than the conservative bound $\tau_\chi = 10^{27}$ s for the
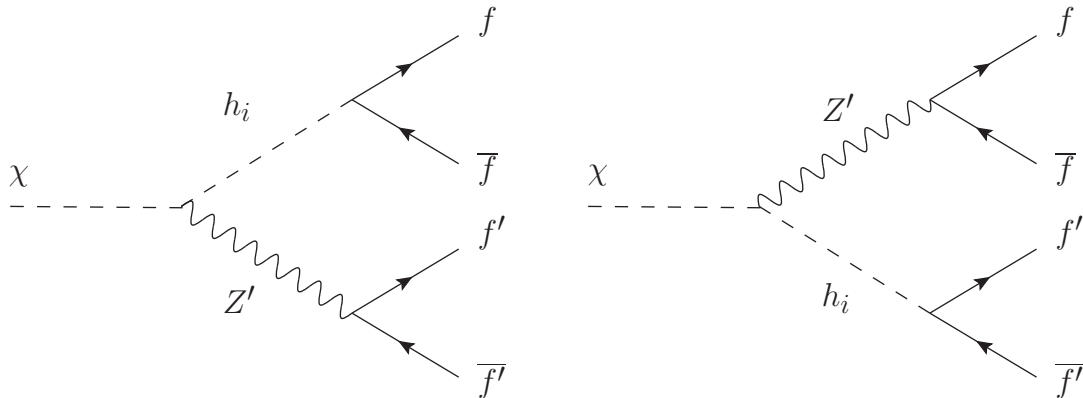
Figure 3.2: The Feynman diagrams for the four body decays $\chi \to f\bar{f}f'\bar{f}'$ are shown [ATTY21].
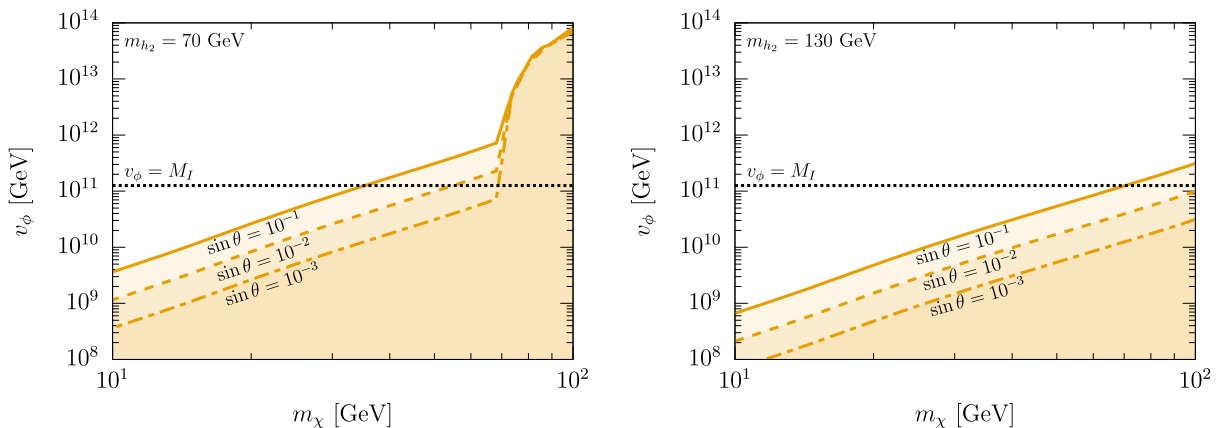
Figure 3.3: Parameter space in the (m_χ, v_ϕ) plane where the second Higgs mass is fixed to be $m_{h_2} = 70\,\mathrm{GeV}$ in the left and $130\,\mathrm{GeV}$ in the right [ATTY21]. The orange region is excluded by the bound of the gamma-ray observations ($\tau_\chi = 10^{27}\,\mathrm{s}$) for $\sin\theta = 10^{-1}, 10^{-2}$ and 10^{-3}.

Higgs mixing angle $\sin\theta = 10^{-1}, 10^{-2}, 10^{-3}$, respectively.[3] The horizontal black dotted line denotes $v_\phi = M_I = 10^{11.10}\,\mathrm{GeV}$. The most part of the region in the plots is dominated by the four body decays except for the region $m_\chi \gtrsim 60\,\mathrm{GeV}$ in the left panel where the three body decay $\chi \to h_2 f\bar{f}$ can open up. One can read off the upper bound of the dark matter mass m_χ for a given mixing angle $\sin\theta$.

Fig. 3.4 shows the parameter space in (m_χ, m_{h_2}) plane for the Higgs mixing angle $\sin\theta = 10^{-1}, 10^{-2}$ and 10^{-3} where $v_\phi = M_I$. The region $m_\chi \gtrsim m_{h_2}$ is strongly constrained by three body decay $\chi \to h_2 f\bar{f}$ while the other region is constrained by four body decays. In particular, if the second Higgs mass is degenerate with the SM-like Higgs boson ($m_{h_1} \approx m_{h_2}$), the four body decay width can be small and the constraint is weaken. This is because

---

[3]The actual bound on the dark matter lifetime for four body decays is weaker than $\tau_\chi \gtrsim 10^{27}\,\mathrm{s}$ since the energy of the emitted gamma rays is softer than two body decays.
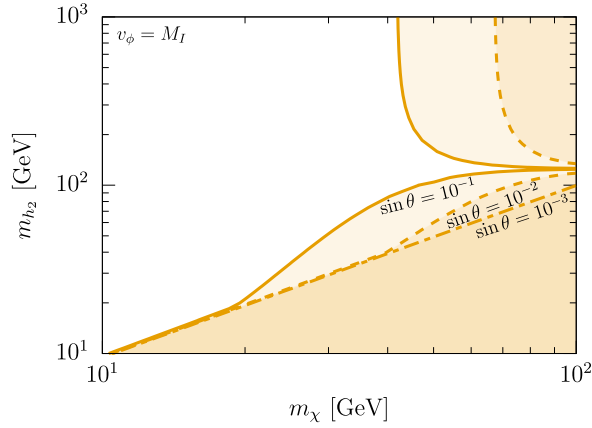
Figure 3.4: Parameter space in (m_χ, h_{h_2}) plane, where the VEV is fixed to be $v_\phi = M_I$ [ATTY21]. The orange region is excluded by the bound of the gamma-ray observations $(\tau_\chi = 10^{27}\,\mathrm{s})$ for $\sin\theta = 10^{-1}, 10^{-2}$ and 10^{-3}.
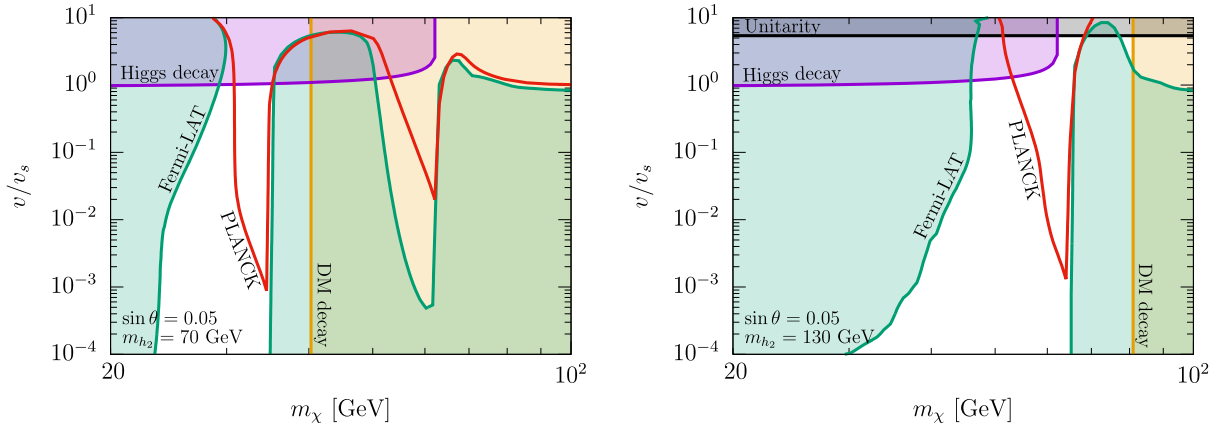
Figure 3.5: Parameter space thermally reproducing the observed relic abundance consistent with some other observations [ATTY21]. The red line represents the parameter space reproducing the correct thermal relic abundance $\Omega_\chi h^2 \approx 0.12$. The orange and green region are excluded by gamma-ray observations coming from the dark matter decay and annihilations, respectively. The purple region are excluded by the constraints of the Higgs invisible decay $h_1 \to \chi\chi$ and the Higgs signal strength. The gray region is perturbative unitarity bound $\lambda_S > 8\pi/3$.

the effective coupling χ-f-f' mediated by h_1 and h_2 becomes small when $m_{h_1} \approx m_{h_2}$.

Thermal relic abundance of dark matter is calculated using `MicrOMEGAs` [BBG+18b]. The results are shown in Fig. 3.5, where the other parameters are fixed to be $m_{h_2} = 70\,\mathrm{GeV}$, $\sin\theta = 0.05$ in the left panel and $m_{h_2} = 130\,\mathrm{GeV}$ and $\sin\theta = 0.05$ the right panel. The red line denotes the parameter space which can reproduce the observed relic abundance of dark matter $\Omega_\chi h^2 \approx 0.12$ [A+20b]. The purple region is excluded by the constraints of the Higgs invisible decay and Higgs signal strength [S+19, A+19a], and the gray region is excluded by the perturbative unitarity bound $\lambda_S < 8\pi/3$ [CDL15]. The

green and orange region are ruled out by the constraints of the gamma-ray observations for dark matter annihilations [A$^+$17b] and four body decays [BGQS16], respectively. One can see that the thermal relic abundance can be consistent with all the constraints when the dark matter mass is rather close to the resonances $m_\chi \lesssim m_{h_i}/2$. This is the characteristic due to the requirement from the gauge coupling unification in the current GUT pNGB model.

We comment on the allowed parameter space $m_\chi \lesssim m_{h_i}/2$. For the second Higgs mass rather heavier than the SM-like Higgs mass, the constraint of the gamma-ray observations can be avoided only if the dark matter mass is light enough $m_\chi \lesssim 35\,\mathrm{GeV}$ as can be seen from Fig. 3.4. On the other hand, this mass region cannot be consistent with the thermal relic abundance of dark matter since it is far from the Higgs resonances. Therefore the mass region $m_{h_2} \gtrsim m_{h_1}$ is completely excluded as long as thermal production mechanism of dark matter is assumed. For more precise calculations in the region $m_\chi \lesssim m_{h_i}/2$, the effect of the early kinetic decoupling from the SM thermal bath should be taken into account [BBGH17, Abe20]. If this effect is included, one can expect that the red line in Fig. 3.3 is shifted slightly upward.

3.5   Summary

In this chapter, we proposed an $SO(10)$ pNGB dark matter model in the framework of GUTs. Each Weyl fermion in **16** of $SO(10)$ contains one generation of quark and leptons. The SM Higgs and two complex scalar fields H, S and Φ in the previous gauged $U(1)_{B-L}$ pNGB dark matter model are embedded into scalar fields in **10**, **16**, and $\overline{\mathbf{126}}$ of $SO(10)$. Assuming a symmetry breaking pattern of $SO(10)$ to G_PS at $\mu = M_U$, and further to G_SM at $\mu = M_I$, the intermediate and unified scales M_I and M_U, the gauge coupling constants of $U(1)_{B-L}$, and the kinetic mixing parameter of between $U(1)_Y$ and $U(1)_{B-L}$ are determined by solving the RGEs with appropriate matching conditions such as gauge coupling unification at $\mu = M_U$.

The dark matter lifetime without GUT has analyzed in Refs. [ATT20, ORS21]. It suggests that the VEV should roughly be the VEV of Φ $v_\phi \gtrsim 10^{13}\,\mathrm{GeV}$ in order to be consistent with the gamma-ray observations if three body decays $\chi \to h_i f \overline{f}$ and $Z f \overline{f}$ are possible. In the current GUT pNGB model, the kinetic mixing and the VEV are fixed to be $\sin\epsilon = -\sqrt{2/5}$ and $v_\phi \approx 10^{11}\,\mathrm{GeV}$, respectively. To satisfy the constraint from the gamma-ray observations, the pNGB dark matter mass must be $m_\chi \lesssim \mathcal{O}(100)\,\mathrm{GeV}$ to forbid the three body decays kinematically. In the mass region, the dominant contribution for dark matter decay channels comes from four body decay channels $\chi \to f \bar{f} f' \bar{f}'$. We find that the thermal relic abundance can be consistent with all the constraints when the dark matter mass is rather close to the resonances $m_\chi \lesssim m_{h_i}/2$.

Appendix 3.A Scalar potential of pNGB dark matter model from $SO(10)$ **GUT**

First, let us devote the scalar potential in the gauged $U(1)_{B-L}$ model (3.2.3) to four parts as follows:

$$
V(H, S, \Phi) = \boxed{-\frac{\mu_H^2}{2}|H|^2 - \frac{\mu_S^2}{2}|S|^2 - \frac{\mu_\Phi^2}{2}|\Phi|^2}
$$
$$
\boxed{+\frac{\lambda_H}{2}|H|^4 + \frac{\lambda_S}{2}|S|^4 + \frac{\lambda_\Phi}{2}|\Phi|^4}
$$
$$
\boxed{+\lambda_{HS}|H|^2|S|^2 + \lambda_{H\Phi}|H|^2|\Phi|^2 + \lambda_{S\Phi}|S|^2|\Phi|^2}
$$
$$
\boxed{-\left(\frac{\mu_c}{\sqrt{2}}\Phi^*S^2 + \text{c.c.}\right)}. \tag{3.A.1}
$$

The first lightgreen line is quadratic couplings, the second lightskyblue line is scalar self couplings, the third lightsalmon line is scalar mixing couplings and the fourth lightgold-enrod line is qubic couplings of Φ and S generating the effective soft breaking mass term S in the low-energy region.

On the other hand, he scalar potential $\mathsf{V}(\Phi_{\mathbf{10}}, \Phi_{\mathbf{16}}, \Phi_{\overline{\mathbf{126}}})$ is given as[4]

$$
\mathsf{V}(\Phi_{\mathbf{10}}, \Phi_{\mathbf{16}}, \Phi_{\overline{\mathbf{126}}}) = -\frac{\mu_{\mathbf{10}}^2}{2}\left(\Phi_{\mathbf{10}}\Phi_{\mathbf{10}}\right)_{\mathbf{1}} - \frac{\mu_{\mathbf{16}}^2}{2}\left(\Phi_{\mathbf{16}}\Phi_{\mathbf{16}}^*\right)_{\mathbf{1}} - \frac{\mu_{\overline{\mathbf{126}}}^2}{2}\left(\Phi_{\overline{\mathbf{126}}}\Phi_{\overline{\mathbf{126}}}^*\right)_{\mathbf{1}}
$$
$$
+ \frac{\lambda_{\mathbf{10}}^{(1)}}{2}\left(\Phi_{\mathbf{10}}\Phi_{\mathbf{10}}\right)_{\mathbf{1}}\left(\Phi_{\mathbf{10}}\Phi_{\mathbf{10}}\right)_{\mathbf{1}} + \frac{\lambda_{\mathbf{10}}^{(2)}}{2}\left(\Phi_{\mathbf{10}}\Phi_{\mathbf{10}}\right)_{\mathbf{54}}\left(\Phi_{\mathbf{10}}\Phi_{\mathbf{10}}\right)_{\mathbf{54}}
$$
$$
+ \frac{\lambda_{\mathbf{16}}^{(1)}}{2}\left(\Phi_{\mathbf{16}}\Phi_{\mathbf{16}}\right)_{\overline{\mathbf{126}}}\left(\Phi_{\mathbf{16}}\Phi_{\mathbf{16}}\right)_{\overline{\mathbf{126}}}^* + \frac{\lambda_{\mathbf{16}}^{(2)}}{2}\left(\Phi_{\mathbf{16}}\Phi_{\mathbf{16}}\right)_{\mathbf{10}}\left(\Phi_{\mathbf{16}}\Phi_{\mathbf{16}}\right)_{\mathbf{10}}^*
$$
$$
+ \frac{\lambda_{\mathbf{16}}^{(3)}}{2}\left(\Phi_{\mathbf{16}}\Phi_{\mathbf{16}}\right)_{\mathbf{10}}\left(\Phi_{\mathbf{16}}\Phi_{\mathbf{16}}\right)_{\mathbf{10}} + \frac{\lambda_{\mathbf{16}}^{(3)*}}{2}\left(\Phi_{\mathbf{16}}\Phi_{\mathbf{16}}\right)_{\mathbf{10}}^*\left(\Phi_{\mathbf{16}}\Phi_{\mathbf{16}}\right)_{\mathbf{10}}^*
$$
$$
+ \frac{\lambda_{\overline{\mathbf{126}}}^{(1)}}{2}\left(\Phi_{\overline{\mathbf{126}}}\Phi_{\overline{\mathbf{126}}}\right)_{\overline{\mathbf{2772}}}\left(\Phi_{\overline{\mathbf{126}}}\Phi_{\overline{\mathbf{126}}}\right)_{\overline{\mathbf{2772}}}^* + \frac{\lambda_{\overline{\mathbf{126}}}^{(2)}}{2}\left(\Phi_{\overline{\mathbf{126}}}\Phi_{\overline{\mathbf{126}}}\right)_{\mathbf{4125}}\left(\Phi_{\overline{\mathbf{126}}}\Phi_{\overline{\mathbf{126}}}\right)_{\mathbf{4125}}^*
$$
$$
+ \frac{\lambda_{\overline{\mathbf{126}}}^{(3)}}{2}\left(\Phi_{\overline{\mathbf{126}}}\Phi_{\overline{\mathbf{16}}}\right)_{\overline{\mathbf{1050}}}\left(\Phi_{\overline{\mathbf{126}}}\Phi_{\overline{\mathbf{126}}}\right)_{\overline{\mathbf{1020}}}^* + \frac{\lambda_{\overline{\mathbf{126}}}^{(4)}}{2}\left(\Phi_{\overline{\mathbf{126}}}\Phi_{\overline{\mathbf{126}}}\right)_{\mathbf{54}}\left(\Phi_{\overline{\mathbf{126}}}\Phi_{\overline{\mathbf{126}}}\right)_{\mathbf{54}}^*
$$
$$
+ \frac{\lambda_{\overline{\mathbf{126}}}^{(5)}}{2}\left(\Phi_{\overline{\mathbf{126}}}\Phi_{\overline{\mathbf{126}}}\right)_{\mathbf{4125}}\left(\Phi_{\overline{\mathbf{126}}}\Phi_{\overline{\mathbf{126}}}\right)_{\mathbf{4125}} + \frac{\lambda_{\overline{\mathbf{126}}}^{(5)*}}{2}\left(\Phi_{\overline{\mathbf{126}}}\Phi_{\overline{\mathbf{126}}}\right)_{\mathbf{4125}}^*\left(\Phi_{\overline{\mathbf{126}}}\Phi_{\overline{\mathbf{126}}}\right)_{\mathbf{4125}}^*
$$
$$
+ \frac{\lambda_{\overline{\mathbf{126}}}^{(6)}}{2}\left(\Phi_{\overline{\mathbf{126}}}\Phi_{\overline{\mathbf{126}}}\right)_{\mathbf{54}}\left(\Phi_{\overline{\mathbf{126}}}\Phi_{\overline{\mathbf{126}}}\right)_{\mathbf{54}} + \frac{\lambda_{\overline{\mathbf{126}}}^{(6)*}}{2}\left(\Phi_{\overline{\mathbf{126}}}\Phi_{\overline{\mathbf{126}}}\right)_{\mathbf{54}}^*\left(\Phi_{\overline{\mathbf{126}}}\Phi_{\overline{\mathbf{126}}}\right)_{\mathbf{54}}^*
$$
$$
+ \lambda_{\mathbf{10},\mathbf{16}}\left(\Phi_{\mathbf{10}}\Phi_{\mathbf{10}}\right)_{\mathbf{1}}\left(\Phi_{\mathbf{16}}\Phi_{\mathbf{16}}^*\right)_{\mathbf{1}}
$$
$$
+ \lambda_{\mathbf{10},\overline{\mathbf{126}}}^{(1)}\left(\Phi_{\mathbf{10}}\Phi_{\mathbf{10}}\right)_{\mathbf{1}}\left(\Phi_{\overline{\mathbf{126}}}\Phi_{\overline{\mathbf{126}}}^*\right)_{\mathbf{1}}
$$
$$
+ \lambda_{\mathbf{10},\overline{\mathbf{126}}}^{(2)}\left(\Phi_{\mathbf{10}}\Phi_{\mathbf{10}}\right)_{\mathbf{54}}\left(\Phi_{\overline{\mathbf{126}}}\Phi_{\overline{\mathbf{126}}}\right)_{\mathbf{54}} + \lambda_{\mathbf{10},\overline{\mathbf{126}}}^{(2)*}\left(\Phi_{\mathbf{10}}\Phi_{\mathbf{10}}\right)_{\mathbf{54}}^*\left(\Phi_{\overline{\mathbf{126}}}\Phi_{\overline{\mathbf{126}}}\right)_{\mathbf{54}}^*
$$
$$
+ \lambda_{\mathbf{16},\overline{\mathbf{126}}}\left(\Phi_{\mathbf{16}}\Phi_{\mathbf{16}}^*\right)_{\mathbf{1}}\left(\Phi_{\overline{\mathbf{126}}}\Phi_{\overline{\mathbf{126}}}^*\right)_{\mathbf{1}}
$$

---

[4]The singlet of the tensor product is able to be read from Ref. [Yam15].

$$-\left(\frac{\mu_{\rm c}}{\sqrt{2}}\big(\Phi_{\overline{\bf 126}}\big)^*\big(\Phi_{\bf 16}\Phi_{\bf 16}\big)_{\overline{\bf 126}} + \frac{\mu_{\rm c}^*}{\sqrt{2}}\big(\Phi_{\overline{\bf 126}}\big)\big(\Phi_{\bf 16}\Phi_{\bf 16}\big)_{\overline{\bf 126}}^*\right)$$
$$-\left(\frac{\mu_{\rm c}'}{\sqrt{2}}\big(\Phi_{\bf 10}\big)\big(\Phi_{\bf 16}\Phi_{\bf 16}\big)_{\bf 10} + \frac{\mu_{\rm c}'^*}{\sqrt{2}}\big(\Phi_{\bf 10}\big)\big(\Phi_{\bf 16}\Phi_{\bf 16}\big)_{\bf 10}^*\right). \tag{3.A.2}$$

The scalar potential of the guaged $U(1)_{B-L}$ model (3.2.3) or (3.A.1) is embeded in the following parts:

$$\mathsf{V}(\Phi_{\bf 10}, \Phi_{\bf 16}, \Phi_{\overline{\bf 126}}) \ni -\frac{\mu_{\bf 10}^2}{2}\big(\Phi_{\bf 10}\Phi_{\bf 10}\big)_{\bf 1} - \frac{\mu_{\bf 16}^2}{2}\big(\Phi_{\bf 16}\Phi_{\bf 16}^*\big)_{\bf 1} - \frac{\mu_{\overline{\bf 126}}^2}{2}\big(\Phi_{\overline{\bf 126}}\Phi_{\overline{\bf 126}}^*\big)_{\bf 1}$$

$$+\frac{\lambda_{\bf 10}^{(1)}}{2}\big(\Phi_{\bf 10}\Phi_{\bf 10}\big)_{\bf 1}\big(\Phi_{\bf 10}\Phi_{\bf 10}\big)_{\bf 1} + \frac{\lambda_{\bf 10}^{(2)}}{2}\big(\Phi_{\bf 10}\Phi_{\bf 10}\big)_{\bf 54}\big(\Phi_{\bf 10}\Phi_{\bf 10}\big)_{\bf 54}$$

$$+\frac{\lambda_{\bf 16}^{(1)}}{2}\big(\Phi_{\bf 16}\Phi_{\bf 16}\big)_{\overline{\bf 126}}\big(\Phi_{\bf 16}\Phi_{\bf 16}\big)_{\overline{\bf 126}}^*$$

$$+\frac{\lambda_{\overline{\bf 126}}^{(1)}}{2}\big(\Phi_{\overline{\bf 126}}\Phi_{\overline{\bf 126}}\big)_{\overline{\bf 2772}}\big(\Phi_{\overline{\bf 126}}\Phi_{\overline{\bf 126}}\big)_{\overline{\bf 2772}}^*$$

$$+\lambda_{\bf 10,16}\big(\Phi_{\bf 10}\Phi_{\bf 10}\big)_{\bf 1}\big(\Phi_{\bf 16}\Phi_{\bf 16}^*\big)_{\bf 1}$$

$$+\lambda_{\bf 10,\overline{\bf 126}}^{(1)}\big(\Phi_{\bf 10}\Phi_{\bf 10}\big)_{\bf 1}\big(\Phi_{\overline{\bf 126}}\Phi_{\overline{\bf 126}}^*\big)_{\bf 1}$$

$$+\lambda_{\bf 16,\overline{\bf 126}}\big(\Phi_{\bf 16}\Phi_{\bf 16}^*\big)_{\bf 1}\big(\Phi_{\overline{\bf 126}}\Phi_{\overline{\bf 126}}^*\big)_{\bf 1}$$

$$-\left(\frac{\mu_{\rm c}}{\sqrt{2}}\big(\Phi_{\overline{\bf 126}}\big)^*\big(\Phi_{\bf 16}\Phi_{\bf 16}\big)_{\overline{\bf 126}} + \frac{\mu_{\rm c}^*}{\sqrt{2}}\big(\Phi_{\overline{\bf 126}}\big)\big(\Phi_{\bf 16}\Phi_{\bf 16}\big)_{\overline{\bf 126}}^*\right)$$

$$-\left(\frac{\mu_{\rm c}'}{\sqrt{2}}\big(\Phi_{\bf 10}\big)\big(\Phi_{\bf 16}\Phi_{\bf 16}\big)_{\bf 10} + \frac{\mu_{\rm c}'^*}{\sqrt{2}}\big(\Phi_{\bf 10}\big)\big(\Phi_{\bf 16}\Phi_{\bf 16}\big)_{\bf 10}^*\right). \tag{3.A.3}$$

We note that $\Phi_{\bf 10}$, $\Phi_{\bf 16}$ and $\Phi_{\overline{\bf 126}}$ are complex scalar fields.

Appendix 3.B   Kinetic mixing as mass mixing

As discussed in the main part of this chapter, the gauge kinetic mixing in Refs. [ATT20, ORS21] is regarded as the mixing angle. In this appendix, we will show this explicitly. The scalar fields in Refs. [ATT20, ORS21] are embedded into the scalars of $SO(10)$ shown in Table 3.3 as

$$\Phi_{\bf 10} \supset \phi_{({\bf 1,2,2})} \supset \phi_{({\bf 1,2},1/2)} = H, \tag{3.B.1}$$

$$\Phi_{\bf 16} \supset \phi_{(\overline{\bf 4},{\bf 1,2})} \supset \phi_{({\bf 1}(+3),{\bf 1},-1/2)} = S, \tag{3.B.2}$$

$$\Phi_{\overline{\bf 126}} \supset \phi_{(\overline{\bf 10},{\bf 1,3})} \supset \phi_{({\bf 1}(+6),{\bf 1},-1)} = \Phi. \tag{3.B.3}$$

Here we will consider the following two symmetry breaking pattern:

$$G_{\rm PS} \to G_{\rm SM}, \quad G_{\rm PS} \to G_{\rm LR} \to G_{\rm SM}. \tag{3.B.4}$$

3.B.1 $G_{\mathrm{PS}} \to G_{\mathrm{SM}}$

First, let us consider the following symmetry breaking pattern

$$SU(4)_C \times SU(2)_R \xrightarrow{\langle\phi_{(\overline{\mathbf{10}},\mathbf{1},\mathbf{3})}\rangle \neq 0, \ \langle\phi_{(\overline{\mathbf{4}},\mathbf{1},\mathbf{2})}\rangle \neq 0} SU(3)_C \times U(1)_Y, \tag{3.B.5}$$

using minimal scalar fields Eqs. (3.B.1)–(3.B.3). This breaking pattern is suitable for the pNGB dark matter model embedding into an $SO(10)$ GUT model because the intermediate scale can be large enough to make the dark matter candidate long-lived.

The covariant derivative of G_{PS} gauge group acts on S and Φ as

$$D_\mu S = \partial_\mu S + ig_4 G'^{\overline{\mathbf{3}},a}_\mu I^{SU(4)_C}_{\overline{\mathbf{3}}(-4),a} S + ig_{B-L} E_\mu Q^S_{B-L} S + i\frac{g_R}{\sqrt{2}} W'^{+}_\mu I^{SU(2)_R}_+ S + ig_R W'^{3}_\mu I^{SU(2)_R}_3 S$$

$$= \partial_\mu S + ig_4 G'^{\overline{\mathbf{3}},a}_\mu I^{SU(4)_C}_{\overline{\mathbf{3}}(-4),a} S + i\frac{g_R}{\sqrt{2}} W'^{+}_\mu I^{SU(2)_R}_+ S + ig_{B-L} E_\mu S - \frac{ig_R}{2} W'^{3}_\mu S, \tag{3.B.6}$$

$$D_\mu \Phi = \partial_\mu \Phi + ig_4 G'^{\mathbf{3},a}_\mu I^{SU(4)_C}_{\mathbf{3}(4),a} \Phi + ig_{B-L} E_\mu Q^\Phi_{B-L} \Phi + i\frac{g_R}{\sqrt{2}} W'^{+}_\mu I^{SU(2)_R}_+ \Phi + ig_R W'^{3}_\mu I^{SU(2)_R}_3 \Phi$$

$$= \partial_\mu \Phi + ig_4 G'^{\mathbf{3},a}_\mu I^{SU(4)_C}_{\mathbf{3}(4),a} \Phi + i\frac{g_R}{\sqrt{2}} W'^{+}_\mu I^{SU(2)_R}_+ \Phi + 2ig_{B-L} E_\mu \Phi - ig_R W'^{3}_\mu \Phi, \tag{3.B.7}$$

where E_μ is the gauge field associated with $U(1)_{B-L} \subset SU(4)_C$ and g_{B-L} is the gauge coupling constant given by $g_{B-L} = \sqrt{\frac{3}{8}} g_4$. The $B-L$ charge comes from the diagonal component of $SU(4)$ denoted by

$$Q_{B-L} = \sqrt{\frac{8}{3}} I^{SU(4)_C}_{15}, \quad I^{SU(4)_C}_{15} = \sqrt{\frac{3}{8}} \operatorname{diag}(1/3, 1/3, 1/3, -1). \tag{3.B.8}$$

$G'^{\mathbf{3},a}_\mu$ and $G'^{\overline{\mathbf{3}},a}_\mu$ are color charged vector boson with the representation $\mathbf{3}(4)$ and $\overline{\mathbf{3}}(-4)$ of $SU(3)_C \times U(1)_{B-L}$ belonging to $\mathbf{15}$ of $SU(4)_C$ respectively. (For the details of the branching rules and the tensor products, see Ref. [Yam15].) These scalars are assumed to develop the following VEVs,

$$\langle S \rangle = \frac{v_s}{\sqrt{2}}, \quad \langle \Phi \rangle = \frac{v_\phi}{\sqrt{2}}, \tag{3.B.9}$$

and these gives the mass terms of the gauge fields

$$\mathcal{L}_{SU(4)_C \times SU(2)_R, \mathrm{mass}} = G'^{\mathbf{3},a\dagger}_\mu M^2_{\mathbf{3},ab} G'^{\mathbf{3},b\mu} + G'^{\overline{\mathbf{3}},a\dagger}_\mu M^2_{\overline{\mathbf{3}},ab} G'^{\overline{\mathbf{3}},b\mu} + \frac{g_R^2}{4}(v_s^2 + 2v_\phi^2) W'^{-}_\mu W'^{+\mu}$$

$$+ \frac{1}{2}\left(\frac{v_s^2}{4} + v_\phi^2\right)\left(2g_{B-L} E_\mu - g_R W'^{3}_\mu\right)^2, \tag{3.B.10}$$

where the mass matrices for the color charged vector bosons $G'^{\mathbf{3},a}_\mu$ and $G'^{\overline{\mathbf{3}},a}_\mu$ are defined by

$$M^2_{\mathbf{3},ab} = \frac{g_4^2 v_\phi^2}{2} \operatorname{tr}\left[\left(I^{SU(4)_C}_{\mathbf{3}(4),a}\right)^\dagger I^{SU(4)_C}_{\mathbf{3}(4),b}\right], \quad M^2_{\overline{\mathbf{3}},ab} = \frac{g_4^2 v_s^2}{2} \operatorname{tr}\left[\left(I^{SU(4)_C}_{\overline{\mathbf{3}}(-4),a}\right)^\dagger I^{SU(4)_C}_{\overline{\mathbf{3}}(-4),b}\right]. \tag{3.B.11}$$

The last term of Eq. (3.B.10) leads the mass mixing between $U(1)_{B-L} \subset SU(4)_C$ and $U(1)_R \subset SU(2)_R$, and the massless direction becomes $U(1)_Y$ in the SM gauge group. From this term, the massive vector boson C'_μ and the orthogonal massless gauge boson B'_μ are introduced by

$$\begin{pmatrix} B'_\mu \\ C'_\mu \end{pmatrix} = \begin{pmatrix} \cos\epsilon & \sin\epsilon \\ -\sin\epsilon & \cos\epsilon \end{pmatrix} \begin{pmatrix} W'^3_\mu \\ E_\mu \end{pmatrix}, \tag{3.B.12}$$

where the mixing angle is defined by

$$\sin\epsilon = \frac{g_R}{\sqrt{g_R^2 + 4g_{B-L}^2}}, \quad \cos\epsilon = \frac{2g_{B-L}}{\sqrt{g_R^2 + 4g_{B-L}^2}}, \tag{3.B.13}$$

and the mass of C'_μ becomes $m_{C'}^2 = (g_R^2 + 4g_{B-L}^2)(v_s^2/4 + v_\phi^2)$. In this basis, the Lagrangian is

$$\mathcal{L} \ni -\frac{1}{4}W^a_{\mu\nu}W^{a\mu\nu} - \frac{1}{4}B'_{\mu\nu}B'^{\mu\nu} - \frac{1}{4}C'_{\mu\nu}C'^{\mu\nu} + \frac{1}{2}m_{C'}^2 C'_\mu C'^\mu \tag{3.B.14}$$

If the color charged vector bosons are dropped, the covariant derivative is rewritten by using these bosons as

$$D_\mu \ni ig_1 B'_\mu + ig_{C'}C'_\mu\left(\frac{Q_{B-L}}{2} - \sin^2\epsilon\, Q_Y\right), \tag{3.B.15}$$

where the hypercharge is defined by

$$Q_Y = I_3^{SU(2)_R} + \frac{Q_{B-L}}{2}, \tag{3.B.16}$$

and the couplings are given by

$$g_1 = \frac{2g_R g_{B-L}}{\sqrt{g_R^2 + 4g_{B-L}^2}}, \quad g_{C'} = \sqrt{g_R^2 + 4g_{B-L}^2}. \tag{3.B.17}$$

Correspondence between the pNGB model [ATT20, ORS21] and the $SO(10)$ pNGB model

We will discuss the kinetic mixing in the GUT model. First, from Eq. (3.B.12), B'_μ is written by using (W'^3_μ, E_μ) as $B'_\mu = W'^3_\mu/\cos\epsilon + \sin\epsilon E_\mu/\cos\epsilon$, and the field redefinition by $\cos\epsilon$ leads the canonically normalized gauge kinetic terms. The massive direction of broken $U(1)$ symmetry does not change in this rewriting. Then Let us introduce new fields after the rescaling by

$$\begin{pmatrix} B'_\mu \\ C'_\mu \end{pmatrix} = \begin{pmatrix} 1 & \sin\epsilon \\ 0 & \cos\epsilon \end{pmatrix}\begin{pmatrix} B_\mu \\ C_\mu \end{pmatrix}, \quad \begin{pmatrix} B_\mu \\ C_\mu \end{pmatrix} = \begin{pmatrix} 1 & -\tan\epsilon \\ 0 & 1/\cos\epsilon \end{pmatrix}\begin{pmatrix} B'_\mu \\ C'_\mu \end{pmatrix}, \tag{3.B.18}$$

Gauged $U(1)_{B-L}$ model [ATT20]	pNGB in $SO(10)$ GUT
$G_{\mathrm{SM}} \times U(1)_{B-L}$	G_{PS}
Q_Y	$Q_Y = I_3^{SU(2)_R} + \frac{Q_{B-L}}{2}$
Q_{B-L}	$Q_{B-L} = \sqrt{\frac{8}{3}} I_{15}^{SU(4)_C}$
B_μ	B_μ in Eq. (3.B.18)
$\hat{B}_\mu$	B'_μ in Eq. (3.B.12)
X_μ	C_μ in Eq. (3.B.18)
$\hat{X}_\mu$	C'_μ in Eq. (3.B.12)
g_1	$g_1 = 2g_R g_{B-L}/\sqrt{g_R^2 + 4g_{B-L}^2}$
g_{B-L}	$g_{B-L} = \sqrt{\frac{3}{8}} g_4$
g_2	g_L
$D_\mu = \partial_\mu + ig_s G_\mu^a I_a^{SU(3)_C} + ig_2 W_\mu^a I_a^{SU(2)_L}$	$D_\mu = \partial_\mu + ig_s G_\mu^a I_a^{SU(3)_C} + ig_L W_\mu^a I_a^{SU(2)_L}$
$+ig_1 Q_Y B_\mu + ig_{B-L} Q_{B-L} X_\mu$	$+ig_1 Q_Y B_\mu + ig_{B-L} Q_{B-L} C_\mu$
kinetic mixing	
gauge kinetic mixing of B_μ and X_μ: ϵ	gauge kinetic mixing of B_μ and C_μ: ϵ
= free parameter	= mixing angle ϵ of $(W_\mu'^3, E_\mu) \mapsto (B'_\mu, C'_\mu)$
	in Eq. (3.B.14)

Table 3.6: The correspondence table of the kinetic mixing and the gauge fields between the gauged $U(1)_{B-L}$ model [ATT20, ORS21] and $SO(10)$ GUT model.

so that the massive direction does not change but the massless component is replaced. The relation between $(W_\mu'^3, E_\mu)$ and (B_μ, C_μ) is given by

$$\begin{pmatrix} W_\mu'^3 \\ E_\mu \end{pmatrix} = \begin{pmatrix} \cos\epsilon & 0 \\ \sin\epsilon & 1 \end{pmatrix} \begin{pmatrix} B_\mu \\ C_\mu \end{pmatrix}. \qquad (3.B.19)$$

The $U(1)_{B-L} \times U(1)_R$ gauge sector in the Lagrangian (3.B.14) is rewritten by using these fields as

$$\mathcal{L} \ni -\frac{1}{4} W_{\mu\nu}^a W^{a\mu\nu} - \frac{1}{4} B_{\mu\nu} B^{\mu\nu} - \frac{1}{4} C_{\mu\nu} C^{\mu\nu} - \frac{\sin\epsilon}{2} B_{\mu\nu} C^{\mu\nu} + \frac{1}{2} m_C^2 C_\mu C^\mu, \qquad (3.B.20)$$

with $M_C^2 = g_{B-L}^2 (v_s^2 + 4v_\phi^2)$, and the covariant derivative is given by

$$D_\mu \ni ig_{B-L} E_\mu Q_{B-L} + ig_R W_\mu'^3 I_3^{SU(2)_R} = ig_{B-L} C_\mu Q_{B-L} + ig_1 B_\mu Q_Y, \qquad (3.B.21)$$

where Eqs. (3.B.16) and (3.B.17) are used. Eqs. (3.B.20) and (3.B.21) are parts of the Lagrangian of the gauged $U(1)_{B-L}$ pNGB model, and the gauge kinetic mixing is naturally regarded as the mixing angle coming from the GUT inspired symmetry breaking. The correspondence is summarized in Table 3.6.

3.B.2 $\quad G_{\mathrm{PS}} \to G_{\mathrm{LR}} \to G_{\mathrm{SM}}$

If the adjoint Higgs bosons $\phi_{(\mathbf{15,1,1})}$ and $\phi_{(\mathbf{1,1,3})}$ are introduced in addition to the scalars Eqs. (3.B.1)–(3.B.3), these VEVs break the Pati-Salam gauge symmetry as

$$SU(4)_C \xrightarrow{\langle \phi_{(\mathbf{15,1,1})} \rangle \neq 0} SU(3)_C \times U(1)_{B-L}, \quad SU(2)_R \xrightarrow{\langle \phi_{(\mathbf{1,1,3})} \rangle \neq 0} U(1)_R. \qquad (3.B.22)$$

By this breaking pattern, the covariant derivative of G_{PS} reduces to that of $SU(3)_C \times SU(2)_L \times U(1)_{R3} \times U(1)_{B-L}$ as

$$D_\mu = \partial_\mu + i g_s G_\mu^a I_a^{SU(3)_C} + i g_{B-L} E_\mu Q_{B-L} + i g_L W_\mu^a I_a^{SU(2)_L} + i g_R W_\mu'^3 I_3^{SU(2)_R}, \qquad (3.B.23)$$

where the $B-L$ charge is defined by Eq. (3.B.8) and the gauge couplings are introduced by $g_s = g_4$, $g_C = \sqrt{\frac{3}{8}} g_4$. The VEVs of S and ϕ (3.B.9) break the residual gauge symmetry as

$$SU(3)_C \times SU(2)_L \times U(1)_R \times U(1)_{B-L} \to G_{\mathrm{SM}}, \qquad (3.B.24)$$

and lead the mass term for the gauge bosons

$$\mathcal{L}_{U(1)_{R3} \times U(1)_{B-L}, \mathrm{mass}} = \frac{1}{2} \left(\frac{v_s^2}{4} + v_\phi^2 \right) \left(2 g_{B-L} E_\mu - g_R W_\mu'^3 \right)^2, \qquad (3.B.25)$$

which is same to the last term of Eq. (3.B.10). In this breaking pattern, the charged gauge bosons become massive via the VEV of the adjoint Higgs fields.

The mixing angle ϵ and correspondence between the mixing angle and kinetic mixing are same in the previous discussions.

Appendix 3.C $\quad$ RGEs for gauge coupling constants

Here we analyze the RGEs for gauge coupling constants of G_{SM} and $G_I = G_{\mathrm{PS}}, G_{\mathrm{LR}}$, and $SO(10)$ in the pNGB dark matter model. (For the RGE analysis, see e.g., Ref. [Moh02].)

The RGE for the gauge coupling constants given in Eq. (3.3.1) can be solve as

$$\alpha_i^{-1}(\mu_1) = \alpha_i^{-1}(\mu_0) - \frac{b_i}{2\pi} \log \left(\frac{\mu_1}{\mu_0} \right). \qquad (3.C.1)$$

when the beta function coefficients b_i are constant in the energy range $\mu_0 < \mu < \mu_1$. In the following, we apply the solution for G_{SM}, and $G_I = G_{\mathrm{PS}}, G_{\mathrm{LR}}$ cases.

In the following, we find the intermediate scale M_I and M_U can be described by using the gauge coupling constants of G_{SM} at $\mu = m_Z$ and the beta function coefficients of G_{SM} and $G_I (= G_{\mathrm{PS}}, G_{\mathrm{LR}})$. Therefore, all the gauge coupling constants such as the unified gauge coupling constant α_U can be analytically solved if they exist.

3.C.1 $G_I = G_{\mathrm{PS}}$ case

We list up the RGEs of G_{SM} and G_{PS} in $m_Z < \mu < M_I$ and $M_I < \mu < M_U$, respectively, and the matching conditions at $\mu = M_I, M_U$.

$m_Z < \mu < M_I$

For $m_Z < \mu < M_I$, the RGEs of the gauge coupling constants of $G_{\mathrm{SM}} = SU(3)_C \times SU(2)_L \times U(1)_Y$ are given by

$$
\begin{aligned}
\alpha_{3C}^{-1}(\mu) &= \alpha_{3C}^{-1}(m_Z) - \frac{b_{3C}}{2\pi} \log\left(\frac{\mu}{m_Z}\right), \\
\alpha_{2L}^{-1}(\mu) &= \alpha_{2L}^{-1}(m_Z) - \frac{b_{2L}}{2\pi} \log\left(\frac{\mu}{m_Z}\right), \\
\alpha_{1Y}^{-1}(\mu) &= \alpha_{1Y}^{-1}(m_Z) - \frac{b_{1Y}}{2\pi} \log\left(\frac{\mu}{m_Z}\right).
\end{aligned}
\tag{3.C.2}
$$

$\mu = M_I$

The matching conditions between G_{SM} and $G_{\mathrm{PS}} = SU(4)_C \times SU(2)_L \times SU(2)_R$ at $\mu = M_I$ are given as

$$
\begin{aligned}
\alpha_{4C}^{-1}(M_I) &= \alpha_{3C}^{-1}(M_I), \\
\alpha_{2L}'^{-1}(M_I) &= \alpha_{2L}^{-1}(M_I), \\
\alpha_{2R}^{-1}(M_I) &= \frac{5}{3}\alpha_{1Y}^{-1}(M_I) - \frac{2}{3}\alpha_{3C}^{-1}(M_I).
\end{aligned}
\tag{3.C.3}
$$

$M_I < \mu < M_U$

For $M_I < \mu < M_U$, the RGEs of the gauge coupling constants of G_{PS} are given by

$$
\begin{aligned}
\alpha_{4C}^{-1}(\mu) &= \alpha_{4C}^{-1}(M_I) - \frac{b_{4C}}{2\pi} \log\left(\frac{\mu}{M_I}\right) = \alpha_{3C}^{-1}(m_Z) - \frac{b_{3C}}{2\pi} \log\left(\frac{M_I}{m_Z}\right) - \frac{b_{4C}}{2\pi} \log\left(\frac{\mu}{M_I}\right), \\
\alpha_{2L}'^{-1}(\mu) &= \alpha_{2L}'^{-1}(M_I) - \frac{b_{2L}'}{2\pi} \log\left(\frac{\mu}{M_I}\right) = \alpha_{2L}^{-1}(m_Z) - \frac{b_{2L}}{2\pi} \log\left(\frac{M_I}{m_Z}\right) - \frac{b_{2L}'}{2\pi} \log\left(\frac{\mu}{M_I}\right), \\
\alpha_{2R}^{-1}(\mu) &= \alpha_{2R}^{-1}(M_I) - \frac{b_{2R}}{2\pi} \log\left(\frac{\mu}{M_I}\right) \\
&= \frac{5}{3}\alpha_{1Y}^{-1}(m_Z) - \frac{2}{3}\alpha_{3C}^{-1}(m_Z) - \left(\frac{5}{3}\frac{b_{1Y}}{2\pi} - \frac{2}{3}\frac{b_{3C}}{2\pi}\right) \log\left(\frac{M_I}{m_Z}\right) - \frac{b_{2R}}{2\pi} \log\left(\frac{\mu}{M_I}\right).
\end{aligned}
\tag{3.C.4}
$$

$\mu = M_U$

For $\mu = M_U$, the matching condition between G_{PS} and $SO(10)$ at $\mu = M_U$ is given by

$$
\alpha_{4C}^{-1}(M_U) = \alpha_{2L}'^{-1}(M_U) = \alpha_{2R}^{-1}(M_U),
\tag{3.C.5}
$$

49

where

$$\alpha_{4C}^{-1}(M_U) = \alpha_{3C}^{-1}(m_Z) - \frac{b_{3C}}{2\pi} \log\left(\frac{M_I}{m_Z}\right) - \frac{b_{4C}}{2\pi} \log\left(\frac{M_U}{M_I}\right),$$

$$\alpha_{2L}'^{-1}(M_U) = \alpha_{2L}^{-1}(m_Z) - \frac{b_{2L}}{2\pi} \log\left(\frac{M_I}{m_Z}\right) - \frac{b_{2L}'}{2\pi} \log\left(\frac{M_U}{M_I}\right),$$

$$\alpha_{2R}^{-1}(M_U) = \frac{5}{3}\alpha_{1Y}^{-1}(m_Z) - \frac{2}{3}\alpha_{3C}^{-1}(m_Z) - \left(\frac{5}{3}\frac{b_{1Y}}{2\pi} - \frac{2}{3}\frac{b_{3C}}{2\pi}\right) \log\left(\frac{M_I}{m_Z}\right) - \frac{b_{2R}}{2\pi} \log\left(\frac{M_U}{M_I}\right).$$

$$(3.C.6)$$

M_I and M_U

From the matching condition in Eq. (3.C.5), we can analytically solve the intermediate scale M_I and unification scale M_U as

$$M_I = m_Z \exp\left[\frac{A_1 B_3 - A_3 B_1}{A_2 B_3 - A_3 B_2}\right],$$

$$M_U = m_Z \exp\left[\left(\frac{A_1 B_3 - A_3 B_1}{A_2 B_3 - A_3 B_2}\right) + \left(\frac{A_1 B_2 - A_2 B_1}{A_3 B_2 - A_2 B_3}\right)\right], \qquad (3.C.7)$$

where

$$A_1 = \alpha_{3C}^{-1}(m_Z) - \alpha_{2L}^{-1}(m_Z), \quad A_2 = \frac{b_{3C} - b_{2L}}{2\pi}, \quad A_3 = \frac{b_{4C} - b_{2L}'}{2\pi},$$

$$B_1 = \frac{5}{3}\left(\alpha_{3C}^{-1}(m_Z) - \alpha_{1Y}^{-1}(m_Z)\right), \quad B_2 = \frac{5}{3}\frac{b_{3C} - b_{1Y}}{2\pi}, \quad B_3 = \frac{b_{4C} - b_{2R}}{2\pi}. \qquad (3.C.8)$$

3.C.2 $\quad G_I = G_{\mathrm{LR}}$ case

We list up the RGEs of G_{SM} and $G_I = G_{\mathrm{LR}}$ in $m_Z < \mu < M_I$ and $M_I < \mu < M_U$, respectively, and the matching conditions at $\mu = M_I, M_U$.

$m_Z < \mu < M_I$

For $m_Z < \mu < M_I$, the RGEs of the gauge coupling constants of $G_{\mathrm{SM}} = SU(3)_C \times SU(2)_L \times U(1)_Y$ are given by

$$\alpha_{3C}^{-1}(\mu) = \alpha_{3C}^{-1}(m_Z) - \frac{b_{3C}}{2\pi} \log\left(\frac{\mu}{m_Z}\right),$$

$$\alpha_{2L}^{-1}(\mu) = \alpha_{2L}^{-1}(m_Z) - \frac{b_{2L}}{2\pi} \log\left(\frac{\mu}{m_Z}\right),$$

$$\alpha_{1Y}^{-1}(\mu) = \alpha_{1Y}^{-1}(m_Z) - \frac{b_{1Y}}{2\pi} \log\left(\frac{\mu}{m_Z}\right). \qquad (3.C.9)$$

$\mu = M_I$

The matching conditions between G_{SM} and $G_{\text{LR}} = SU(3)_C \times SU(2)_L \times SU(2)_R \times U(1)_{B-L}$ at $\mu = M_I$ are given as

$$
\begin{aligned}
\alpha_{3C}'^{-1}(M_I) &= \alpha_{3C}^{-1}(M_I), \\
\alpha_{2L}'^{-1}(M_I) &= \alpha_{2L}^{-1}(M_I), \\
\alpha_{2R}^{-1}(M_I) &= \frac{5}{3}\alpha_{1Y}^{-1}(M_I) - \frac{2}{3}\alpha_{B-L}^{-1}(M_I).
\end{aligned}
\tag{3.C.10}
$$

Note that unlike the above $G_I = G_{\text{PS}}$ case, the gauge coupling constants of G_{LR} at $\mu = M_I$ cannot be determined only by using those of G_{SM} at $\mu = M_I$. To fix them, we need to use the matching conditions of the gauge coupling constants at $\mu = M_U$.

$M_I < \mu < M_U$

For $M_I < \mu < M_U$, the RGEs of the gauge coupling constants of G_{LR} are given by

$$
\begin{aligned}
\alpha_{3C}'^{-1}(\mu) &= \alpha_{3C}'^{-1}(M_I) - \frac{b_{3C}'}{2\pi}\log\left(\frac{\mu}{M_I}\right) = \alpha_{3C}^{-1}(m_Z) - \frac{b_{3C}}{2\pi}\log\left(\frac{M_I}{m_Z}\right) - \frac{b_{3C}'}{2\pi}\log\left(\frac{\mu}{M_I}\right), \\
\alpha_{2L}'^{-1}(\mu) &= \alpha_{2L}'^{-1}(M_I) - \frac{b_{2L}'}{2\pi}\log\left(\frac{\mu}{M_I}\right) = \alpha_{2L}^{-1}(m_Z) - \frac{b_{2L}}{2\pi}\log\left(\frac{M_I}{m_Z}\right) - \frac{b_{2L}'}{2\pi}\log\left(\frac{\mu}{M_I}\right), \\
\alpha_{2R}^{-1}(\mu) &= \alpha_{2R}^{-1}(M_I) - \frac{b_{2R}}{2\pi}\log\left(\frac{\mu}{M_I}\right), \\
\alpha_{B-L}^{-1}(\mu) &= \alpha_{B-L}^{-1}(M_I) - \frac{b_{B-L}}{2\pi}\log\left(\frac{\mu}{M_I}\right).
\end{aligned}
\tag{3.C.11}
$$

$\mu = M_U$

For $\mu = M_U$, the matching condition between G_{LR} and $SO(10)$ at $\mu = M_U$ is given by

$$
\alpha_{3C}'^{-1}(M_U) = \alpha_{2L}'^{-1}(M_U) = \alpha_{2R}^{-1}(M_U) = \alpha_{B-L}^{-1}(M_U),
\tag{3.C.12}
$$

where

$$
\begin{aligned}
\alpha_{3C}'^{-1}(M_U) &= \alpha_{3C}^{-1}(m_Z) - \frac{b_{3C}}{2\pi}\log\left(\frac{M_I}{m_Z}\right) - \frac{b_{3C}'}{2\pi}\log\left(\frac{M_U}{M_I}\right), \\
\alpha_{2L}'^{-1}(M_U) &= \alpha_{2L}^{-1}(m_Z) - \frac{b_{2L}}{2\pi}\log\left(\frac{M_I}{m_Z}\right) - \frac{b_{2L}'}{2\pi}\log\left(\frac{M_U}{M_I}\right), \\
\alpha_{2R}^{-1}(M_U) &= \frac{5}{3}\alpha_{1Y}^{-1}(m_Z) - \frac{2}{3}\alpha_{B-L}^{-1}(M_I) - \frac{5}{3}\frac{b_{1Y}}{2\pi}\log\left(\frac{M_I}{m_Z}\right) - \frac{b_{2R}}{2\pi}\log\left(\frac{M_U}{M_I}\right), \\
\alpha_{B-L}^{-1}(M_U) &= \alpha_{B-L}^{-1}(M_I) - \frac{b_{B-L}}{2\pi}\log\left(\frac{M_U}{M_I}\right).
\end{aligned}
\tag{3.C.13}
$$

M_I and M_U

From the matching condition in Eq. (3.C.12), we can analytically solve the intermediate scale M_I and unification scale M_U as

$$M_I = m_Z \, \exp\left[\frac{C_1 D_3 - C_3 D_1}{C_2 D_3 - C_3 D_2}\right],$$

$$M_U = m_Z \, \exp\left[\left(\frac{C_1 D_3 - C_3 D_1}{C_2 D_3 - C_3 D_2}\right) + \left(\frac{C_1 D_2 - C_2 D_1}{C_3 D_2 - C_2 D_3}\right)\right], \qquad (3.C.14)$$

where

$$C_1 = \alpha_{3C}^{-1}(m_Z) - \alpha_{2L}^{-1}(m_Z), \; C_2 = \frac{b_{3C} - b_{2L}}{2\pi}, \; C_3 = \frac{b'_{3C} - b'_{2L}}{2\pi},$$

$$D_1 = \alpha_{2L}^{-1}(m_Z) - \alpha_{1Y}^{-1}(m_Z), \; D_2 = \frac{b_{2L} - b_{1Y}}{2\pi}, \; D_3 = \frac{b'_{2L} - \frac{3b_{2R}+2b_{B-L}}{5}}{2\pi}. \qquad (3.C.15)$$

Chapter 4

Non-thermal production of pseudo-Nambu-Goldstone dark matter and inflation

4.1 Feeble interaction in pNGB dark matter model and inflationary scenario

As we discussed in Chapters 2 and 3, one of the ways naturally evading the severe constraints from direct detection is to identify a pNGB as dark matter. In these cases, it is found due to the nature of NGB that all couplings of dark matter are inversely proportional to the VEV associated with the symmetry breaking, and then highly suppressed if the VEV is large enough.

Such a large VEV may in fact be connected to generate the small neutrino masses in the framework of Majoron models where the right-handed neutrino Majorana masses are induced by the large VEV [CMP80, CMP81, GR81, GMS10, MY10, QS14]. In this case, the pNGB is identified as Majoron. In order to make the canonical seesaw mechanism work with $\mathcal{O}(1)$ Yukawa couplings, the VEV should be as large as $\mathcal{O}(10^{14})$ GeV. Therefore from this viewpoint, it is motivated to consider the pNGB as FIMPs (Feebly Interacting Massive Particles) produced by freeze-in mechanism [AIM06, AIM07, HJMRW10] with extremely suppressed interactions, e.g., due to a large VEV. In the framework of freeze-in mechanism, dark matter is assumed to be never thermalized with the SM particles. A typical magnitude of FIMP coupling for reproducing the relic abundance observed by the PLANCK Collaboration [A$^+$20b] is $\mathcal{O}(10^{-11})$ for dimensionless couplings [HJMRW10].

In this chapter, we calculate the dark matter relic abundance via Higgs portal in the pNGB dark matter model [GLT17] with large symmetry breaking scale, and study in detail the freeze-in parameter space consistent with the observations. In addition, we examine if successful inflation can occur through the non-minimal coupling to gravity

where the field associated with the symmetry breaking is identified as the inflaton. That implies the inflaton also necessarily induces the pNGB dark matter relic, which would significantly modify the relevant parameter space.

The rest part is organized as follows. In Section 4.2, we briefly review the pNGB model in this chapter's notation in the non-linear representation. In Section 4.3, the relic abundance of pNGB dark matter via the Higgs portal freeze-in is calculated, including the thermal mass of the Higgs boson which is important to evaluate the reaction rates of relevant processes. We also derive the Boltzmann equations for the pNGB FIMP, evaluate the time evolution of the dark matter yield, and show some parameter sets consistent with the present relic abundance observed by experiments. In Section 4.4, we examine the possibility that the radial component of symmetry breaking scalar plays an role of the inflaton. The allowed parameter space is identified taking into account the direct production of the pNGB dark matter from the inflaton decay. Section 4.5 is devoted to our summary.

4.2   Simple pNGB dark matter model

In the simple pNGB model, the SM is extended with a complex singlet scalar Φ[1], and the Lagrangian is given by

$$\mathcal{L} = \mathcal{L}_{\text{SM}} + |\partial_\mu \Phi|^2 - \mathcal{V}(H, \Phi), \tag{4.2.1}$$

where the scalar potential including the SM Higgs doublet H is given by

$$\mathcal{V}(H, \Phi) = -\frac{\mu_H^2}{2}|H|^2 + \frac{\lambda_H}{2}|H|^4 - \frac{\mu_\Phi^2}{2}|\Phi|^2 + \frac{\lambda_\Phi}{2}|\Phi|^4 + \lambda_{H\Phi}|H|^2|\Phi|^2$$
$$-\frac{m^2}{4}\left(\Phi^2 + \Phi^{*2}\right). \tag{4.2.2}$$

The last term is the soft-breaking mass term which is introduced in order to generate the mass of pNGB. We do not consider the origin of this term (UV completion of the model). The Higgs doublet H and the singlet scalar Φ are assumed to develop non-vanishing VEVs and are parametrized as

$$H = \frac{1}{\sqrt{2}}\begin{pmatrix} 0 \\ v + h \end{pmatrix}, \qquad \Phi = \frac{v_\phi + \phi}{\sqrt{2}}\, e^{i\chi/v_\phi}, \tag{4.2.3}$$

where we have dropped the would-be NG modes in H (the unitary gauge). Note that the pNGB χ is stable due to a remnant $\mathbb{Z}_2$ symmetry after the spontaneous symmetry breaking, thus it can be a dark matter candidate. The stationary conditions of the VEVs v and v_ϕ impose the following relations between the parameters in the scalar potential

$$\mu_H^2 = \lambda_H v^2 + \lambda_{H\Phi}v_\phi^2, \qquad \mu_\Phi^2 = \lambda_\Phi v_\phi^2 + \lambda_{H\Phi}v^2 - m^2. \tag{4.2.4}$$

---

[1]In this chapter, Φ denotes the singlet scalar producing the pNGB, which is written as S in the previous chapters.

Using these relations, the masses of the scalar fields are evaluated in the following two phases:

- The electroweak symmetry is unbroken, $\langle H \rangle = (0,0)$ and $\langle \Phi \rangle = v_\phi/\sqrt{2}$. In this phase, only the components of Φ acquire the masses as

$$m_\phi^2 = \lambda_\Phi v_\phi^2, \qquad m_\chi^2 = m^2. \tag{4.2.5}$$

- The electroweak symmetry is spontaneously broken, $\langle H \rangle = (0, v/\sqrt{2})$ and $\langle \Phi \rangle = v_\phi/\sqrt{2}$. In this phase, the physical component of H is massive and the mass eigenvalues of the scalar fields are given by

$$m_{h_1}^2 = \frac{1}{2}\left[\lambda_H v^2 + \lambda_\Phi v_\phi^2 - \sqrt{(\lambda_\Phi v_\phi^2 - \lambda_H v^2)^2 + 4\lambda_{H\Phi}^2 v^2 v_\phi^2}\right], \tag{4.2.6}$$

$$m_{h_2}^2 = \frac{1}{2}\left[\lambda_H v^2 + \lambda_\Phi v_\phi^2 + \sqrt{(\lambda_\Phi v_\phi^2 - \lambda_H v^2)^2 + 4\lambda_{H\Phi}^2 v^2 v_\phi^2}\right], \tag{4.2.7}$$

$$m_\chi^2 = m^2. \tag{4.2.8}$$

The lighter CP-even scalar h_1 is identified as the SM-like Higgs boson with the mass 125 GeV. The mass eigenstates are introduce as

$$\begin{pmatrix} h \\ \phi \end{pmatrix} = \begin{pmatrix} \cos\theta & \sin\theta \\ -\sin\theta & \cos\theta \end{pmatrix} \begin{pmatrix} h_1 \\ h_2 \end{pmatrix}, \quad \tan 2\theta = \frac{2\lambda_{H\Phi} v v_\phi}{\lambda_\Phi v_\phi^2 - \lambda_H v^2}. \tag{4.2.9}$$

Note that the mixing can safely be ignored in our setup with a large hierarchy between the VEVs ($v \ll v_\phi$).

These are the same to results in the linear representation shown in Section 2.2. The difference of the representation appears in the interaction Lagrangian shown below.

In this chapter, we mainly use the non-linear representation for the fluctuations of Φ field as given in Eq. (4.2.3). The same physics is obtained also in the linear representation. The Lagrangian in the broken phase of Φ contains

$$\mathcal{L} \ni \frac{1}{2}\left[(\partial_\mu\phi)^2 - m_\phi^2\phi^2\right] + \frac{1}{2}\left(1 + \frac{\phi}{v_\phi}\right)^2\left[(\partial_\mu\chi)^2 - m_\chi^2 v_\phi^2 \sin^2\left(\frac{\chi}{v_\phi}\right)\right]$$
$$- \frac{\lambda_\Phi}{8}\phi^4 - \frac{\lambda_\Phi v_\phi}{2}\phi^3 - \frac{\lambda_{H\Phi}}{2}|H|^2\left(v_\phi + \phi\right)^2. \tag{4.2.10}$$

The interaction terms of pNGB dark matter χ are originated from the scalar kinetic term and the $U(1)$ soft-breaking mass term in this representation.[2]

---

[2]The contact interaction of the pNGB in the scalar potential appears in the linear representation. However, the contribution is cancelled by the tree-level scattering mediated by the massive mode ϕ in the IR limit and gives the same amplitude to that in the non-linear representation. The explicit calculation is shown in Chapter 5.

4.3 PNGB Production via Freeze-in

In this section, we discuss how the pNGB dark matter relics are produced via the freeze-in mechanism and the parameter set consistent with the observations. We assume that the relic abundance of dark matter is determined in the radiation dominant era of the universe, in which the Hubble parameter H and entropy density s are given as the functions of the temperature T as

$$H = \sqrt{\frac{\pi^2}{90} g_*} \frac{T^2}{M_P}, \qquad s = \frac{2\pi^2}{45} g_*^S T^3, \tag{4.3.1}$$

where g_* and g_*^S denote the total numbers of effective massless degrees of freedom contributing to the energy and entropy densities, respectively [KT90], and M_P is the reduced Planck mass $M_P = 1/\sqrt{8\pi G_N} = 2.4 \times 10^{18}$ GeV (G_N is the gravitational constant).

4.3.1 Boltzmann equations

We are interested in the case that both of dark matter χ and the CP-even scalar ϕ ($\simeq h_2$) are never thermalized with the SM particles. This is achieved by tiny values of quartic couplings $\lambda_{H\Phi}$ and λ_Φ, roughly speaking, $\lambda_{H\Phi}, \lambda_\Phi \lesssim 10^{-6}$. From the theoretical side, a radiative correction to the $|\Phi|^4$ term would imply its lower bound, $\lambda_\Phi \gtrsim \lambda_{H\Phi}^2/16\pi^2$. With these feeble couplings, both of ϕ and χ become the FIMPs, and the Boltzmann equations for the number densities n_ϕ and n_χ are given by

$$\frac{dn_\phi}{dt} + 3Hn_\phi = C_{H^\dagger H \leftrightarrow \phi\phi} + C_{\chi\chi \leftrightarrow \phi\phi} + C_{H^\dagger H \leftrightarrow \phi} + C_{\chi\chi \leftrightarrow \phi}, \tag{4.3.2}$$

$$\frac{dn_\chi}{dt} + 3Hn_\chi = C_{\phi\phi \leftrightarrow \chi\chi} + C_{H^\dagger H \leftrightarrow \chi\chi} + C_{\phi \leftrightarrow \chi\chi}, \tag{4.3.3}$$

where $C_{A \leftrightarrow B}$ in the right-hand side denotes the collision term corresponding to the process $A \leftrightarrow B$. Here the broken phase of Φ is assumed and the scalars in the dark sector interact with the SM only through the Higgs doublet. The explicit form of collision terms is

$$C_{ij...\leftrightarrow ab...} = \int \prod_i d\Pi_i f_i \prod_a d\Pi_a (1 + f_a) \, (2\pi)^4 \delta^4 \left(\sum_i p_i - \sum_a p_a \right) |\mathcal{M}_{ij...\rightarrow ab...}|^2$$
$$- \int \prod_a d\Pi_a f_a \prod_i d\Pi_i (1 + f_i) \, (2\pi)^4 \delta^4 \left(\sum_a p_a - \sum_i p_i \right) |\mathcal{M}_{ab...\rightarrow ij...}|^2, \tag{4.3.4}$$

where f_x is the distribution function of particle x, $d\Pi_x$ is the Lorentz-invariant phase space expressed as $d\Pi_x = \frac{d^3 \boldsymbol{p}_x}{(2\pi)^3 2E_{\boldsymbol{p}_x}}$, and $\mathcal{M}_X$ denotes the amplitude of the process X.

Since dark matter is produced by the freeze-in mechanism from the SM thermal bath, the magnitude of distribution functions is tiny for ϕ and χ. Thus the $\mathcal{O}(f_{\phi,\chi}^2)$ terms can be dropped in the above equations. This approximation is valid as long as the distribution

functions $f_{\phi,\chi}$ are not close to the equilibrium one before the abundance is frozen. The Boltzmann equations are thus reduced to

$$\frac{dn_\phi}{dt} + 3Hn_\phi = C_{H^\dagger H \to \phi\phi} + C_{H^\dagger H \to \phi} - \int d\Pi_\phi \, f_\phi(\boldsymbol{p}_\phi) \, 2m_\phi\big(\Gamma_{\phi \to H^\dagger H} + \Gamma_{\phi \to \chi\chi}\big), \quad (4.3.5)$$

$$\frac{dn_\chi}{dt} + 3Hn_\chi = C_{H^\dagger H \to \chi\chi} + 2\int d\Pi_\phi \, f_\phi(\boldsymbol{p}_\phi) \, 2m_\phi\Gamma_{\phi \to \chi\chi}, \quad (4.3.6)$$

where the decay widths are given by

$$\Gamma_{\phi \to H^\dagger H} = \frac{\lambda_{H\Phi}^2 m_\phi}{8\pi\lambda_\Phi}\sqrt{1 - \frac{4m_H^2}{m_\phi^2}}, \qquad \Gamma_{\phi \to \chi\chi} = \frac{\lambda_\Phi m_\phi}{32\pi}\sqrt{1 - \frac{4m_\chi^2}{m_\phi^2}}. \quad (4.3.7)$$

Note that we have used the relation $m_\phi^2 = \lambda_\Phi v_\phi^2$ in the above equations and the SM Higgs doublet contains real four components, leading to the difference of numerical factors. The mass parameter m_H for the H field will be discussed in the next section. Introducing the net dark matter number density $n_D = n_\chi + 2\text{Br}^{\phi \to \chi\chi}n_\phi$, the Boltzmann equation for n_D is recast as

$$\frac{dn_D}{dt} + 3Hn_D = C_{H^\dagger H \to \chi\chi} + 2\text{Br}^{\phi \to \chi\chi}\big(C_{H^\dagger H \to \phi\phi} + C_{H^\dagger H \to \phi}\big), \quad (4.3.8)$$

where $\text{Br}^{\phi \to \chi\chi}$ is the branching ratio defined by $\text{Br}^{\phi \to \chi\chi} = \Gamma_{\phi \to \chi\chi}/(\Gamma_{\phi \to H^\dagger H} + \Gamma_{\phi \to \chi\chi})$. The collision terms are written by using the thermally averaged cross sections and the number density of the SM Higgs doublet in thermal bath, n_H^{eq}. Then we obtain

$$\frac{dn_D}{dt} + 3Hn_D = 2\left[\langle\sigma_{H^\dagger H \to \chi\chi}v_{\text{rel}}\rangle + 2\text{Br}^{\phi \to \chi\chi}\langle\sigma_{H^\dagger H \to \phi\phi}v_{\text{rel}}\rangle + \text{Br}^{\phi \to \chi\chi}\langle\sigma_{H^\dagger H \to \phi}v_{\text{rel}}\rangle\right](n_H^{\text{eq}})^2.$$
$$(4.3.9)$$

The first term in the right-hand side denotes the dark matter production directly from the thermal bath, and the second and third terms are the contributions from the decays of ϕ produced from the thermal bath. The thermally averaged cross sections are explicitly calculated as

$$\langle\sigma_{H^\dagger H \to \chi\chi}v_{\text{rel}}\rangle \, (n_H^{\text{eq}})^2 = \frac{\lambda_{H\Phi}^2 T^4}{256\pi^5}\int_{2\bar{x}_\chi}^\infty dz \, \sqrt{z^2 - 4x_\chi^2}\sqrt{z^2 - 4x_H^2}\frac{z^4 K_1(z)}{(z^2 - x_\phi^2)^2 + x_\phi^2\gamma_\phi^2}, \quad (4.3.10)$$

$$\langle\sigma_{H^\dagger H \to \phi\phi}v_{\text{rel}}\rangle \, (n_H^{\text{eq}})^2 = \frac{\lambda_{H\Phi}^2 T^4}{256\pi^5}\int_{2\bar{x}_\phi}^\infty dz \, \sqrt{z^2 - 4x_\phi^2}\sqrt{z^2 - 4x_H^2}\frac{(z^2 + 2x_\phi^2)^2 + x_\phi^2\gamma_\phi^2}{(z^2 - x_\phi^2)^2 + x_\phi^2\gamma_\phi^2}K_1(z),$$
$$(4.3.11)$$

$$\langle\sigma_{H^\dagger H \to \phi}v_{\text{rel}}\rangle \, (n_H^{\text{eq}})^2 = \frac{\lambda_{H\Phi}^2 m_\phi^3 T}{16\pi^3\lambda_\Phi}K_1(x_\phi)\sqrt{1 - \frac{4m_H^2}{m_\phi^2}}, \quad (4.3.12)$$

where we have defined the integral variable $z := \sqrt{s}/T$ for the Mandelstam s variable, the dimensionless parameters $x_i := m_i/T$ and $\gamma_i := \Gamma_i/T$ for a particle i with the mass m_i and the total decay width Γ_i. v_{rel} denotes the relative velocity of the initial states

given by $v_{\rm rel} = 2\frac{\sqrt{\lambda(s,m_H^2,m_H^2)}}{s}$ with the kinematic function $\lambda(x,y,z) = x^2 + y^2 + z^2 - 2xy - 2yz - 2zx$. In the integrals, the lower limits are given by $\bar{x}_{\chi,\phi} = \max[x_{\chi,\phi}, x_H]$ and $K_1(z)$ is the modified Bessel function of second kind of order 1. Here thermal bath particles are assumed to obey the Maxwell-Boltzmann distribution.[3] Note that the integrand in Eq. (4.3.10) contains the factor z^4 due to the derivative coupling of pNGB dark matter. This behavior implies that even if the portal coupling $\lambda_{H\Phi}$ is large, the dark matter reaction rate with the SM is suppressed in lower energy than m_ϕ and the usual freeze-out does not work in the case of the hierarchical VEV $v_\phi \gg v$ $(m_\phi \gg m_h)$.

4.3.2 Thermal mass of the Higgs boson

The one-loop effect of bath particles leads to the mass corrections quadratically scaling by the temperature, which are called thermal masses. Including thermal mass corrections gives important effects for collision terms (reaction rates) and hence for the evaluation of relic abundance of dark matter. The detailed calculation of thermal mass for the SM Higgs boson is summarized in Appendix 4.A. The electroweak gauge bosons, all SM fermions, and all components of H including the NGBs eaten by the gauge bosons contribute to the thermal mass, which is given by

$$\Delta_h = \left(\frac{g_1^2}{16} + \frac{3g_2^2}{16} + \frac{y_t^2}{4} + \frac{\lambda_H}{4}\right)T^2, \qquad (4.3.13)$$

where g_Y and g_2 are the gauge couplings of $U(1)_Y$ and $SU(2)_L$, and y_t is the top Yukawa coupling which is dominant over the other Yukawa couplings. Including this thermal contribution, the mass of the SM Higgs boson is given by

$$m_H^2 = m_{h_1}^2 + \Delta_h, \qquad (4.3.14)$$

which plays a role of regulator in the reaction rates in the Boltzmann equations.

4.3.3 IR freeze-in $(T_R \gg m_\phi)$

When the reheating temperature of the universe, T_R, is higher than the heavy mediator mass m_ϕ, the final abundance of dark matter is determined independently of the reheating temperature. This is so-called the IR freeze-in [HJMRW10]. The analytic formula of the dark matter yield $Y_D = n_D/s$ derived from Eq. (4.3.9) is approximately given by

$$Y_D^{\rm IR} \approx \frac{405\sqrt{10}}{(2\pi)^5}\frac{{\rm Br}^{\phi\to\chi\chi}\lambda_{H\Phi}^2 M_P}{g_*^S g_*^{1/2}\lambda_\Phi m_\phi}\sqrt{1 - \frac{4m_h^2}{m_\phi^2}}. \qquad (4.3.15)$$

The result is found to be independent of the dark matter mass because the dominant production process comes from the ϕ decay around $T \sim m_\phi$, as shown in the following

---

[3]Quantum statistical distributions may give a small factor difference in numerical calculations [LT19].
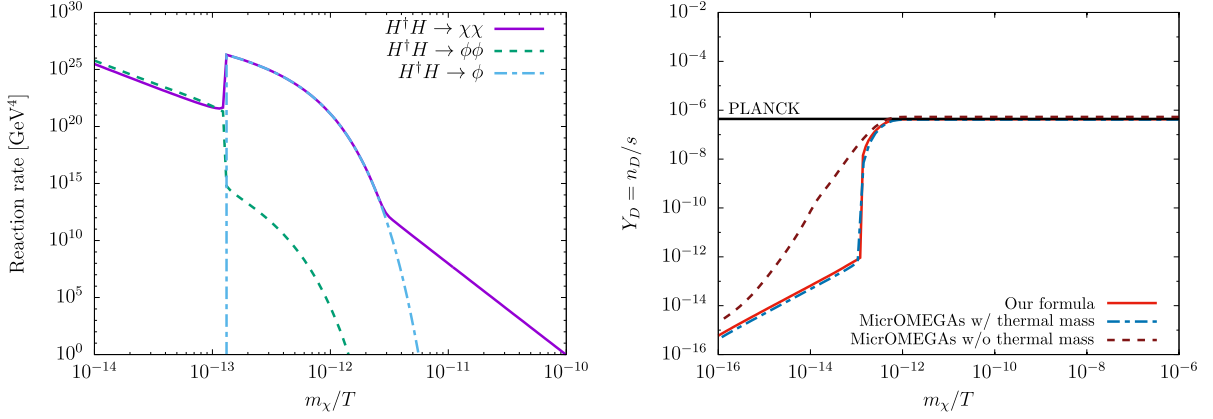
Figure 4.1: (Left): Evolution of the reaction rates for three processes Eqs. (4.3.10)–(4.3.12). (Right): Evolution of the dark matter yield determined by solving the Boltzmann equation. The red solid, dot-dashed dark blue and dashed brown lines denote the results using our formula (4.3.9), the public code `MicrOMEGAs` with and without the thermal mass effect for the SM Higgs boson, respectively. The black horizontal line corresponds to the correct dark matter abundance for $m_\chi = 1$ MeV. These figures are from Ref. [ATY21].

part. In the limit where the scalar VEV and the mass of ϕ are much larger than the masses of the SM Higgs boson and dark matter, the factor of quartic couplings $\mathrm{Br}^{\phi \to \chi\chi} \lambda_{H\Phi}^2$ reduces to

$$\mathrm{Br}^{\phi \to \chi\chi} \lambda_{H\Phi}^2 \approx \frac{\lambda_\Phi^2 \lambda_{H\Phi}^2}{\lambda_\Phi^2 + 4\lambda_{H\Phi}^2} \approx \begin{cases} \lambda_{H\Phi}^2 & \text{for } \lambda_\Phi \gg \lambda_{H\Phi} \\ \frac{\lambda_\Phi^2}{4} & \text{for } \lambda_\Phi \ll \lambda_{H\Phi} \end{cases}. \tag{4.3.16}$$

Thus combining the IR freeze-in relic Eq. (4.3.15) and the yield corresponding to the observed value $Y_D^{\text{obs.}} = 4.4 \times 10^{-7} \, (m_\chi/\text{MeV})^{-1}$ [A+20b] with $g_* \sim g_*^S \sim 100$, we obtain the following relations

$$\left(\frac{\lambda_\Phi}{10^{-8}}\right) \approx \left(\frac{\lambda_{H\Phi}}{2 \times 10^{-9}}\right)^2 \left(\frac{m_\chi}{1 \text{ MeV}}\right) \left(\frac{10^{10} \text{ GeV}}{m_\phi}\right) \qquad \text{for } \lambda_\Phi \gg \lambda_{H\Phi}, \tag{4.3.17}$$

$$\left(\frac{\lambda_\Phi}{7 \times 10^{-11}}\right) \approx \left(\frac{1 \text{ MeV}}{m_\chi}\right) \left(\frac{m_\phi}{10^{10} \text{ GeV}}\right) \qquad \text{for } \lambda_\Phi \ll \lambda_{H\Phi}. \tag{4.3.18}$$

The evolution of the reaction rates including the thermal mass effects is shown in the left panel of Fig. 4.1 where we choose the following parameter set

$$\lambda_\phi = 7 \times 10^{-11}, \quad \lambda_{H\Phi} = 10^{-7}, \quad m_\chi = 1 \text{ MeV}, \quad m_\phi = 10^{10} \text{ GeV}, \tag{4.3.19}$$

as a benchmark. This is chosen so that the parameter relation Eq. (4.3.18) is realized. Note that the portal coupling should satisfy $\lambda_{H\Phi} \lesssim 10^{-6}$ in order for the dark sector particles not to enter into the thermal bath. When the temperature cools down to the mediator mass scale $T \sim m_\phi$, a number of on-shell ϕ are resonantly produced. As a result
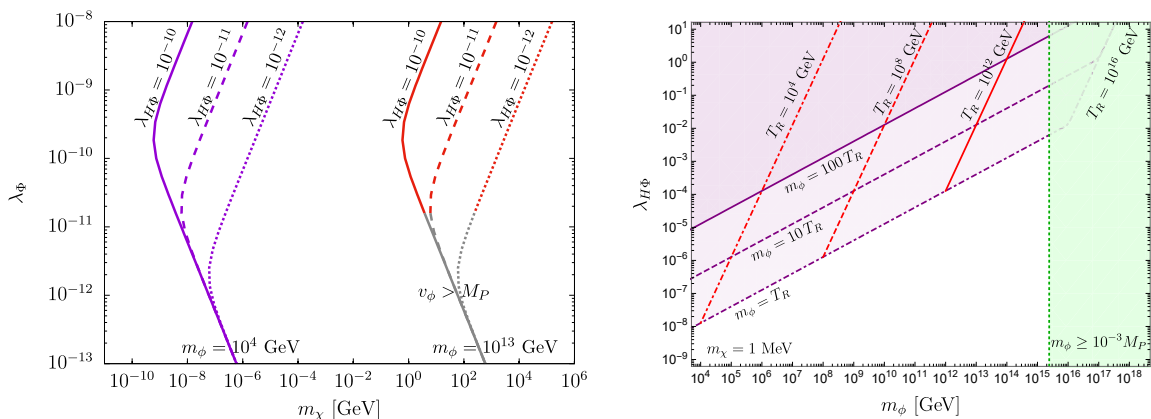
Figure 4.2: (Left): Contours reproducing the observed relic abundance in the (m_χ, λ_Φ) plane where the mediator mass is fixed to be $m_\phi = 10^4$ GeV (10^{13} GeV) in the purple (red) line. The solid, dashed and dotted lines correspond to $\lambda_{H\Phi} = 10^{-10}$, 10^{-11} and 10^{-12}, respectively. The gray parts of the red lines are excluded by the criterion $v_\phi > M_P$. (Right): The purple region can realize the observed relic abundance via the UV freeze-in in the $(m_\phi, \lambda_{H\Phi})$ plane. Each contour reproduces the abundance for a specific parameter set. The solid, dashed and dot-dashed red lines correspond to $T_R = 10^{12}$ GeV, 10^8 GeV and 10^4 GeV, respectively. The green region, $m_\phi \geq 10^{-3} M_P$, is excluded (see the text). These figures are from Ref. [ATY21].

the magnitude of the reaction rate for the process $H^\dagger H \to \chi\chi$ rapidly increases as can be seen in Fig. 4.1.

For the same benchmark parameter set, the evolution of the dark matter yield is shown in the right panel of Fig. 4.1, assuming the vanishing initial conditions of the dark sector

$$Y_\chi(T = T_R) = Y_\phi(T = T_R) = 0. \tag{4.3.20}$$

We also show for comparison the results calculated by the public code `MicrOMEGAs` [BBG+18b] with and without the thermal mass effect for the SM Higgs boson.[4] As obvious from the plot, the thermal mass effect gives an impact on the evolution of the dark matter yield, in particular when the temperature is $T \gtrsim m_\phi$. Including thermal mass also affects the final dark matter abundance, while its impact is not so large and only gives a few factor difference. One can see from the plot that the yield of dark matter rapidly grows at $T \sim m_\phi$ due to the resonant production of ϕ, and then the evolution is almost frozen afterwards.

The purple and red lines in the left panel of Fig. 4.2 show the contours in the (m_χ, λ_Φ) plane reproducing the dark matter relic abundance observed by the PLANCK Collaboration [A+20b]. The reheating temperature is assumed to be much higher than the mediator mass scale ($T_R \gg m_\phi$). As can be seen in the plots, for a larger m_ϕ the lines

---

[4]In the current version of `MicrOMEGAs`, full thermal mass effects are not implemented. However it is possible to include the thermal mass only for the Higgs boson by hand without difficulty.

simply shift to the right (purple to red), namely the direction of heavier dark matter mass which compensates a smaller yield Y_D^{IR}. The behavior of the lines change around $\lambda_\Phi \sim \lambda_{H\Phi}$ as explained in Eqs. (4.3.17) and (4.3.18). While one can take a heavier dark matter mass m_χ if a larger mediator mass m_ϕ is chosen, there is an upper bound on m_χ if the criterion for the VEV $v_\phi < M_P$ is taken into account. As we will discuss in the next section, a feeble value of the scalar self-coupling, typically $\lambda_\Phi \gtrsim \mathcal{O}(10^{-12})$ is suitable for ϕ being the inflaton.

4.3.4 UV freeze-in $(T_R \ll m_\phi)$

When m_ϕ is much larger than the reheating temperature, the dark matter relic abundance is determined by the portal coupling $\lambda_{H\Phi}$ and the reheating temperature T_R. This is so called the UV freeze-in discussed in Refs. [HJMRW10, EKU15]. For $T < T_R \ll m_\phi$, only the $H^\dagger H \to \chi\chi$ process is effective for the dark matter production (see the left panel of Fig. 4.1). In the $H^\dagger H \to \chi\chi$ reaction rate (4.3.10), we can safely assume $m_\phi \gg \sqrt{s} \gg m_h, m_\chi$ since the modified Bessel function regarded as the window function with a cut-off T and the large s contribution is dominant due to the $s^{5/2}$ behavior of the integrand. Thus the reaction rate is approximated by

$$\langle \sigma_{H^\dagger H \to \chi\chi} \bar{v} \rangle \left(n_H^{\mathrm{eq}} \right)^2 \approx \frac{\lambda_{H\Phi}^2 T}{512\pi^5} \int_0^\infty ds\, \frac{s^{5/2}}{m_\phi^4} K_1(\sqrt{s}/T) = \frac{3\lambda_{H\Phi}^2 T^8}{2\pi^5 m_\phi^4}. \tag{4.3.21}$$

By integrating the Boltzmann equations for the dark sector using this approximation, the pNGB dark matter yield is evaluated as

$$Y_D^{\mathrm{UV}} \approx \frac{135\sqrt{10}\lambda_{H\Phi}^2 M_P T_R^3}{4\pi^8 g_*^S g_*^{1/2} m_\phi^4}. \tag{4.3.22}$$

Combining with the observed value $Y_D^{\mathrm{obs.}} = 4.4 \times 10^{-7} \left(m_\chi/\mathrm{MeV} \right)^{-1}$ with $g_* \sim g_*^S \sim 100$, we obtain the following relation[5]

$$\left(\frac{\lambda_{H\Phi}}{10^{-6}} \right)^2 \approx \left(\frac{1\ \mathrm{MeV}}{m_\chi} \right) \left(\frac{m_\phi}{10^5\ \mathrm{GeV}} \right)^4 \left(\frac{10^4\ \mathrm{GeV}}{T_R} \right)^3. \tag{4.3.23}$$

The right panel of Fig. 4.2 shows the parameter space where the dark matter relic can be realized by the UV freeze-in, which is denoted by the purple region. The purple solid, dashed and dot-dashed lines denote $m_\phi = 100\, T_R$, $10\, T_R$ and T_R (the UV freeze-in (4.3.22) is valid for $m_\phi \gg T_R$). The red lines show the contours in the $(m_\chi, \lambda_{H\Phi})$ plane reproducing the dark matter relic for various given reheating temperatures. Note that the green colored region $m_\phi \geq 10^{-3} M_P$ is excluded by the conditions $v_\phi \leq M_P$ and $\lambda_\Phi \leq 10^{-6}$, the latter of which is required for the dark sector not being thermalized.

---

[5]For a heavier pNGB dark matter case, the broader parameter space in the $(m_\phi, \lambda_{H\Phi})$ plane has been discussed in Ref. [AHO+20].

4.4 Inflation

In the previous section, we have seen the pNGB dark matter relic abundance realized via feeble scalar couplings, where the radial component ϕ of the symmetry breaking scalar plays a role of the mediator of pNGB production. In this section, we investigate the possibility that ϕ also plays another important role, namely, the inflaton.[6]

4.4.1 Inflation dynamics and constraints

The inflation gives a plausible solution for the flatness and horizon problems in the universe. A successful inflation scenario can occur in our model if a non-minimal coupling between the complex scalar Φ and gravity is introduced. Then the Lagrangian relevant for the inflation dynamics is given by

$$\frac{\mathcal{L}}{\sqrt{-g}} = -\frac{M_P^2}{2}\mathcal{R} - \xi|\Phi|^2\mathcal{R} + g^{\mu\nu}(\partial_\mu\Phi)^*(\partial_\nu\Phi) - \mathcal{V}(\Phi), \qquad (4.4.1)$$

where $\mathcal{R}$ is the Ricci scalar and ξ is the so-called non-minimal coupling constant. During the inflation era, the scalar potential is assumed to be dominated by the field value of Φ, thus $\mathcal{V}(\Phi) \approx \lambda_\Phi|\Phi|^4/2 \approx \lambda_\Phi\phi^4/8$, and the $|\Phi|^2$ part can be written as $|\Phi|^2 \approx \phi^2/2$ with the non-linear representation $\Phi = (v_\phi + \phi)\,e^{i\chi/v_\phi}/\sqrt{2}$.

The non-minimal coupling is removed by the conformal transformation,

$$g_{\mu\nu} \to g_{\mu\nu} = \Omega^{-2}\hat{g}_{\mu\nu} \quad \text{with} \quad \Omega = \sqrt{1 + \frac{\xi\phi^2}{M_P^2}}, \qquad (4.4.2)$$

where $\hat{g}_{\mu\nu}$ corresponds to the metric in the Einstein frame. As a result of this transformation[7], the Lagrangian becomes

$$\frac{\hat{\mathcal{L}}}{\sqrt{-\hat{g}}} = -\frac{M_P^2}{2}\hat{\mathcal{R}} + \frac{\hat{g}^{\mu\nu}}{2}(\partial_\mu\varphi)(\partial_\nu\varphi) + \frac{\hat{g}^{\mu\nu}}{2}(\partial_\mu\hat{\chi})(\partial_\nu\hat{\chi}) - \hat{\mathcal{V}}(\varphi), \qquad (4.4.4)$$

where φ and $\hat{\chi}$ are the canonically normalized fields satisfying the differential equations

$$\frac{d\varphi}{d\phi} = \sqrt{\frac{M_P^2\Omega^2 + 6\xi^2\phi^2}{M_P^2\Omega^4}}, \qquad \frac{d\hat{\chi}}{d\chi} = \Omega^{-1}. \qquad (4.4.5)$$

---

[6]Some different types of models are studied in the literature, e.g. [BMSV14, ENTT14] about possible common origins of the inflaton and dark matter.

[7]In D-dimentional spacetime, the Ricci scalar is transformed under the Weyl rescaling $g_{MN} = e^w\hat{g}_{MN}$ as

$$\mathcal{R}_D = e^{-w}\left[\hat{\mathcal{R}}_D - (D-1)\hat{\nabla}_M^2 w - \frac{(D-1)(D-2)}{4}(\partial_M w)^2\right], \qquad (4.4.3)$$

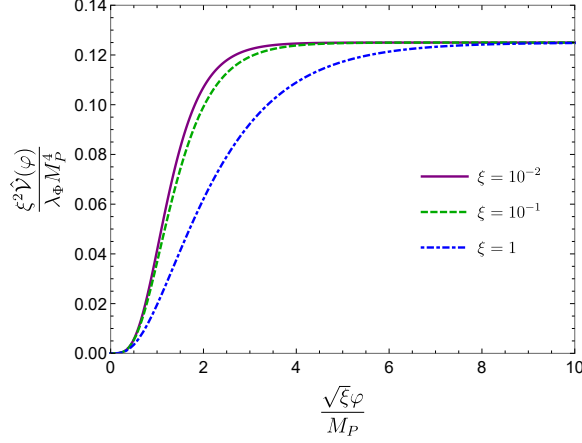where $\hat{\nabla}_M^2 = \frac{1}{\sqrt{-\hat{g}}}\partial_M\sqrt{-\hat{g}}\hat{g}^{MN}\partial_N$.

Figure 4.3: Inflation potential with the non-minimal coupling $\xi = 10^{-2} \ 10^{-1}$, and 1 [ATY21].

If $\xi \gg 1$, which is similar to the case of the Higgs inflation [BS08b], the differential equation is simplified and the explicit expressions of φ and $\hat{\mathcal{V}}(\varphi)$ are obtained. However in the present pNGB model with feeble couplings, we will show later that a smaller ξ is favored for successful inflation. The shape of the scalar potential is numerically evaluated and shown in Fig. 4.3 where the non-minimal coupling is fixed to be $\xi = 10^{-2}, 10^{-1}, 1$. The flat part of the potential gets longer for a smaller value of ξ.

While one cannot write down the explicit form of the scalar potential $\hat{\mathcal{V}}(\varphi)$, the slow-roll parameters are expressed in terms of ϕ,

$$\epsilon_V := \frac{M_P^2}{2} \left(\frac{\hat{\mathcal{V}}_\varphi}{\hat{\mathcal{V}}} \right)^2 = \frac{8M_P^4}{\phi^2 [M_P^2 + \xi (1 + 6\xi) \phi^2]}, \tag{4.4.6}$$

$$\eta_V := M_P^2 \frac{\hat{\mathcal{V}}_{\varphi\varphi}}{\hat{\mathcal{V}}} = \frac{4M_P^2 [3M_P^4 + M_P^2 \xi (1 + 12\xi) \phi^2 - 2\xi^2 (1 + 6\xi) \phi^4]}{\phi^2 [M_P^2 + \xi (1 + 6\xi) \phi^2]^2}, \tag{4.4.7}$$

where $\hat{\mathcal{V}}_\varphi := \partial \hat{\mathcal{V}}/\partial \varphi$ and $\hat{\mathcal{V}}_{\varphi\varphi} := \partial^2 \hat{\mathcal{V}}/\partial \varphi^2$. Using the slow-roll approximation, the spectral index n_s and the tensor-to-scalar ratio r are given by

$$n_s = 1 - 6\epsilon_V + 2\eta_V, \qquad r = 16\epsilon_V. \tag{4.4.8}$$

The e-folding number N_* between the time of horizon exit (t_*) and the end of inflation $(t_{\rm end})$ is given by

$$N_* = \int_{t_*}^{t_{\rm end}} H dt \approx \frac{-1}{M_P^2} \int_{\phi_*}^{\phi_{\rm end}} \frac{d\varphi}{d\phi} \frac{\hat{\mathcal{V}}}{\hat{\mathcal{V}}_\varphi} d\phi = \frac{(1 + 6\xi) (\phi_*^2 - \phi_{\rm end}^2)}{8M_P^2} - \frac{3}{4} \log \left(\frac{M_P^2 + \xi \phi_*^2}{M_P^2 + \xi \phi_{\rm end}^2} \right), \tag{4.4.9}$$

where ϕ_* and $\phi_{\rm end}$ are the field values at t_* and $t_{\rm end}$, respectively. Defining $t_{\rm end}$ as the time giving the slow-roll parameter $\epsilon = 1$ in Eq. (4.4.6), $\phi_{\rm end}$ satisfies

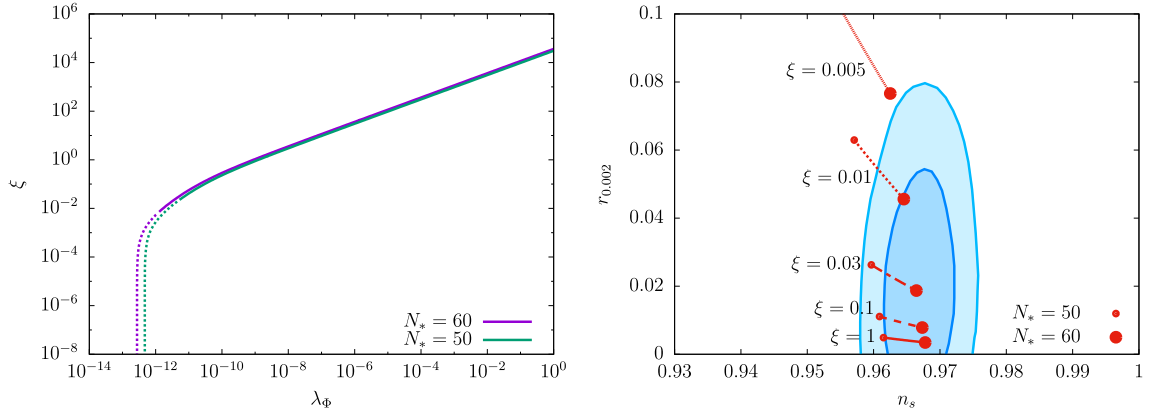$$\phi_{\rm end}^2 = \frac{M_P^2}{2} \frac{\sqrt{1 + 32\xi + 192\xi^2} - 1}{\xi (1 + 6\xi)}. \tag{4.4.10}$$

Figure 4.4: (Left): Contours in the (ξ, λ_Φ) plane for successful inflation where N_* is fixed as $N_* = 50$ and 60. (Right): Predictions for the spectral index (n_s) and the tensor-to-scalar ratio (r) where the non-minimal coupling ξ is taken as $\xi = 1$, 0.1, 0.03, 0.01 and 0.005. The blue and light blue regions are allowed by the PLANCK observation at 1σ and 2σ confidence level, respectively. These figures are from Ref. [ATY21].

On the other hand, ϕ_* is numerically evaluated, giving the amplitude of the scalar power spectrum at the horizon exit observed by the Planck Collaboration [A+20c]: $A_s = \hat{\mathcal{V}}(\varphi(\phi_*))/(24\pi^2 M_P^4 \epsilon_V(\phi_*)) = 2.10 \times 10^{-9}$. From these relations, the non-minimal coupling ξ and the scalar self-coupling λ_Φ for successful inflation can be read. The contour of the e-folding number N_* on the (ξ, λ_Φ) plane is shown in the left panel of Fig. 4.4 where $N_* = 50$ and 60. When the non-minimal coupling ξ is small enough ($\xi \lesssim 10^{-3}$), the dependence on λ_Φ disappears. This region has the same behavior as the ϕ^4 chaotic inflation.

The predictions for the spectral index n_s and the tensor-to-scalar ratio r at the pivot scale $k_* = 0.002$ Mpc^{-1} are shown in the right panel of Fig. 4.4 where N_* is taken to be between 50 and 60. The blue and light blue regions represent the 1σ and 2σ confidence levels observed by the Planck Collaboration [A+20c]. It can be found that the lower bounds for the non-minimal coupling are required

$$\xi \gtrsim 0.02 \quad (N_* = 50), \qquad \xi \gtrsim 0.0055 \quad (N_* = 60), \tag{4.4.11}$$

for the scenario consistent with the observation.

In the left panel of Fig. 4.4, the solid (dotted) part of each contour represents the parameter region consistent (inconsistent) with the PLANCK observation at 2σ confidence level, when combined with the lower bounds of ξ obtained in the right panel. We find that the self-coupling λ_Φ should be in the range $\lambda_\Phi \gtrsim 10^{-12}$ in the pNGB dark matter model with large symmetry breaking, if the inflation is induced by the coupling ξ.

4.4.2 pNGB production from inflaton

There is another important physical implication of the possibility that the radial scalar component ϕ plays the role of inflaton in the pNGB dark matter model. That is the direct production process of dark matter χ from the inflaton decay, which is inevitable because of the interaction between ϕ and χ. In this section, we investigate the parameter space consistent with the inflationary scenario discussed above and the dark matter relic abundance taking into account both the freeze-in and inflaton-induced dark matter.

As discussed in Refs. [Tak08, GP11], the number density of the inflaton induced χ particle is estimated as

$$n_\chi^{\rm inf} \approx \frac{\rho_{\rm rh}}{m_\phi} \frac{\Gamma_{\phi \to \chi\chi}}{\sqrt{3}H(T_R)}, \tag{4.4.12}$$

where $\rho_{\rm rh}$ and $H(T_R)$ are the energy density of radiation and the Hubble rate at the reheating temperature T_R. We here define the reheating temperature T_R at which the Hubble rate is equal to the decay width of the inflaton to the SM sector ($H(T_R) \approx \Gamma_{\phi \to H^\dagger H}$), and then

$$T_R^2 \approx \frac{3\sqrt{10}}{8\pi^2 g_*^{1/2}} \frac{\lambda_{H\Phi}^2}{\lambda_\Phi} M_P m_\phi \sqrt{1 - \frac{4m_h^2}{m_\phi^2}}. \tag{4.4.13}$$

Note that the effective degrees of freedom g_* in the right-hand side also depends on the temperature in general. Using the explicit form of the decay widths and the reheating temperature (4.4.13), we obtain the pNGB dark matter yield directly produced from the inflaton as

$$Y_\chi^{\rm inf} \approx \left(\frac{9\sqrt{10}}{2048\pi^2} \right)^{1/2} \frac{g_*^{3/4} \lambda_\Phi^{3/2} M_P^{1/2}}{g_*^S \lambda_{H\Phi} m_\phi^{1/2}} \left(1 - \frac{4m_\chi^2}{m_\phi^2} \right)^{\frac{1}{2}} \left(1 - \frac{4m_h^2}{m_\phi^2} \right)^{-\frac{1}{4}}. \tag{4.4.14}$$

As previously, we impose the portal coupling satisfies $\lambda_{H\Phi} \lesssim 10^{-6}$ such that dark matter does not get into the SM thermal bath.

We here comment on the comparison between the three contributions of pNGB dark matter yields, $Y_D^{\rm IR}$, $Y_D^{\rm UV}$ and $Y_\chi^{\rm inf}$. Typical behaviors are shown in Fig. 4.5 as the functions of the mediator mass m_ϕ, which behaviors are evaluated by `MicrOMEGAs` for $\lambda_{H\Phi} = 10^{-7}$ and 10^{-11}. The reheating temperature is given by Eq. (4.4.13) in the left panel, while it is treated as a free parameter in the right panel (see the detail in the next subsection). The IR and UV freeze-in productions are effective in the smaller and larger m_ϕ regions, respectively. These freeze-in yields are smoothly connected in the gray region where $T_R \lesssim m_\phi \lesssim 100\,T_R$, which is denoted by the purple dashed line. Since $Y_D^{\rm IR} \propto m_\phi^{-1}$ and $Y_\chi^{\rm inf} \propto m_\phi^{-1/2}$, the IR freeze-in is dominant for a lighter mediator. Further, $Y_D^{\rm IR}$ becomes equal to $Y_\chi^{\rm inf}$ at $m_\phi = m_{\rm eq}$. It is easy to find from Eqs. (4.3.15), (4.4.13) and (4.4.14) that $m_{\rm eq} \lesssim 10^{-2}\,T_R$, and then the inflaton-induced yield necessarily becomes dominant
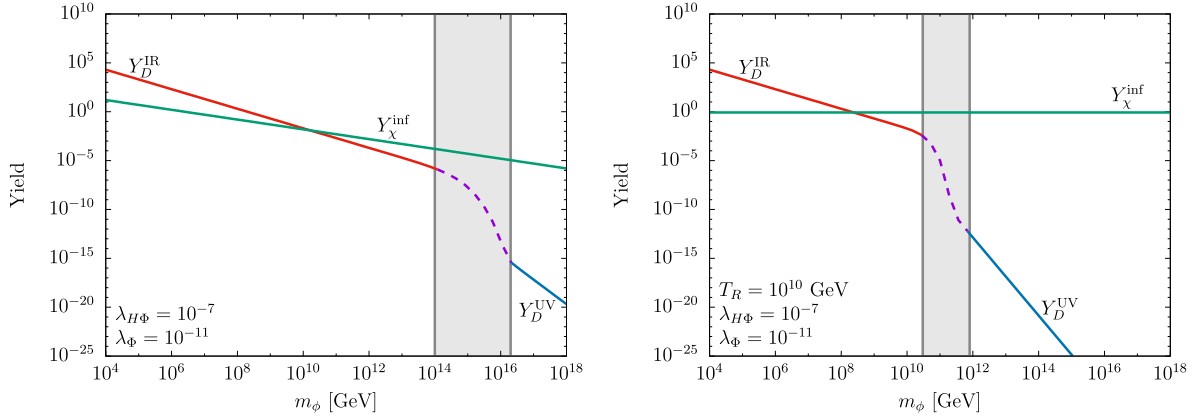
Figure 4.5: Comparisons of the pNGB dark matter yields, Y_D^{IR} (red), Y_D^{UV} (green) and Y_χ^{inf} (blue) for $\lambda_{H\Phi} = 10^{-7}$ and $\lambda_\Phi = 10^{-11}$ [ATY21]. The reheating temperature is given by Eq. (4.4.13) in the left panel and a free parameter in the right panel, chosen as $T_R = 10^{10}$ GeV. The IR and UV freeze-in are smoothly connected in the gray region, typically $T_R \lesssim m_\phi \lesssim 100\, T_R$.

in the left side of the gray band. On the other hand, the UV freeze-in abundance takes the value $Y_D^{\mathrm{UV}}/Y_\chi^{\mathrm{inf}} \simeq 10^{-3}\lambda_{H\Phi}^2/\lambda_\Phi$ around $m_\phi = T_R$. This ratio is much smaller than 1 due to the constraints $\lambda_{H\Phi} \lesssim 10^{-6}$ and $\lambda_\Phi \gtrsim 10^{-12}$ as we explained from the cosmological arguments. Since $Y_D^{\mathrm{UV}} \propto m_\phi^{-5/2}$, the UV freeze-in contribution is always subdominant compared to the inflaton decay.

4.4.3 Dark matter abundance

Fig. 4.6 shows the parameter space realizing the correct dark matter relic abundance in the (m_χ, λ_Φ) plane taking into account the pNGB production from the freeze-in and inflaton decay. The portal coupling is chosen as $\lambda_{H\Phi} = 10^{-7}$, 10^{-8} and 10^{-9} and the mediator mass is $m_\phi = 10^4$ GeV, 10^6 GeV and 10^8 GeV. The purple line represents the parameters reproducing the dark matter abundance only by the freeze-in contribution. The gray region represents the parameter space where the inflaton induced dark matter abundance is larger than 10 % of the observed value. In order to be consistent with the inflation observables at 2σ confidence level as discussed in the previous subsection, the scalar self-coupling has to satisfy $\lambda_\Phi \gtrsim 10^{-12}$ and the lower orange region is excluded by this condition.

The behavior of the purple lines in the most of panels can be understood by the IR freeze-in as discussed in Section 4.3.3, except the right-bottom one. The region $\lambda_\Phi \gtrsim 10^{-9}$ of that plot corresponds to the intermediate state between the IR and UV freeze-in, namely $T_R \sim m_\phi$, while the contribution to the relic from the inflaton decay is eventually dominant in this region. In case that the reheating temperature determined by the inflaton decay is much lower than the mediator mass m_ϕ, since the reheating temperature scales
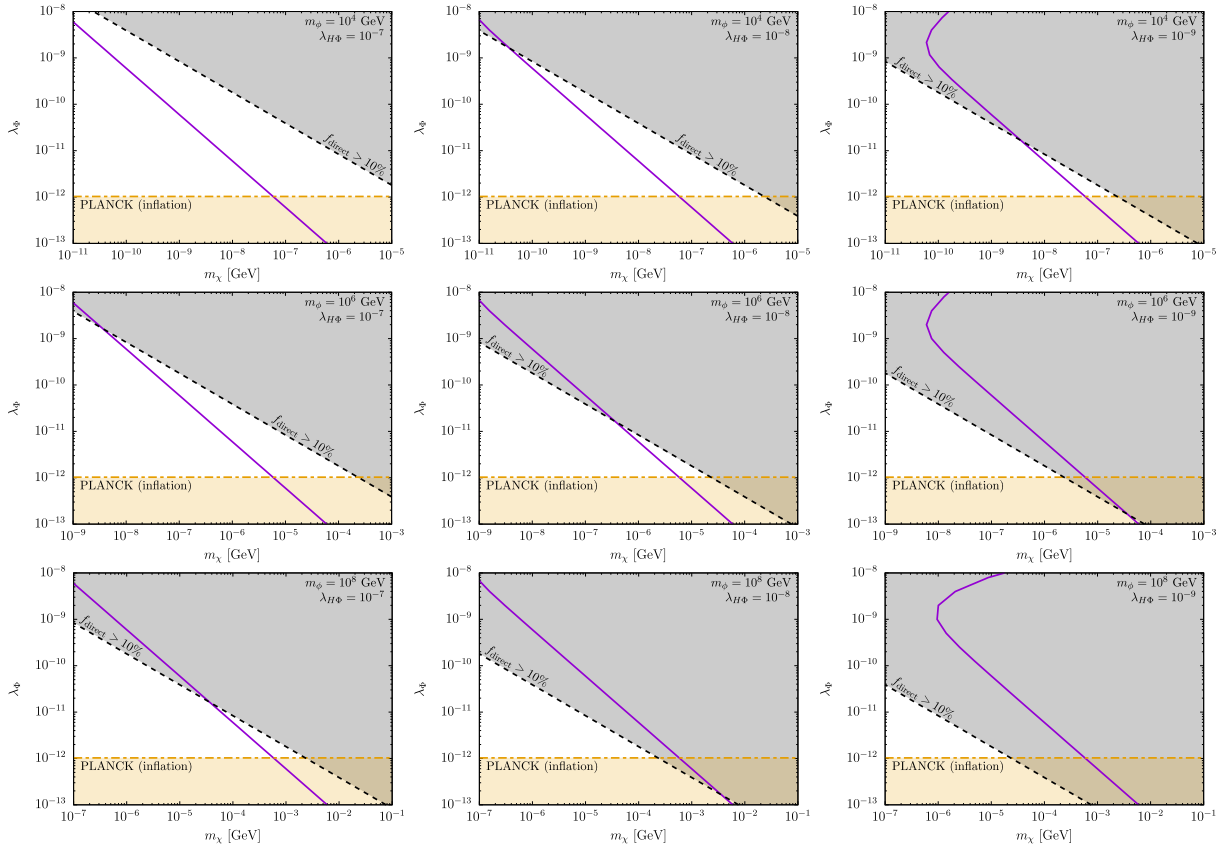
Figure 4.6: Parameter space in the (m_χ, λ_Φ) plane where the reheating of the universe is assumed to occur via the perturbative inflaton decay into the SM sector [ATY21]. The purple lines reproduce the correct relic abundance of dark matter only by the freeze-in production. The gray regions represent the parameter space that the dark matter abundance created by the inflaton decay is larger than 10 % of the observed value. The lower orange region cannot be consistent with the inflation observables at 2σ confidence level.
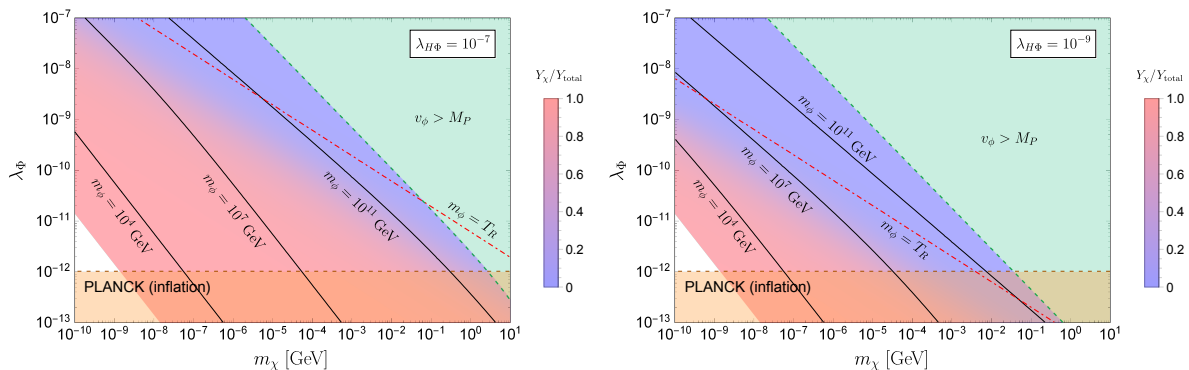
Figure 4.7: Parameter space in the (m_χ, λ_Φ) plane where the correct relic abundance of dark matter is realized by the non-thermal production (the freeze-in and the inflaton decay). The portal coupling is chosen as $\lambda_{H\Phi} = 10^{-7}$ (left) and $\lambda_{H\Phi} = 10^{-9}$ (right). The freeze-in production is dominant in the red region and the inflaton decay dominant in the blue region. The lower orange region is not consistent with the inflation observables as in Fig. 4.6. In the green region, the scalar VEV becomes trans-Planckian.

as $T_R \propto \lambda_{H\Phi} \lambda_\Phi^{-1/2} m_\phi^{1/2}$ which can be seen in Eq. (4.4.13), it finds that the self-coupling goes as $\lambda_\Phi \propto m_\chi^{2/3}$ to reproduce the correct relic abundance from Eq. (4.3.23) for the UV freeze-in. This behavior has been numerically checked in our computation.

Fig. 4.7 shows the parameter space in the (m_χ, λ_Φ) plane realizing the correct dark matter relic abundance via both contributions from the freeze-in and inflaton induced productions. The red and blue regions mean the abundance is dominated by the freeze-in and the inflaton, respectively. The red dot-dashed line denotes $m_\phi = T_R$. In the green region, the singlet scalar VEV (v_ϕ) becomes trans-Planckian, where the low-energy field description is not valid.[8] When the dark sector scalars ϕ and/or χ are heavy, the inflaton decay tends to be the dominant process for the dark matter creation. A physical implication of Fig. 4.7 is that in the pNGB dark matter model with large symmetry breaking, the dark matter should be lighter than MeV–GeV if the freeze-in production is assumed to be dominant. A heavier dark matter is also possible if taking the inflaton induced contribution into account.

In the above analysis, we have assumed that the reheating of the universe simply occurs via the inflaton perturbative decay to the Higgs field. However if there exists some other decay modes of the inflaton, the reheating temperature generally takes a different value. In this situation, the inflaton induced dark matter is estimated by

$$Y_\chi^{\text{inf}} \approx \frac{3\sqrt{30}}{128\pi^2} \frac{g_*^{1/2} \lambda_\Phi M_P}{g_*^S T_R} \sqrt{1 - \frac{4m_\chi^2}{m_\phi^2}}, \tag{4.4.15}$$

---

[8]When one considers graviton loop effect, its form may be $\frac{m^2}{16\pi^2 M_P^2}$ where m is a typical scale in low-energy theory. Therefore the low-energy perturbative description is violated above $m_P \simeq 4\pi M_P$. If one imposes the condition $v_\phi < m_P$ in Fig. 4.7, the green excluded region is relaxed by 4π.
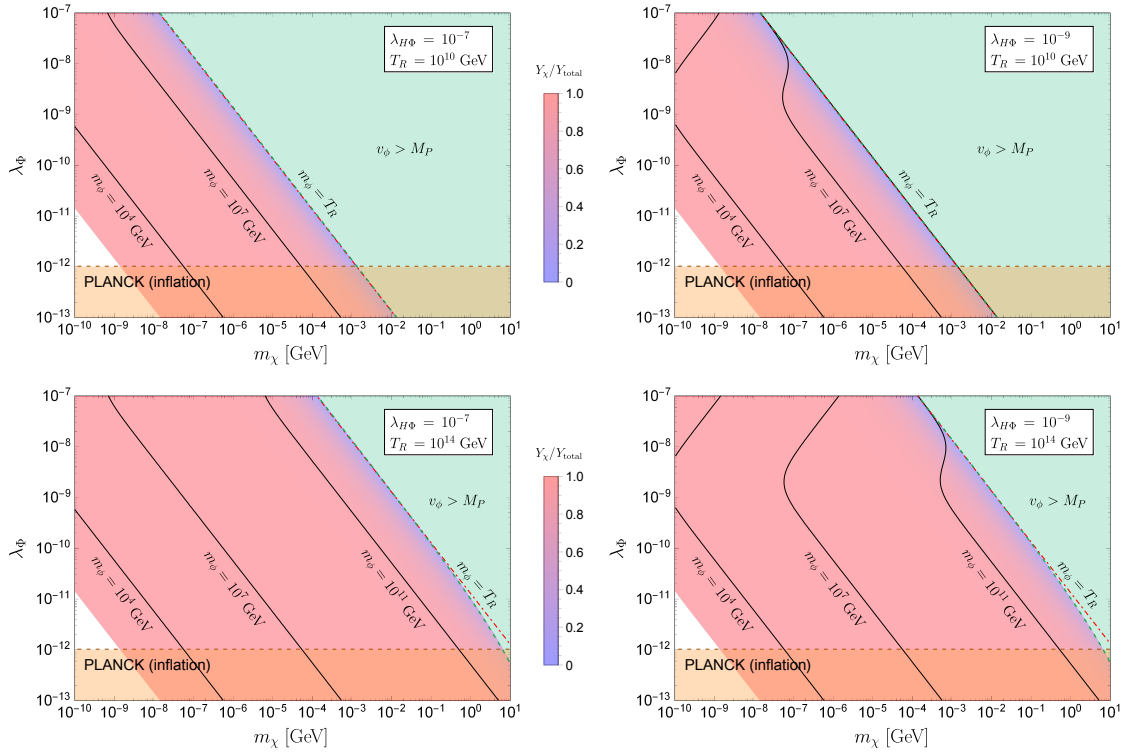
68

Figure 4.8: Same plots as Fig. 4.7 while the reheating temperature is taken to be a free parameter [ATY21]. The portal coupling is chosen as $\lambda_{H\Phi} = 10^{-7}$ (left) and 10^{-9} (right), and the reheating temperature is $T_R = 10^{10}$ GeV (above) and 10^{14} GeV (below).

which is independent of the Higgs portal coupling $\lambda_{H\Phi}$ and almost independent of m_ϕ for a relatively heavy ϕ. The pNGB abundance from the UV freeze-in is also implicitly changed since the parameter dependence of T_R is modified from Eq. (4.4.13) to a free parameter, though the formula of Y_D^{UV} is still valid. In the same fashion in Fig. 4.7, we draw the parameter space realizing the correct dark matter abundance via both of freeze-in and inflaton decay (Fig. 4.8). We find in almost all allowed regions the freeze-in production is dominant. This comes from the fact that the inflaton induced abundance Eq. (4.4.15) is almost insensitive to m_ϕ. Compared with Fig. 4.7, a heavier dark matter is possible up to $\mathcal{O}(10-100)$ GeV with a higher reheating temperature.

4.5   Summary

The pNGB dark matter model has been originally motivated from the fact that the strong constraint of direct detection can naturally be evaded even when it is a WIMP with sufficiently large couplings with the SM particles. On the other hand, the pNGB dark matter can also be regarded as a natural FIMP candidate if the VEV of the symmetry-breaking scalar is large enough. That is because all couplings of the pNGB are suppressed by the large VEV due to its NG property.

We have studied the model parameters for which the dark matter relic is reproduced by the feeble couplings of pNGB, taking into account the effect of thermal mass of the Higgs field. The dark matter relic abundance is mainly determined by the mediator mass and a smaller coupling of λ_Φ and $\lambda_{H\Phi}$ when the reheating temperature of the universe is larger than the mediator mass. On the contrary, the abundance depends on the reheating temperature if it is not large as the mediator mass. These feature are similar to typical FIMPs.

We have also investigated the possibility that the radial component of the symmetry-breaking scalar Φ plays a role of the inflaton. Introducing the non-minimal coupling of Φ to gravity, the flat potential is understood by the rescaling, and the parameter space consistent with the observations has been explored. We have found that the scalar self coupling is tiny $\lambda_\Phi \gtrsim 10^{-12}$ and the non-minimal coupling should be $\xi \gtrsim 10^{-2}$, which are rather different from the Higgs inflation scenario. Furthermore, it is important the inflaton decay into the pNGB is unavoidable. We have examined the allowed parameter regions taking into account both of the freeze-in and the inflaton decay. Combining these requirements for the dark matter relic and the successful inflation, it is found that the pNGB FIMP dark matter should be lighter than a few GeV when the freeze-in contribution is assumed to be dominant. A heavier pNGB dark matter with $\mathcal{O}(10^{1-2})$ GeV mass is possible if the inflaton-induced contribution comes to be effective and/or the reheating process depends on some other dynamics.

In the present model, since the pNGB dark matter is stable due to the $\mathbb{Z}_2$ symmetry: $\chi \mapsto -\chi$ coming from the CP invariance of the scalar potential, one may feel there

is no detectable signals from the pNGB dark matter with feeble couplings. However if the remnant symmetry is not exact as easily expected in a UV completion of the model [ATT20], the pNGB can decay into lighter SM particles. Even if its couplings are highly suppressed by the large VEV, some signals may be detectable in cosmic-ray observations. That is left for future study.

Appendix 4.A   Thermal mass contribution

Referring to [KP14], we summarize the derivation of thermal mass and its formula in the high temperature era.

We consider a field variable decomposed to the background configuration σ and its fluctuation ρ, and integrate out the latter. Then the one-loop effective potential for the background σ is given by

$$\mathcal{V}_{\text{eff}}^T(\sigma) = \mathcal{V}_0(\sigma) + \mathcal{V}_1(\sigma) + \mathcal{V}_1^T(\sigma; T), \tag{4.A.1}$$

where $\mathcal{V}_0(\sigma)$ is the classical potential for σ, and $\mathcal{V}_1(\sigma)$, $\mathcal{V}_1^T(\sigma)$ are the one-loop contributions. According to Refs. [DJ74, Wei74], the effective potential is evaluated on $\mathbb{R}^3 \times S^1$ with the radius $1/T$ in order to take the thermal effect into account.

The effective potential for a real scalar is expressed as

$$\mathcal{V}_{1B}(\sigma) = \int \frac{d^3 k}{(2\pi)^3} \frac{E_{\boldsymbol{k}}}{2}, \qquad \mathcal{V}_{1B}^T(\sigma; T) = \frac{T^4}{2\pi^2} J_B(M/T), \tag{4.A.2}$$

where $E_{\boldsymbol{k}}^2 = \boldsymbol{k}^2 + M^2$, and M denotes the ρ mass in the σ background. The mass M is typically given by $M^2 = M(\sigma)^2 = m_b^2 + \frac{\lambda}{2}\sigma^2$ for the ρ mass m_b and the scalar self quartic coupling λ. The function $J_B(y)$ is given by

$$J_B(y) = \int_0^\infty dx\, x^2 \log\left(1 - e^{-(x^2+y^2)^{1/2}}\right). \tag{4.A.3}$$

In the high-temperature region corresponding to $y \ll 1$, the function $J_B(y)$ is approximately written as

$$J_B(y) \approx -\frac{\pi^4}{45} + \frac{\pi^2}{12}y^2 - \frac{\pi}{6}y^3 - \frac{y^4}{32}\log\left(\frac{y^2}{a_B}\right), \tag{4.A.4}$$

with $a_B = \pi^2 e^{3/2 - 2\gamma_E}$ and γ_E is the Euler constant. The y^2 term contributes to the thermal mass.

For a Dirac fermion, the one-loop effective potential is given by

$$\mathcal{V}_{1F}(\sigma) = -4\int \frac{d^3 k}{(2\pi)^3} \frac{E_{\boldsymbol{k}}}{2}, \qquad \mathcal{V}_{1F}^T(\sigma; T) = -\frac{2T^4}{\pi^2} J_F(M/T), \tag{4.A.5}$$

with

$$J_F(y) = -\int_0^\infty dx\, x^2 \log\left(1 + e^{-(x^2+y^2)^{1/2}}\right). \tag{4.A.6}$$

The mass in the σ background is typically given by using a Yukawa coupling g as $M = M(\sigma) = m_f + g\frac{\sigma}{\sqrt{2}}$, for the fermion mass m_f. As in the bosonic case, the function $J_F(y)$ is approximately written as

$$J_F(y) \approx \frac{7\pi^4}{360} - \frac{\pi^2}{24}y^2 - \frac{y^4}{32}\log\left(\frac{y^4}{a_F}\right), \tag{4.A.7}$$

with $a_F = 16\pi^2 e^{3/2 - 2\gamma_E}$ in the high-temperature region corresponding to $y \ll 1$.

The thermal mass is defined from the one-loop effective potential $\mathcal{V}_1^T(\sigma; T)$ as

$$\Delta := \left.\frac{\partial^2 \mathcal{V}_1^T}{\partial \sigma^2}\right|_{\sigma=0}. \tag{4.A.8}$$

Using the above formulae, the thermal mass contributions of particle i are given by

$$\begin{cases} \Delta^B = g_i \frac{T^4}{2\pi^2}\frac{\pi^2}{12}\frac{M^2(\sigma)''}{T^2} = \frac{g_i T^2 M^2(\sigma)''}{24} & \text{for bosons} \\ \Delta^F = -g_i \frac{T^4}{2\pi^2}\left(\frac{-\pi^2}{24}\right)\frac{M^2(\sigma)''}{T^2} = \frac{g_i T^2 M^2(\sigma)''}{48} & \text{for fermions} \end{cases} \tag{4.A.9}$$

where g_i is the degrees of freedom of the particle i and the prime means the derivative with respect to σ.

For the SM Higgs boson, there are three sources of thermal mass; electroweak gauge bosons, quarks and leptons, and Higgs scalar. Applying the above result to the SM, the thermal mass contributions are found

$$\Delta_h^{\text{gauge}} = \frac{g_1^2}{16}T^2 + \frac{3g_2^2}{16}T^2, \tag{4.A.10}$$

$$\Delta_h^{\text{fermion}} = \frac{T^2}{12}\left[y_e^2 + y_\mu^2 + y_\tau^2 + 3\left(y_u^2 + y_d^2 + y_c^2 + y_s^2 + y_t^2 + y_b^2\right)\right] \approx \frac{y_t^2}{4}T^2, \tag{4.A.11}$$

$$\Delta_h^{\text{scalar}} = \frac{\lambda_H}{4}T^2. \tag{4.A.12}$$

Chapter 5

TeV-scale majorogenesis

5.1 Tev-scale Majoron dark matter and feeble interactions

Some cosmic-ray observations are known to suggest the existence of leptophilic TeV-scale dark matter. That motivates us to consider a TeV-scale Majoron dark matter, whose mass scale is heavier than those in previous works. The heavy Majoron can decay to neutrinos, which requires the SM singlet scalar VEV is around the unification scale. It can also decay to heavy quarks such as the top quark, and that imposes strong upper bound on the Yukawa couplings between the Majoron and the right-handed neutrinos. The Majoron interactions are too small to realize the dark matter relic abundance via the thermal freeze-out mechanism [ABD+20]. Hence the creation of Majoron dark matter (dubbed as Majorogenesis) at TeV scale should be realized in a way other than the freeze-out mechanism, such as the freeze-in production [HJMRW10].

In this chapter, we investigate the Majorogenesis for TeV-scale Majoron. We then consider the following three scenarios; (A) introducing explicit Majoron masses, (B) using the interaction with the SM Higgs doublet (C) using the resonant production from non-thermal right-handed neutrinos. All of these scenarios are found to have the parameter space compatible with the tiny Yukawa coupling and the dark matter relic abundance.

This chapter is organized as follows. In Section 5.2, we discuss the Majoron model and its phenomenological constraints from heavy Majoron dark matter decays. In Section 5.3, we show the difficulty of creating the heavy Majoron in the reference model, and then consider three ways to realize the TeV-scale Majorogenesis. In each case, we will evaluate the Majoron relic abundance and show the parameter space realizing the TeV-scale Majorogenesis. Section 5.4 is devoted to summarizing our results and discussing future work.

5.2 Majoron dark matter

5.2.1 The model

First of all, we consider the reference Majoron model for the following discussion. We introduce a new SM-singlet complex scalar which has the Yukawa coupling to right-handed neutrinos. The Lagrangian for the right-handed neutrinos ν_{Ri} are written as

$$\mathcal{L}_N = i\overline{\nu_{Ri}}\slashed{\partial}\nu_{Ri} - \frac{f_{ij}}{2}\Phi\overline{\nu_{Ri}^c}\nu_{Rj} - y_{\alpha i}^{\nu\dagger}\,\overline{L_\alpha}\tilde{H}\nu_{Ri} + \text{h.c.} \tag{5.2.1}$$

where the right-handed neutrinos and the new scalar Φ have the lepton number $+1$ and -2, respectively.[1] The neutrino Yukawa coupling $y_{\alpha i}^\nu$ gives the Dirac mass $m_D = y^\nu v/\sqrt{2}$ after the electroweak symmetry breaking, where v is the electroweak VEV $v \approx 246$ GeV. In addition, the new Yukawa coupling with Φ gives the Majorana mass $M_N = fv_\phi/\sqrt{2}$. Thus, the small masses for active neutrinos are generated by the type-I seesaw mechanism as $(m_\nu)_{\alpha\beta} \approx -(m_D)_{\alpha i}(M_N^{-1})_{ij}({}^t m_D)_{j\beta}$. We use Geek indices $\alpha, \beta, \ldots$ for the generation of the SM leptons and Latin indices $i, j, \ldots$ for the generation of the right-handed neutrinos here.

The scalar potential in the model is written as

$$\mathcal{V}(H, \Phi) = V_H(H) - \frac{\mu_\Phi^2}{2}|\Phi|^2 + \frac{\lambda_\Phi}{2}|\Phi|^4 - \frac{m^2}{4}\left(\Phi^2 + \Phi^{*2}\right), \tag{5.2.2}$$

where V_H is the Higgs potential in the SM (shonw in Eq. (A.2.2)) and the coupling between Φ and H will be taken into account in Section 5.3.3. The last quadratic term proportional to m^2 is the soft-breaking term to generate the pNGB mass. This term breaks the $U(1)_L$ symmetry of the scalar potential into $\mathbb{Z}_2$, which corresponds to $\Phi \mapsto -\Phi$.[2] For the potential stability, the quartic coupling satisfies $\lambda_\Phi > 0$. The scalar field develops a VEV v_ϕ, and is parametrized as

$$\Phi = \frac{v_\phi + \phi + i\chi}{\sqrt{2}}. \tag{5.2.3}$$

The stationary conditions are solved as $\mu_\Phi^2 = \lambda_\Phi v_\phi^2 - m^2$, and the scalar masses in the $U(1)_L$ breaking vacuum are given by

$$m_\phi^2 = \lambda_\Phi v_\phi^2, \quad m_\chi^2 = m^2. \tag{5.2.4}$$

The CP-odd component χ is a pNGB called as the Majoron, whose mass is given by the soft-breaking parameter m. In the following parts of this chapter, we will see that this Majoron can be a dark matter candidate.

---

[1] The NGB from this complex scalar field is eaten if the symmetry is gauged such as the gauged $U(1)_{B-L}$.

[2] The total Lagrangian with this soft-breaking term is invariant under the $\mathbb{Z}_4$ symmetry, which is the residual discrete symmetry of the global $U(1)_L$.
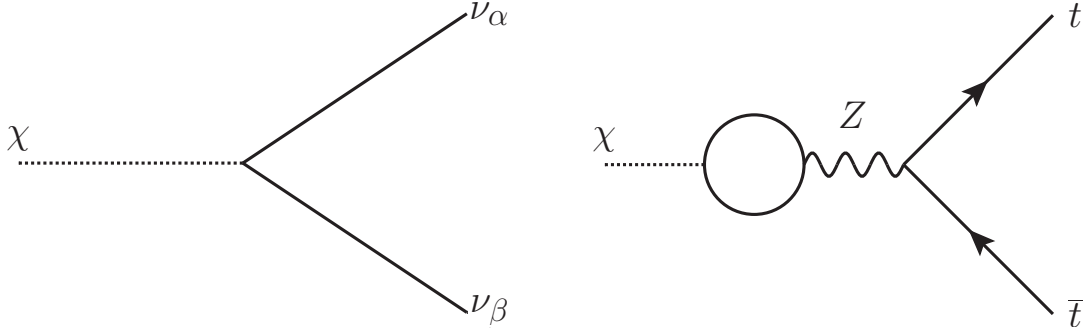
Figure 5.1: The Feynman diagrams for the dark matter decay processes [AHO+20]. (left): $\chi \to \nu_\alpha \nu_\beta$. (right): $\chi \to t\bar{t}$. The internal lines in the loop represent the active and heavy neutrinos.

In general, the Yukawa matrix f_{ij} in Eq. (5.2.1) can be diagonalized into $f_i \delta_{ij}$ by the redefinition of the right-handed neutrinos and the diagonal couplings f_i are taken to be real. The Majorana fermion in this mass basis is denoted by $N_i = \nu_{Ri} + \nu_{Ri}^c$, in which we denote the redefined right-handed neutrino as ν_{Ri}. The Lagrangian is rewritten using these Majorana fermions as

$$
\mathcal{L}_N = \frac{i}{2} \overline{N_i} \slashed{\partial} N_i - \frac{M_{N_i}}{2} \overline{N_i} N_i - \frac{f_i}{2\sqrt{2}} \phi \overline{N_i} N_i - \frac{i f_i}{2\sqrt{2}} \chi \overline{N_i} \gamma_5 N_i \\
- Y_{\alpha i}^{\nu\dagger} \overline{L_\alpha} \tilde{H} P_R N_i + \text{h.c.},
\tag{5.2.5}
$$

where $Y_{\alpha i}^\nu$ is the neutrino Yukawa matrix in the right-handed neutrino mass basis and $P_{R/L}$ is the chirality projection. An important point is that the flavor changing off-diagonal interaction between the Majoron and the right-handed neutrinos such as $\chi \overline{N_1} N_2$ disappears in the mass diagonal basis.

5.2.2 Decaying dark matter

In this subsection, we see features of the TeV-scale Majoron and the phenomenological constraints as the dark matter candidate. The Majoron is assumed to be lighter than the lightest right-handed neutrino to prevent it from decaying into the right-handed neutrinos. Otherwise, the Yukawa coupling f is required to be highly suppressed and/or the VEV v_ϕ must be huge due to astrophysical constraints.

The massive Majoron is unstable due to its interaction with right-handed neutrinos and the neutrino Yukawa couplings. The main decay channels are expressed by the Feynman diagrams of Fig. 5.1. The decay width to the neutrinos is given by

$$
\Gamma_{\chi \to \nu_\alpha \nu_\beta} = \frac{m_\chi}{16\pi v_\phi^2} \left| (m_\nu)_{\alpha\beta} \right|^2,
\tag{5.2.6}
$$

where $(m_\nu)_{\alpha\beta}$ is the neutrino mass matrix. To realize the long-lived dark matter, the VEV v_ϕ has a lower bound for a fixed value of the dark matter mass m_χ. The constraints on

the dark matter mass and lifetime for this decay mode are discussed e.g., in Refs. [PR08, CGIT10]. For example, the VEV v_ϕ is found to satisfy $v_\phi \gtrsim 10^{15}$ GeV for TeV-scale dark matter. In the following parts, we assume $v_\phi \approx 10^{15}$ GeV. In addition, the Majoron is so heavy that it can decay to (the top) quark pair through the one-loop diagram shown Fig. 5.1. As the width is generally proportional to the quark mass, the dominant radiative decay is given by $\chi \to t\bar{t}$, if possible, and its width is evaluated as

$$\Gamma_{\chi \to t\bar{t}} = \frac{3\alpha_W C_{\chi Z}^2}{8\cos^2\theta_W} \frac{m_\chi m_t^2}{m_Z^4} \sqrt{1 - \frac{4m_t^2}{m_\chi^2}}, \tag{5.2.7}$$

where m_t and m_Z are the masses of the top quark and the Z boson, respectively, and α_W is the fine structure constant of $SU(2)_L$ gauge coupling. The overall factor 3 comes from the summation of color indices of the final states. The neutrino loop factor connecting χ and Z is given by

$$C_{\chi Z} = \sum_{i,j} \frac{g|(m_D)_{ij}|^2}{16\pi^2 v_\phi \cos\theta_W} \int_0^1 dx \int_0^{1-x} dy \int_0^{1-x-y} dz \frac{F(2m_\chi^2/M_{N_i}^2)}{F(m_\chi^2/M_{N_i}^2)^2}, \tag{5.2.8}$$

where $F(\omega) := (x+y) + (y+z)(y+z-1)\omega$. The main decay modes of the Majoron are these $\chi \to \nu_\alpha \nu_\beta$, $\chi \to t\bar{t}$, and the model parameters are constrained by the cosmic-ray observations such as anti-protons and gamma-rays. The decay widths of the Majoron to other SM particles are much smaller, then the constraints are irrelevant.[3] In general, analyzing the constraints on the model parameters are very complicated due to many degrees of freedom and indeterminacy [IYY], which is beyond the scope of this chapter. In this chapter, we impose a conservative upper bound on the Yukawa coupling $f_i \lesssim 10^{-(10-11)}$ with reference to the past analysis, but the precise value of f_i is irrelevant to the Majoron creation.

From these results and analysis, we find the following three statements are inseparable in the TeV-scale Majoron dark matter model:

1. Light right-handed neutrinos with TeV-PeV-scale masses

2. Heavy Majoron feebly interacting with right-handed neutrinos

3. Large VEV of Φ around the unification scale

5.3 Dark matter creation: majorogenesis

In this section, we will show the difficulty to realize the dark matter relic abundance, and discuss some improved scenarios for the Majorogenesis to take place.

---

[3]In the case of the Majoron being light, see a previous work [GCH17] for the constraints from the Majoron decay.

5.3.1 Flaw and improvements of the model

As we have seen in the last section, the three conditions,

1. light right-handed neutrinos,

2. heavy Majoron,

3. large v_ϕ,

are inseparable when we consider a TeV-scale Majoron dark matter. In the model in Section 2, the Majoron couples to the SM particles only through the right-handed neutrinos and the coupling is too small to realize the freeze-out mechanism. Even if we introduce the mixing coupling such as $\lambda_{H\Phi}|H|^2|\Phi|^2$, it is hard for pNGB dark matter with the large VEV to realize the relic abundance as by the freeze-out mechanism [ABD+20]. Then another option to create the Majoron is the freeze-in mechanism discussed in Ref. [HJMRW10]. The magnitude of the coupling that is necessary for the freeze-in to work is typically $\mathcal{O}(10^{-11})$, and thus the tiny Yukawa couplings in the model of Section 2, $f_{ij} \lesssim \mathcal{O}(10^{-(10-11)})$, seem useful for the Majoron creation via the freeze-in. However, the Yukawa interaction between the Majoron and the right-handed neutrinos is flavor diagonal in the right-handed neutrino mass basis, and flavor changing off-diagonal interactions such as $\chi \overline{N_1} N_2$ are absent in the Lagrangian (see Eq. (5.2.5)). The other processes are too tiny to explain the relic abundance by the freeze-in mechanism. The scattering amplitude of the annihilation $NN \to \chi\chi$ via t-channel is proportional to f^2. In addition, the decay $N \to \chi\nu$ is highly suppressed by the neutrino mass on top of f. Therefore, it is impossible to realize the dark matter relic abundance by the freeze-in mechanism using the right-handed neutrino decay in that model. Here let us consider the following three scenarios to avoid this flaw.

(A): The first is to modify the universality of mass/coupling ratios for the pNGB Majoron. A simple way for this is to introduce Majorana masses for right-handed neutrinos, which break the $U(1)_L$ symmetry similarly to the soft breaking term for Φ. Then flavor changing couplings of the Majoron generally appear in the right-handed neutrino mass basis, and could lead to the freeze-in production of Majoron.

(B): The second is adding the mixing coupling between the SM Higgs H and the SM singlet scalar Φ such as $\lambda_{H\Phi}|H|^2|\Phi|^2$ to the scalar potential (5.2.2). The Majoron can interact with the SM Higgs via this coupling on top of neutrinos, but the typical magnitude of the interaction is also too small to realize the thermal relic because of the nature of NGB [RSW20] as we stated above. As an alternative option, we consider the freeze-in mechanism through this portal coupling.

(C): The third option is using a non-thermal creation of the right-handed neutrinos during the reheating after the cosmological inflation. The scattering process mediated by the CP-even scalar particle arising from Φ is essential to explain the dark matter relic abundance.
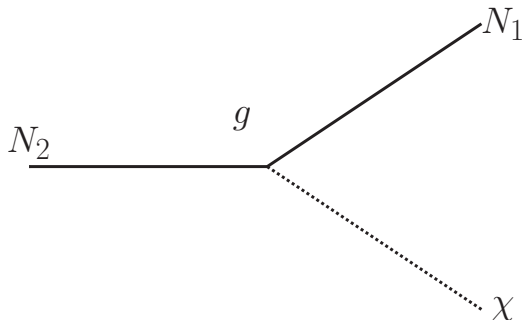
Figure 5.2: The Feynman diagram for Majorogenesis in the scenario (A) [AHO+20].

In the rest part of this section, we discuss the above three scenarios (A)–(C) and investigate the parameter space realizing the TeV-scale Majorogenesis for each case.

5.3.2 (A): Heavy right-handed neutrino decay

Let us consider the scenario (A), in which Majorana mass terms for the right-handed neutrinos are introduced:

$$\Delta \mathcal{L}_{\text{Majorana}} = -\frac{1}{2} m_{ij} \overline{\nu_{Ri}^c} \nu_{Rj} + \text{h.c.} \tag{5.3.1}$$

which enables the flavor changing interactions in the mass-diagonal basis. In this subsection, we consider only two right-handed neutrinos ($i = 1, 2$), or equivalently, we assume that one of the three is sufficiently heavy. Hereafter, we use g for the off-diagonal Yukawa interaction giving $\chi \overline{N_1} N_2$ vertex, which is assumed to have the constraint,

$$g \lesssim 10^{-10}, \tag{5.3.2}$$

as in the Majoron model.

The dark matter creation process is $N_2 \xrightarrow{g} N_1 \chi$ ($M_{N_2} > M_{N_1} + m_\chi$), which is shown in Fig. 5.2, and the decay width is given by

$$\Gamma_{N_2 \to N_1 \chi} = \frac{g^2 M_{N_2}}{32\pi} I\left(\frac{M_{N_1}}{M_{N_2}}, \frac{m_\chi}{M_{N_2}}\right), \tag{5.3.3}$$

where the function $I(x, y)$ is defined by $I(x, y) := [(1 - x)^2 - y^2]^{3/2} [(1 + x)^2 - y^2]^{1/2}$. On the other hand, the thermal creation process of the right-handed neutrinos are given by $N_i \longleftrightarrow L_\alpha H$ ($L_\alpha^c H^\dagger$), and the decay width is expressed as

$$\Gamma_{N_i \to \text{B}} = \frac{|Y_{\alpha i}^{\nu \dagger}|^2 M_{N_i}}{8\pi}. \tag{5.3.4}$$

The Boltzmann equations for the right-handed neutrinos and the Majoron are given by

$$\frac{dY_{N_2}(x)}{dx} = -\frac{\Gamma_{N_2 \to N_1 \chi}}{Hx} \frac{K_1(r_2 x)}{K_2(r_2 x)} Y_{N_2}(x)$$

$$-\frac{\Gamma_{N_2 \to \text{B}}}{Hx}\frac{K_1(r_2 x)}{K_2(r_2 x)}\left[Y_{N_2}(x) - Y_{N_2}^{\text{eq}}(r_2 x)\right], \tag{5.3.5}$$

$$\frac{dY_{N_1}(x)}{dx} = +\frac{\Gamma_{N_2 \to N_1 \chi}}{Hx}\frac{K_1(r_2 x)}{K_2(r_2 x)}Y_{N_2}(x)$$

$$-\frac{\Gamma_{N_1 \to \text{B}}}{Hx}\frac{K_1(r_1 x)}{K_2(r_1 x)}\left[Y_{N_1}(x) - Y_{N_1}^{\text{eq}}(r_1 x)\right], \tag{5.3.6}$$

$$\frac{dY_{\chi}(x)}{dx} = +\frac{\Gamma_{N_2 \to N_1 \chi}}{Hx}\frac{K_1(r_2 x)}{K_2(r_2 x)}Y_{N_2}(x), \tag{5.3.7}$$

where K_n is the modified Bessel function of the second kind. We introduce the dimensionless parameter x by $x := m_{\chi}/T$ for the temperature T and the mass ratios by $r_i := M_{N_i}/m_{\chi}$. The Hubble parameter and the entropy density are defined by Eq. (4.3.1) and $\dot{T} \approx -HT$ is used. The yield of a particle a is defined by $Y_a := n_a/s$ with the number density n_a. The function form of Y_X in the thermal equilibrium is given by

$$Y_X^{\text{eq}}(z) = g_X\left(\frac{45}{4\pi^4 g_*^S}\right)z^2 K_2(z), \tag{5.3.8}$$

with g_X being the number of the degrees of freedom for the particle X. We assume that the SM particles are always in the thermal bath and neglect the inverse decay $N_1\chi \to N_2$ because the contribution from this process is small.

Using Eqs. (5.3.5)–(5.3.7), we obtain

$$Y_{\chi}(\infty) = \int_{x_I}^{\infty} dx\,\frac{dY_{\chi}(x)}{dx}$$

$$= \frac{\Gamma_{N_2 \to N_1 \chi}\Gamma_{N_2 \to \text{B}}}{\Gamma_{N_2 \to N_1 \chi} + \Gamma_{N_2 \to \text{B}}}\int_{x_I}^{\infty} dx\,\frac{1}{Hx}\frac{K_1(r_2 x)}{K_2(r_2 x)}Y_{N_2}^{\text{eq}}(r_2 x), \tag{5.3.9}$$

where we have assumed $Y_{N_2}(x_I) = Y_{N_2}(\infty) = 0$. The integral Eq. (5.3.9) can be carried out approximately and the Majoron relic abundance is evaluated as

$$Y_{\chi}(\infty) \approx \left(\frac{\Gamma_{N_2 \to N_1 \chi}\Gamma_{N_2 \to \text{B}}}{\Gamma_{N_2 \to N_1 \chi} + \Gamma_{N_2 \to \text{B}}}\right)\frac{405\sqrt{5}}{8\pi^{9/2}g_*^S g_*^{1/2}}\frac{m_{\text{Pl}}}{M_{N_2}^2} \tag{5.3.10}$$

$$\approx \Gamma_{N_2 \to N_1 \chi}\frac{405\sqrt{5}}{8\pi^{9/2}g_*^S g_*^{1/2}}\frac{m_{\text{Pl}}}{M_{N_2}^2}, \tag{5.3.11}$$

where we have used $\Gamma_{N_2 \to N_1 \chi} \ll \Gamma_{N_2 \to \text{B}}$ and the explicit expressions of the Hubble parameter and the entropy density.

The time evolution of the yields are shown in Fig. 5.3. The masses for the particle contents are fixed as $M_{N_1} = 5$ TeV, $M_{N_2} = 20$ TeV and $m_{\chi} = 1$ TeV, and the off-diagonal Yukawa coupling is chosen as $g = 10^{-11}$. The decay parameter D_i is defined by the ratio of the decay width of $N_i \to$ SM to the Hubble parameter H as $D_i = \Gamma_{N_i \to \text{B}}/H(T = M_{N_i})$ and is related to the neutrino Yukawa couplings $Y_{\alpha i}^{\nu}$ (see Eq. (5.3.4)). In the left panel, the two decay parameters are unity, and then the right-handed neutrinos go into the
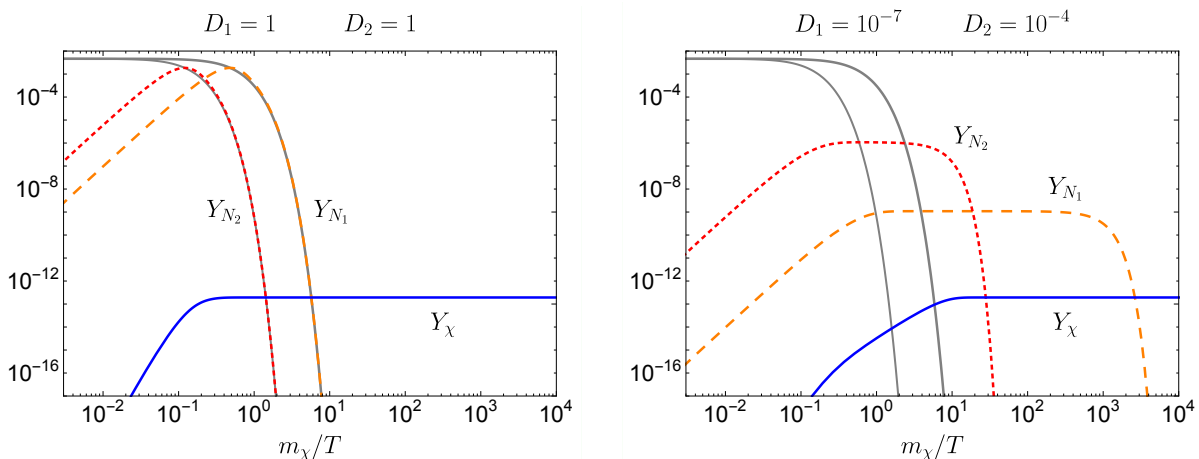
Figure 5.3: The solutions of the Boltzmann equations with the masses $M_{N_1} = 5$ TeV, $M_{N_2} = 20$ TeV, $m_\chi = 1$ TeV and the Yukawa coupling $g = 10^{-11}$ [AHO+20]. The black solid lines indicate the yields in the thermal equilibrium, $Y_{N_i}^{\text{eq}}$. The decay parameters $D_i = \Gamma_{N_i \to B}/H(T = M_{N_i})$ are changed. In the left panel, the decay parameters are unity. In the right panel, the decay parameters are hierarchical and tiny values.

thermal bath and the yields follow the thermal equilibrium distribution (black solid lines in the figure). In the right panel, the two decay parameters are too small to put Y_{N_i} into the thermal bath. It is interesting that the final result $Y_\chi(\infty)$ converges to the same value independently of the magnitudes of the neutrino Yukawa couplings $Y_{\alpha i}^\nu$, which is clear from Eq. (5.3.11). This is because, for small $Y_{\alpha i}^\nu$, the thermally induced amount of the right-handed neutrinos around their mass scale becomes small while the branching ratio decaying into the Majoron becomes large and these two effects are canceled out. In the thermal historical point of view, the independence of neutrino Yukawa couplings is understood by the fact that thermally induced N_2 is proportional to D_2 and the time interval where the decay $N_2 \to N_1 \chi$ is effective is inversely proportional to D_2.

Then the relic abundance of the Majoron is given by

$$
\begin{aligned}
\Omega_\chi h^2 &= \frac{m_\chi Y_\chi(\infty) s_0}{\varepsilon_{c,0}/h^2} \\
&\approx 0.1075 \times \left(\frac{g}{10^{-11}}\right)^2 \left(\frac{100}{g_*^S}\right) \left(\frac{100}{g_*}\right)^{1/2} \left(\frac{m_\chi}{1 \text{ TeV}}\right) \left(\frac{20 \text{ TeV}}{M_{N_2}}\right) I\left(\frac{M_{N_1}}{M_{N_2}}, \frac{m_\chi}{M_{N_2}}\right),
\end{aligned}
\tag{5.3.12}
$$

where $s_0 = 2891$ cm^{-3} is the today entropy density, and $\varepsilon_{c,0} = 5.16(h/0.7)^2$ GeV m^{-3} is the today critical energy density. The current observed value of dark matter abundance is $\Omega_{\text{darkmatter}} h^2 = 0.1200(12)$ [A+20b]. As we stated above, the relic abundance is independent of the neutrino Yukawa couplings $Y_{\alpha i}^\nu$.

In Fig. 5.4, we show the allowed parameter regions in (m_χ, g) and (M_{N_1}, M_{N_2}) planes. In the left panel, each line represents the parameter space realizing the dark matter relic
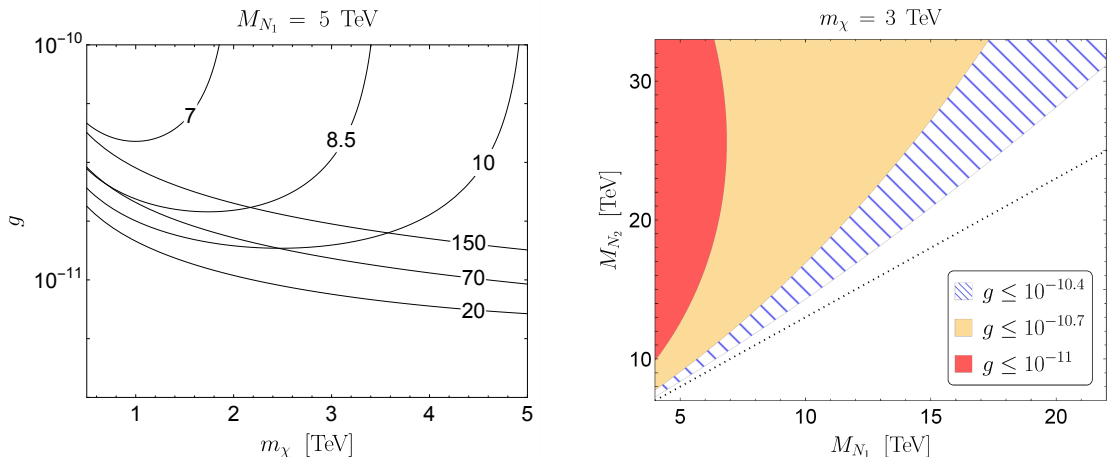
Figure 5.4: The allowed region to realize the dark matter relic abundance in (m_χ, g)- and (M_{N_1}, M_{N_2})-planes [AHO+20]. See the text for details.

abundance for several choices of M_{N_2} with M_{N_1} fixed as 5 TeV. Note that the stronger Yukawa coupling g is required for the smaller Majorana mass M_{N_2} since the phase factor $I(M_{N_1}/M_{N_2}, m_\chi/M_{N_2})$ becomes smaller. On the other hand, large g is also required for larger M_{N_2} because $I \sim 1$ and the relic abundance is inversely proportional to M_{N_2}. The allowed region regarding M_{N_2} as a free parameter is bounded from below by the critical line corresponding to $M_{N_2} \sim 20$ TeV. Thus the lower bound for g is around $g \sim 10^{-11}$. In the right panel, we show the allowed region with the dark matter mass $m_\chi = 3$ TeV and the Yukawa coupling $g \le 10^{-10.4}$, $10^{-10.7}$, 10^{-11}. If we take a severer bound for the off-diagonal Yukawa coupling $g \le 10^{-11}$ (red region in the figure), the lightest right-handed neutrino mass has to be in 3 TeV $\le M_{N_1} \le 7$ TeV, and the mass M_{N_2} has to be larger than 10 TeV.

Interestingly, the bound on g for this scenario to work is marginally comparable with the experimentally constrained upper bound Eq. (5.3.2). Therefore, the scenario (A) can be proved or excluded in the near future observations.

5.3.3   (B): Scalar potential interaction

Let us move to another scenario, in which we introduce the mixing coupling $\lambda_{H\Phi}|H|^2|\Phi|^2$. We consider the freeze-in creation of the Majoron in this model. The scalar potential is written as

$$\mathcal{V}(H, \Phi) = V_H(H) - \frac{\mu_\Phi^2}{2}|\Phi|^2 + \frac{\lambda_\Phi}{2}|\Phi|^4 + \lambda_{H\Phi}|H|^2|\Phi|^2 - \frac{m^2}{4}(\Phi^2 + \Phi^{*2}), \qquad (5.3.13)$$

and the conditions for the quartic couplings such that the potential is bounded from below are $\lambda_H > 0$, $\lambda_\Phi > 0$, $\sqrt{\lambda_H \lambda_\Phi} + \lambda_{H\Phi} > 0$. In addition, the quartic coupling λ_Φ has the upper bound $8\pi/3$ from the perturbative unitarity as discussed in Ref. [CDL15]. The
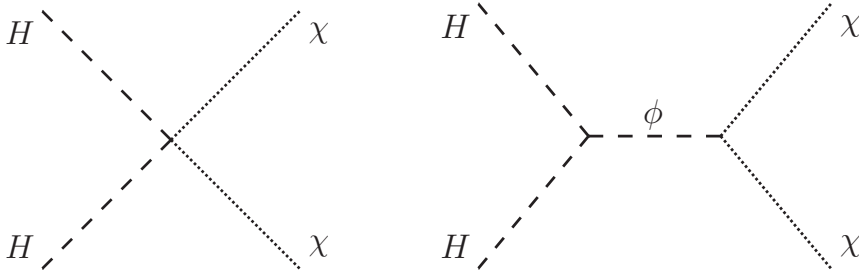
Figure 5.5: The Feynman diagrams for the Majorogenesis in the scenario (B) [AHO+20]. The contact type interaction in the left panel is canceled by the low-energy contribution from the scalar mediated interaction in the right panel.

quartic coupling $\lambda_{H\Phi}$ is also constrained by the bound of the mixing angle between the CP-even components [FGL15].

One important feature of the Majoron is a cancellation due to the nature of NGB in two-body scattering processes such as Fig. 5.5. The contribution from the contact type four-point interaction (left panel) is canceled by the one from the ϕ-mediated interaction (right panel) in the soft limit, and the remaining value is suppressed by the large decay constant. Indeed, the leading contribution after the cancellation comes from the portal energy in the propagator, which is written as

$$i\mathcal{M}(H^\dagger H \to \chi\chi)(s) = -i\frac{\lambda_{H\Phi}}{s - m_\phi^2}s, \tag{5.3.14}$$

where s is the Mandelstam's s variable and $m_\phi^2 = \lambda_\Phi v_\phi^2$ is the mass of ϕ. This is consistent with the result implied by the soft-pion theorem, and is easily understood in the non-linear representation:

$$\Phi = \frac{v_\phi + \phi}{\sqrt{2}}e^{i\pi/v_\phi}. \tag{5.3.15}$$

The phase field π is the Majoron in this representation and is the same as χ to the leading order of $1/v_\phi$. We have the following interaction vertices in the Lagrangian:

$$\mathcal{L}_{\text{int}} \ni \frac{\phi}{v_\phi}\left[(\partial_\mu\pi)^2 - m_\chi^2\pi^2\right] - \lambda_{H\Phi}v_\phi\phi|H|^2, \tag{5.3.16}$$

where the derivative coupling between the (p)NGB π and the CP-even scalar particle ϕ has come from the kinetic term of Φ. The scattering amplitude for $HH \to \pi\pi$ evaluated from this interaction Lagrangian Eq. (5.3.16) is the same as Eq. (5.3.14), which is now given by a single diagram like the right-panel of Fig. 5.5 and the energy (s) dependence originates from the derivative coupling.

The Boltzmann equation for the Majoron dark matter is given by

$$\frac{dY_\chi(x)}{dx} = \frac{2}{sHx}\gamma^{\chi\chi}{}_{H^\dagger H}, \tag{5.3.17}$$
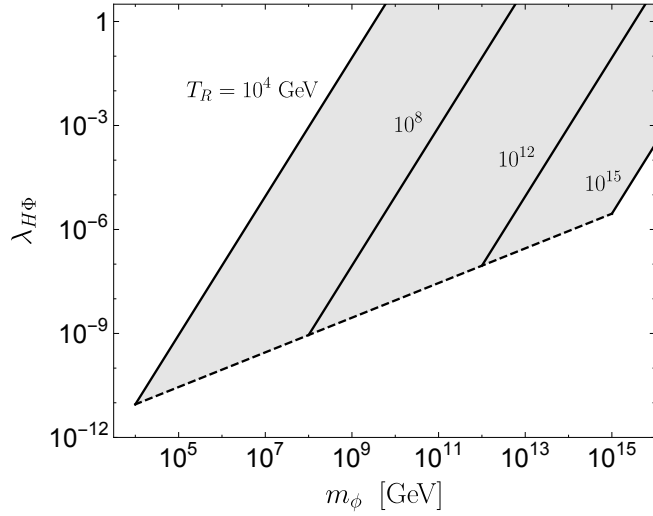
82

Figure 5.6: The parameter space in the $(m_\phi, \lambda_{H\Phi})$ plane explaining the dark matter relic by the TeV scale Majoron [AHO$^+$20]. See the text for details.

where $\gamma^{\chi\chi}{}_{H^\dagger H}$ is the interaction density defined by

$$\gamma^{\chi\chi}{}_{H^\dagger H} := \frac{4}{2!2!} \frac{T\lambda_{H\Phi}^2}{2^9\pi^5} \int_{4m_\chi^2}^\infty ds \sqrt{s - 4m_\chi^2} K_1(\sqrt{s}/T) \frac{s^2}{(s - m_\phi^2)^2}. \tag{5.3.18}$$

The prefactor 4 comes from the degrees of freedom of the Higgs doublet in the symmetric phase. We integrate the Boltzmann equation with the initial condition $Y_\chi(x_R) = 0$, then the Majoron abundance can be analytically evaluated as

$$\Omega_\chi h^2 \approx 1.5 \times 10^{25} \text{ GeV} \left(\frac{100}{g_*^S}\right) \left(\frac{100}{g_*}\right)^{1/2} \left(\frac{m_\chi}{1 \text{ TeV}}\right) \frac{\lambda_{H\Phi}^2 T_R^3}{m_\phi^4}, \tag{5.3.19}$$

where T_R is the reheating temperature satisfying $x_R := m_\chi/T_R$. In Eq. (5.3.19), we have assumed that m_ϕ is larger than the reheating temperature. Due to the energy dependence of the amplitude (5.3.14) and the heavy portal scalar, the relic abundance is dominated by the contribution from the UV-region unlike the previous case (A) and depends on the reheating temperature T_R, which arises from the UV physics. A similar type of freeze-in effect is discussed in the context of higher dimensional operators [HJMRW10].

In Fig. 5.6, we show the allowed region in the $(m_\phi, \lambda_{H\Phi})$ plane. Each solid line represents the parameter space realizing the dark matter relic abundance and the region above each line for T_R being fixed is excluded by the over creation. The dashed line means the case $m_\phi = T_R$, and the region below this line is not valid because we assumed that the mass of ϕ is larger than the reheating temperature such that ϕ is inactive in thermal evolution after the reheating. The shaded region shows the parameter space in which the dark matter relic abundance is realized regarding the reheating temperature as a free parameter. The region of m_ϕ is taken as 10^4 GeV $\leq m_\phi \leq 10^{15}$ GeV. We note the
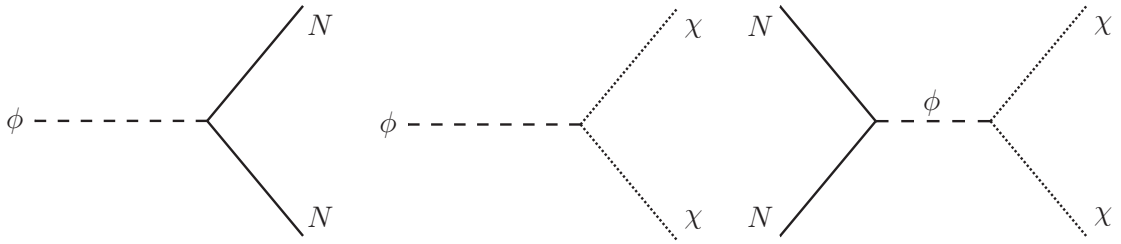
Figure 5.7: The Feynman diagrams for the Majorogenesis in the scenario (C) [AHO$^+$20].

VEV v_ϕ is large for the TeV-scale Majoron and the constraint from the mixing among the CP-even components is negligible due to the suppression by v_ϕ.

We here give a comment on other previous work. The portal-like coupling of pNGB has also been discussed in various contexts, e.g., Refs. [GMS10, QS14]. The existence of the contact type interaction by the quartic coupling $\lambda_{H\Phi}$ is usually assumed, but that is canceled by heavy scalar mediated contribution, as stated above. Consequently, it seems that the thermal freeze-out creation and collider search of the pNGB dark matter are inaccessible in case of the large decay constant.

5.3.4 (C): Resonant creation from non-thermal source

Let us consider the third scenario that the Majoron dark matter is created by the right-handed neutrino annihilation process mediated by the heavy CP-even scalar ϕ. We here assume that the mass m_ϕ is smaller than the reheating temperature T_R so that ϕ plays an important role in the thermal history of the universe. In this subsection, we consider the case of one generation right-handed neutrino for simplicity, but the generalization to three generations right-handed neutrino is straightforward.

We further assume that the right-handed neutrino has a Yukawa coupling to the inflaton field φ with mass m_φ. This coupling generates the right-handed neutrinos non-thermally during the reheating, and the yield at T_R is evaluated as

$$Y_N = \frac{3}{2}\frac{T_R}{m_\varphi}\mathrm{Br}(\varphi \to NN). \tag{5.3.20}$$

Here $\mathrm{Br}(\varphi \to NN)$ is the branching ratio of $\varphi \to NN$ process, which is given by $\Gamma_{\varphi \to NN}/\Gamma_\varphi$ with Γ_φ being the total decay width of the inflaton. The reheating temperature T_R is defined by $H(T = T_R) = \Gamma_\varphi$.

The right-handed neutrinos created by the inflaton can annihilate into the Majoron through the scattering process mediated by ϕ: $NN \overset{\phi}{\longleftrightarrow} \chi\chi$ as shown by Fig. 5.7. The Yukawa coupling f corresponding to $\phi\overline{N}N$ should be small from astrophysical constraints, and the three point coupling $\phi\chi\chi$ is also suppressed. As we will see in the following, even for these tiny couplings, a sufficient amount of the Majoron dark matter can be generated with the resonant contribution of ϕ. The partial decay widths of ϕ to right-handed
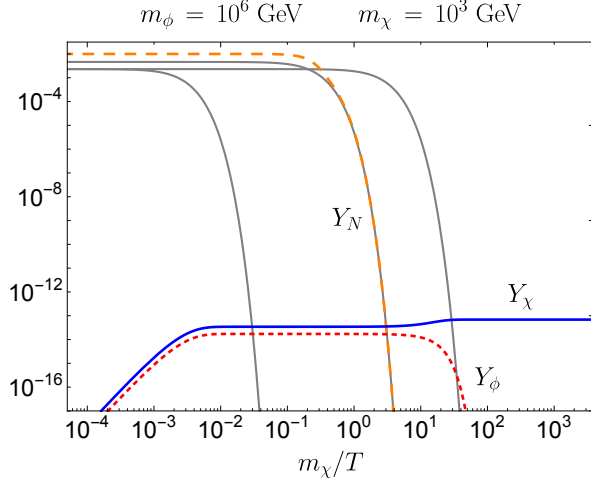
Figure 5.8: The solution of the Boltzmann equations with $m_\phi = 10^6$ GeV, $m_\chi = 10^3$ GeV and the initial value of the right-handed neutrino yield $Y_N(x_R) = 10^{-2}$ [AHO+20]. The right-handed neutrino mass is fixed as $M_N = 10^4$ GeV, but the dark matter abundance $Y_\chi(\infty)$ does not depend on it.

neutrinos and Majoron

$$\Gamma_{\phi \to NN} = \frac{f^2 m_\phi}{32\pi} \left[1 - \frac{4M_N^2}{m_\phi^2} \right]^{3/2}, \quad \Gamma_{\phi \to \chi\chi} = \frac{\lambda_\Phi m_\phi}{32\pi} \left[1 - \frac{4m_\chi^2}{m_\phi^2} \right]^{1/2}. \tag{5.3.21}$$

The contribution to the Boltzmann equations from the ϕ portal annihilation process, $NN \overset{\phi}{\to} \chi\chi$, is evaluated as

$$\gamma^{NN}{}_{\chi\chi} = \frac{\lambda_\Phi f^2 T}{2^{11} \pi^5} \int_{4M_N^2}^\infty ds \, \frac{(s - 4M_N^2)^{3/2} (s - 4m_\chi^2)^{1/2}}{s^{1/2} (s - m_\phi^2)^2} K_1(\sqrt{s}/T)$$

$$\approx \frac{f^2 m_\phi^3 T}{2^6 \pi^3} \left[1 - \frac{4M_N^2}{m_\phi^2} \right]^{3/2} K_1(m_\phi/T), \tag{5.3.22}$$

where we use the narrow width approximation.

The Boltzmann equations for the Majorogenesis in this system are expressed as

$$\frac{dY_N(x)}{dx} = 2 \frac{\Gamma_{\phi \to NN}}{Hx} \frac{K_1(r_\phi x)}{K_2(r_\phi x)} Y_\phi^{\text{eq}}(r_\phi x) \left[\frac{Y_\phi(x)}{Y_\phi^{\text{eq}}(r_\phi x)} - \left(\frac{Y_N(x)}{Y_N^{\text{eq}}(rx)} \right)^2 \right]$$

$$- \frac{2}{Hsx} \gamma^{NN}{}_{\chi\chi} \left(\frac{Y_N(x)}{Y_N^{\text{eq}}(rx)} \right)^2 - \frac{\Gamma_{N \to B}}{Hx} \frac{K_1(rx)}{K_2(rx)} \left[Y_N(x) - Y_N^{\text{eq}}(rx) \right], \tag{5.3.23}$$

$$\frac{dY_\phi(x)}{dx} = - \frac{\Gamma_{\phi \to NN}}{Hx} \frac{K_1(r_\phi x)}{K_2(r_\phi x)} Y_\phi^{\text{eq}}(r_\phi x) \left[\frac{Y_\phi(x)}{Y_\phi^{\text{eq}}(r_\phi x)} - \left(\frac{Y_N(x)}{Y_N^{\text{eq}}(rx)} \right)^2 \right]$$

$$- \frac{\Gamma_{\phi \to \chi\chi}}{Hx} \frac{K_1(r_\phi x)}{K_2(r_\phi x)} Y_\phi(x), \tag{5.3.24}$$

$$\frac{dY_\chi(x)}{dx} = 2 \frac{\Gamma_{\phi \to \chi\chi}}{Hx} \frac{K_1(r_\phi x)}{K_2(r_\phi x)} Y_\phi(x) + \frac{2}{Hsx} \gamma^{NN}{}_{\chi\chi} \left(\frac{Y_N(x)}{Y_N^{\text{eq}}(rx)} \right)^2, \tag{5.3.25}$$
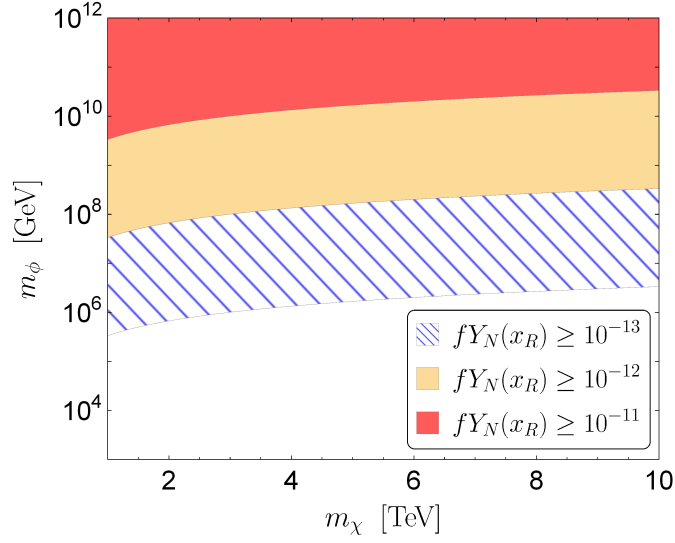
Figure 5.9: The allowed region in (m_χ, m_ϕ) plane when the initial yield of the right-handed neutrino is given [AHO+20]. The initial yield is fixed as $fY_N(x_R) \geq 10^{-13}$, 10^{-12}, 10^{-11}, and the small ϕ mass is favored.

where we have assumed that the SM particles are in the thermal bath. r_ϕ and r are defined as $r_\phi := m_\phi/m_\chi$ and $r := M_N/m_\chi$, respectively. The relic density of the Majoron dark matter is found by solving these equations and evaluated approximately as

$$Y_\chi(\infty) \approx \frac{f^2 m_\phi}{16\pi} \left(1 - \frac{4M_N^2}{m_\phi^2}\right)^{3/2} \int_{x_R}^\infty dx \, \frac{2}{Hx} \frac{K_1(r_\phi x)}{K_2(r_\phi x)} Y_\phi^{\mathrm{eq}}(r_\phi x) \left(\frac{Y_N(x)}{Y_N^{\mathrm{eq}}(rx)}\right)^2, \quad (5.3.26)$$

where we have used the boundary conditions $Y_\phi(x_R) = Y_\chi(x_R) = Y_N(\infty) = Y_\phi(\infty) = 0$. The final result is given by

$$Y_\chi(\infty) \approx \frac{\pi^{5/2} g_*^S}{128\sqrt{5} g_*^{1/2}} \frac{m_{\mathrm{Pl}}}{m_\phi} f^2 Y_N(x_R)^2. \quad (5.3.27)$$

The relic abundance of the Majoron dark matter is evaluated as

$$\Omega_\chi h^2 \approx 4.02 \times 10^{27} \left(\frac{100}{g_*^S}\right) \left(\frac{100}{g_*}\right)^{1/2} \frac{m_\chi}{m_\phi} f^2 Y_N(x_R)^2. \quad (5.3.28)$$

This result depends on the Yukawa coupling f, the scalar mass m_ϕ, and the initial amount of right-handed neutrinos, but is independent of the right-handed neutrino mass.

The time evolution of the yields are shown in Fig. 5.8, in which the masses are fixed as $m_\phi = 10^6$ GeV, $m_\chi = 10^3$ GeV and $M_N = 10^4$ GeV. The yield Y_N initially created by the inflaton decay is large and remains the constant for $T \gtrsim m_\phi$, during which ϕ and Majoron are generated through the decay and scattering processes. After the creation of Majoron dark matter by this process, the relic abundance is frozen-in at the temperature

just below m_ϕ.[4] On the other hand, the heavy scalar ϕ similarly created by the N decay finally disappears after the $\phi \to \chi\chi$ process becomes effective in the thermal history.

In Fig. 5.9, we show the allowed region in (m_χ, m_ϕ) plane with the initial yield $fY_N(x_R) \geq 10^{-11}$, 10^{-12}, 10^{-13}. A smaller ϕ mass is favored to realize the dark matter relic abundance. The figure shows that a tiny value of the coupling f is compatible with the observations, while that depends on the other parameters.

5.4 Summary

We have studied the scenarios where the Majoron, a pNGB of lepton number symmetry with TeV-scale mass, can be the dark matter of the universe. Since the decay constant of the Majoron is large and the coupling to the SM is tiny, it is nontrivial how to create the Majoron in the early universe, called Majorogenesis. The Majoron model can realize neither freeze-out nor freeze-in production of the Majoron dark matter with the large VEV because the Majoron couplings to the SM particles are tiny and the Yukawa couplings to the right-handed neutrinos are flavor-diagonal in the mass basis of the right-handed neutrinos. To avoid this flaw, we have discussed three scenarios (A)–(C) for Majorogenesis via the freeze-in mechanism; (A) introducing explicit Majorana masses, (B) using the interaction with the SM Higgs doublet, (C) using the resonant production from the non-thermally induced right-handed neutrinos.

In (A), we find the lower bound on the Majoron Yukawa coupling for the freeze-in Majorogenesis to work, and the bound is roughly comparable with the tiny value of Yukawa coupling constrained from astrophysics. Therefore, this scenario could be proved or excluded in the near future observations such as Cherenkov Telescope Array (CTA) [C+16] and IceCube Neutrino Observatory [A+19b].

In (B), the toal coupling between the Majoron and the SM Higgs is found to be canceled and suppressed by the large mass scale, and is useful to create the Majoron via the freeze-in mechanism. Note that this scenario is quite general because we have used only the fact that χ is the pNGB having the large VEV and the mixing coupling to the SM Higgs.

In (C), the sufficient amount of right-handed neutrinos are produced by the decay of the inflaton during the reheating. After that, the ϕ-mediated $NN\chi\chi$ interaction, whose magnitude is constrained by cosmic-ray observations, can be used to realize the freeze-in production.

In all the scenarios (A)–(C), there are the parameter regions realizing the dark matter relic abundance and avoiding the astrophysical constraints. Therefore, the Majoron with the TeV-scale mass (or heavier) can play the role of dark matter in the universe.

---

[4]The relic abundance of the Majoron could be slightly changed by thermalized right-handed neutrinos. However, it is not large effect unless m_ϕ is close to M_N.

For further study, it may be intersting to examine the leptogenesis [FY86] in these scenarios. A straightforward way is using resonances between the right-handed neutrinos [PU04]. A more challenging is introducing other particles whose masses are at an intermediate scale between v and v_ϕ. One can use radiative decay processes of right-handed neutrinos where the new particles appear in the loop to generate lepton asymmetry. This motivates us to consider an extension in which one more SM-singlet $U(1)_L$-charged scalar is added. Whether such type of leptogenesis can be compatible with the TeV-scale Majorogeneis is left for future work.

Chapter 6

Electroweak axion string and superconductivity

6.1 Strong CP problem, axions and axion strings

In the Quantum Chromodynamics (QCD) sector, the general Lagrangian is given by

$$\mathcal{L}_{\text{QCD}} = -\frac{1}{2g_s^2} \text{tr}(G_{\mu\nu})^2 + \frac{i\theta}{8\pi^2} \text{tr}(G_{\mu\nu}\tilde{G}^{\mu\nu}) + \mathcal{L}_{\text{matter}}, \tag{6.1.1}$$

where $G_{\mu\nu}$ denotes the field strength of the Gluon field and $\tilde{G}^{\mu\nu} = \frac{1}{2}\epsilon^{\mu\nu\rho\sigma}G_{\mu\nu}$. The second term is the CP violating term, which is called θ-term and $\theta \in [0, 2\pi]$. The non-vanishing θ value leads the non-trivial electric dipole moment of the neutron, but the observed value is highly suppressed $|d_n| < 2.9 \times 10^{-26} \, e$ cm [B$^+$06] and the constraint on the θ parameter is typically given by $|\theta| \lesssim 10^{-10}$ [H$^+$99]. While there is no reason in QCD, the the value of *theta* is fine tunned, this is known as the strong CP problem.

This strong CP problem is one of the unresolved mysteries in SM. The problem can be naturally solved by the Peccei-Quinn (PQ) mechanism, in which a global symmetry denoted by $U(1)_{\text{PQ}}$ is assumed to be spontaneously broken and provides a pNGB, the axion [PQ77a, PQ77b, Wei78, Wil78]. In other words, the PQ mechanism solves the strong CP problem dynamically by promoting the parameter θ to a scalar field. The axion is a promising candidate for a viable cold dark matter [PWW83, AS83, DF83].

Among various models bringing the axion (for recent reviews, see, e.g., Refs. [Sik08, Mar16, Rin12, WS10, KC10]), the DFSZ model [Zhi80, DFS81] has been studied extensively, as well as the KSVZ model [Kim79, SVZ80]. In the DFSZ model, the scalar sector of the SM is extended to have two Higgs doublets and one SM-singlet complex scalar. The scalar fields and the SM fermions are assumed to be charged under the $U(1)_{\text{PQ}}$ symmetry, which is spontaneously broken by a VEV of the complex scalar. The axion is a linear combination of imaginary components of the doublets and the complex scalar.

The $U(1)_{\text{PQ}}$ symmetry in the DFSZ model is anomalous due to one-loop contributions from the SM fermions and is broken down to a discrete subgroup $\mathbb{Z}_3$ (or $\mathbb{Z}_6$), which

produces a domain wall at the QCD phase transition. The energy density of the domain walls dominate soon that of the universe, leading to the domain wall problem. One possible scenario to solve the problem is to assume that the $U(1)_{\rm PQ}$ symmetry is broken during or before the cosmological inflation. There exists, however, a stringent constraint on isocurvature perturbation produced by the axion during the inflation [A$^+$20c]. Another simple way is introducing a tiny term breaking the symmetry explicitly, called the bias [GGK89, LSW97], which resolves the vacuum degeneracy [Sik82, CHS99, Vil81]. For other scenarios and their studies, see, e.g., Refs. [PWY86, KW86, LS82, CHN20, KTY16, STY18].

As well as most axion models enjoying the $U(1)_{\rm PQ}$ symmetry, the DFSZ model predicts the axion string [Dav86], which is a global cosmic string. The axion string is created by the Kibble-Zurek mechanism [Kib80, Zur85] (see also Ref. [MS10]) when the $U(1)_{\rm PQ}$ symmetry is spontaneously broken. For the scenario that the domain wall problem is avoided by the inflation, the axion strings are diluted away and seem to play no role in cosmology. But for the other scenarios, they become interesting ingredients in the universe and have been studied in various contexts (see Ref. [VS00]). We assume the latter scenarios in this chapter. After the creation, the strings form a network whose energy density has a scaling property. To understand the evolution of the network, it is important to study the interaction between the axion strings. The interaction is thought to be dominated by exchange of the (massless) axion as a long-range force.

On the other hand, cosmic strings sometimes can be superconducting strings [Wit85] when the electromagnetic gauge symmetry is spontaneously broken inside the strings. It is known that the axion strings necessarily become superconducting states [LS85, Iwa97, GL89, LPS88] because they must have fermionic zero modes traveling on the string [JR81, CH85]. The maximum amount of the supercurrent is determined by the (bulk) mass of the fermions. In the DFSZ model, however, the axion string cannot carry significant amount of the current because the model has no heavy fermion. Thus, the superconductivity seems to play no crucial role for cosmological properties.

In this chapter, we show that the axion string in the DFSZ model becomes the electroweak string after the breaking of the electroweak symmetry. The electroweak string is a string containing flux tubes of the $SU(2)_L \times U(1)_Y$ gauge fields like the Abrikosov-Nielsen-Olesen vortex [Abr57, NO73] and has been studied in the SM [Nam77, Vac93, Vac92, JPV92, JPV93, VF94, BVB94, Bar95, EKNO13] (see Ref. [AV00] for review), and in two Higgs doublet models (2HDM) [Per93, La93, DS93, DS94, BL94, BRT99, Iva08, BBP11, EHKN20b, EHKN20a] (for recent comprehensive studies, see Refs. [EKN18a, EKN18b]). An essence is that the two Higgs doublets in the DFSZ model also acquire the VEVs after the electroweak phase transition and they must have winding in the $SU(2)_L \times U(1)_Y$ gauge orbits for the single-valuedness, as well as the winding for $U(1)_{\rm PQ}$. We call such strings *the electroweak axion strings*. In particular, we show that there are at least three types of the electroweak axion string in the DFSZ model. Interestingly, some of them have very similar properties to those of the electroweak string in 2HDM.

	H_1	H_2	S
$SU(2)_L$	**2**	**2**	**1**
$U(1)_Y$	1	1	0
$U(1)_{\mathrm{PQ}}$	X_1	X_2	X_s

Table 6.1: The scalar field contents and their quantum charges.

Furthermore, we show that one of the electroweak axion strings (dubbed the type-C string) can be a superconducting string *without* fermionic fields. This is because the charged fields, the charged Higgs and W bosons, acquire non-zero values inside the string and the $U(1)_{\mathrm{EM}}$ symmetry is spontaneously broken there. This is a similar situation to superconductivity of non-Abelian vortices [ABC$^+$90, ABC$^+$91] and of the $U(1) \times \tilde{U}(1)$ model considered by Witten [Wit85]. Remarkably, due to the coupling between the Higgs doublets and the complex scalar, the amount of the supercurrent can be of order of the $U(1)_{\mathrm{PQ}}$ breaking scale resulting in large magnetic energy even in the DFSZ model. As a consequence, the strings feel a large magnetic interaction, which can overcome the one from the axion exchange. Therefore, superconductivity could drastically change the cosmological scenario of the axion strings after the electroweak phase transition in the DFSZ model.

The rest of this chapter is organized as follows. In Section 6.2, the DFSZ axion model is reviewed and our notation is introduced. For later use, we present a definition of the $U(1)_{\mathrm{EM}}$ in general soliton backgrounds. In Section 6.3, after a brief review of the conventional axion string, we discuss the electroweak axion strings. There are at least three types of the electroweak axion strings (type-A, B and C). We compare the tensions of the strings. In Section 6.4, we show that the type-C string can be superconducting. A linearized equation of motion for massless zero modes traveling on the string is presented. In addition, we estimate the maximum amount of the supercurrent flowing on the string to be of order of the $U(1)_{\mathrm{PQ}}$ breaking scale. Section 6.5 is devoted to the summary. In Appendix. 6.B, we present the derivation of the linearized equation used in Section 6.4.

6.2 The model

6.2.1 DFSZ axion model

The particle contents and the charge assignments under the SM gauge group and the $U(1)_{\mathrm{PQ}}$ are shown in Tab. 6.1. We introduce a SM-singlet complex scalar S and two $SU(2)_L$ doublets, H_1 and H_2, both with the hypercharge $Q_Y = 1/2$. The Lagrangian which describes the electroweak and scalar sectors is written as

$$\mathcal{L} = -\frac{1}{4}(B_{\mu\nu})^2 - \frac{1}{4}(W^a_{\mu\nu})^2 + \sum_{i=1,2}|D_\mu H_i|^2 + |\partial_\mu S|^2 - V(H_1, H_2, S). \tag{6.2.1}$$

Here, $B_{\mu\nu}$ and $W_{\mu\nu}^a$ describe field strength tensors of the hypercharge and weak gauge interactions, respectively, with μ (ν) and a being Lorentz and weak iso-spin indices, respectively. D_μ represents the covariant derivative acting on the Higgs fields, and the index i runs $i = 1, 2$. The scalar potential $V(H_1, H_2, S)$ being invariant under the charge assignments of Tab. 6.1 is

$$V(H_1, H_2, S) = V_H + V_S + V_{\mathrm{mix}}, \tag{6.2.2}$$

where each part is given by

$$\begin{aligned} V_H =& m_{11}^2 H_1^\dagger H_1 + m_{22}^2 H_2^\dagger H_2 + \frac{\beta_1}{2}\left(H_1^\dagger H_1\right)^2 + \frac{\beta_2}{2}\left(H_2^\dagger H_2\right)^2 \\ &+ \beta_3 \left(H_1^\dagger H_1\right)\left(H_2^\dagger H_2\right) + \beta_4 \left(H_1^\dagger H_2\right)\left(H_2^\dagger H_1\right), \end{aligned} \tag{6.2.3}$$

$$V_S = -m_S^2 |S|^2 + \lambda_S |S|^4, \tag{6.2.4}$$

$$V_{\mathrm{mix}} = \left(\kappa S^2 H_1^\dagger H_2 + \mathrm{h.c.}\right) + \kappa_{1S}|S|^2|H_1|^2 + \kappa_{2S}|S|^2|H_2|^2, \tag{6.2.5}$$

with $m_S^2 > 0$ which admits S to acquire a non-zero VEV: $\langle S \rangle = v_s$. Without loss of generality, we can suppose that the Higgs fields develop VEVs as $\langle H_1 \rangle = (0, v_1)$, $\langle H_2 \rangle = (0, v_2)$ with $v_1, v_2 \in \mathbb{R}$.[1] Then the electroweak scale, v_{EW} (≈ 246 GeV), can be expressed by these VEVs as $v_{\mathrm{EW}}^2 = 2(v_1^2 + v_2^2)$. We also define $\tan\beta := v_2/v_1$. In order for V_{mix} to be invariant under the $U(1)_{\mathrm{PQ}}$ symmetry, the $U(1)_{\mathrm{PQ}}$ charges in Tab. 6.1 should satisfy the relation $2X_s - X_1 + X_2 = 0$. If the first term in Eq. (6.2.5) has a structure like $SH_1^\dagger H_2$ instead of $S^2 H_1^\dagger H_2$, the assignment of the $U(1)_{\mathrm{PQ}}$ charges should change, but qualitative properties of the axion strings we discuss below are almost same. In particular, the string becomes superconducting also in such a case.

The Yukawa interaction terms are given by

$$\mathcal{L}_{\mathrm{Yukawa}} = -y^U \overline{u_R} \tilde{H}_1 Q - y^D \overline{d_R} H_2 Q - y^e \overline{e_R} H_2 L + \mathrm{h.c.}, \tag{6.2.6}$$

and the SM fermions carry the $U(1)_{\mathrm{PQ}}$ charge so that this Lagrangian is invariant under $U(1)_{\mathrm{PQ}}$. The new singlet scalar S couples to the SM fermions via Higgs sector. In the following parts of this chapter, we leave aside the Yukawa terms.

For later use, we rewrite the Higgs fields in a two-by-two matrix form [GMW11], H, defined by

$$\mathsf{H} = \left(i\sigma^2 H_1^*,\ H_2\right) = \left(\tilde{H}_1, H_2\right). \tag{6.2.7}$$

The matrix field H transforms under the electroweak $SU(2)_L \times U(1)_Y$ symmetry as

$$\mathsf{H} \mapsto \exp\left[\frac{i}{2}\theta_a(x)\sigma^a\right] \mathsf{H} \, \exp\left[-\frac{i}{2}\theta_Y(x)\sigma^3\right], \tag{6.2.8}$$

---

[1]Note that we drop "$1/\sqrt{2}$" in our notation for the VEVs.

where the group element acting from the left belongs to $SU(2)_L$ and the other element acting from the right belongs to $U(1)_Y$. Therefore the covariant derivative on H can be expressed as

$$D_\mu \mathsf{H} = \partial_\mu \mathsf{H} - i\frac{g_2}{2}\sigma^a W_\mu^a \mathsf{H} + i\frac{g_1}{2}\mathsf{H}\sigma^3 B_\mu. \tag{6.2.9}$$

The VEV of H is expressed by a diagonal matrix $\langle \mathsf{H} \rangle = \mathrm{diag}(v_1, v_2)$, and the Higgs potential V_H can be written by using H as follows:

$$\begin{aligned} V_H = &- m_1^2 \operatorname{tr}|\mathsf{H}|^2 - m_2^2 \operatorname{tr}\left(|\mathsf{H}|^2\sigma^3\right) + \alpha_1 \operatorname{tr}|\mathsf{H}|^4 \\ &+ \alpha_2\left(\operatorname{tr}|\mathsf{H}|^2\right)^2 + \alpha_3 \operatorname{tr}\left(|\mathsf{H}|^2\sigma^3|\mathsf{H}|^2\sigma^3\right) + \alpha_4 \operatorname{tr}\left(|\mathsf{H}|^2\sigma^3|\mathsf{H}|^2\right), \end{aligned} \tag{6.2.10}$$

where the relations between the parameters in Eq. (6.2.3) and in Eq. (6.2.10) are given by

$$m_{11}^2 = -m_1^2 - m_2^2, \qquad m_{22}^2 = -m_1^2 + m_2^2, \tag{6.2.11}$$

$$\beta_1 = 2(\alpha_1 + \alpha_2 + \alpha_3 + \alpha_4), \qquad \beta_2 = 2(\alpha_1 + \alpha_2 + \alpha_3 - \alpha_4), \tag{6.2.12}$$

$$\beta_3 = 2(\alpha_1 + \alpha_2 - \alpha_3), \qquad \beta_4 = 2(\alpha_3 - \alpha_1). \tag{6.2.13}$$

The formulae in the bilinear formalism is summarized in Appendix 6.A.2. The mixing term V_{mix} is also rewritten by H as

$$\begin{aligned} V_{\mathrm{mix}} = &\left(\kappa S^2 \det \mathsf{H} + \mathrm{h.c.}\right) + \frac{1}{2}(\kappa_{1S} + \kappa_{2S})|S|^2 \operatorname{tr}|\mathsf{H}|^2 \\ &+ \frac{1}{2}(\kappa_{1S} - \kappa_{2S})|S|^2 \operatorname{tr}(|\mathsf{H}|^2\sigma^3). \end{aligned} \tag{6.2.14}$$

The custodial transformation $SU(2)_C$ in the two Higgs doublet model [GMW11,PV94] is identified as the global unitary transformation of the Higgs matrix H as

$$\mathsf{H} \mapsto U^\dagger \mathsf{H} U, \quad U \in SU(2)_C. \tag{6.2.15}$$

If $m_2^2 = \alpha_3 = \alpha_4 = 0$, and $\kappa_{1S} = \kappa_{2S}$, the scalar potential is invariant under the custodial transformation. This symmetry makes the two VEVs be equal, $\tan\beta = 1$.

6.2.2 Mass spectra and PQ transformation

The scalar fields develop the following VEVs

$$\langle \mathsf{H} \rangle = \begin{pmatrix} v_1 & 0 \\ 0 & v_2 \end{pmatrix}, \quad \langle S \rangle = v_s. \tag{6.2.16}$$

The stationary conditions are solved with the mass parameters m_1^2, m_2^2, m_S^2 as

$$\begin{aligned} m_1^2 = &(\alpha_1 + 2\alpha_2 + \alpha_3 + \alpha_4)v_1^2 + (\alpha_1 + 2\alpha_2 + \alpha_3 - \alpha_4)v_2^2 \\ &+ \frac{1}{2}\left[\kappa\left(\frac{v_1}{v_2} + \frac{v_2}{v_1}\right) + \kappa_{1S} + \kappa_{2S}\right]v_s^2, \end{aligned} \tag{6.2.17}$$

$$m_2^2 = (\alpha_1 + \alpha_3 + \alpha_4)v_1^2 - (\alpha_1 + \alpha_3 - \alpha_4)v_2^2 + \frac{1}{2}\left[\kappa\left(\frac{v_2}{v_1} - \frac{v_1}{v_2}\right) + \kappa_{1S} - \kappa_{2S}\right]v_s^2, \quad (6.2.18)$$

$$m_S^2 = 2\lambda_S v_s^2 + \kappa_{1S}v_1^2 + \kappa_{2S}v_2^2 + 2\kappa v_1 v_2. \quad (6.2.19)$$

After the symmetry breaking, the gauge bosons and scalars become massive due to the above VEVs. The masses of the weak gauge bosons are given by

$$m_W = \frac{g_2 v_{\text{EW}}}{2}, \quad m_Z = \frac{g_2 v_{\text{EW}}}{2\cos\theta_W}, \quad (6.2.20)$$

with the standard definitions of the weak mixing angle $\cos\theta_W = g_2/\sqrt{g_2^2 + g_1^2}$, the Z boson $Z_\mu = W_\mu^3 \cos\theta_W - B_\mu \sin\theta_W$, and the photon $A_\mu = W_\mu^3 \sin\theta_W + B_\mu \cos\theta_W$.

In the scalar sector, we have three scalars, three pseudo scalars, and two charged scalars. Among these, one massless pseudo scalar and one massless charged scalar are eaten by the weak gauge bosons, and the other massless pseudo scalar becomes the axion, which obtains a mass from the non-perturbative QCD effect. There remain five physical scalar bosons after the symmetry breaking. For example, the lightest real scalar has the mass eigenvalue

$$m_{h_1}^2 \approx 4(\alpha_1 + \alpha_3)\frac{v_1^4 + v_2^4}{v_1^2 + v_2^2} + 4\alpha_2(v_1^2 + v_2^2) + 4\alpha_4(v_1^2 - v_2^2)$$
$$- \frac{\left(\kappa_{1S}v_1^2 + \kappa_{2S}v_2^2 + 2\kappa v_1 v_2\right)^2}{\lambda_S(v_1^2 + v_2^2)}, \quad (6.2.21)$$

up to $\mathcal{O}(v_{\text{EW}}^2/v_s^2)$, and we identify it as the SM Higgs boson. The mass squared matrix for three pseudo scalars is expressed as

$$\kappa\begin{pmatrix} -\frac{v_2 v_s^2}{v_1} & v_s^2 & 2v_2 v_s \\ v_s^2 & -\frac{v_1 v_s^2}{v_2} & -2v_1 v_s \\ 2v_2 v_s & -2v_1 v_s & -4v_1 v_2 \end{pmatrix}. \quad (6.2.22)$$

This matrix has one massive and two exact zero modes. The non-vanishing mass eigenvalue is

$$m_{A_0}^2 = -\kappa\frac{4v_1^2 v_2^2 + v_1^2 v_s^2 + v_2^2 v_s^2}{v_1 v_2}. \quad (6.2.23)$$

In order to avoid the tachyonic mass, the portal coupling κ should be negative. One of the massless eigenvector is $(\cos\beta, \sin\beta, 0)$ which corresponds to the longitudinal mode of the Z boson. Another zero eigenvector is given by $(X_1 v_1, X_2 v_2, X_s v_s)$ as long as $2X_s - X_1 + X_2 = 0$ is satisfied. This flat direction corresponds to the axion. Imposing these two massless modes are orthogonal, we find

$$X_1 = 2\sin^2\beta, \quad X_2 = -2\cos^2\beta, \quad X_s = 1, \quad (6.2.24)$$

where X_s determines the normalization. Then the $U(1)_{\text{PQ}}$ transformation acts on the scalars as

$$H_1 \to e^{2i\alpha \sin^2 \beta} H_1, \quad H_2 \to e^{-2i\alpha \cos^2 \beta} H_2, \quad S \to e^{i\alpha} S. \tag{6.2.25}$$

The same result is obtained by defining the $U(1)_{\text{PQ}}$ current not to couple to the Z boson. For the matrix field H, the $U(1)_{\text{PQ}}$ transformation becomes

$$\mathsf{H} \to e^{-i\alpha} \mathsf{H} e^{i\alpha\sigma^3 \cos 2\beta}. \tag{6.2.26}$$

6.2.3 Definition of unbroken $U(1)_{\text{EM}}$ group

Unlike in the vacuum, in the presence of a soliton background, the definition of the unbroken $U(1)_{\text{EM}}$ generator is non-trivial. In this chapter, it is defined as [2]

$$\hat{Q}\mathsf{H} := -n^a \frac{\sigma^a}{2}\mathsf{H} - \mathsf{H}\frac{\sigma^3}{2}, \tag{6.2.27}$$

where

$$n^a := \frac{\sum_{i=1,2} |\mathsf{H}_i|^2 n_i^a}{C}, \tag{6.2.28}$$

$$n_1^a := \frac{H_1^\dagger \sigma^a H_1}{|H_1|^2}, \qquad n_2^a := \frac{H_2^\dagger \sigma^a H_2}{|H_2|^2}. \tag{6.2.29}$$

The positive normalization factor C is determined to satisfy $n^a n^a = 1$. Correspondingly, the $U(1)_Z$ subgroup in the $SU(2)_L \times U(1)_Y$ group is defined as

$$\hat{T}_Z\mathsf{H} := -n^a \frac{\sigma^a}{2}\mathsf{H} - \sin^2 \theta_W \hat{Q}\mathsf{H}. \tag{6.2.30}$$

Also, the $U(1)_Z$ and $U(1)_{\text{EM}}$ gauge fields are defined as

$$Z_\mu := -n^a W_\mu^a \cos \theta_W - B_\mu \sin \theta_W, \tag{6.2.31}$$

$$A_\mu := -n^a W_\mu^a \sin \theta_W + B_\mu \cos \theta_W. \tag{6.2.32}$$

In addition, the charged components of $SU(2)_L$ gauge group is defined as orthogonal components to $n^a \sigma^a$. In the vacuum, the Higgs field takes a constant VEV $\langle \mathsf{H} \rangle = \text{diag}(v_1, v_2)$, and $n^a \sigma^a = -\sigma^3$. The above definitions reduce to the conventional ones. The VEV is invariant under $U(1)_{\text{EM}}$,

$$\hat{Q} \langle \mathsf{H} \rangle = 0, \tag{6.2.33}$$

which means that the $U(1)_{\text{EM}}$ symmetry is not spontaneously broken in the vacuum.

It may be useful to rewrite the above expressions for the two doublets H_1 and H_2,

$$\hat{Q}H_i = \left(-n^a \frac{\sigma^a}{2} + \frac{1}{2}\mathbf{1}\right) H_i, \tag{6.2.34}$$

$$\hat{T}_Z H_i = \left(-n^a \frac{\sigma^a}{2} - \sin^2 \theta_W \hat{Q}\right) H_i, \tag{6.2.35}$$

for $i = 1, 2$.

_____

[2]The vector n^a corresponds to $\tilde{n}^a$ in Ref. [EHN20].

6.3 Electroweak axion strings

Similarly to other axion models, the DFSZ axion model provides a vortex string solution known as the axion string corresponding to the breaking of $U(1)_{\rm PQ}$. On the other hand, after the electroweak phase transition, the axion string can contain flux tubes of the $SU(2)_L \times U(1)_Y$ gauge fields like the Abrikosov-Nielsen-Olesen vortex [Abr57, NO73] since the two Higgs doublets also acquire the VEVs. We call such vortex strings the electroweak axion strings. In this section, we show that there are (at least) three types of the electroweak axion strings in the DFSZ model. Interestingly, some of them have similar properties to those of (non-Abelian) vortices in two Higgs doublet models, in which there is a global symmetry for a relative rotation of the two Higgs doublets. In particular, some part of our argument in this section refers to that in Refs. [EKN18a, EKN18b].

6.3.1 Axion string in DFSZ model

We first review the conventional axion string in this subsection. Let us consider a case that the $U(1)_{\rm PQ}$ symmetry is spontaneously broken by $\langle S \rangle \neq 0$ but the electroweak symmetry remains, $\langle H_1 \rangle = \langle H_2 \rangle = (0,0)$. This situation realized in the early universe when the temperature T satisfies $v_{\rm EW} \ll T \ll v_s$. In this case, as is well-known, a vortex-string configuration associated with the global $U(1)_{\rm PQ}$ symmetry exists as a solution to the equation of motion (EOM), which is called the axion string in the literature. The configuration located on the z-axis is described by the following ansatz

$$
S = v_s e^{i\theta} \phi(r), \qquad H_1 = H_2 = \begin{pmatrix} 0 \\ 0 \end{pmatrix}, \tag{6.3.1}
$$

where r and θ are the distance from the z-axis and the rotational angle, respectively. Namely, $x + iy = re^{i\theta}$. The profile function $\phi(r)$ satisfies the boundary conditions

$$
\phi(0) = 0, \qquad \phi(\infty) = 1. \tag{6.3.2}
$$

The detailed form of $\phi(r)$ is determined by solving the EOM. This string has a winding number associated with the $U(1)_{\rm PQ}$ symmetry, and hence is topologically stable. The $U(1)_{\rm PQ}$ symmetry is restored on the string core because of $\phi(0) = 0$.

It is known that such strings are necessarily produced during the phase transition of the $U(1)_{\rm PQ}$ symmetry breaking by the Kibble-Zurek mechanism. In the viewpoint of phenomenology, one of the important aspects of cosmic strings is the interaction between a pair of the cosmic strings having the same topological charge. For axion strings, the interaction is dominated by exchange of massless axion particles, resulting in the long-range repulsive force. The potential of the interaction $V_{\rm st.}$ is approximately given as $V_{\rm st.} \sim -v_s^2 \log R$ with R being the distance between the pair. Due to the repulsive interaction, a pair of the strings reconnects with probability of the order of unity when they collide

to each other and does not form a bound state of the strings (such as the Y-junction [BLM97,BK94,CKS06,CKS07,SAC$^+$08,BS08a,BCM$^+$09,HEK$^+$14,HST$^+$13]). As a result, the strings form a stationary network whose typical length scale remains to be the Hubble horizon scale (scaling regime). Such a scale-invariant evolution of the network prevents the energy density of the strings from dominating that of the universe, and thus axion models producing the axion strings are cosmologically viable as far as concerning the strings.

6.3.2 Vortex string with Z-flux (type-A string)

Next, we discuss the electroweak axion strings. Let us consider a string configuration after the electroweak phase transition $T_{th} \lesssim v_{\rm EW}$. The two doublets also acquire the VEVs and their phases must also wind because they also have the $U(1)_{\rm PQ}$ charges, otherwise divergent energy arises from $V_{\rm mix}$.[3] From the single-valuedness of the doublets, the string configuration has the form

$$
\begin{cases}
S = v_s e^{i\theta} \phi(r) \\[2mm]
H_1 = v_1 e^{i\theta} \begin{pmatrix} 0 \\ f(r) \end{pmatrix} \\[4mm]
H_2 = v_2 e^{-i\theta} \begin{pmatrix} 0 \\ h(r) \end{pmatrix}
\end{cases}
,
\tag{6.3.3}
$$

$$
Z_i = \frac{2\cos 2\beta}{g_Z} \frac{\epsilon_{ij} x_j}{r^2} (1 - z(r)),
\tag{6.3.4}
$$

and $W_i^{\pm} = A_i = 0$. g_Z is the coupling of Z-boson given by $g_Z = \sqrt{g_2^2 + g_1^2}$. ϵ_{ij} is the anti-symmetric tensor satisfying $\epsilon_{12} = -\epsilon_{21} = 1$. We call this string configuration the type-A electroweak axion string.

The last two configurations in Eq. (6.3.3) are equivalent to

$$
\mathsf{H} = e^{-i\theta} \begin{pmatrix} v_1 f(r) & 0 \\ 0 & v_2 h(r) \end{pmatrix}.
\tag{6.3.5}
$$

The profile functions $f(r), h(r)$ satisfy the same boundary conditions as that of $\phi(r)$, i.e.,

$$
\phi(0) = f(0) = h(0) = 0, \qquad \phi(\infty) = f(\infty) = h(\infty) = 1.
\tag{6.3.6}
$$

The profile function for the gauge field $z(r)$ should satisfy the boundary conditions

$$
z(0) = 1, \quad z(\infty) = 0.
\tag{6.3.7}
$$

---

[3]If the two doublets had no windings, the mixing term provides $\kappa v_s^2 v_1 v_2 \cos 2\theta$ at large distances, which means a divergent potential energy after the spatial integration.
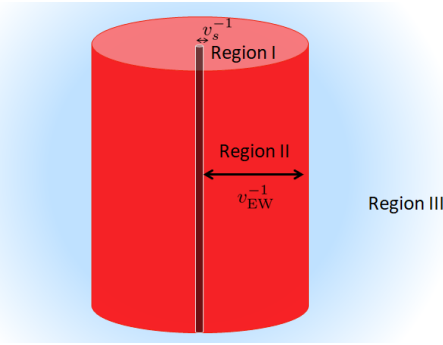
Figure 6.1: Schematic picture of the energy density profile of the electroweak axion strings (type-A, B and C) [AHY21]. The energy density consists of three parts. There is a one-dimensional thin object consisting of the radial component of the complex scalar $\phi(r)$ in Region I: $r \lesssim v_s^{-1}$. We call this region the core of the string. In Region II: $v_s^{-1} \lesssim r \lesssim (v_{\rm EW})^{-1}$ (red region), the energy density is dominated by the Higgs fields and the electroweak gauge fields. This region is much fatter than Region I. In addition, there is the fattest part made from the gradient energy of the axion, leading to the logarithmically divergent tension. This is denoted by Region III: $r \gtrsim (v_{\rm EW})^{-1}$ (blue cloud). Note that the type-A string with $\tan \beta = 1$ is a special case since it has only the global winding and its energy density does not have the Region II.

Eq. (6.3.6) indicates that the electroweak symmetry is restored inside the string as well as $U(1)_{\rm PQ}$.

Noting that the two doublets have $U(1)_{\rm PQ}$ charges as given in Eq. (6.2.25), it is convenient to decompose the winding phases as

$$H_1 = v_1 e^{2i\theta s_\beta^2} e^{-i\theta \sigma^3 c_{2\beta}} \begin{pmatrix} 0 \\ f(r) \end{pmatrix}, \tag{6.3.8}$$

$$H_2 = v_2 e^{-2i\theta c_\beta^2} e^{-i\theta \sigma^3 c_{2\beta}} \begin{pmatrix} 0 \\ h(r) \end{pmatrix}, \tag{6.3.9}$$

with $c_X := \cos(X)$ and $s_X := \sin(X)$. Eqs. (6.3.8) and (6.3.9) mean that the configurations of the doublets have the winding number unity for the global $U(1)_{\rm PQ}$ symmetry and the fractional winding number $-\cos 2\beta$ for the $U(1)_Z$ subgroup of the $SU(2)_L \times U(1)_Y$ gauge symmetry. Therefore, the gradient energy from the $U(1)_Z$ windings is canceled by the Z gauge field (6.3.4) with Eq. (6.3.7) at large distances $r \to \infty$. It follows from Eq. (6.3.4) that the string configuration has the Z-flux,

$$\Phi_Z = \oint_{r=\infty} dx_i \, Z_i = \frac{-4\pi \cos 2\beta}{g_Z}, \tag{6.3.10}$$

which is fractionally quantized because of the fractional winding number.

We discuss a qualitative property of the profile functions. The typical length scale for $\phi(r)$ is v_s^{-1} while those of $f(r), h(r)$ and $z(r)$ are given as $(v_{\rm EW})^{-1}$. Thus the string is a

"multi-scale solution". Fig. 6.1 shows a schematic picture of the energy density profile of the electroweak axion strings. The energy density has three structures. One is that from the radial component of the complex scalar, $\phi(r)$, whose typical scale is v_s^{-1}. This part looks as a thin object (Region I: $r \lesssim v_s^{-1}$). Another is from those of the two Higgs doublets and the gauge fields, whose typical scale is the EW-scale $(v_{\mathrm{EW}})^{-1}$. This region, which we call Region II, is much fatter than Region I and is shown as the red region. The third part is the fattest part from the gradient energy of the axion. This is denoted by Region III: $r \gtrsim (v_{\mathrm{EW}})^{-1}$ (blue cloud in the figure). When one calculates the tension of the string (energy per unit length) by integrating the energy density on the xy plane, the third part leads to the log-divergent tension $\sim 2\pi v_s^2 \log L$ where L is the IR-cutoff and is usually taken as the distance between neighbor two strings. The coefficient of the log divergence is the same as that of the conventional axion string shown in the last subsection because it depends only on the winding number of the global $U(1)_{\mathrm{PQ}}$ symmetry.

Let us obtain the profile functions and calculate the string tension for the type-A string in a numerical way. For simplicity, we take $m_2^2 = \alpha_4 = 0$ and $\kappa_{1S} = \kappa_{2S}$, leading to $\tan\beta = 1$ (see the stationary condition (6.2.18)). The VEVs are denoted as $v_1 = v_2 := v$. We should note that in this case, the Higgs doublets do not have winding number for the $U(1)_Z$ gauge subgroup, and thus the right hand side of Eq. (6.3.4) vanishes. The Z-flux is constantly zero. After substituting the ansatz, the energy density is given by

$$
\mathcal{E} := |\partial_i S|^2 + \mathrm{tr}\,|D_i \mathsf{H}|^2 + \frac{1}{4}(W_{ij}^a)^2 + \frac{1}{4}(B_{ij})^2 + V(\mathsf{H}, S) \tag{6.3.11}
$$

$$
\begin{aligned}
&= \frac{v^2}{r^2}\left[r^2\left(f'(r)^2 + h'(r)^2\right) + f(r)^2 + h(r)^2\right] \\
&\quad + v^2\left[-m_1^2(f(r)^2 + h(r)^2) + 2\alpha_2 v^2 f(r)^2 h(r)^2 + v^2\alpha_{123}(f(r)^4 + h(r)^4)\right] \\
&\quad + v^2 v_s^2\left[2\kappa f(r)h(r)\phi(r)^2 + \kappa_{1S}(f(r)^2 + h(r)^2)\phi(r)^2\right] \\
&\quad + v_s^2\left(-m_S^2\phi(r)^2 + \lambda_S v_s^2 \phi(r)^4\right) + \frac{v_s^2}{r^2}\left(r^2\phi'(r)^2 + \phi(r)^2\right),
\end{aligned} \tag{6.3.12}
$$

with $\alpha_{123} := \alpha_1 + \alpha_2 + \alpha_3$ and $'$ denoting the derivative with respect to r.

The EOMs are obtained as

$$
\begin{aligned}
&f''(r) + \frac{f'(r)}{r} - \frac{f(r)}{r^2} \\
&- \left(2\alpha_{123}\,v^2 f(r)^2 + 2\alpha_2 v^2 h(r)^2 + \kappa_{1S} v_s^2 \phi(r)^2 - m_1^2\right)f(r) - \kappa v_s^2 h(r)\phi(r)^2 = 0, \tag{6.3.13}
\end{aligned}
$$

$$
\begin{aligned}
&h''(r) + \frac{h'(r)}{r} - \frac{h(r)}{r^2} \\
&- \left(2\alpha_{123}\,v^2 h(r)^2 + 2\alpha_2 v^2 f(r)^2 + \kappa_{1S} v_s^2 \phi(r)^2 - m_1^2\right)h(r) - \kappa v_s^2 f(r)\phi(r)^2 = 0, \tag{6.3.14}
\end{aligned}
$$

$$
\begin{aligned}
&\phi''(r) + \frac{\phi'(r)}{r} - \frac{\phi(r)}{r^2} \\
&- \left(2\lambda_S v_s^2 \phi(r)^2 + 2\kappa_{1S} v^2(f(r)^2 + h(r)^2) + 2\kappa v^2 f(r)h(r) - m_S^2\right)\phi(r) = 0. \tag{6.3.15}
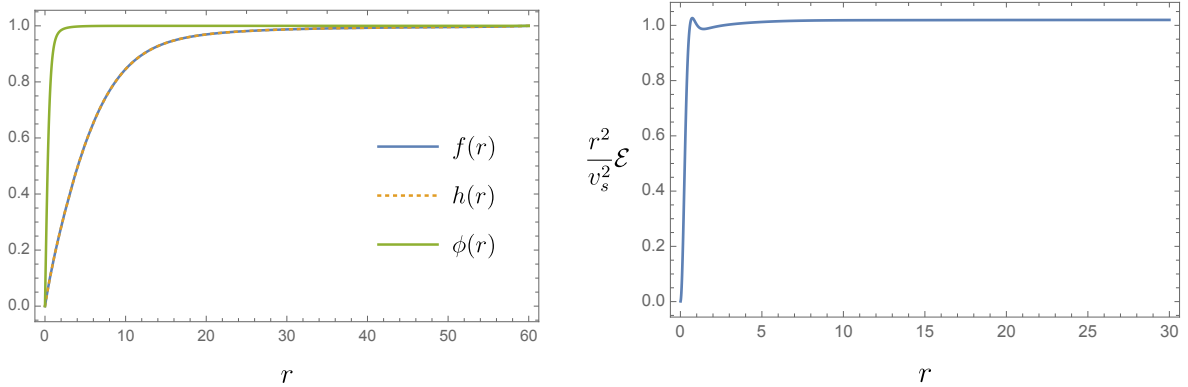\end{aligned}
$$

99

Figure 6.2: Numerical solution for the type-A string [AHY21]. We take benchmark parameters as Eq. (6.3.16) and $v_s = 10\,v$. Also we adopt a length unit as $v_s^{-1} = 0.5$. (left): Plots of profile functions. Note $f(r)$ (blue line) is equal to $h(r)$ (dotted orange line) everywhere. $\phi(r)$ increases as $\phi \sim v_s r$ for $r \sim 0$ while $f = h \sim vr$. All of them approach to unity for $r \to \infty$. (right): Plot of energy density $\mathcal{E}$ (Eq. (6.3.11)) divided by v_s^2/r^2. Clearly, the energy density has a polynomial tail like r^{-2}, instead of an exponential one. This leads to the logarithmically divergent tension. The integrated value of the tension over $0 \le r \le 120\,v_s^{-1}$ is 140.321.

We adopt the so-called relaxation method to solve the EOMs. As a benchmark case, we take the parameters as

$$\alpha_1 = 1, \quad \alpha_2 = -0.3348, \quad \alpha_3 = 0, \quad \lambda_S = 1, \quad \kappa = -2\left(\frac{v}{v_s}\right)^2, \quad \kappa_{1S} = 0.4, \quad (6.3.16)$$

such that the lightest scalar mass $m_{h_1}^2$ reproduces the SM Higgs mass $(125 \text{ GeV})^2$. In addition, we set the VEV for S as $v_s = 10\,v$. Although this is too small and not viable in the phenomenological viewpoint, it does not matter because the qualitative picture of the type-A string does not change. If one takes them more hierarchical, huge numerical costs arise in the calculation. The obtained numerical solutions are shown in Fig. 6.2. In the left panel, $f(r)$ (blue line) is equal to $h(r)$ (dotted orange line) everywhere. $\phi(r)$ increases as $\phi \sim v_s r$ for $r \sim 0$ while $f = h \sim vr$. All of them approach to unity for $r \to \infty$. The right panel shows the energy density $\mathcal{E}$ (Eq. (6.3.11)) divided by v_s^2/r^2. The divided value approaches to unity, which means that the energy density has a polynomial tail like r^{-2}, instead of an exponential one. This leads to the logarithmically divergent tension.

6.3.3 Type-B string with Z-flux

We have shown that the phases of the two Higgs doublets must wind after the electroweak phase transition $T_{th} \lesssim v_{\text{EW}}$. Actually, there is another type of vortex string that is consistent with the single-valuedness and the potential minimum. This is obtained by giving an *additional winding* in the $U(1)_Z$ gauge orbit to the type-A string. We call this

string the type-B electroweak axion string. The ansatz describing the string is given as

$$
\begin{cases}
S = v_s e^{i\theta} \phi(r) \\[2mm]
H_1 = v_1 e^{2i\theta} \begin{pmatrix} 0 \\ f(r) \end{pmatrix} \\[4mm]
H_2 = v_2 \begin{pmatrix} 0 \\ h(r) \end{pmatrix}
\end{cases}
\tag{6.3.17}
$$

$$
Z_i = \frac{4 \cos^2 \beta}{g_Z} \frac{\epsilon_{ij} x_j}{r^2} (1 - z(r)).
\tag{6.3.18}
$$

The last two configurations in Eq. (6.3.17) are equivalent to

$$
\mathsf{H} = e^{-i\theta} e^{-i\theta\sigma^3} \begin{pmatrix} v_1 f(r) & 0 \\ 0 & v_2 h(r) \end{pmatrix}.
\tag{6.3.19}
$$

The profile functions $f(r)$ and $\phi(r)$ satisfy the same boundary conditions,

$$
\phi(0) = f(0) = 0, \quad \phi(\infty) = f(\infty) = 1,
\tag{6.3.20}
$$

but $h(r)$ should satisfy the following boundary conditions:

$$
\partial_r h|_{r=0} = 0, \quad h(\infty) = 1.
\tag{6.3.21}
$$

The profile function for the gauge field $z(r)$ satisfies

$$
z(0) = 1, \quad z(\infty) = 0.
\tag{6.3.22}
$$

Note that $h(r)$ is not fixed to zero on the center of the string because it does not have a winding phase. Therefore, the electroweak symmetry is *not* restored inside the string core (see Fig. 6.3.)

Again, we decompose the winding phases as

$$
H_1 = v_1 e^{2i\theta s_\beta^2} e^{-2i\theta\sigma^3 c_\beta^2} \begin{pmatrix} 0 \\ f(r) \end{pmatrix},
\tag{6.3.23}
$$

$$
H_2 = v_2 e^{-2i\theta c_\beta^2} e^{-2i\theta\sigma^3 c_\beta^2} \begin{pmatrix} 0 \\ h(r) \end{pmatrix},
\tag{6.3.24}
$$

which mean that the configurations of the doublets have the winding number unity for the global $U(1)_{\mathrm{PQ}}$ symmetry and the fractional winding number $-2\cos^2\beta$ for the $U(1)_Z$ subgroup. The difference between the winding number of the type-A and type-B strings is unity. Similarly to the previous case, the Z gauge field (6.3.18) cancels the gradient
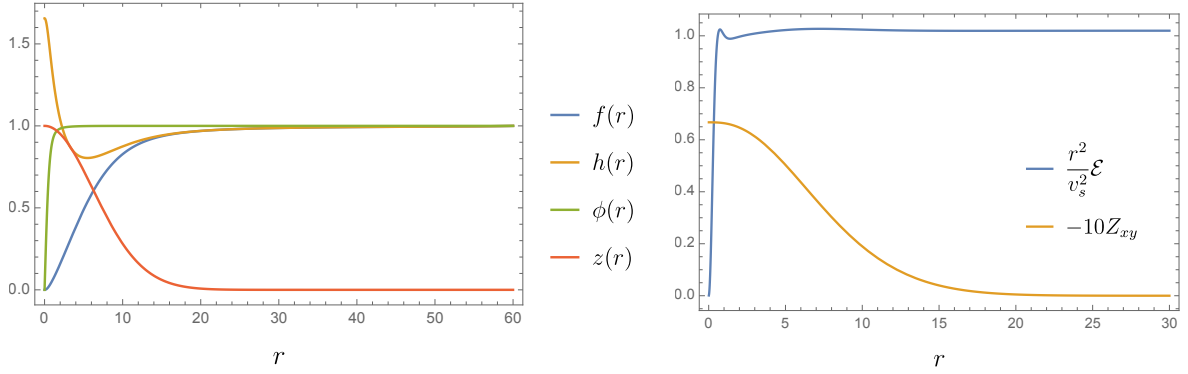
Figure 6.3: Numerical solution for the type-B string [AHY21]. We take the same parameters as ones in Fig. 6.2. Also we adopt a length unit as $v_s^{-1} = 0.5$. (left): Plots of profile functions. $\phi(r)$ increases as $\phi \sim v_s r$ for $r \sim 0$ while $f(r)$ behaves as a quadratic function with respect to r. The three profile functions f, h and ϕ approach to unity for $r \to \infty$. The profile function of the Z field, $z(r)$, approaches to zero as $r \to \infty$ starting from unity at $r = 0$. (right): Plots of energy density (6.3.26) divided by v_s^2/r^2 and the Z-flux density multiplied by -10. The energy density has a polynomial tail like r^{-2} like the type-A string. The tension T integrated over $0 \le r \le 120\, v_s^{-1}$ is 140.524. The Z-flux density decays exponentially for $r \to \infty$ like the usual Abrikosov-Nielsen-Olesen vortex. The total value of the Z-flux is calculated to -16.9539, which is consistent with Eq. (6.3.25).

energy from the $U(1)_Z$ windings. It follows from Eq. (6.3.4) that the string configuration has the Z-flux, which is calculated as

$$\Phi_Z = \oint_{r=\infty} dx_i \, Z_i = \frac{-8\pi \cos^2 \beta}{g_Z}. \tag{6.3.25}$$

Interestingly, this string configuration is quite similar to the topologically stable Z-string (topological vortex with the Z-flux) in 2HDM [DS93,DS94,EKN18a,EKN18b]. In addition to the winding number of $U(1)_Z$, the difference from the 2HDM is the existence of the singlet complex scalar carrying the $U(1)_{\mathrm{PQ}}$ charge, which is replaced by the relative phase rotation of the two doublets in the 2HDM.

Let us obtain the profile functions and calculate the string tension for the type-B string in a numerical way. Again, we take $m_2^2 = \alpha_4 = 0$ and $\kappa_{1S} = \kappa_{2S}$, leading to $\tan \beta = 1$. The VEVs are denoted as $v_1 = v_2 := v$. Unlike the type-A string, the Higgs doublets have winding numbers for the $U(1)_Z$ gauge subgroup even for $\tan \beta = 1$. Consequently, the Z-flux is non-zero and confined inside the string. The energy density is

$$\begin{aligned}
\mathcal{E} =\ & \frac{v^2}{r^2} \left[r^2 \left(f'(r)^2 + h'(r)^2 \right) + f(r)^2(1 + z(r))^2 + h(r)^2(1 - z(r))^2 \right] \\
& + v^2 \left[-m_1^2(f(r)^2 + h(r)^2) + 2\alpha_2 v^2 f(r)^2 h(r)^2 + v^2 \alpha_{123}(f(r)^4 + h(r)^4) \right] \\
& + v^2 v_s^2 \left[2\kappa f(r)h(r)\phi(r)^2 + \kappa_{1S}(f(r)^2 + h(r)^2)\phi(r)^2 \right]
\end{aligned}$$

102

$$+ v_s^2 \left(-m_S^2 \phi(r)^2 + \lambda_S v_S^2 \phi(r)^4\right) + \frac{v_s^2}{r^2}\left(r^2\phi'(r)^2 + \phi(r)^2\right) + 2\frac{z'(r)^2}{g_Z^2 r^2} \qquad (6.3.26)$$

Then, the EOMs are obtained as

$$f''(r) + \frac{f'(r)}{r} - \frac{(1+z(r))^2}{r^2}f(r)$$
$$- \left(2\alpha_{123}\, v^2 f(r)^2 + 2\alpha_2 v^2 h(r)^2 + \kappa_{1S} v_s^2 \phi(r)^2 - m_1^2\right)f(r) - \kappa v_s^2 h(r)\phi(r)^2 = 0, \quad (6.3.27)$$

$$h''(r) + \frac{h'(r)}{r} - \frac{(-1+z(r))^2}{r^2}h(r)$$
$$- \left(2\alpha_{123}\, v^2 h(r)^2 + 2\alpha_2 v^2 f(r)^2 + \kappa_{1S} v_s^2 \phi(r)^2 - m_1^2\right)h(r) - \kappa v_s^2 f(r)\phi(r)^2 = 0, \quad (6.3.28)$$

$$\phi''(r) + \frac{\phi'(r)}{r} - \frac{\phi(r)}{r^2}$$
$$- \left(2\lambda_S v_s^2 \phi(r)^2 + \kappa_{1S} v^2 (f(r)^2 + h(r)^2) + 2\kappa v^2 f(r)h(r) - m_S^2\right)\phi(r) = 0, \qquad (6.3.29)$$

$$z''(r) - \frac{z'(r)}{r} - \frac{g_Z^2 v^2}{2}f(r)^2(1+z(r)) - \frac{g_Z^2 v^2}{2}h(r)^2(-1+z(r)) = 0. \qquad (6.3.30)$$

We take the same parameter choice as Eq. (6.3.16). In addition, we set the VEV for S as $v_s = 10\,v$. The obtained numerical solutions are shown in Fig. 6.3. In the left panel, $f(r)$ ($\phi(r)$) behaves like $v_s r$ (vr^2) at the origin because the phases of $\phi(r)$ and $f(r)$ wind once and twice, respectively. $h(r)$ does not start from zero at the origin due to the Neumann condition at the origin. All of the scalar profile functions approach to unity for $r \to \infty$. The profile function for the gauge field $z(r)$ approaches to zero starting from unity. The right panel shows the energy density $\mathcal{E}$ (Eq. (6.3.11)) divided by v_s^2/r^2 and the Z-flux density multiplied by -10. Similarly to the previous case, the type-A string, the energy density has a polynomial tail like r^{-2}, instead of an exponential one. This leads to the logarithmically divergent tension. The schematic picture of the energy density profile is the same as Fig. 6.1. On the other hand, the Z-flux has an exponential tail.

In the above ansatz for the type-B string, only the one doublet H_1 has the winding number. There may be also an alternative string in which only H_2 has the winding phase. Roughly speaking, they are related by exchange of the two doublets H_1 and H_2. Since the property is similar to the former, we do not study the latter one in this chapter and also categorize the latter one as the type-B string.

6.3.4 Type-C string with W-flux

Finally, we consider the third type of the vortex string, called the type-C electroweak axion string. While the type-B string has been obtained by performing an additional rotation of $U(1)_Z$ on the type-A one, the type-C string has a winding in the $U(1)_{W^1}$

subgroup of the $SU(2)_L \times U(1)_Y$ symmetry. The ansatz for the scalar fields is given as

$$
\begin{cases}
S = v_s e^{i\theta} \phi(r) \\[2mm]
H_1 = \frac{1}{2} v_1 e^{i\theta} \begin{pmatrix} f(r)e^{i\theta} - h(r)e^{-i\theta} \\ f(r)e^{i\theta} + h(r)e^{-i\theta} \end{pmatrix} \\[4mm]
H_2 = \frac{1}{2} v_2 e^{-i\theta} \begin{pmatrix} h(r)e^{i\theta} - f(r)e^{-i\theta} \\ h(r)e^{i\theta} + f(r)e^{-i\theta} \end{pmatrix}
\end{cases}
\tag{6.3.31}
$$

The profile functions $f(r), h(r), \phi(r)$ satisfy similar boundary conditions to those of the type-B string, (6.3.20) and (6.3.21), i.e.,

$$
f(0) = \phi(0) = 0, \quad \partial_r h|_{r=0} = 0, \quad f(\infty) = h(\infty) = \phi(\infty) = 1. \tag{6.3.32}
$$

Due to the non-zero value of $h(0)$, the electroweak symmetry is not restored inside the string as the type-B string.

Unlike the type-A and type-B strings, in the background of the type-C string, the $U(1)_{\text{EM}}$ and $U(1)_Z$ generators depend on the positions. As explained in Section 6.2, the $U(1)_{\text{EM}}$ generator is defined by Eq. (6.2.27) or Eq. (6.2.34). Substituting the ansatz Eq. (6.3.31), we obtain

$$
n_1^a = \frac{H_1^\dagger \sigma^a H_1}{|H_1|^2} = \frac{2}{f^2 + h^2} \left((f^2 - h^2)/2, -fh \sin 2\theta, -fh \cos 2\theta \right), \tag{6.3.33}
$$

$$
n_2^a = \frac{H_2^\dagger \sigma^a H_2}{|H_2|^2} = \frac{2}{f^2 + h^2} \left((h^2 - f^2)/2, -fh \sin 2\theta, -fh \cos 2\theta \right), \tag{6.3.34}
$$

and

$$
n^a \frac{\sigma^a}{2} = -\frac{\sigma^2}{2} \sin 2\theta - \frac{\sigma^3}{2} \cos 2\theta. \tag{6.3.35}
$$

Then the $U(1)_{\text{EM}}$ and $U(1)_Z$ generators are given by

$$
\hat{Q} H_i = \left(\frac{\sigma^2}{2} \sin 2\theta + \frac{\sigma^3}{2} \cos 2\theta + \frac{1}{2} \mathbf{1} \right) H_i, \tag{6.3.36}
$$

$$
\hat{T}_Z H_i = \left(\sigma^2 \sin 2\theta + \sigma^3 \cos 2\theta - \sin^2 \theta_W \hat{Q} \right) H_i, \tag{6.3.37}
$$

which depend on θ.

Let us see the asymptotic behaviors of the two doublets at large distances $r \to \infty$. From Eq. (6.3.32), we obtain

$$
H_1 \sim v_1 e^{i\theta} \begin{pmatrix} i \sin \theta \\ \cos \theta \end{pmatrix} = v_1 e^{2i\theta s_\beta^2} e^{-i\theta c_{2\beta} \sigma^Z} e^{i\theta \sigma^1} \begin{pmatrix} 0 \\ 1 \end{pmatrix}, \tag{6.3.38}
$$

$$
H_2 \sim v_2 e^{-i\theta} \begin{pmatrix} i \sin \theta \\ \cos \theta \end{pmatrix} = v_2 e^{-2i\theta c_\beta^2} e^{-i\theta c_{2\beta} \sigma^Z} e^{i\theta \sigma^1} \begin{pmatrix} 0 \\ 1 \end{pmatrix}, \tag{6.3.39}
$$

where $\sigma^Z := 2\hat{T}_Z$ (note $\hat{Q}H_i = 0$ for $r \to \infty$). It is clear that these configurations have a winding number unity for $U(1)_{\text{PQ}}$, $-\cos 2\beta$ for $U(1)_Z$ and unity for the $U(1)_{W^1}$ subgroup (σ^1 rotation) of the gauge symmetry. Therefore, to cancel the gradient energy from the windings for $U(1)_Z$ and $U(1)_{W^1}$, the ansatz for the gauge fields are given as

$$Z_i = \frac{2\cos 2\beta}{g_Z} \frac{\epsilon_{ij} x_j}{r^2} (1 - z(r)), \tag{6.3.40}$$

$$W_i^1 = \frac{-2}{g_2} \frac{\epsilon_{ij} x_j}{r^2} (1 - w(r)), \tag{6.3.41}$$

and $A_i = 0$, where we have used the definitions of the gauge fields Eqs. (6.2.31) and (6.2.32). The profile functions for the gauge fields $w(r)$ and $z(r)$ satisfy

$$w(0) = z(0) = 1, \quad w(\infty) = z(\infty) = 0. \tag{6.3.42}$$

Interestingly, the type-C string has both of the Z and W-fluxes for $\tan\beta \neq 1$. It follows from the ansatz (6.3.40) and (6.3.41) that

$$\Phi_Z = \oint_{r=\infty} dx_i \, Z_i = \frac{-4\pi \cos 2\beta}{g_Z}, \tag{6.3.43}$$

$$\Phi_{W^1} = \oint_{r=\infty} dx_i \, W_i^1 = \frac{4\pi}{g}, \tag{6.3.44}$$

where the latter flux is independent of $\tan\beta$.

The most important difference from the type-A and type-B strings is that the $U(1)_{\text{EM}}$ symmetry is broken inside the type-C string. This can be seen by using the concrete expression, Eq. (6.3.31), as $\hat{Q}H_i \neq 0$ ($i = 1, 2$). Actually, that is generally inevitable for a configuration with a non-vanishing winding number for charged components, i.e., a configuration whose asymptotic form is $\exp[i\hat{T}(\theta)]H(\theta = 0)$ with a non-Abelian generator $\hat{T}(\theta)$ satisfying $[\hat{T}(\theta), \hat{Q}] \neq 0$ [ABC$^+$90, ABC$^+$91]. ($\hat{T} = \sigma^1\theta$ in our case.) Due to the winding, the charged components cannot remain zero, and they acquire non-zero values inside the string, leading to the breaking of $U(1)_{\text{EM}}$. We should note that $U(1)_{\text{EM}}$ is restored at large distances from the string, $r \to \infty$.

Let us solve the EOMs with respect to the profile functions and calculate the string tension for the type-C string. Again, we take $m_2^2 = \alpha_4 = 0$ and $\kappa_{1S} = \kappa_{2S}$, leading to $\tan\beta = 1$. The VEVs are denoted as $v_1 = v_2 := v$. The Higgs doublets have winding numbers for the $U(1)_{W^1}$ gauge subgroup but not for $U(1)_Z$. Consequently, only the W^1-flux is non-zero and confined inside the string. Substituting the ansatz, the energy density is given by

$$\begin{aligned}
\mathcal{E} = &\frac{v^2}{r^2} \left[r^2 \left(f'(r)^2 + h'(r)^2 \right) + f(r)^2 (w(r) + 1)^2 + h(r)^2 (w(r) - 1)^2 \right] \\
&- m_1^2 v^2 (f(r)^2 + h(r)^2) + v^4 \left[2(\alpha_2 + \alpha_3) f(r)^2 h(r)^2 + (\alpha_1 + \alpha_2)(f(r)^4 + h(r)^4) \right] \\
&+ v^2 v_s^2 \left[2\kappa f(r)h(r)\phi(r)^2 + \kappa_{1S}(f(r)^2 + h(r)^2)\phi(r)^2 \right]
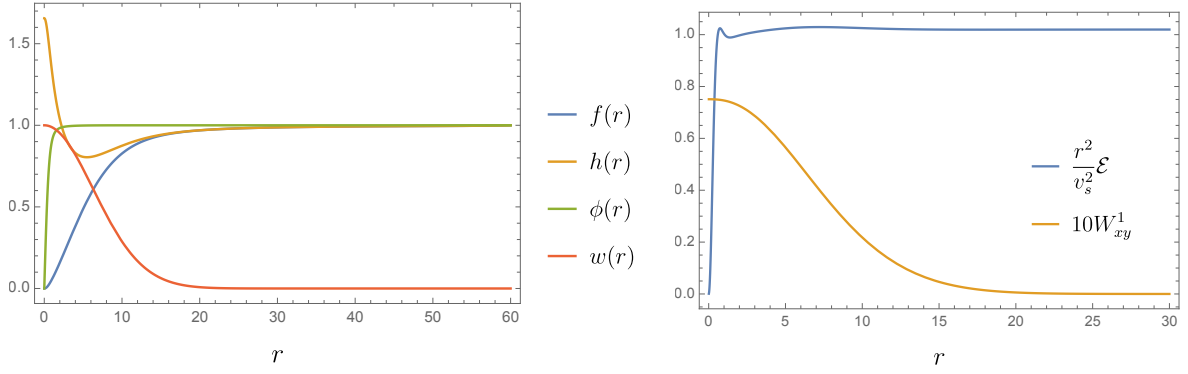\end{aligned}$$

Figure 6.4: Numerical solution for the type-C string [AHY21]. We take the same benchmark parameters as Fig. 6.2. Also we adopt a length unit as $v_s^{-1} = 0.5$. (left): Plots of profile functions. The behavior of the scalar profile functions are the same as one in Fig. 6.3. The profile function of the W^1 field, $w(r)$, approaches to zero as $r \to \infty$ starting from unity at $r = 0$. (right): Plots of energy density (6.3.45) divided by v_s^2/r^2 and the W^1-flux density multiplied by 10. The tension integrated over $0 \leq r \leq 120 \, v_s^{-1}$ is 140.604. The total value of the W^1-flux is calculated to 19.3208, which is consistent with Eq. (6.3.44).

$$+ \frac{2w'(r)^2}{g^2 r^2} + v_s^2 \left(-m_S^2 \phi(r)^2 + \lambda_S v_s^2 \phi(r)^4\right) + \frac{v_s^2}{r^2} \left(r^2 \phi'(r)^2 + \phi(r)^2\right), \tag{6.3.45}$$

and, the EOMs are given as follows:

$$f''(r) + \frac{f'(r)}{r} - \frac{(1 + w(r))^2}{r^2} f(r)$$
$$- \left(2(\alpha_1 + \alpha_2)v^2 f(r)^2 + 2(\alpha_2 + \alpha_3)v^2 h(r)^2 + \kappa_{1S} v_s^2 \phi(r)^2 - m_1^2\right) f(r) - \kappa v_s^2 h(r)\phi(r)^2 = 0, \tag{6.3.46}$$

$$h''(r) + \frac{h'(r)}{r} - \frac{(-1 + w(r))^2}{r^2} h(r)$$
$$- \left(2(\alpha_1 + \alpha_2)v^2 h(r)^2 + 2(\alpha_2 + \alpha_3)v^2 f(r)^2 + \kappa_{1S} v_s^2 \phi(r)^2 - m_1^2\right) h(r) - \kappa v_s^2 f(r)\phi(r)^2 = 0, \tag{6.3.47}$$

$$\phi''(r) + \frac{\phi'(r)}{r} - \frac{\phi(r)}{r^2}$$
$$- \left(2\lambda_S v_s^2 \phi(r)^2 + \kappa_{1S} v^2(f(r)^2 + h(r)^2) + 2\kappa v^2 f(r)h(r)\right)\phi(r) = 0, \tag{6.3.48}$$

$$w''(r) - \frac{w'(r)}{r} - \frac{g_2^2 v^2}{2} f(r)^2 (1 + w(r)) - \frac{g_2^2 v^2}{2} h(r)^2 (-1 + w(r)) = 0. \tag{6.3.49}$$

The obtained numerical solutions are shown in Fig. 6.4. We take the same parameter choice as Eq. (6.3.16) and set the VEV for S as $v_s = 10\, v$. The shapes of the profile functions, the energy density and the flux density are almost similar to those of the type-B string (Fig. 6.3). This can be understood by the argument on non-Abelian moduli in

106

2HDM in Ref. [EKN18b]. That is, when $\tan\beta = 1$, the two ansatz for the Higgs fields (Eqs. (6.3.17) and (6.3.31)) are related by the $SU(2)_C$ custodial transformation:

$$\mathsf{H} \to U^\dagger \mathsf{H} U \tag{6.3.50}$$

with $U = \exp\left[i\frac{\pi}{4}\sigma^2\right]$. This symmetry is respected in the potential $V(H, S)$ when $m_2^2 = \alpha_3 = \alpha_4 = 0$ and $\kappa_{1S} = \kappa_{2S}$, but is explicitly broken in the gauge sector because of $g_1 \neq 0$. Thus the shapes and hence the string tension are slightly different between them.

While the above ansatz has the Z- and W^1-fluxes in the string, there is also a string in which the W^2-flux (and also mixtures of them in general) is confined. Due to the $U(1)_{\mathrm{EM}}$ symmetry in the Lagrangian, they have the degenerated tension. Since the property is almost the same as the one we studied above, we do not consider them in this chapter.

6.3.5 String tensions

The vortex strings we have considered above have the same winding number (unity) associated with the $U(1)_{\mathrm{PQ}}$ symmetry. Because all possible configurations in the theory are classified into topological sectors characterized by the non-trivial first homotopy group $\pi_1(U(1)_{\mathrm{PQ}}) = \mathbb{Z}$, the above fact means that they are in the same topological sector with the topological charge $1 \in \pi_1(U(1)_{\mathrm{PQ}}) = \mathbb{Z}$ and that they can continuously deform to each others. Since their string tensions (energy per length unit) are generically not degenerated, heavier strings decay into the lightest one, which does not decay any further and is a stable solution to the EOMs.We here study the string tensions, i.e., stability of the strings.

For simplicity, we focus on a case with $\tan\beta = 1$. This is realized when $m_2^2 = \alpha_4 = 0$ in the Higgs potential (6.2.10) and $\kappa_{1S} = \kappa_{2S}$ in the mixing term (6.2.14). In this case, as stated above, the type-A string does not have the Z-flux and the type-B one has the winding number unity for $U(1)_Z$. In addition, the type-C string does not have the $U(1)_Z$ winding but does for $U(1)_{W^1}$. It may seem that the type-A one is lighter than type-B and type-C ones since the latter two have the Z and W-fluxes. However, this is not the case when the potential energy is more dominant than that of the gauge sector. Indeed, both the profile functions for the doublets in the type-A string vanish on the core, and thus that leads to a larger amount of the potential energy than those of the type-B and type-C.

On the other hand, the difference of the tensions between the type-B and type-C strings is controlled by the parameter α_3. As explained in the last subsection, in the case $\tan\beta = 1$, the type-C string has only the W^1-flux, and the two strings are related by the custodial $SU(2)_C$ transformation. If $\alpha_3 = 0$ (and $m_2^2 = \alpha_4 = 0$), the Higgs potential V_H respects this symmetry but the gauge sector does not due to the $U(1)_Y$ coupling constant $g_1 \neq 0$. This slightly lifts up the tension of the type-C because of $g_Z = \sqrt{g_2^2 + g_1^2} > g$. The non-zero value of α_3 can change this relation. In Refs. [EKN18b, EHKN20a], it is shown that, in 2HDM, the smaller (larger) value of α_3 tends to make the tension of the
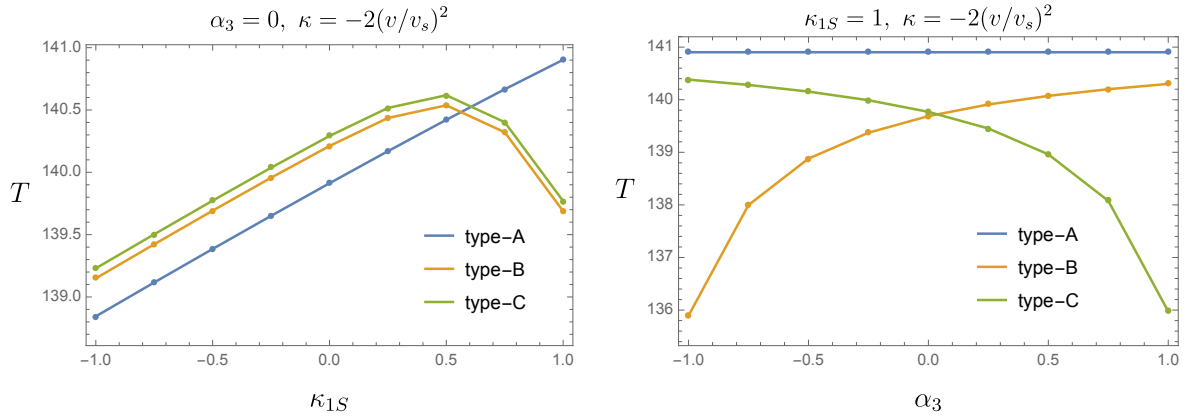
Figure 6.5: String tensions of the type-A, type-B and type-C strings [AHY21]. The parameters are taken as Eq. (6.3.51) and the tension is calculated by integration over $0 \leq r \leq 120\, v_s^{-1}$. (left): α_3 is fixed as 0 and κ_{1S} is taken as a free parameter. The tension of the type-A string increases as κ_{1S} becomes larger, but those of the type-B and type-C ones change to decrease for $\kappa_{1S} \gtrsim 0.5$. (right): κ_{1S} is fixed as 1.0 and α_3 is taken as a free parameter. As is expected, the tension of the type-B (type-C) strings decreases (increases) as α_3 becomes larger. The type-C string becomes the lightest one for $\alpha_3 \gtrsim 0$.

string with the W-flux heavier (lighter) than that of the string with the Z-flux. Thus, in our case, we expect that the type-C string is lighter than the type-A and type-B ones when α_3 is larger than a critical value depending on other parameters.

Keeping $\kappa_{1S} = \kappa_{2S}$, we take the benchmark parameters as

$$\alpha_1 = 1, \quad \lambda_S = 1, \quad \kappa = -2\left(\frac{v}{v_s}\right)^2, \quad v_s = 10\, v, \quad m_2^2 = \alpha_4 = 0, \tag{6.3.51}$$

and take α_2 such that the lightest scalar mass $m_{h_1}^2$ is equal to the SM Higgs mass $(125\,\text{GeV})^2$. We use a length unit $v_s^{-1} = 0.5$. The remaining two parameters α_3 and κ_{1S} are taken as free parameters. The tensions T are calculated over $0 \leq r \leq L$ with the IR cutoff $L = 120\, v_s^{-1}$. Note that, although each tension depends on the IR cutoff as $\sim \log L$, the differences do not, so that we can compare them as far as L is fixed.

Fig. 6.5 shows the relation of the string tensions between the three strings. In the left panel, we fix $\alpha_3 = 0$ and scan κ_{1S} in the range $-1 \leq \kappa_{1S} \leq 1$. The tension of the type-A string increases as κ_{1S} becomes larger, but those of the type-B and type-C ones change to decrease for $\kappa_{1S} \gtrsim 0.5$. It can be seen that the difference of the tensions between type-B and type-C is independent of κ_{1S}, which is reasonable because it is controlled only by the $SU(2)_C$ breaking parameters g_1 and α_3 as stated above.

In the right panel, we fix $\kappa_{1S} = 1.0$ and scan α_3 in the range $-1 \leq \alpha_3 \leq 1$. As is expected, the tension of the type-C (type-B) strings increases (decreases) as α_3 increases. In this parameter choice, that of the type-A string is almost constant, but this tendency depends on the parameters in general. The type-C string becomes the lightest one for $\alpha_3 \gtrsim 0$.

Before closing this section, we stress that the type-C string can be the lightest and stable string for rather wide parameter space. Although we have concentrated on the case of $\tan\beta = 1$, it would not be crucial. Therefore, the axion string produced by the breaking of $U(1)_{\mathrm{PQ}}$ in the early universe necessarily becomes the type-C electroweak axion string after the electroweak phase transition, depending on the parameters in the DFSZ model. In the string, the $U(1)_{\mathrm{EM}}$ symmetry is spontaneously broken. This property causes an interesting phenomenon on the string, superconductivity of vortex strings, as we see in the next section.

6.4   Superconducting DFSZ string

It is known [Wit85] that cosmic strings can be superconductors, i.e., the electric current can flow along a string without resistance, when the electromagnetic gauge symmetry is broken inside the string core. Superconducting strings are often realized by using scalar fields that develop non-zero VEVs only inside the strings or fermionic fields whose gapless modes are confined on the string. Further, non-Abelian vortex strings, in which charged particles such as charged vector bosons are condensed, can also support superconductivity [ABC$^+$91, ABC$^+$90]. In this section, we show that the type-C string discussed in Section 6.3 can be a superconducting string.

In the type-C string, the W^1-flux is confined, and the $U(1)_{\mathrm{EM}}$ symmetry is broken by the charged Higgs components and the W^1 gauge field. Corresponding to the breaking of $U(1)_{\mathrm{EM}}$, the string has a $U(1)_{\mathrm{EM}}$ moduli parameter, which is a flat direction around the string configuration. The existence of the moduli ensures that a (z, t)-dependent fluctuation in the direction of the moduli is a zero mode (massless excitation) in the string background and can travel on the string with the speed of light. It can carry an electric current without resistance, resulting in a supercurrent. We can rephrase this explanation into a more concrete one. The breaking of $U(1)_{\mathrm{EM}}$ means that the charged components of the Higgs field gets the non-zero VEV inside the string, $\hat{Q}H \neq 0$, and that they can play a similar role to the charged scalar field in Ref. [Wit85].

In addition, the string can carry large electric current which induces a large magnetic interaction between the strings. That may affect the cosmological evolution of the string in the DFSZ axion model. In the following analysis, we assume $\tan\beta = 1$ for simplicity, but it is irrelevant to the argument on superconductivity.

6.4.1   Zero modes along the string

Let $\overline{S}$, $\overline{\mathsf{H}}$, $\overline{W}_\mu$ and $\overline{B}_\mu$ be the background configuration for the type-C string given by Eqs. (6.3.31) and (6.3.41). Note that $\overline{Z}_\mu = 0$ due to $\tan\beta = 1$. To find a zero mode excitation, we consider the (z, t)-modulated "gauge transformation" around the type-C

string:

$$S = \overline{S}, \tag{6.4.1}$$

$$\mathsf{H} = \exp\left[i\eta(z,t)\chi(r,\theta)\right]\,\overline{\mathsf{H}}\,\exp\left[i\eta(z,t)\xi(r,\theta)\frac{\sigma^3}{2}\right], \tag{6.4.2}$$

$$W_\mu = \exp[i\eta(z,t)\chi(r,\theta)]\left(\overline{W}_\mu - \frac{i}{g}\delta_\mu^j\partial_j\right)\exp[-i\eta(z,t)\chi(r,\theta)], \tag{6.4.3}$$

$$B_\mu = \overline{B}_\mu + \frac{1}{g_1}\delta_\mu^j\,\eta(z,t)\partial_j\xi(r,\theta) \tag{6.4.4}$$

where $\chi = \chi^a\sigma^a/2$ and $j = r,\theta$. This is not a mere gauge transformation unless η is independent of z and t, but is a (z,t)-dependent physical excitation described by $\eta(z,t)$, $\xi(r,\theta)$ and $\chi^a(r,\theta)$.

Instead of the above expressions, for later use, we analyze an alternative ansatz that is obtained by performing the $SU(2)_L \times U(1)_Y$ gauge transformation with the gauge parameters $(\eta\chi, \eta\xi)$. The transformed ansatz is given by

$$S = \overline{S}, \tag{6.4.5}$$
$$\mathsf{H} = \overline{\mathsf{H}}, \tag{6.4.6}$$
$$W_\mu = \overline{W}_\mu + \delta W_\mu, \tag{6.4.7}$$
$$B_\mu = \overline{B}_\mu + \delta B_\mu \tag{6.4.8}$$

with

$$\delta W_\mu = \frac{1}{g_2}\delta_\mu^\alpha\,\chi\partial_\alpha\eta, \tag{6.4.9}$$

$$\delta B_\mu = -\frac{1}{g_1}\delta_\mu^\alpha\,\xi\partial_\alpha\eta, \tag{6.4.10}$$

where $\alpha = t,z$. For these ansatz (6.4.5)–(6.4.8), the field strength tensors are given by

$$W_{\mu\nu} = \overline{W}_{\mu\nu} + \overline{D}_\mu\delta W_\nu - \overline{D}_\nu\delta W_\mu, \tag{6.4.11}$$
$$B_{\mu\nu} = \overline{B}_{\mu\nu} + \partial_\mu\delta B_\nu - \partial_\nu\delta B_\mu, \tag{6.4.12}$$

where $\overline{W}_{\mu\nu}$, $\overline{B}_{\mu\nu}$ and $\overline{D}_\mu$ are the field strengths and the covariant derivative consisting of the background gauge configurations $\overline{W}_\mu$ and $\overline{Y}_\mu$.

The linearized EOMs for the excitation η, χ^a and ξ are obtained by substituting the ansatz into the full EOMs,

$$(D_\nu W^{\nu\mu})^a = -j_W^{\mu,a}, \tag{6.4.13}$$

$$\partial_\nu B^{\nu\mu} = -j_Y^\mu, \tag{6.4.14}$$

$$D_\mu D^\mu\mathsf{H} = -\frac{\delta V(\mathsf{H},S)}{\delta\mathsf{H}^\dagger}, \tag{6.4.15}$$

110

where $j_W^{\mu,a}$ and j_Y^μ are the $SU(2)_L$ and $U(1)_Y$ currents:

$$j_W^{\mu,a} = \frac{i}{2} g_2 \operatorname{tr} \left[\mathsf{H}^\dagger \sigma^a D^\mu \mathsf{H} - (D^\mu \mathsf{H})^\dagger \sigma^a \mathsf{H} \right], \tag{6.4.16}$$

$$j_Y^\mu = -\frac{i}{2} g_1 \operatorname{tr} \left[\sigma^3 \mathsf{H}^\dagger D^\mu \mathsf{H} - (D^\mu \mathsf{H})^\dagger \mathsf{H} \sigma^3 \right]. \tag{6.4.17}$$

Then we obtain the following equations from Eqs. (6.4.13) and (6.4.14) (see Appendix 6.B for the derivation),

$$\partial^\alpha \eta \left(\overline{D}_j \overline{D}^j \chi \right)^a = \frac{-g_2^2}{2} \partial^\alpha \eta \left(\chi^a \operatorname{tr} |\overline{\mathsf{H}}|^2 + \xi \operatorname{tr} \left[\overline{\mathsf{H}}^\dagger \sigma^a \overline{\mathsf{H}} \sigma^3 \right] \right), \tag{6.4.18}$$

$$\partial^\alpha \eta \partial_j \partial^j \xi = \frac{-g_1^2}{2} \partial^\alpha \eta \left(\xi \operatorname{tr} |\overline{\mathsf{H}}|^2 + 2 \operatorname{tr} \left[\overline{\mathsf{H}}^\dagger \chi \overline{\mathsf{H}} \sigma^3 \right] \right), \tag{6.4.19}$$

$$\overline{D}^j \chi \, \partial^\alpha \partial_\alpha \eta = 0, \tag{6.4.20}$$

$$\partial^j \xi \, \partial^\alpha \partial_\alpha \eta = 0, \tag{6.4.21}$$

and from the EOM for H (6.4.15)

$$\partial^\alpha \partial_\alpha \eta \left(2\chi \overline{\mathsf{H}} + \xi \overline{\mathsf{H}} \sigma^3 \right) = 0. \tag{6.4.22}$$

We have used the fact that the background configurations $\overline{\mathsf{H}}$, $\overline{W}_\mu$ and $\overline{Y}_\mu$ solve the EOMs.

The above equations (6.4.20), (6.4.21) and (6.4.22) are satisfied with

$$\partial^\alpha \partial_\alpha \eta = (\partial_t^2 - \partial_z^2)\eta = 0, \tag{6.4.23}$$

which is a (1+1)-dimensional wave equation. This has the zero mode solutions $\eta = \eta^+(z+t)$ and $\eta = \eta^-(z-t)$ with some functions $\eta^\pm$, and the general solution can be written by a linear combination of these modes. When one is particularly interested in the static case, the t-independent solution is given by

$$\eta(z) = \omega z, \qquad (\omega : \text{const.}) \tag{6.4.24}$$

implying the constant current along the z direction. On the other hand, the radial and angular dependence of the excitations is determined by Eqs. (6.4.18) and (6.4.19). We can see that there are four independent zero modes corresponding to the solutions χ^a ($a = 1, 2, 3$) and ξ. This is understood from the fact that the whole symmetry of $SU(2)_L \times U(1)_Y$ (even $U(1)_{\text{EM}}$) is broken inside the string. In other words, four zero modes can induce the $SU(2)_L$ and $U(1)_Y$ currents on the string.

However, only one of them induces the $U(1)_{\text{EM}}$ current, which generates two-dimensional Coulomb (magnetic) potential far from the string. To illustrate this, let us consider the asymptotic behavior of χ and ξ at $r \to \infty$. At infinity, the $U(1)_{\text{EM}}$ is restored, in which the background configuration $\overline{\mathsf{H}}$ satisfies [EHN20]

$$\overline{\mathsf{H}} \sigma^3 + n^a \sigma^a \overline{\mathsf{H}} = 0, \qquad n^a = -\frac{\operatorname{tr} \left(\sigma^3 \overline{\mathsf{H}}^\dagger \sigma^a \overline{\mathsf{H}} \right)}{\operatorname{tr} |\overline{\mathsf{H}}|^2}, \tag{6.4.25}$$

and $(\overline{D}_\mu n)^a = 0$ and $\mathrm{tr}\,|\overline{\mathsf{H}}|^2 = 2\,v^2$. Using these conditions, the Poisson-like equations (6.4.18) and (6.4.19) become

$$\left(\overline{D}_j\overline{D}^j\chi\right)^a = -g_2^2 v^2 \left(\chi^a - n^a\xi\right), \tag{6.4.26}$$

$$\partial_j\partial^j\xi = -g_1^2 v^2 \left(\xi - \chi^a n^a\right), \tag{6.4.27}$$

which describe the long-range behavior on the xy plane only when $\chi^a - \xi n^a = 0$. Thus, we have the two-dimensional Laplace equation:

$$\frac{1}{r}\partial_r(r\partial_r\xi) = 0 \tag{6.4.28}$$

with $\chi^a = \xi n^a$ for ξ being rotationally invariant ($\partial_\theta\xi = 0$). The asymptotic solution of Eq. (6.4.28) behaves as $\xi \sim \log r$. Substituting this into the expressions of gauge fields gives

$$\delta W_z^a \sim \frac{\omega}{g_2}n^a \log r, \qquad \delta B_z \sim -\frac{\omega}{g_1}\log r, \tag{6.4.29}$$

where we have taken the normalization of ξ such that $\xi \to \log r$ for $r \to \infty$. We find the form of the $U(1)_{\mathrm{EM}}$ field strength

$$F_{rz}^{\mathrm{EM}} = -\sin\theta_W n^a W_{rz}^a + \cos\theta_W Y_{rz}, \tag{6.4.30}$$

$$= -\sin\theta_W n^a \partial_r \delta W_z^a + \cos\theta_W \partial_r \delta Y_z, \tag{6.4.31}$$

$$\sim -\frac{\omega}{er} \quad (r \to \infty). \tag{6.4.32}$$

This is nothing but the magnetic long-range force on the two-dimensional xy plane. Correspondingly, the total amount of $U(1)_{\mathrm{EM}}$ current J_{EM} along the string is estimated from Eq. (6.4.32) as

$$J_{\mathrm{EM}} := -2\pi r F_{rz}^{\mathrm{EM}} \sim \frac{2\pi\omega}{e}. \tag{6.4.33}$$

6.4.2 Current quenching and string interaction

In the above argument, it may seem that the magnitude of the current is given by the parameter ω and can be taken arbitrarily large. However this is not the case since we have ignored the backreaction from the zero modes to the background fields $\overline{S}$, $\overline{\mathsf{H}}$, $\overline{W}_\mu$ and $\overline{Y}_\mu$ by linearizing the EOMs. To examine the backreaction, we look at the following term in the Lagrangian:

$$\mathcal{L} \supset -\mathrm{tr}\left|-ig_2\delta W_z\overline{\mathsf{H}} + i\frac{g_1}{2}\overline{\mathsf{H}}\sigma^3\delta B_z\right|^2 \tag{6.4.34}$$

$$= -\omega^2\,\mathrm{tr}\left|\chi\overline{\mathsf{H}} + \xi\overline{\mathsf{H}}\frac{\sigma^3}{2}\right|^2, \tag{6.4.35}$$

which is obtained by substituting the string ansatz and the solution for $\eta(z)$. This term induces a positive squared mass for the $SU(2)_L \times U(1)_Y$ charged components of $\overline{\mathsf{H}}$. For

$\omega \to \infty$, the charged components vanish, $\chi\overline{\mathsf{H}}+\xi\overline{\mathsf{H}}\frac{\sigma^3}{2} \to 0$, which decreases the $SU(2)_L$ and $U(1)_Y$ currents from the Higgs field, $j_W^{z,a}$ and j_Y^z ((6.4.16) and (6.4.17)). Correspondingly, the right hand sides of Eqs. (6.4.18) and (6.4.19) vanish everywhere, and they have only a trivial solution $\xi = \chi^a = 0$.[4] Thus, the backreaction from an extremely large ω reduces the amount of the current. Such behavior is known as the current quenching [Wit85].

Now, let us estimate the maximum value of the current. For the $U(1)_{\text{EM}}$ zero mode, $\chi^a = \xi n^a$, the mass term (6.4.35) reads

$$- (\omega\xi)^2 \operatorname{tr} |\hat{Q}\overline{\mathsf{H}}|^2 = -(\omega\xi)^2 \frac{v^2}{2}(f - h)^2, \tag{6.4.36}$$

where $\hat{Q}$ is the $U(1)_{\text{EM}}$ generator defined in Eq. (6.2.27), and we have used the concrete expression of $\overline{\mathsf{H}}$ for the type-C string, Eq. (6.3.31). On the other hand, using $\kappa_{1S} = \kappa_{2S}$ for $v_1 = v_2 = v$, the mass terms for f and h that are originally present in the Lagrangian are

$$- \mathcal{L} \ni \frac{v^2}{r^2} \left[(1 + w)^2 f^2 + (1 - w)^2 h^2 \right] + (-m_1^2 + \kappa_{1S} v_s^2 \phi^2)(f^2 + h^2). \tag{6.4.37}$$

Due to the backreaction term Eq. (6.4.36), the two-by-two mass matrix M^2 for (f, h) is changed and not diagonal. It is sufficient to consider the signs of the eigenvalues of M^2. If they are positive inside the string, then f and h tend to vanish, and hence $(f - h)^2 \propto \operatorname{tr} |\hat{Q}H|^2 = 0$, which means that the $U(1)_{\text{EM}}$ symmetry is restored even inside the string. On the other hand, if one of them is negative, the quenching is not significant and the $U(1)_{\text{EM}}$ symmetry is still broken. Then the current can be increased with $|\omega|$.

Inside the string, $r \lesssim v^{-1}$, the determinant of the matrix M^2 is calculated as

$$\det \mathsf{M}^2 \sim m_1^4 + \frac{4}{r^2} \left(\omega^2 \xi^2 - m_1^2 + \kappa_{1S}\phi^2 \right) + \left(-m_1^2 + \kappa_{1S} v_s^2 \phi^2 \right) \omega^2 \xi^2, \tag{6.4.38}$$

where we have used $w(r) \sim 1$ there. Note that the mass matrix and hence the determinant vary with the radius r in and out the string core as

$$\det \mathsf{M}^2 \sim \begin{cases} v_s^4 + \frac{4}{r^2} \left(\omega^2 \xi^2 - v^2 \right) - v^2 \omega^2 \xi^2 & \text{for } r \gtrsim v_s^{-1}, \\ v_s^4 + \frac{4}{r^2} \left(\omega^2 \xi^2 - v_s^2 \right) - v_s^2 \omega^2 \xi^2 & \text{for } r \lesssim v_s^{-1}. \end{cases} \tag{6.4.39}$$

Clearly, there is a critical value of $|\omega\xi|$, for which the sign of the term proportional to r^{-2} changes from negative to positive. For a value smaller than the critical one, there exists a region where the determinant is negative, avoiding the current quenching. The critical value of $|\omega\xi|$ is $\sim v_s$ around the core. Then the current magnitude becomes maximum for this value. Note that ξ is of order unity inside the core to be connected with the asymptotic form $\xi \to \log r$. Thus, $|\omega| \sim v_s$ in this case. Note that the definition of the $U(1)_{\text{EM}}$ moduli may be different a bit from $\chi^a = \xi n^a$ inside the string [EHN20]. The difference is however subleading and negligible for the maximum amount of the supercurrent.

---

[4]A solution behaving like $\sim \log r$ for all r is singular at $r = 0$.

Finally, we consider the tension of the string (energy per unit length). When $\omega = 0$, the string reduces to the type-C string and the tension T is dominated by the gradient energy from the axion:

$$T(\omega = 0) \sim 2\pi \int^L r dr |\partial_i S|^2 \sim 2\pi v_s^2 \log L, \qquad (6.4.40)$$

with L being an IR cutoff. The logarithmic divergence is natural because $U(1)_{\text{PQ}}$ is a global symmetry. On the other hand, for $\omega \neq 0$, there should be an additional contribution to the tension from the magnetic field induced by the $U(1)_{\text{EM}}$ current:

$$T(\omega) = T(0) + T_{\text{EM}} \qquad (6.4.41)$$

where

$$T_{\text{EM}} \sim 2\pi \int^L r dr \left(F_{rz}^{\text{EM}} \right)^2 \sim \frac{2\pi\omega^2}{e^2} \log L. \qquad (6.4.42)$$

Thus the current also induces a logarithmically divergent energy, which is comparable to that from the gradient term, for the maximal current $|\omega| \sim v_s$ discussed above.

This result provides an interesting sight for the interaction between the strings. Let us consider two superconducting strings that are well separated in the xy plane. They are assumed to have the same winding for $U(1)_{\text{PQ}}$ and $U(1)_{W^1}$, and contain the superconducting currents with the same sign. As is well-known, the gradient energy of S gives a repulsive force $\sim v_s^2/R_0$ with R_0 being the distance between them. However, the magnetic interaction induced from the supercurrent provides an attractive force,

$$F = -\frac{(J_{\text{EM}})^2}{2\pi R_0} \sim -\frac{2\pi\omega^2}{e^2 R_0}. \qquad (6.4.43)$$

Therefore, the superconducting strings can receive the attractive force overcoming the repulsive one with $|\omega| \sim v_s$.

6.4.3 Y-junction formation

In usual cases, a pair of axion strings reconnects with a probability of the order of unity when they collide. Thanks to this reconnection process, a network of strings in the early universe produces small string loops, which soon shrink and disappear by emitting radiations, and sufficiently looses the energy if the network is dense. The time evolution of the energy density approaches the so-called scaling behavior, and the total energy density of the universe is not dominated by the string network. However, the attractive interaction discussed above, which is induced by superconducting current, can change this picture drastically. In particular, it is known that an attractive interaction between strings could form the Y-junction [BLM97, BK94, CKS06, CKS07, SAC$^+$08, BS08a, BCM$^+$09, HEK$^+$14, HST$^+$13], which is a bound state of two strings (see Fig. 6.6). If Y-junctions are formed frequently, that reduces the effective reconnection probability and
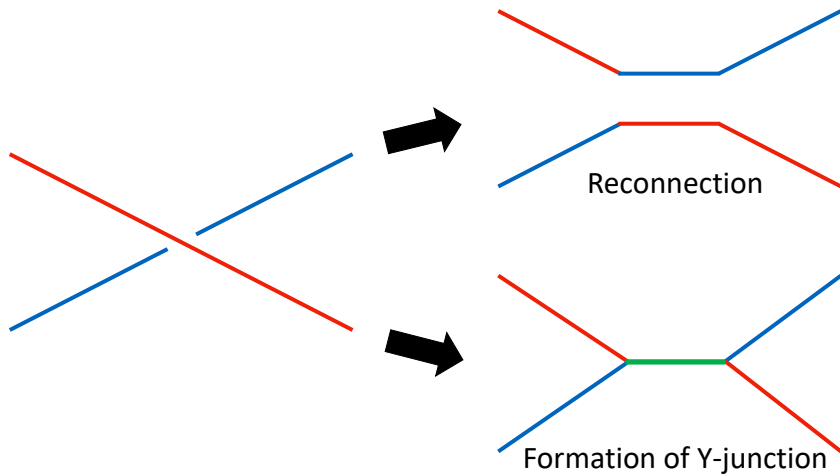
Figure 6.6: Reconnection process and formation of a Y-junction [AHY21].

makes non-trivial whether the string network evolves to the scaling solution. As the first step to study the Y-junctions of the axion strings, we present a rough estimation of the formation probability of Y-junctions in this section.

Firstly, let us assume the presence of a primordial magnetic field (PMF) after the electroweak phase transition. PMF is well motivated as an origin of intergalactic magnetic fields in order to explain the galactic magnetic fields observed today via the dinamo mechanism [Par55]. (For a review, see, e.g., Ref. [DN13].) There are the observational lower and upper bounds on the present strength of intergalactic magnetic fields for a coherent length $\lambda \gtrsim 0.1\,\mathrm{Mpc}$ as $3 \times 10^{-16}\,\mathrm{G} \lesssim B_0 \lesssim 10^{-11}\,\mathrm{G}$, where the lower one is set by the non-observation of secondary photons from the emission of highly collimated gamma rays by blazars [NV10] and the upper one is from the CMB observations [JS19]. For simplicity, we further assume that the power spectrum of PMF is scale invariant and almost coherent over the entire Hubble horizon, which could be realized for the inflationary magnetogenesis [DN13].

We then show that PMF can induce large superconducting currents on the strings. Such large currents are sufficient to form the Y-junctions. The scale invariant PMF evolves as

$$B(t) \propto a(t)^{-2}\,,\tag{6.4.44}$$

where $B(t)$ and $a(t)$ are the magnetic field strength and the scale factor at the cosmological time t, respectively. It is convenient to define a ratio of the energy density of PMF (ρ_B) to that of photon (ρ_γ),

$$\epsilon := \frac{\rho_B}{\rho_\gamma} \sim B(t)^2 G_N t^2,\tag{6.4.45}$$

with G_N being the Newton constant. The ratio ϵ is a constant as the universe expands.
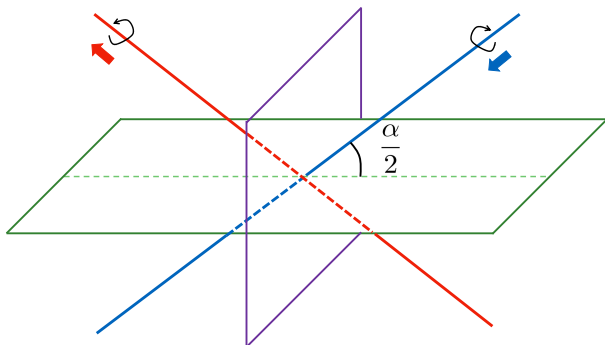
Figure 6.7: Two strings (red and blue lines) collide with the crossing angle α [AHY21]. The black arrows indicate the directions of the topological winding number of $U(1)_{\mathrm{PQ}}$. The red and blue arrows indicate the directions of the flowing electric currents, which are parallel for $\alpha = 0$. The green and purple planes are orthogonal and include the collision point.

If we take the upper limit on B_0, we have $\epsilon \sim 10^{-11}$.

In the early universe, the superconducting strings (Type-C EW axion strings) move with velocity v_{str} ($\sim \mathcal{O}(1)$) in the presence of PMF and hence feel the electric fields $E \sim B(t)v_{\mathrm{str}}$, which induce the superconducting current,

$$J_{\mathrm{PMF}} \sim e^2 B(t)\xi v_{\mathrm{str}}, \tag{6.4.46}$$

with ξ being a string typical length. Since there are no superconducting strings before the electroweak phase transition, we can assume that the scaling property $\xi \sim t$ holds at least just after the phase transition, and obtain

$$J_{\mathrm{PMF}} \sim 10^{12} \left(\frac{\epsilon}{10^{-11}}\right)^{1/2} \mathrm{GeV} \sim 10^{12} \left(\frac{B_0}{10^{-11}\,\mathrm{G}}\right) \mathrm{GeV}. \tag{6.4.47}$$

Note that this is independent of t. For the upper limit of B_0, yielding $\epsilon \sim 10^{-11}$, the induced current (6.4.47) is larger than the maximum current estimated in the last subsection, $J_{\mathrm{EM}} \sim 2\pi v_s/e$, with $v_s \approx 10^{9-12}\,\mathrm{GeV}$. Therefore, the current is saturated to the maximum value by PMF. In the following argument, we use this maximum current as those the strings carry in the early universe.

Let us discuss the formation of Y-junctions. They can be formed by collisions of two superconducting strings when they feel an attractive force and are trapped in the potential. We suppose that the two strings collide with the crossing angle α and that they are identical and parallel for $\alpha = 0$. The superconducting currents are assumed to flow in the same direction for $\alpha = 0$ (the opposite case will be considered later). The three-dimensional dynamics of the collision event is rather complicated and difficult to analyze. However a qualitative picture can be understood by reducing it on two orthogonal planes

116

including the colliding point [CT86, She87, She88] (see Fig. 6.7). On one of them (purple plane in Fig. 6.7), the situation is regarded as a collision (scattering) event of two point-like vortices in two dimensions while, on the other plane (green plane in Fig. 6.7), as a vortex-antivortex collision resulting in the annihilation in two dimensions. Note that this picture reproduces the reconnection process shown in the upper-right picture in Fig. 6.6 when the strings have no superconducting current; two scattered vortices on the purple plane and nothing on the green one.

We concentrate on the two-dimensional analysis of the superconducting vortex-vortex collision since the current does not change the annihilation. Unlike the non-superconducting case leading to the $90°$ scattering, the long-range magnetic interaction plays a crucial role in our case. On the reduced plane, the vortex-vortex pair feel a net interaction potential,

$$V \sim \frac{v_s^2}{e^2} \cos \frac{\alpha}{2} \log r \,, \tag{6.4.48}$$

where r is the distance between the two vortices and we have ignored the axion-mediated repulsive interaction, which should be subleading by a factor e^2 compared to Eq. (6.4.48). If the vortices do not have sufficient kinetic energy to escape to infinity, they become trapped by the potential. Thus we obtain a condition to form a bound state,

$$\frac{v_s^2}{e^2} \cos \frac{\alpha}{2} \log \frac{L}{\delta} \geq (\gamma - 1)\mu \,, \tag{6.4.49}$$

where γ and μ are the Lorentz factor and the tension of the colliding vortices. L and δ are the IR and UV cutoff for the potential, which we take as the Hubble radius and the width of the strings, respectively. As considering just after the electroweak phase transition, the logarithmic factor gives $\log(10^{17} \times v_s/v_{\text{EW}}) \sim 50$. In addition, we take a mildly relativistic velocity ~ 0.6 for the vortices, yielding $\gamma \sim 1.25$, and thus Eq. (6.4.49) gives

$$\cos \frac{\alpha}{2} \geq 10^{-3} \,, \tag{6.4.50}$$

which means that they *almost always* form the bound state except for $\alpha \approx \pi$.

On the other hand, they cannot form such a bound state in the case that the currents flow in the opposite directions (anti-parallel) on the vortex-vortex plane because they always feel a repulsive force. Therefore, we obtain a rough estimation for the formation probability of the bound state,

$$\begin{cases} \text{Y-junction formed} & \text{(current in the same directions)} \\ \text{not formed} & \text{(current in the opposite directions)} \end{cases} \Rightarrow \text{probability} \approx \frac{1}{2} \,. \tag{6.4.51}$$

Note that this is based on the two-dimensional analysis focusing on the collision point. This picture may break down for the case that the dynamics after colliding is dominated by other parts of the strings than the collision point. Furthermore, the formed Y-junction could be peeled off, depending on the velocities and the crossing angle of the strings. For a
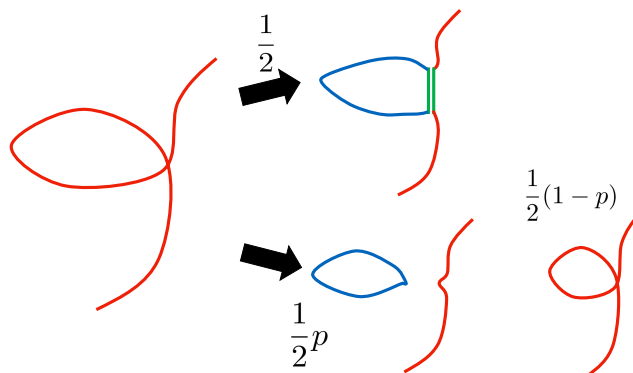
Figure 6.8: Self-intersection of a superconducting string [AHY21]. The Y-junction (green doubled line) is formed with probability $\frac{1}{2}$. Otherwise, it reconnects producing a small loop (blue line) or passes through. The reconnection probability is $p \sim 1$.

more detailed study including these effects, it is necessary to perform a three-dimensional simulation, which is beyond the scope of the present paper.

Finally, we discuss a consequence of the formation of Y-junctions. When a superconducting string intersects with itself, it forms the Y-junction with probability $1/2$, produces a small loop with probability $p/2$, or passes through with probability $(1-p)/2$ (see Fig. 6.8), where p is the reconnection probability without the current ($p \sim 1$). If such a Y-junction-connected loop (upper one in Fig. 6.8) is produced, it is not obvious whether the strings sufficiently loose their energy, and the scaling behavior of the energy density of strings is not ensured. Once the energy density of the universe is dominated by such superconducting strings, it causes large impacts on cosmology, and hence some parameter region in the DFSZ axion model may be constrained.

6.5 Summary

We have studied the axion strings with the electroweak gauge flux, and their superconductivity in the DFSZ model. We constructed three types of the electroweak axion string solutions, which have similar properties to those of (non-Abelian) vortices in two Higgs doublet model. We also showed that in some parameter space, the string with W-flux, we called the type-C string, can be lighter than those with Z-flux. The type-C string exhibits superconductivity and a large electric current can flow along the string. This large current may realize a net attractive force between the axion strings, which could form the so-called Y-junctions in the early universe. By considering the string collision reduced onto two-dimensional planes, the probability of the formation of the Y-junctions is estimated to be $\sim 1/2$.

Type	Comments	up-type quarks	donw-type quark	charge lepton
Type I	Fermiophilic	H_2	H_2	H_2
Type II	MSSM-like	H_2	H_1	H_1
X	lepton-specific	H_2	H_2	H_1
Y	Filipped	H_2	H_1	H_2

Table 6.2: Classification of THDM

Once such Y-junctions are formed, they can affect the evolution of the string network and make non-trivial whether the network evolves to the scaling solution. If no obeying the scaling behavior, the string network could dominate the energy density of the the universe and the model is severely constrained. To conclude whether this is true or not, we need detailed numerical simulations on the time evolution of the network taking into account both the axionic and magnetic interactions. In addition, the Y-junction provides characteristic signals in astrophysical observations. It is worthwhile to study the Y-junction dynamics of the DFSZ axion strings[5] within a phenomenologically allowed parameter space.

In this chapter, we focus on the $U(1)_{\mathrm{EM}}$ symmetry breaking through the W-flux and the charged Higgs components. On the other hand, the type-A and type-B strings also could be superconducting. The Z-flux give a negative mass contribution to the W-boson as

$$ig \cos\theta_W \overline{Z}_{\mu\nu} W^{-\mu} W^{+\nu}, \tag{6.5.1}$$

which leads the instability called the W-condensate [AO92, AO90b, AO90a]. This can be another possible mechanism realizing superconductivity. If the magnitude of the background flux is sufficiently large, the type-A and type-B strings also can be superconducting.

Appendix 6.A   Memo for Two Higgs doublet model

In this section, we show brief summary of the Two Higgs doublet model (THDM) and its bilinear formalism.

6.A.1   Two Higgs doublet model

In THDM, we have two Higgs doublets and the general scalar potential is given by

$$V_H = m_{11}^2 |H_1|^2 m_{22}^2 |H_2|^2 - \left(m_{12}^2 H_1^\dagger H_2 + \text{h.c.}\right)$$

---

[5]Y-junctions could also be formed in the KSVZ model when heavy extra fermions are $U(1)_{\mathrm{EM}}$ charged and the strings are superconducting.

$$+ \frac{\beta_1}{2}|H_1|^4 + \frac{\beta_2}{2}|H_2|^4$$
$$+ \beta_3|H_1|^2|H_2|^2 + \beta_4(H_1^\dagger H_2)(H_2^\dagger H_1) + \left\{ \frac{\beta_5}{2}\left(H_1^\dagger H_2\right)^2 + \text{h.c.} \right\}, \tag{6.A.1}$$

where m_{12}^2 is a $\mathbb{Z}_2$ soft breaking parameter. Depending on the Yukawa couplings between two Higgs doublets and SM fermions, some types are able to be considered (shown in Table 6.2).

6.A.2   Higgs bilinear formlism in THDM

According to Ref. [GMW11], we introduce the Higgs bilinear H by using the Higgs doublets as,

$$\mathsf{H} = (i\sigma^2 H_1^*, H_2) = (\tilde{H}_1, H_2), \tag{6.A.2}$$

which transforms under the $SU(2)_L \times U(1)_Y$ gauge transformation as

$$\mathsf{H} \mapsto \exp\left(i\alpha^a(x)\frac{\sigma^a}{2}\right)\mathsf{H}\exp\left(-i\beta(x)\frac{\sigma^3}{2}\right). \tag{6.A.3}$$

The trace and determinant of H's polynomials are expressed as [EKN18b]

$$\text{tr}(\mathsf{H}^\dagger\mathsf{H}) = H_1^\dagger H_1 + H_2^\dagger H_2, \tag{6.A.4}$$
$$\text{tr}(\mathsf{H}^\dagger\mathsf{H}\sigma^3) = H_1^\dagger H_1 - H_2^\dagger H_2, \tag{6.A.5}$$
$$\det\mathsf{H} = H_1^\dagger H_2, \quad \det\mathsf{H}^\dagger = H_2^\dagger H_1, \tag{6.A.6}$$
$$\text{tr}\left[(\mathsf{H}^\dagger\mathsf{H})(\mathsf{H}^\dagger\mathsf{H})\right] = (H_1^\dagger H_1 + H_2^\dagger H_2)^2 - 2(H_1^\dagger H_2)(H_2^\dagger H_1), \tag{6.A.7}$$
$$\text{tr}\left[(\mathsf{H}^\dagger\mathsf{H})\sigma^3(\mathsf{H}^\dagger\mathsf{H})\right] = (H_1^\dagger H_1)^2 - (H_2^\dagger H_2)^2, \tag{6.A.8}$$
$$\text{tr}\left[(\mathsf{H}^\dagger\mathsf{H})\sigma^3(\mathsf{H}^\dagger\mathsf{H})\sigma^3\right] = (H_1^\dagger H_1 - H_2^\dagger H_2)^2 + 2(H_1^\dagger H_2)(H_2^\dagger H_1), \tag{6.A.9}$$
$$\det\mathsf{H}^2 = (H_1^\dagger H_2)^2, \quad \det\mathsf{H}^{\dagger 2} = (H_2^\dagger H_1)^2, \tag{6.A.10}$$
$$\det\mathsf{H}^\dagger\mathsf{H} = (H_2^\dagger H_1)(H_1^\dagger H_2). \tag{6.A.11}$$

From these equations, we can express products of H_i by the bilinear Higgs matrix H as

$$H_1^\dagger H_1 = \frac{1}{2}\left[\text{tr}(\mathsf{H}^\dagger\mathsf{H}) + \text{tr}(\mathsf{H}^\dagger\mathsf{H}\sigma^3)\right], \tag{6.A.12}$$

$$H_2^\dagger H_2 = \frac{1}{2}\left[\text{tr}(\mathsf{H}^\dagger\mathsf{H}) - \text{tr}(\mathsf{H}^\dagger\mathsf{H}\sigma^3)\right], \tag{6.A.13}$$

$$H_1^\dagger H_2 = \det\mathsf{H}, \quad H_2^\dagger H_1 = \det\mathsf{H}^\dagger, \tag{6.A.14}$$

$$(H_1^\dagger H_1)^2 = \frac{1}{4}\left\{\text{tr}\left[(\mathsf{H}^\dagger\mathsf{H})(\mathsf{H}^\dagger\mathsf{H})\right] + 2\,\text{tr}\left[(\mathsf{H}^\dagger\mathsf{H})\sigma^3(\mathsf{H}^\dagger\mathsf{H})\right] + \text{tr}\left[(\mathsf{H}^\dagger\mathsf{H})\sigma^3(\mathsf{H}^\dagger\mathsf{H})\sigma^3\right]\right\},$$
$$\tag{6.A.15}$$

$$(H_2^\dagger H_2)^2 = \frac{1}{4}\left\{\text{tr}\left[(\mathsf{H}^\dagger\mathsf{H})(\mathsf{H}^\dagger\mathsf{H})\right] - 2\,\text{tr}\left[(\mathsf{H}^\dagger\mathsf{H})\sigma^3(\mathsf{H}^\dagger\mathsf{H})\right] + \text{tr}\left[(\mathsf{H}^\dagger\mathsf{H})\sigma^3(\mathsf{H}^\dagger\mathsf{H})\sigma^3\right]\right\},$$
$$\tag{6.A.16}$$

$$(H_1^\dagger H_1)(H_2^\dagger H_2) = \frac{1}{4}\left\{\mathrm{tr}\left[(H^\dagger H)(H^\dagger H)\right] - \mathrm{tr}\left[(H^\dagger H)\sigma^3(H^\dagger H)\sigma^3\right]\right\} + \det H^\dagger H, \tag{6.A.17}$$

$$(H_1^\dagger H_2)^2 = \det H^2, \quad (H_2^\dagger H_1)^2 = \det H^{\dagger 2}, \quad (H_1^\dagger H_2)(H_2^\dagger H_1) = \det(H^\dagger H). \tag{6.A.18}$$

Using these equations, the scalar potential (6.A.1) is rewritten as

$$
\begin{aligned}
V_H &= \frac{m_{11}^2 + m_{22}^2}{2}\,\mathrm{tr}(H^\dagger H) - \frac{m_{11}^2 - m_{22}^2}{2}\,\mathrm{tr}(H^\dagger H\sigma^3) - m_{12}^2(\det H + \text{h.c.}) \\
&\quad + \frac{\beta_1 + \beta_2 + 2\beta_3}{8}\,\mathrm{tr}\left[(H^\dagger H)(H^\dagger H)\right] + \frac{\beta_1 + \beta_2 - 2\beta_3}{8}\,\mathrm{tr}\left[(H^\dagger H)\sigma^3(H^\dagger H)\sigma^3\right] \\
&\quad + \frac{\beta_1 - \beta_2}{4}\,\mathrm{tr}\left[(H^\dagger H)\sigma^3(H^\dagger H)\right] + (\beta_3 + \beta_4)\det(H^\dagger H) \\
&\quad + \left\{\frac{\beta_5}{2}\det H^2 + \text{h.c.}\right\} \tag{6.A.19}
\end{aligned}
$$

$$
\begin{aligned}
&= \frac{m_{11}^2 + m_{22}^2}{2}\,\mathrm{tr}\,|H|^2 - \frac{m_{11}^2 - m_{22}^2}{2}\,\mathrm{tr}(|H|^2\sigma^3) - m_{12}^2(\det H + \text{h.c.}) \\
&\quad + \frac{\beta_1 + \beta_2 - 2\beta_3 - 4\beta_4}{8}\,\mathrm{tr}\,|H|^4 + \frac{\beta_3 + \beta_4}{2}\left(\mathrm{tr}\,|H|^2\right)^2 + \frac{\beta_1 + \beta_2 - 2\beta_3}{8}\,\mathrm{tr}\left[|H|^2\sigma^3|H|^2\sigma^3\right] \\
&\quad + \frac{\beta_1 - \beta_2}{4}\,\mathrm{tr}\left[|H|^2\sigma^3|H|^2\right] \\
&\quad + \left\{\frac{\beta_5}{2}\det H^2 + \text{h.c.}\right\} \tag{6.A.20}
\end{aligned}
$$

$$
\begin{aligned}
=: &\ m_1^2\,\mathrm{tr}\,|H|^2 - m_2^2\,\mathrm{tr}(|H|^2\sigma^3) - m_3^2(\det H + \text{h.c.}) \\
&+ \alpha_1\,\mathrm{tr}\,|H|^4 + \alpha_2\left(\mathrm{tr}\,|H|^2\right)^2 + \alpha_3\,\mathrm{tr}\left(|H|^2\sigma^3|H|^2\sigma^3\right) + \alpha_4\,\mathrm{tr}\left(|H|^2\sigma^3|H|^2\right) \\
&+ \left\{\frac{\alpha_5}{2}\det H^2 + \text{h.c.}\right\}, \tag{6.A.21}
\end{aligned}
$$

where we used the Cayley-Hamilotn identity

$$\mathrm{tr}[A^2] - (\mathrm{tr}\,A)^2 + 2\det A = 0,$$

and we can obtain the following coupling of the scalar potential relations:

$$
\begin{aligned}
m_1^2 &= \frac{m_{11}^2 + m_{22}^2}{2}, \quad m_2^2 = \frac{m_{11}^2 - m_{22}^2}{2}, \quad m_3^2 = m_{12}^2, \\
\alpha_1 &= \frac{\beta_1 + \beta_2 - 2\beta_3 - 4\beta_4}{8}, \quad \alpha_2 = \frac{\beta_3 + \beta_4}{2}, \\
\alpha_3 &= \frac{\beta_1 + \beta_2 - 2\beta_3}{8}, \quad \alpha_4 = \frac{\beta_1 - \beta_2}{4}, \quad \alpha_5 = \beta_5,
\end{aligned} \tag{6.A.22}
$$

$$
\begin{aligned}
m_{11}^2 &= m_1^2 + m_2^2, \quad m_{22}^2 = m_1^2 - m_2^2, \quad m_{12}^2 = m_3^2, \\
\beta_1 &= 2(\alpha_1 + \alpha_2 + \alpha_3 + \alpha_4), \quad \beta_2 = 2(\alpha_1 + \alpha_2 + \alpha_3 - \alpha_4), \\
\beta_3 &= 2(\alpha_1 + \alpha_2 - \alpha_3), \quad \beta = -2(\alpha_1 - \alpha_3), \quad \beta_5 = \alpha_5.
\end{aligned} \tag{6.A.23}
$$

Appendix 6.B Derivation of the linearized EOMs

By substituting the string ansatz into the EOM (6.4.13) for $\mu = \alpha$, we have

$$\left(\overline{D}_j\overline{D}^j\delta W^\alpha\right)^a = \frac{-i}{2}g_2\,\mathrm{tr}\left[\overline{\mathsf{H}}^\dagger\sigma^a\left(-ig\delta W^\alpha\overline{\mathsf{H}} + i\frac{g_1}{2}\delta B^\alpha\overline{\mathsf{H}}\sigma^3\right) - \mathrm{h.c.}\right], \qquad (6.\mathrm{B}.1)$$

where we have used the fact that the background configurations $\overline{\mathsf{H}}$, $\overline{W}_\mu$ and $\overline{B}_\mu$ solve the EOMs. The equation is explicitly written by the functions η, χ and ξ :

$$(\text{l.h.s.}) = \frac{1}{g_2}\partial^\alpha\eta\left(\overline{D}_j\overline{D}^j\chi\right)^a, \qquad (6.\mathrm{B}.2)$$

$$(\text{r.h.s}) = \frac{-g_2}{2}\partial^\alpha\eta\,\mathrm{tr}\left[\overline{\mathsf{H}}^\dagger\{\sigma^a,\chi\}\overline{\mathsf{H}} + \left(\overline{\mathsf{H}}^\dagger\sigma^a\overline{\mathsf{H}}\frac{\sigma^3}{2} + \frac{\sigma^3}{2}\overline{\mathsf{H}}^\dagger\sigma^a\overline{\mathsf{H}}\right)\xi\right] \qquad (6.\mathrm{B}.3)$$

$$= \frac{-g_2}{2}\partial^\alpha\eta\left(\chi^a\,\mathrm{tr}\,|\overline{\mathsf{H}}|^2 + \xi\,\mathrm{tr}\left[\overline{\mathsf{H}}^\dagger\sigma^a\overline{\mathsf{H}}\sigma^3\right]\right), \qquad (6.\mathrm{B}.4)$$

which implies the linearized EOM (6.4.18). A similar procedure for the EOM of B_μ (6.4.14) leads to the linearized one (6.4.19). On the other hand, for the EOM (6.4.13) for $\mu = j$, we have

$$\left(D_\nu W^{\nu j}\right)^a = -\frac{i}{2}g_2\,\mathrm{tr}\left[\overline{\mathsf{H}}^\dagger\sigma^a\overline{D}^j\overline{\mathsf{H}} - (\overline{D}^j\overline{\mathsf{H}})^\dagger\sigma^a\overline{\mathsf{H}}\right]. \qquad (6.\mathrm{B}.5)$$

The l.h.s. is divided into two pieces

$$\left(D_\nu W^{\nu j}\right)^a = \left(\overline{D}_k W^{kj}\right)^a + \left(D_\alpha W^{\alpha j}\right)^a \qquad (6.\mathrm{B}.6)$$

with $k = r,\theta$. The first term in the r.h.s. of Eq. (6.B.6) is found to be equal to the r.h.s. of Eq. (6.B.5), and they are cancelled out from the EOM. The remaining second term is given at the leading order of δW as

$$D_\alpha W^{\alpha j} = -\partial_\alpha\overline{D}^j\delta W^\alpha + ig_2\left[\delta W_\alpha,\overline{D}^j\delta W^\alpha\right] \approx \frac{-1}{g_2}\overline{D}^j\chi\,\partial^\alpha\partial_\alpha\eta, \qquad (6.\mathrm{B}.7)$$

which implies the linearized EOM (6.4.20). The similar derivation holds for the gauge field B_μ.

Appendix 6.C Aharonov-Bohm string, axion string and anomaly inflow

Let us consider the system of two gauge fields $F_2 = dA_1$, $\tilde{F}_2 = d\tilde{A}_1$, two form field B_2 and the axion a:

$$S = \int_M \left(\frac{1}{2}F_2 \wedge *_4 F_2 + \frac{1}{2}\tilde{F} \wedge *_4\tilde{F}_2 + \frac{1}{2}dB_2 \wedge *_4 dB_2 + \frac{1}{2}da \wedge *_4 da\right.$$

$$\left. + B_2 \wedge \tilde{F}_2 + \kappa a F_2 \wedge F_2\right), \qquad (6.\mathrm{C}.1)$$

where M denotes the total spacetime. We assume that a has 2π periodicity $a \simeq a + 2\pi$. In this system, there exist two-types of string objects.
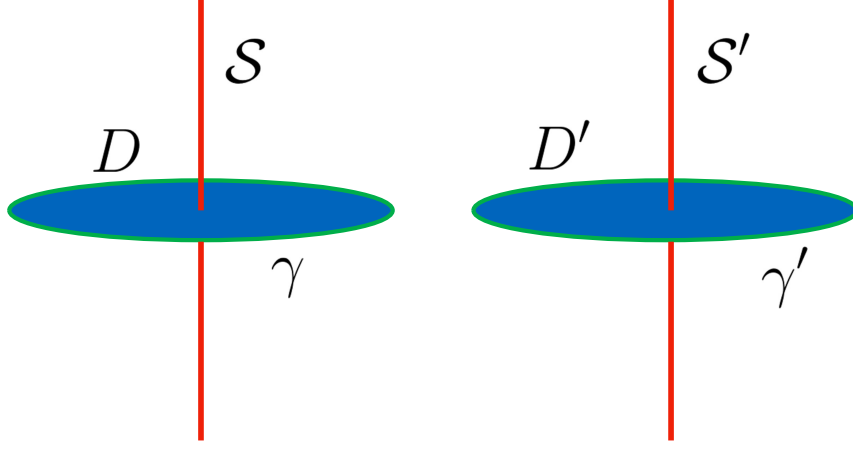
Figure 6.9: Schematic picture of string objects.

6.C.1 Aharonov-Bohm string

The first one is a string charactrized by the holonomy around the string

$$\mathrm{hol}(\gamma) = \exp i \int_\gamma \tilde{A}_1 = \exp i \int_D \tilde{F}_2 = \exp i\Phi, \tag{6.C.2}$$

which has non-trivial gauge flux. The string electrically interacts with the two form field and the gauge field has the following Lagrangian:

$$\int_M B_2 \wedge \tilde{F}_2 + \int_{\mathcal{S}} B_2, \tag{6.C.3}$$

which dual picture is discussed in Section 2.B.

6.C.2 Axion string and anomaly inflow

Another string is a so called axion string, which is characterized by the monodromy of the axion field around the string

$$\int_{\gamma'} da = 2\pi, \tag{6.C.4}$$

which implies that this is a magnetic object for the axion field. The EOM of the axion is

$$d *_4 da = \kappa F_2 \wedge F_2, \tag{6.C.5}$$

the right-handed side comes from the Chern-Simons coupling $\kappa a F_2 \wedge F_2$. This equation is rewritten as

$$-d *_4 da + \kappa F_2 \wedge F_2 = d\big(- *_4 da + \kappa A_1 \wedge dA_1\big) = 0. \tag{6.C.6}$$

If we consider the following large grauge transformation

$$A_1 \mapsto A_1 + \beta_1, \qquad d\beta_1 = 0, \quad \beta_1 \neq d\alpha, \tag{6.C.7}$$

the second term in Eq. (6.C.6) is transformed as

$$\int_M \delta_A \big(\kappa A_1 \wedge dA_1\big) = \int_M \big(\kappa \beta_1 \wedge dA_1\big) = -\int_{\partial M} \kappa \beta_1 \wedge A_1, \tag{6.C.8}$$

and this implies that the object should have localized anomalous degree of freedom such that it can cancel this contribution. This is an anomaly inflow.

This can be seen in the Lagrangian level. We introduce the Chern-Simons form by $F_2 \wedge F_2 = d\omega_3$, $\omega_3 = A_1 dA_1$, then the Chern-Simons term is rewritten as

$$\int_M a F_2 \wedge F_2 = -\int_M da \wedge \omega_3. \tag{6.C.9}$$

From the descent equation, we assume that the trasformation of the Chern-Simons form is given by $\delta\omega_3 = dG_2$, and the transformation of the above Chern-Simons term becomes

$$\delta\left(-\int_M da \wedge \omega_3\right) = -\int_M da \wedge dG_2 = \int_M dda \wedge G_2. \tag{6.C.10}$$

If a has a non-trivial monodromy, $dda \neq 0$ and this implies the existence of the delta function source

$$dda \sim \delta_W. \tag{6.C.11}$$

Then the localized degree of freedom on the object δ_W produces the new contribution to cancel the anomaly of G_2 such as

$$\int_M \delta_W \wedge G_2. \tag{6.C.12}$$

Chapter 7

Conclusion

In this thesis, we consider a scalar sector extension by an SM singlet scalar field, which can carry other charges such as $U(1)_{B-L}$ or $U(1)_L$ and the dynamics and phenomenology of pNGB arising from the spontaneous symmetry breaking of the scalar potential.

In Chapter 2 and Chapter 3, we investigate the UV completion of the pNGB dark matter model motivated by the swampland conjecture of no-global symmetry. The pNGB is an attractive candidate of WIMPs and avoid the severe constraints of the direct detection experiments thanks to the its derivative couplings which is typically evaluated by the ratio of the electroweak scale and the VEV of the singlet scalar. In Chapter 2, we propose the pNGB dark matter model based on the gauged $U(1)_{B-L}$ symmetry where the symmetry of the scalar sector is realized as the discrete gauge symmetry. The soft breaking mass term of the pNGB arises from the cubic coupling such as $\Phi^* S^2$. However, this pNGB is not a stable dark matter candidate due to the interaction with the $B-L$ gauge boson and the scalar mixing, and becomes a decaying dark matter. We evaluate the life-time of the pNGB and show the parameter space realizing the current dark matter relic as the thermal relic consistently with the experimental and observational results. In Chapter 3, we consider the embedding of the $U(1)_{B-L}$ pNGB dark matter model to the $SO(10)$ GUT. In order to realize this model in the low energy region, the symmetry breaking pattern of $SO(10) \to G_{\mathrm{PS}} \to G_{\mathrm{SM}} \times U(1)_{B-L}$ is favored. It is found that the $B-L$ gauge coupling, the gauge kinetic mixing ϵ and the $B-L$ breaking intermediate scale $M_I \sim v_\phi$ are determined by the grand unification. The intermediate scale is lower than that in Chapter 2, which implies that the lighter dark matter mass is required in order to make the life-time long. We find that the thermal relic abundance can be consistent with all the constraints when the dark matter mass is rather close to the resonances $m_\chi \lesssim m_{h_i}/2$.

In Chapter 4 and Chapter 5, we consider the phenomenology in other aspects of the simple singlet scalar extension, where the VEV of the singlet scalar is much larger than the electroweak scale. In such situation, the interaction of the pNGB is highly suppressed by the huge VEV. This kind of invisible pNGB is discussed in some BSM models. In Chapter 4, we show that the pNGB with large VEV becomes a typical FIMP

candidate and the dark matter relic is realized by the freeze-in production through the portal interactions between the singlet scalar and the SM Higgs boson. In addition to this FIMP pNGB, the possibility is pursued that the symmetry breaking scalar causes the inflationary expansion, reheats the SM thermal bath and directly produce the pNGB. We show the allowed region in the (m_χ, λ_Φ) plane. In Chapter 5, we consider the case that the singlet scalar field carries the lepton number and becomes Majoron with the TeV-scale mass. The life-time constraint and the cosmic-ray observations give a strong constraint on the interactions of the TeV-scale Majoron via the VEV and neutrino sector Yukawa couplings, which implies that the TeV-scale Majoron is also FIMP dark matter candidate. We propose three production scenarios and show the parameter space realizing the current dark matter relic.

We study the situation that the pNGB becomes another type scalar field, called axion in Chapter 6. We consider the DFSZ axion model and find that the axion string in this model has novel structure, named as an electroweak axion string: it has a thin axion string core and the SM gauge flux surrounds this. We construct the solution describing this string object, and discuss that the electromagnetic symmetry can be broken around the string core, and the axion string can be superconducting in some parameter space. If the electromagnetic symmetry is broken, the zero mode current can travel along the string and gives the long-range attractive force between these strings. We discuss the possibility that this attractive force can form a bound state of the axion string called Y-shaped junction and its cosmological impacts.

These days, it is pointed out that the consistency conditions of quantum gravity theory gives constraints on the low-energy effective theory. The classification of the constraints is discussed in the context of the Swampland Programs [Vaf05] (and reviews [Pal19, vBCIMV21, GnH21]). In this thesis, the BSM model motivated by the swampland conjectures was proposed and we discussed the possibility that the existence of dark matter and the quantum gravity consistency may imply the grand unification of the fundamental forces. The soliton in such models and the interactions between them can be suitable for testing the swampland conjectures in the phenomenology. In addition to these, the scalar potential plays the crucial role for the phenomenology and it can be directly connected to the dynamics of quantum gravity. Thus, the author thinks that it will be important to develop quantum gravity theory and phenomenology in a complementary manner in order to reveal the theory of everything.

Acknowledgement

Appendix A

Notation and convention

A.1 Notation

In the main part of this thesis, we use the notation of Ref. [PS95]. The signature of Minkowski metric is the almost minus one,

$$\eta_{ab} = \eta^{ab} = \text{diag}(+1, -1, -1, -1), \tag{A.1.1}$$

and the Clifford algebra is given by

$$\{\gamma^a, \gamma^b\} = 2\eta^{ab}. \tag{A.1.2}$$

The hermitian conjugate of the gamma matrices is expressed as

$$(\gamma^a)^\dagger = \gamma_a = \gamma^0 \gamma^a \gamma^0. \tag{A.1.3}$$

The Weyl representation of the gamma matrices is

$$\gamma^0 = \begin{pmatrix} 0 & \mathbb{1} \\ \mathbb{1} & 0 \end{pmatrix}, \qquad \vec{\gamma} = \begin{pmatrix} 0 & \vec{\sigma} \\ -\vec{\sigma} & 0 \end{pmatrix}, \tag{A.1.4}$$

with the Pauli matrices $\vec{\sigma}$. For the four component Dirac fermion ψ, the Dirac conjugate is defined by

$$\overline{\psi} = \psi^\dagger \gamma^0. \tag{A.1.5}$$

The chirality operator is defined by

$$\gamma^5 := i\gamma^0 \gamma^1 \gamma^2 \gamma^3 = \begin{pmatrix} -\mathbb{1} & 0 \\ 0 & \mathbb{1} \end{pmatrix}, \tag{A.1.6}$$

which satisfies the following normalization,

$$\text{tr}\, \gamma^a \gamma^b \gamma^c \gamma^d \gamma^5 = -4i\epsilon^{abcd}, \tag{A.1.7}$$

with $\epsilon^{0123} = +1$. The left-handed and right-handed projection operator is given by

$$P_L := \frac{\mathbb{1} - \gamma^5}{2}, \qquad P_R := \frac{\mathbb{1} + \gamma^5}{2}, \tag{A.1.8}$$

and they satisfy $\gamma^5 P_L = -P_L$ and $\gamma^5 P_R = +P_R$.[1]

In the curved background, the vielbein field is defined by

$$g_{\mu\nu} = \eta_{ab} e^a{}_\mu e^b{}_\nu, \tag{A.1.13}$$

and the volume element becomes

$$\sqrt{-g} := \sqrt{-\det g_{\mu\nu}} = \det e^a{}_\mu =: e. \tag{A.1.14}$$

The Levi-Civita connection and curvatures are introduced by

$$\Gamma^\mu_{\nu\rho} = \frac{1}{2} g^{\mu\sigma} (\partial_\mu g_{\sigma\nu} + \partial_\nu g_{\mu\sigma} - \partial_\sigma g_{\mu\nu}), \tag{A.1.15}$$

$$\mathcal{R}_{\mu\nu}{}^\rho{}_\sigma = \partial_\mu \Gamma^\rho_{\nu\sigma} - \partial_\nu \Gamma^\rho_{\mu\sigma} + \Gamma^\rho_{\mu\tau} \Gamma^\tau_{\nu\sigma} - \Gamma^\rho_{\nu\tau} \Gamma^\tau_{\mu\sigma}, \tag{A.1.16}$$

$$\mathcal{R}_{\mu\nu} = \mathcal{R}_{\rho\mu}{}^\rho{}_\nu, \tag{A.1.17}$$

$$\mathcal{R} = g^{\mu\nu} \mathcal{R}_{\mu\nu}. \tag{A.1.18}$$

In the convention of Eq. (A.1.1), the Einstein-Hilbert action becomes

$$S_{\text{EH}} = -\frac{1}{2\kappa_4^2} \int d^4x \sqrt{-g} \mathcal{R}. \tag{A.1.19}$$

---

[1] In the almost plus signature of the Minkowski metric $\eta_{ab} = \text{diag}(-1, +1, +1, +1)$ notation, the Clifford algebra

$$\{\gamma^a, \gamma^b\} = 2\eta^{ab}, \tag{A.1.9}$$

leads the anti-hermite $(\gamma^0)^\dagger = -\gamma^0$ and the hermite $(\vec{\gamma})^\dagger = +\vec{\gamma}$. The representation of these gamma matrices is given by the replacement with $\gamma^a \to -i\gamma^a$ in Eq. (A.1.4) [Wei05, Wei13a, Wei13b]. The Dirac conjugate of the Dirac fermion ψ is given by $\overline{\psi} := i\psi^\dagger \gamma^0$, and the canonically normalized kinetic term for the massive free Dirac fermion is

$$\mathcal{L} = -\overline{\psi}(\gamma^\mu \partial_\mu + m)\psi. \tag{A.1.10}$$

In this convention, the chirality operator is defined by

$$\gamma^5 = -i\gamma^0 \gamma^1 \gamma^2 \gamma^3 = \begin{pmatrix} \mathbb{1} & 0 \\ 0 & -\mathbb{1} \end{pmatrix}, \tag{A.1.11}$$

and the left, right-handed projection operators are given by

$$P_L = \frac{\mathbb{1} + \gamma^5}{2}, \qquad P_R = \frac{\mathbb{1} - \gamma^5}{2}. \tag{A.1.12}$$

Name	Field	$SU(3)_c$	$SU(2)_L$	$U(1)_Y$
$SU(3)_c$ gauge boson (Gluon)	$G_\mu^{a=1-8}$	**8** (adj)	**1**	0
$SU(2)_L$ gauge boson	$W_\mu^{a=1-3}$	**1**	**3** (adj)	0
$U(1)_Y$ gauge boson	B_μ	**1**	**1**	adj
Quark doublet (left)	$Q_L^{i=1,2,3}$	**3**	**2**	$+1/6$
Up quark (right)	$(u_R^C)^{i=1,2,3}$	$\bar{\mathbf{3}}$	**1**	$-2/3$
Down quark (right)	$(d_R^C)^{i=1,2,3}$	$\bar{\mathbf{3}}$	**1**	$+1/3$
Lepton (right)	$L_L^{i=1,2,3}$	**1**	**2**	$-1/2$
Electron (right)	$(e_R^C)^{i=1,2,3}$	**1**	**1**	-1
Higgs doublet	H	**1**	**2**	$+1/2$

Table A.1: Particle contents and their quantum charges of the SM.

where $\kappa_4^2 = 1/M_P^2$ with the reduced Planck mass M_P. We expand the graviton around the flat Minkowski background as $g_{\mu\nu} = \eta_{\mu\nu} + h_{\mu\nu}$, this action reduces to

$$S_{\rm EH} = \frac{1}{2\kappa_4^2} \int d^4x \left[\frac{1}{4}\partial_\mu h_{\alpha\beta}\partial^\mu h^{\alpha\beta} - \frac{1}{2}\partial_\mu h_{\alpha\beta}\partial^\alpha h^{\mu\beta} + \frac{1}{2}\partial_\alpha h\partial_\beta h^{\alpha\beta} - \frac{1}{4}\partial_\alpha h\partial^\alpha h \right], \quad \text{(A.1.20)}$$

with $h \coloneqq \eta^{\mu\nu}h_{\mu\nu}$, which leads the canonical kinetic term of the graviton fluctuation.

A.2 Standard Model Lagrangian

The particle contents and their quantum charges of the SM are summarized in Table A.1 and the Lagrangian is given by

$$\begin{aligned}
\mathcal{L}_{\rm SM} = &-\frac{1}{4}\sum_{a=1}^{8}(G_{\mu\nu}^a)^2 - \frac{1}{4}\sum_{a=1}^{3}(W_{\mu\nu}^a)^2 - \frac{1}{4}(B_{\mu\nu})^2 \\
&+ i\overline{Q_i}\slashed{D}Q_i + i\overline{u_{Ri}}\slashed{D}u_{Ri} + i\overline{d_{Ri}}\slashed{D}d_{Ri} + i\overline{L_i}\slashed{D}L_i + i\overline{e_{Ri}}\slashed{D}e_{Ri} \\
&- \left(y_{ij}^D \overline{d_{Ri}}H^\dagger Q_j + y_{ij}^U \overline{u_{Ri}}\tilde{H}^\dagger Q_j + y_{ij}^e \overline{e_{Ri}}H^\dagger L_j + \text{h.c.} \right) \\
&+ (D_\mu H)^\dagger(D^\mu H) - V_H(H), \quad &\text{(A.2.1)} \\
V_H(H) = &-\frac{\mu_H^2}{2}|H|^2 + \frac{\lambda_H}{2}|H|^4, \quad &\text{(A.2.2)}
\end{aligned}$$

with $\tilde{H} = i\sigma^2 H^*$. The covariant derivative of the SM gauge boson is

$$D_\mu = \partial_\mu + ig_s G_\mu^a \frac{\lambda^a}{2} + ig_2 W_\mu^a \frac{\sigma^a}{2} + ig_1 Q_Y B_\mu \quad \text{(A.2.3)}$$

$$= \partial_\mu + ig_s G_\mu^a \frac{\lambda^a}{2} + \frac{ig_2}{\sqrt{2}}(W_\mu^+ T^+ + W_\mu^- T^-) + \frac{ig_2}{\cos\theta_W}Z_\mu(T^3 - \sin^2\theta_W Q_{\rm EM}) + ieA_\mu Q_{\rm EM}, \quad \text{(A.2.4)}$$

where λ^a and σ^a denote the Gell-Mann matrices and the Pauli matrices, respectively. $T^\pm := T^1 \pm iT^2$ and T^i denotes the i th component of weak isospin. The electromagnetic charge and the coupling constant are defined by $Q_{\rm EM} := T^3 + Q_Y$ and $e := g_2 g_1 / \sqrt{g_2^2 + g_1^2}$. The gauge bosons are introduced by

$$W_\mu^\pm = \frac{W_\mu^1 \mp iW_\mu^2}{\sqrt{2}}, \qquad \begin{pmatrix} Z_\mu \\ A_\mu \end{pmatrix} = \begin{pmatrix} \cos\theta_W & -\sin\theta_W \\ \sin\theta_W & \cos\theta_W \end{pmatrix} \begin{pmatrix} W_\mu^3 \\ B_\mu \end{pmatrix}, \tag{A.2.5}$$

wheresin $\theta_W = g_1/\sqrt{g_1^2 + g_2^2}, \ \cos\theta_W = g_2/\sqrt{g_1^2 + g_2^2}$.

A.3 Differential forms

In this section, we will summarize the notation of the differential forms.

Let us consider the D-dimensional space-time with the following Minkowski metric for simplicity of the signature[2]

$$\eta_{AB} = {\rm diag}(-1, +1, \ldots, +1). \tag{A.3.1}$$

The infinitesimal distance ds^2 is given by

$$ds^2 = g_{MN} dx^M dx^N, \tag{A.3.2}$$

and the vielberin $e^A{}_M$ is defined by

$$g_{MN} = \eta_{AB} e^A{}_M e^A{}_N. \tag{A.3.3}$$

The determinant is

$$\sqrt{-g} := \sqrt{-\det g_{MN}} = \det e^A{}_M =: e \tag{A.3.4}$$

Differential forms

p-fomrs is introduced by

$$\omega_p = \frac{1}{p!} \omega_{M_1 \cdots M_p} dx^{M_1} \wedge \cdots \wedge dx^{M_p}. \tag{A.3.5}$$

The exterior product of p-forms and q-forms satisfy

$$\omega_p \wedge \eta_q = (-1)^{pq} \eta_q \wedge \omega_p. \tag{A.3.6}$$

---

[2]If we use the almost minus notation $\eta_{AB} = {\rm diag}(+1, -1, \ldots, -1)$, the signature of $\epsilon_{01\cdots D-1}$ is depend on the number of the space dimensions. In the case of four-dimensional spacetime, the we can discuss in the similar manner. The difference is the overall signature of the canonically normalized kinetic terms (A.3.45).

The exterior derivative d acts the p-form as

$$d\omega_p = \frac{1}{p!}\partial_M \omega_{M_1 \cdots M_p} \, dx^M \wedge dx^{M_1} \wedge \cdots \wedge dx^{M_p}, \tag{A.3.7}$$

which is $d : p$-forms $\mapsto (p+1)$-forms as

$$dA_p = \frac{1}{p!}\partial_N A_{M_1 \cdots M_p} dx^N \wedge dx^{M_1} \cdots \wedge dx^{M_p} =: F_{p+1}, \tag{A.3.8}$$

$$F_{p+1} := \frac{1}{(p+1)!} F_{M_1 \cdots M_{p+1}} dx^{M_1} \wedge \cdots \wedge dx^{M_{p+1}}, \tag{A.3.9}$$

$$F_{M_1 \cdots M_{p+1}} := (p+1)\partial_{[M_1} A_{M_2 \cdots M_{p+1}]}. \tag{A.3.10}$$

The exterior derivative of the exterior product is defined as

$$d(\omega_p \wedge \eta_q) = (d\omega_p) \wedge \eta_q + (-1)^p \omega_p \wedge (d\eta_p). \tag{A.3.11}$$

d is a nilpotent operator $d^2 = 0$:

$$d^2\omega_p = -d^2\omega_p = 0. \tag{A.3.12}$$

The interior product of the p-form ω_p and the vector field V is defined by

$$I_V \omega_p = \frac{1}{(p-1)!} V^M \omega_{MM_1 \cdots M_{p-1}} \, dx^M \wedge \cdots \wedge dx^{M_{p-1}}. \tag{A.3.13}$$

I_V maps p-forms to $(p-1)$-forms.

The Lie derivative is defined by

$$L_V := d\,I_V + I_V\,d, \tag{A.3.14}$$

which maps p-forms to p-forms.

Invariant tensor and volume form in Lorentz signature

We choose the following normalization of the invariant tensors

$$\epsilon^{01\cdots(D-1)} = +\alpha, \quad \epsilon_{01\cdots(D-1)} = -\alpha. \tag{A.3.15}$$

In this normalization, the anti-symmetric symbols (Levi-Civita symbols) are defined by

$$\varepsilon^{M_1 M_2 \cdots M_D} := e\, \epsilon^{A_1 A_2 \cdots A_D} e_{A_1}{}^{M_1} e_{A_2}{}^{M_2} \cdots e_{A_D}{}^{M_D} \tag{A.3.16}$$

$$\varepsilon_{M_1 M_2 \cdots M_D} := e^{-1} \epsilon_{A_1 A_2 \cdots A_D} e^{A_1}{}_{M_1} e^{A_2}{}_{M_2} \cdots e^{A_D}{}_{M_D}. \tag{A.3.17}$$

We note that $\epsilon^{A_1 A_2 \cdots A_D}$ is a tensor, but $\varepsilon^{M_1 M_2 \cdots M_D}$ is not a tensor but an anti-symmetric symbol.

$\epsilon^{A_1 A_2 \cdots A_D}$ and $\varepsilon^{M_1 M_2 \cdots M_D}$ satisfy the following relations:

$$\epsilon^{01\cdots(D-1)} = +\alpha, \tag{A.3.18}$$

132

$$\epsilon_{01\cdots(D-1)} = -\alpha, \tag{A.3.19}$$

$$\varepsilon^{M_1 M_2 \cdots M_D} := e\, \epsilon^{A_1 A_2 \cdots A_D} e_{A_1}{}^{M_1} e_{A_2}{}^{M_2} \cdots e_{A_D}{}^{M_D} \tag{A.3.20}$$

$$\varepsilon_{M_1 M_2 \cdots M_D} := e^{-1} \epsilon_{A_1 A_2 \cdots A_D} e^{A_1}{}_{M_1} e^{A_2}{}_{M_2} \cdots e^{A_D}{}_{M_D}, \tag{A.3.21}$$

$$\epsilon^{A_1 A_2 \cdots A_D} = e^{-1} \varepsilon^{M_1 M_2 \cdots M_D} e^{A_1}{}_{M_1} e^{A_2}{}_{M_2} \cdots e^{A_D}{}_{M_D}, \tag{A.3.22}$$

$$\epsilon_{A_1 A_2 \cdots A_D} = e\, \varepsilon_{M_1 M_2 \cdots M_D} e_{A_1}{}^{M_1} e_{A_2}{}^{M_2} \cdots e_{A_D}{}^{M_D}, \tag{A.3.23}$$

$$\epsilon^{A_1 A_2 \cdots A_D} \epsilon_{A_1 A_2 \cdots A_D} = -D!\alpha^2, \tag{A.3.24}$$

$$\varepsilon^{M_1 M_2 \cdots M_D} \varepsilon_{M_1 M_2 \cdots M_D} = -D!\alpha^2 \tag{A.3.25}$$

$$\epsilon^{A_1 \cdots A_p C_1 \cdots C_{D-p}} \epsilon_{B_1 \cdots B_p C_1 \cdots C_{D-p}} = -p!(D-p)!\alpha^2 \delta^{A_1 \cdots A_p}_{B_1 \cdots B_p}, \tag{A.3.26}$$

$$\varepsilon^{M_1 \cdots M_p L_1 \cdots L_{D-p}} \varepsilon_{N_1 \cdots N_p L_1 \cdots L_{D-p}} = -p!(D-p)!\alpha^2 \delta^{M_1 \cdots M_p}_{N_1 \cdots N_p} \tag{A.3.27}$$

$$\epsilon_{A_1 A_2 \cdots A_D} e^{A_1} \wedge e^{A_2} \wedge \cdots \wedge e^{A_D} = \frac{1}{\alpha} \epsilon^{A_1 A_2 \cdots A_D} dV_D, \tag{A.3.28}$$

$$d^D x = dx^0 \wedge dx^1 \wedge \cdots \wedge dx^D = -\frac{1}{D!\alpha} \varepsilon_{M_1 M_2 \cdots M_D} dx^{M_1} \wedge dx^{M_2} \wedge \cdots \wedge dx^{M_D}, \tag{A.3.29}$$

$$dx^{M_1} \wedge dx^{M_2} \wedge \cdots \wedge dx^{M_D} = \frac{1}{\alpha} \varepsilon^{M_1 M_2 \cdots M_D} d^D x \tag{A.3.30}$$

where $\delta^{A_1 \cdots A_p}_{B_1 \cdots B_p}$ is given by

$$\delta^{A_1 \cdots A_p}_{B_1 \cdots B_p} = \frac{1}{p!} \sum_{\sigma \in S_D} \mathrm{sgn}(\sigma) \delta^{A_1}_{\sigma(B_1)} \cdots \delta^{A_p}_{\sigma(B_p)}. \tag{A.3.31}$$

The volume form dV_D is defined by

$$dV_D = e^0 \wedge e^1 \wedge \cdots \wedge e^{D-1} = -\frac{1}{D!\alpha} \epsilon_{A_1 \cdots A_D} e^{A_1} \wedge \cdots \wedge e^{A_D} \tag{A.3.32}$$

$$= e^0{}_{M_1} e^1{}_{M_2} \cdots e^{D-1}{}_{M_D} dx^{M_1} \wedge dx^{M_2} \wedge \cdots \wedge dx^{M_D} =: e\, d^D x. \tag{A.3.33}$$

Hodge duality

The Hodge duality for the frame fields e^{A_1} is defined by

$$*_D\left(e^{A_1} \wedge \cdots \wedge e^{A_p}\right) = \frac{1}{(D-p)!} \epsilon^{A_1 \cdots A_p}{}_{B_1 \cdots B_{D-p}} e^{B_1} \wedge \cdots \wedge e^{B_{D-p}}. \tag{A.3.34}$$

The Hodge dual of the unity is

$$*_D 1 := \frac{1}{D!} \epsilon_{A_1 A_2 \cdots A_D} e^{A_1} \wedge e^{A_2} \wedge \cdots \wedge e^{A_D} = -\alpha dV_D \tag{A.3.35}$$

and that of the volume form is given by

$$*_D dV_D = *_D \left(-\frac{1}{D!\alpha} \epsilon_{A_1 A_2 \cdots A_D} e^{A_1} \wedge e^{A_2} \wedge \cdots \wedge e^{A_D} \right)$$

$$= -\frac{1}{D!\alpha} \epsilon_{A_1 A_2 \cdots A_D} \epsilon^{A_1 A_2 \cdots A_D} = \alpha. \tag{A.3.36}$$

Let us evaluate the operations of acting on the Hodge dual in twice:

$$*_D(*_D1) = *_D\left(-\alpha dV_D\right) = -\alpha^2, \tag{A.3.37}$$

$$*_D\left(*_D dV_D\right) = *_D\,\alpha = -\alpha^2 dV_D \tag{A.3.38}$$

From these, we can get the following relations

$$*_D *_D 1 = -\alpha^2, \quad *_D *_D\, dV_D = -\alpha^2\, dV_D. \tag{A.3.39}$$

The Hodge dual of the basis of the curved space-time is defined as

$$*_D\left(dx^{M_1} \wedge \cdots \wedge dx^{M_p}\right) = \frac{e}{(D-p)!}\, g^{M_1 K_1} \cdots g^{M_p K_p}\, \varepsilon_{K_1 \cdots K_p N_1 \cdots N_{D-p}}\, dx^{N_1} \wedge \cdots \wedge dx^{N_{D-p}}. \tag{A.3.40}$$

Then, the Hodge dual of the p-form field is given by

$$\begin{aligned}
*_D\omega_p &= \frac{1}{p!(D-p)!}\omega^{A_1 A_2 \cdots A_p}\epsilon_{A_1 A_2 \cdots A_p B_1 B_2 \cdots B_{D-p}}\, e^{B_1} \wedge e^{B_2} \wedge \cdots \wedge e^{B_{D-p}} \\
&= \frac{e}{p!(D-p)!}\,\omega^{N_1 \cdots N_p}\varepsilon_{N_1 \cdots N_p M_1 \cdots M_{D-p}}\, dx^{M_1} \wedge \cdots \wedge dx^{M_{D-p}}, \tag{A.3.41}
\end{aligned}$$

and the operations of acting on the Hodge dual of the p-forms in twice satisfy

$$*_D *_D\, \omega_p = \alpha^2(-1)^{p(D-p)+1}\omega_p. \tag{A.3.42}$$

$*_D1$ is also written as

$$*_D1 = \frac{\sqrt{-g_D}}{D!}\,\varepsilon_{M_1 \cdots M_D}\, dx^{M_1} \wedge \cdots \wedge dx^{M_D} = -\alpha\sqrt{-g_D}\,d^D x = -\alpha dV_D. \tag{A.3.43}$$

Using the Hodge dual, the kinetic term of $F_{p+1} = dC_p$ is written in the differential form as

$$\begin{aligned}
&\int F_{p+1} \wedge *_D F_{p+1} \\
&= \int \left(\frac{1}{(p+1)!}F_{M_1 \cdots M_{p+1}}dx^{M_1} \wedge \cdots \wedge dx^{M_p}\right) \wedge \left(\frac{e}{(p+1)!(D-p-1)!}\omega^{N_1 \cdots N_{p+1}} \right. \\
&\quad \left. \times \varepsilon_{N_1 \cdots N_{p+1} K_1 \cdots K_{D-p-1}}dx^{K_1} \wedge \cdots \wedge dx^{K_{D-p-1}}\right) \\
&= \int \frac{e}{(p+1)!(p+1)!(D-p-1)!}F_{M_1 \cdots M_{p+1}}F^{N_1 \cdots N_{p+1}}\varepsilon_{N_1 \cdots N_p K_1 \cdots K_{D-p-1}} \\
&\quad \times \frac{1}{\alpha}\varepsilon^{M_1 \cdots M_{p+1} K_1 \cdots K_{D-p-1}}d^D x \\
&= \int d^D x\, \frac{e}{(p+1)!(p+1)!(D-p-1)!}\frac{1}{\alpha}(-\alpha^2)(p+1)!(D-p-1)!\,\delta^{N_1 \cdots N_{p+1}}_{M_1 \cdots M_{p+1}}F_{M_1 \cdots M_{p+1}}F^{N_1 \cdots N_{p+1}} \\
&= (-\alpha)\int d^D x\, e\frac{1}{(p+1)!}F^{M_1 \cdots M_{p+1}}F_{M_1 \cdots M_{p+1}} = (-\alpha)\int d^D x\, e|F_{p+1}|^2, \tag{A.3.44}
\end{aligned}$$

where $|F_{p+1}|^2 = \frac{1}{(p+1)!}F^{M_1\cdots M_{p+1}}F_{M_1\cdots M_{p+1}}$. Then the kinetic term of C_p in the Minkowski metric (A.3.1) is written as

$$\mathcal{L}_{\text{kin. of } C_p} = -\frac{1}{2}\int d^D x\sqrt{-g}\frac{1}{p!}F^{M_1\cdots M_{p+1}}F_{M_1\cdots M_{p+1}} = -\frac{1}{2}\int d^D x\sqrt{-g}|F_{p+1}|^2$$

$$= \frac{1}{2\alpha}\int F_{p+1}\wedge *_D F_{p+1}. \tag{A.3.45}$$

In the same way, the Einstein-Hilbert action is written as

$$S_{\text{EH}} = \frac{M_P^2}{2}\int d^D x\sqrt{-g}\mathcal{R} = -\frac{M_P^2}{2\alpha}\int \mathcal{R}\wedge *_D 1. \tag{A.3.46}$$

Appendix B

Implications of the weak gravity conjecture in anomalous quiver gauge theories

B.1 Swampland conjecture and weak gravity conjecture

Swampland conjectures attract much attention recently in various aspects [Vaf05, OV07, AHMNV07, OOSV18, GK19, OPSV19, Pal19]. The conjectures are expected to constrain effective field theories to be consistent with quantum gravity, and give us new insights into not only the string theory as a candidate of quantum gravity but also physics of BSM.

Among them, the weak gravity conjecture (WGC) requires theories consistent with quantum gravity to include a charged state with a charge q and a mass m satisfying the weak gravity bound [AHMNV07],

$$eq \geq \frac{m}{\sqrt{2}M_P}, \tag{B.1.1}$$

so that an extremal black holes can have a decay channel. The WGC briefly states that the gravity is the weakest force. Here, e is an anomaly-free gauge coupling and M_P is the reduced Planck mass. The WGC can be extended to theories with multiple $U(1)$ groups [CR14] and also to a scalar exchange force such as a Yukawa interaction [Pal17, LP18, GIn19, ACE20, BBLM20]. The latter extension is called the scalar weak gravity conjecture (SWGC) . These conjectures also have been checked in several aspects [LLW19a, LLW19b], and indicate that repulsive forces of gauge interactions among the same species of particles are stronger than attractive forces of gravity and Yukawa interactions among them [HRR19].

The situation may not be so simple in chiral gauge theories. IR symmetries are often obtained through the breaking of UV symmetries, and an IR gauge coupling is given by

a linear combination of UV gauge couplings as in the SM. The linear combinations are determined by the Stückelberg couplings among the gauge bosons and would-be NGB (or axions) associated with the symmetry breaking. This is applicable not only to anomaly-free gauge theories but also to consistent theories possessing anomalous $U(1)$ gauge groups. In theories with an anomalous $U(1)$, an axion field plays an important role to cancel the gauge anomalies: the gauge invariance is (non-linearly) restored owing to the axion coupling to topological terms of the gauge fields on top of the Stückelberg couplings.[1] As in the ordinary spontaneous symmetry breaking, these Stückelberg couplings lead to the gauge boson mass and determine the eigenstate of massless gauge boson. Thus the gauge boson of anomalous $U(1)$ symmetry is decoupled in the low energy limit.[2] In the string theory, this anomaly cancellation is realized by the Green-Schwarz mechanism [GS84] involving string theoretic axions. 4D string models with anomalous $U(1)$'s have been well-discussed for realizing the SM [AIQU00, AFI$^+$01b, AFI$^+$01a, BLS03, BHW05, BKLS07].

In this chapter, we will focus on models with multiple $U(1)$ symmetries and chiral fermions. For models with $U(1)^k$, an anomaly-free $U(1)$ is given by a linear combination of the original symmetries:

$$U(1)_{\text{anomaly-free}} = \sum_{i=1}^{k} c_i U(1)_i, \qquad (B.1.2)$$

where k is the number of $U(1)$ symmetries, c_i $(i = 1, 2, \ldots, k)$ is a model-dependent $\mathcal{O}(1)$ coefficient and $U(1)_i$ is the i-th gauge group. We will discuss some examples in the following section. Then, the corresponding anomaly-free gauge coupling e is given by

$$\frac{1}{e^2} = \sum_{i=1}^{k} \frac{c_i^2}{g_i^2}, \qquad (B.1.3)$$

where g_i is the gauge coupling of the $U(1)_i$ symmetry. The gauge coupling e will become necessarily very weak and smaller than the original coupling g_i as the number of $U(1)$ gauge groups increases in the large k limit.[3] Thus, the WGC condition in Eq. (B.1.1) looks hard to be satisfied with an assumption that chiral anomlies can be canceled. In other words, the repulsive force among particles will then become very weak. It is conjectured that a certain class of chiral gauge theories with too many $U(1)$ symmetries can be in the swampland.[4] It is noted that the gauge groups in 10D superstring theories are restricted [Pol07], while those in 4D brane models seem less-constrained in the view point of tadpole condition.[5] When magnitude of all the gauge couplings is comparable to each other, the

---

[1]See also a recent work [CGGK20].

[2]Some of gauge bosons in the anomaly-free gauge groups can also become massive through the Stückelberg couplings.

[3]The WGC with a similar gauge coupling is discussed in Ref. [Sar17].

[4]This will generally be applicable to theories with a semi-simple gauge group of $G = \prod_{i=1}^{k} G_i$ in the large k limit, when G is spontaneously broken to a simple group. Here G_i is a simple group.

[5]In the heterotic string, the rank of the gauge group is sixteen.

Eq. (B.1.3) is rewitten as

$$eq \sim \frac{\tilde{g}}{\sqrt{k}}q \gtrsim \frac{m}{M_P}, \tag{B.1.4}$$

where $\tilde{g} \sim g_i$ for $\forall i$ is the average of the gauge couplings. We find that the gauge coupling is scaling as $e \sim k^{-1/2}$ for a large k and there exists an upper bound on k, $k \lesssim (q\tilde{g}\frac{M_P}{m})^2$, if the WGC is correct and the mass m remains non-zero in the large k limit. This upper bound on k is similar to the species bound [DR08], but k is not the number of species but the number of $U(1)$ gauge groups in our case.[6] Similar conditions for theories with a discrete $\mathbb{Z}_k$ (gauge) symmetry are also discussed in Refs. [CGGK19,BCMU20]. Eq. (B.1.4) could be regarded as an example of the weak coupling conjecture [BCMU20].

A notion of quiver gauge theory is often used for theories in the presence of multiple gauge groups and bi-fundamental chiral fermions, and matches model building involving D-branes well [IMR01, CIM02b, CIM02a, VW07, CHR09, KDMQ10, DKQ11, DM96, Ura00, BLPZ06, Yam08]. Instead of concrete string models, in this chapter we will consider quiver gauge theories with $U(1)^k$ gauge groups and focus on the anomaly-free gauge groups and the (S)WGC in a bottom-up approach, supposing that the remaining anomalies are canceled and then the anomalous gauge bosons get massive. In general, computation of anomalies depends on the matter content in models. In order to check anomaly-free $U(1)$'s systematically and study concretely the (S)WGC constraints on the gauge couplings, we restrict ourselves to several types of models controlled by discrete symmetries. However, a behavior of the anomaly-free gauge coupling in Eq. (B.1.3) does not change in general models with anomalous $U(1)$'s. The (S)WGC can constrain range of free parameters in low energy theories and show what parameter values are favored by UV theory in the view point of IR physics. In some quiver gauge theories of our interest, there exist a discrete symmetry associated with cyclic permutations between the gauge groups in certain quiver gauge theories, and the symmetry can generally be broken in anomaly-free $U(1)$ theories by a linear combination of $U(1)$'s as in Eq. (B.1.3). Some of quiver gauge theories remind us of deconstructed extra dimension [AHCG01, AKMY03], which could relate our approach to the weak coupling conjecture in holography [BCMU20]. Also new insights can be given to chiral abelian gauge theories which may be a candidate of hidden sectors of dark matter models in particle physics [CDF20].

This appendix is based on Ref. [AHT20] and organized as follows. In Section B.2, we give a brief review of the (S)WGC and anomalous $U(1)$ symmetries. In Section B.3, we will discuss concrete quiver gauge theories with $U(1)^k$, then identify the anomaly-free $U(1)$ symmetries. In Section B.4, we numerically show the SWGC constraint on the gauge couplings and Yukawa couplings in a $U(1)^4$ quiver gauge theory. We discuss also a toy model from 5D orbifold compactification similarly. Section B.5 is devoted to summary

---

[6]If we have too large c_i's, the theory would be in the swampland owing to the appearance of very weak coupling.

and conclusion. In this chapter, we will discuss the above arguments with the tree level parameters.

B.2 Brief reviews of the (S)WGC and anomalous $U(1)$'s

B.2.1 The WGC and the SWGC

In this subsection, we give a brief review of the WGC and the SWGC in four dimension. The WGC claims that there exists a state with a charge q and a mass m satisfying the inequality

$$eq \geq \frac{m}{\sqrt{2}M_P} \tag{B.2.1}$$

in a theory consistent with quantum gravity [AHMNV07]. The factor of $1/\sqrt{2}$ comes from the relative normalization of the Newton force against the Coulomb one, and a generalization to an arbitrary dimension is straightforward [Rob06]. This conjecture makes (super)extremal black holes decay into lighter ones.

The WGC can be extended to theories including a scalar exchange force such as a Yukawa interaction. This is called the SWGC [Pal17, LP18, LLW19a]. Let us consider a theory with multiple $U(1)$ gauge groups:

$$S_{\text{EM}} = \int d^4x \sqrt{-g} \left[-\frac{M_P^2}{2}\mathcal{R} + \sum_{a,b} \frac{1}{2} K_{ab}\partial_\mu \phi^a \partial^\mu \phi^b - \frac{1}{4} \sum_{i,j} f_{ij}(\phi) F_{\mu\nu}^{(i)} F^{(j)\mu\nu} \right] \tag{B.2.2}$$

where $\mathcal{R}$ is a Ricci scalar, ϕ^a is a real scalar field, $F_{\mu\nu}^{(i)}$ is a field strength of $U(1)_i$, K_{ab} is a scalar kinetic matrix, f_{ij} is a gauge kinetic function, and i, j ($= 1, 2, \ldots, k$) and a, b denote the labels of $U(1)$ gauge groups and those of scalar fields respectively. The diagonal parts of f_{ij} give the gauge couplings of $U(1)_i$'s and the off-diagonal components are kinetic mixings. The matter part action is given by

$$S_{\text{matter}} = \int d^4x \sqrt{-g} \left[\frac{1}{2} \sum_{a,b} K_{ab}\partial_\mu \Phi^a \partial^\mu \Phi^b + \overline{\psi} i\gamma^\mu \left(\nabla_\mu + i \sum_j q_j A_\mu^{(j)} \right)\psi - m(\Phi)\overline{\psi}\psi \right] \tag{B.2.3}$$

where ψ is a Dirac spinor of a test particle for the SWGC and has a charge q_i under the gauge group $U(1)_i$ and a mass $m(\Phi)$, and Φ^a is a real scalar field which may be different from ϕ^a in general. Here, the covariant derivative ∇_μ includes the spin connection. The Φ^a is decomposed as

$$\Phi^a = \overline{\varphi}^a + \varphi^a, \tag{B.2.4}$$

where $\overline{\varphi}^a$ is the background configuration of Φ^a and φ^a denotes a fluctuation around the background. With these, the mass $m(\Phi)$ is rewritten as

$$m(\Phi) = m(\overline{\varphi}) + \frac{\partial m}{\partial \varphi^a}\varphi^a + \cdots. \tag{B.2.5}$$

$m(\overline{\varphi})$ is the mass of the ψ in the background $\overline{\varphi}^a$, and the higher order terms of φ^a give the interaction terms between φ^a's and ψ. Thus the Yukawa coupling reads:

$$S_{\text{matter}} \supset \int d^4x \sqrt{-g} \sum_a y_a(\overline{\varphi})\varphi^a \overline{\psi}\psi, \tag{B.2.6}$$

$$y_a(\overline{\varphi}) := \frac{\partial m}{\partial \varphi^a}(\overline{\varphi}) = \partial_a m(\overline{\varphi}). \tag{B.2.7}$$

Then the SWGC for ψ is given by

$$\sum_{i,j} f^{ij}q_i q_j \geq \frac{m^2}{2M_P^2} + \sum_{a,b} K^{ab}y_a y_b, \tag{B.2.8}$$

where f^{ij} and K^{ab} are the inverse matrix of the f_{ij} and K_{ab} respectively. This inequality can be interpreted as the total gauge repulsive force is stronger than the sum of the attractive forces of the gravity and the total Yukawa interactions when we focus on forces acting between the test particle ψ: $|\vec{F}_{\text{Coulomb}}| \geq |\vec{F}_{\text{gravity}}| + |\vec{F}_{\text{Yukawa}}|$. The absolute value of long-range force mediated by massless fields in four dimension is expressed as

$$|\vec{F}| = \frac{A}{4\pi r^2}, \tag{B.2.9}$$

where a numerator A is the factor corresponding to each force:

$$A_{\text{Coulomb}} = \sum_{i,j} f^{ij}q_i q_j, \quad A_{\text{gravity}} = \frac{m^2}{2M_P^2}, \quad A_{\text{Yukawa}} = \sum_{a,b} K^{ab}y_a y_b \tag{B.2.10}$$

If the scalars φ^a are heavy, Yukawa interactions are short-range forces and neglected. Then the SWGC gets back to the WGC.

B.2.2 Anomalous $U(1)$ symmetries

In this subsection, we review cancellation of chiral $U(1)$ gauge anomalies by axion fields. In 4D effective field theories, gauge transformation of the axions can cancel the chiral anomalies produced by light chiral fermions in the presence of topological terms of the gauge fields and the Stückelberg couplings. In field theories with an anomaly-free $U(1)$ gauge symmetry, such axions are would-be Nambu-Goldstone bosons associated with the spontaneous breaking of the $U(1)$ symmetry. After integrating out heavy fermions with chiral $U(1)$ charges, we can obtain anomalous $U(1)$ in the low energy limit [ABDK06, CGGK20]. In 4D string models, anomalies can be canceled by the Green-Schwarz mechanism involving string theoretic axions that originate from tensor fields, when tadpoles of brane charges are canceled [DSW87, JL05].

We shall consider the 4D action involving axions in addition to chiral fermions leading to chiral anomalies:

$$S_{\text{axion}} = \sum_{i \in U(1)_{\text{anomaly}}} \int d^4x \left[\frac{1}{2}\frac{m_i^2}{g_i^2}\left(\sum_{I \in \text{axions}} B_{iI}\partial_\mu \theta_I + A_\mu^{(i)}\right)^2 + \sum_{I \in \text{axions}} \frac{C_{iI}\theta_I}{32\pi^2}\epsilon^{\mu\nu\rho\sigma}F_{\mu\nu}^{(i)}F_{\rho\sigma}^{(i)}\right]. \tag{B.2.11}$$

Here, θ_I is an axion, B_{iI} and C_{iI} are constants, m_i is the gauge boson mass. For the anomalous $U(1)$ symmetries, the fields transform as

$$\theta_I \to \theta_I - D_{Ii}\Lambda_i, \qquad A_\mu^{(i)} \to A_\mu^{(i)} + \partial_\mu\Lambda_i, \tag{B.2.12}$$

where Λ_i is the transformation parameter, and we assume that D_{Ii} satisfies $\sum_I B_{iI}D_{Ij} = \delta_{ij}$. The theory is invariant in the presence of chiral anomalies produced by gauge transformations against chiral fermions:

$$S_{\text{anomaly}} = \sum_{i \in U(1)_{\text{anomaly}}} \int d^4x \left[\sum_{I \in \text{axions}} \Lambda_i \frac{C_{iI}D_{Ii}}{32\pi^2} \epsilon^{\mu\nu\rho\sigma} F_{\mu\nu}^{(i)} F_{\rho\sigma}^{(i)} \right], \tag{B.2.13}$$

such that $\delta_\Lambda S_{\text{total}} = S_{\text{anomaly}} + \delta_\Lambda S_{\text{axion}} = 0$. Thus, in terms of axions the anomaly-free $U(1)$'s are determined such that the coefficients of C_{iI}'s are vanishing[7]. 4D effective action from 5D theory is also discussed, for instance, in Refs. [LOSW99,CGN20]. The anomalous gauge bosons become massive as

$$\frac{1}{2}\frac{m_i^2}{g_i^2}\left(B_{iI}\partial_\mu\theta_I + A_\mu^{(i)}\right)^2 =: \frac{1}{2}\frac{m_i^2}{g_i^2}\left(\tilde{A}_\mu^{(i)}\right)^2, \tag{B.2.14}$$

after θ's are eaten by them as in spontaneous gauge symmetry breaking. Further, for some non-anomalous gauge bosons, there can exist Stückelberg couplings

$$S_{\text{axion}} = \sum_{i \in U(1)_{\text{non-anomalous}}} \int d^4x \left[\frac{1}{2}\frac{m_i^2}{g_i^2}\left(\sum_{I \in \text{axions}} B_{iI}'\partial_\mu\theta_I + A_\mu'^{(i)} \right)^2 \right]. \tag{B.2.15}$$

The non-anomalous gauge bosons can become massive as the anomalous ones. Then, the repulsive forces mediated by such massive gauge bosons will not contribute to the WGC.

Hereafter, we suppose that this mechanism works in the quiver gauge theories studied in this chapter, and these terms are ignored otherwise stated.

B.3 Quiver gauge theories and the WGC

In this section, we discuss quiver theories with $U(1)^k$ gauge symmetry and identify anomaly-free gauge groups. In general, computation of anomalies depends on the matter content in models. To check anomaly-free $U(1)$'s systematically and identify the gauge couplings concretely, we focus on several types of models controlled by discrete symmetries. However, an anomaly-free gauge coupling will be given by Eq. (B.1.3) in general cases. As for a quiver diagram in this chapter, each node implies a gauge group whereas each arrow among two nodes shows a left-handed chiral fermion charged under two gauge

---

[7]Once anomalous gauge fields are written as $A_\mu^{\text{anomalous}} = \sum_i b_i A_\mu^{(i)}$, b_i's would be related to c_i's in Eq. (B.1.3) through the orthogonality among $U(1)$'s. If there exists a large hierarchy among b_i's in $b_i(\partial^\mu\theta)A_\mu^{(i)}$, some c_i's would become very large.
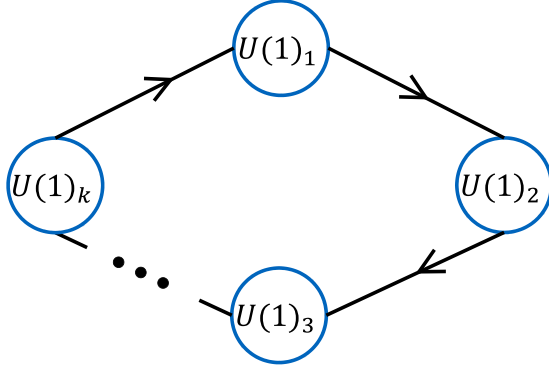
Figure B.1: A quiver diagram with k nodes [AHT20].

groups. The number of arrows shows that of matters and a direction of an arrow is corresponding to the representation against two gauge groups. An arrowhead corresponds to anti-fundamental representation while its opposite side means fundamental one. For theories only with multiple $U(1)$ groups, (anti-)fundamental representation is supposed to have a charge $+1$ (-1). A solid line shows a chiral (left-handed) fermion whereas a dashed line shows a complex scalar.

At first, we shall focus on non-supersymmetric gauge theories with bi-fundamental chiral fermions of $(\boldsymbol{N}_1, \overline{\boldsymbol{N}_2})$ representation under $U(N_1) \times U(N_2) \times \cdots$ gauge group, which is inspired by D-brane models. Although there exist many types of quiver diagrams corresponding to gauge theories, for simplicity we focus on theories including only $U(1)$ groups in the diagrams such as Fig. B.1. Since there exist chiral fermions, chiral gauge anomalies can generally be produced as a consequence. We study cancellation condition of chiral anomalies to identify anomaly-free gauge couplings at the tree level, and apply the couplings to the WGC. Anomaly-free conditions for $U(N)^3$ and $U(N)^4$ are discussed in Appendix B.A. For instance, in $SU(N)^k$ theories with a general N, non-abelian gauge anomaly cancellations require that the number of incoming arrows is equal to that of outgoing ones at each node. In $U(1)^k$ theories we will simply mimic $SU(N)^k$ cases because in D-brane models a gauge group can be given by $U(N) = U(1) \times SU(N)$ rather than just $SU(N)$, hence $U(1)$ and $SU(N)$ are considered simultaneously. We suppose that the anomalies are canceled as in Section B.2.2 and then (non-)anomalous gauge fields get massive in a gauge invariant form. Quiver gauge theories associated with deconstructed extra dimension [AHCG01, AKMY03] could relate our approach to the weak coupling conjecture [BCMU20].

In quiver gauge theories with $U(1)^k$ of our interest, the action is written by

$$S = \sum_{j=1}^{k} \int d^4x \left[-\frac{1}{4g_j^2} F_{\mu\nu}^{(j)} F^{(j)\mu\nu} + \overline{\psi}_{j,j+1} i\gamma^\mu \left(\partial_\mu + iA_\mu^{(j)} - iA_\mu^{(j+1)}\right) \psi_{j,j+1} + \cdots \right], \quad \text{(B.3.1)}$$

where ellipsis shows gravity and interaction terms among fermions which we have neglected. We assume that kinetic mixings among gauge fields are absent at the tree level for simplicity, and will ignore them in this chapter. The gauge field of $U(1)_j$ is denoted by $A_\mu^{(j)}$ and $\psi_{j,j+1}$ is a left-handed spinor with a charge of $(+1, -1)$ against the $(U(1)_j, U(1)_{j+1})$ gauge group as noted above. The index runs as $j = 1, 2, \ldots, k$ and satisfies $k + 1 \equiv 1$. There will exist a symmetry[8] that shifts labels simultaneously as $j \to j + 1$:

$$g_j \to g_{j+1}, \quad A_\mu^{(j)} \to A_\mu^{(j+1)}, \quad \psi_{j,j+1} \to \psi_{j+1,j+2}, \quad \text{(B.3.2)}$$

when we treat the gauge couplings as spurion fields, which are expected to be moduli fields in the string theory. This can be regarded as a $\mathbb{Z}_k$ symmetry acting on k nodes with a element of

$$\begin{pmatrix} 0 & 1 & 0 & 0 & \cdots & 0 \\ 0 & 0 & 1 & 0 & \cdots & 0 \\ 0 & 0 & 0 & 1 & \cdots & 0 \\ & & & & \ddots & \\ 1 & 0 & 0 & 0 & \cdots & 0 \end{pmatrix}. \quad \text{(B.3.3)}$$

We can study anomalies and identify anomaly-free $U(1)$'s systematically owing to this symmetry as seen below. This symmetry will be broken in the low energies when an anomaly-free gauge group is given by a linear combination of UV $U(1)$'s. So, interactions of axions to gauge fields are expected to violate this discrete symmetry.

In terms of particle phenomenology, this theory may be the hidden sector for dark matter apart from the visible sector [CDF20]. In Appendix B.B, we discussed also several quiver models not shown in this section.

B.3.1 $U(1)^{2k-1}$

We consider quiver gauge theories with $U(1)^{2k-1}$ groups as shown in Fig. B.1. These types of (supersymmetric) models have often been studied in D-brane models on orbifolds or intersecting/magnetized D-brane models. They are used also to realize realistic Yukawa couplings or higher order couplings. We hereafter focus just on fermions producing anomalies. As seen below, these theories can have an unique anomaly-free $U(1)$.
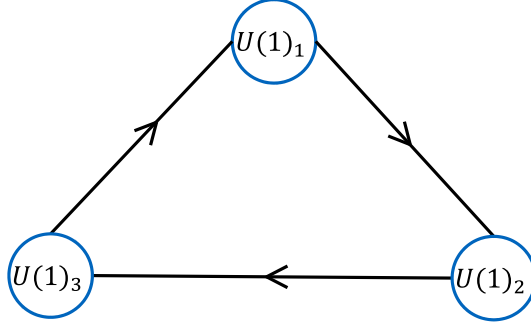
Figure B.2: Three nodes quiver diagram [AHT20].

$U(1)^3$

One of the simplest case is the quiver gauge theory with $U(1)^3 = U(1)_1 \times U(1)_2 \times U(1)_3$ groups[9] in Fig. B.2. As in Eq. (B.3.1), there exist three left-handed chiral fermions ψ_{Li} ($i = 1, 2, 3$), which have charges of $(1, -1, 0)$, $(0, 1, -1)$ and $(-1, 0, 1)$ against $(U(1)_1, U(1)_2, U(1)_3)$ respectively.[10] This model will have a $\mathbb{Z}_3$ symmetry as noted above, and there is no other choices to connect each node. The divergences of $U(1)^3$ chiral currents $j^{i\mu}$ ($i = 1, 2, 3$) are given by

$$
\begin{cases}
\partial \cdot j^1 = Q_2 - Q_3 \\
\partial \cdot j^2 = Q_3 - Q_1 \\
\partial \cdot j^3 = Q_1 - Q_2,
\end{cases}
\tag{B.3.4}
$$

where $\partial \cdot j^i = \partial_\mu j^{i\mu}$ and Q_i is the topological charge density, $Q_i = \frac{1}{32\pi^2} \epsilon^{\mu\nu\rho\sigma} F_{\mu\nu}^{(i)} F_{\rho\sigma}^{(i)}$. Thus we define the anomaly-free $U(1)$ by

$$
U(1)_X := c_1 U(1)_1 + c_2 U(1)_2 + c_3 U(1)_3,
\tag{B.3.5}
$$

and impose the divergence of its current to vanish

$$
\partial \cdot j^X = \sum_{i=1,2,3} c_i \partial \cdot j^i = (-c_2 + c_3)Q_1 + (c_1 - c_3)Q_2 + (-c_1 + c_2)Q_3 \equiv 0.
\tag{B.3.6}
$$

Then the solution is

$$
U(1)_X = U(1)_1 + U(1)_2 + U(1)_3.
\tag{B.3.7}
$$

---

[8]See also Refs. [GRW98, BLPZ06, GVMU19].

[9]In a supersymmetric case, we have a Yukawa coupling.

[10]These charge vectors will not satisfy the convex-hull condition if the same masses are given to the matters by hand. This is seen on the two dimensional section with two charge vectors whose magnitudes are $\sqrt{2}$ and between which the angle is $2\pi/3$.

In this model, the anomaly-free gauge group is determined uniquely (up to overall normalization of the charges), and its gauge coupling is given by

$$\frac{1}{e_X^2} = \frac{1}{g_1^2} + \frac{1}{g_2^2} + \frac{1}{g_3^2}. \tag{B.3.8}$$

Here, the anomaly-free gauge coupling e_X is written so that the gauge kinetic term becomes the canonical form:

$$-\sum_j \frac{1}{4g_j^2} F_{\mu\nu}^{(j)} F^{(j)\mu\nu} = -\frac{1}{4e_X^2} F_{\mu\nu}^{(X)} F^{(X)\mu\nu} + (\text{anomalous gauge fields}). \tag{B.3.9}$$

Thus, the anomaly-free gauge coupling e_X can be smaller than the original $U(1)$ gauge couplings g_i's.

It is noted that all the matters are then neutral under this anomaly-free $U(1)_X$, i.e., $\forall\, q_X = 0$. It seems that this model may not be naively applied to the WGC, but the presence of global symmetries is important. The low energy Lagrangian will be given by

$$\mathcal{L} = \sum_{i \in \text{ matter}} i\overline{\psi_{Li}} \slashed{\partial} \psi_{Li} - \frac{1}{4e_X^2} \left(F_{\mu\nu}^{(X)} \right)^2 + \cdots, \tag{B.3.10}$$

if anomaly-free gauge boson $A_\mu^{(X)}$ survives in low energy limit. Ellipsis includes interactions among fermions and anomaly-free gauge boson and there will additionally exist kinetic mixings such as $K_{ij}\overline{\psi_{iL}}\slashed{\partial}\psi_{jL}$ and Majorana mass terms of $-M_{ij}\overline{\psi_{iL}^C}\psi_{jL}$ in low energy limit after anomalous massive bosons are integrated out. These terms will violate invariance under phase rotations of fermions. Now the original $\mathbb{Z}_3$ symmetry acts as $e_X \to e_X$, $A_\mu^{(X)} \to A_\mu^{(X)}$ and $\psi_{Li} \to \psi_{Li+1}$, but whether this low energy theory has the $\mathbb{Z}_3$ symmetry depends on parameters for fermions. Since all fermions are neutral under $U(1)_X$, global symmetries will be hard to survive in the low energy limit while discrete gauge symmetries originating from the anomalous $U(1)$'s can survive if any. If global symmetries survive, this model is in the swampland. It will be necessary to embed this model into string theory in order to know what kind of symmetries survives. This is beyond the scope of this work and left for future work.

$U(1)^{2k-1}$

We consider quiver gauge theories with more general $U(1)^{2k-1}$ groups. Fig. B.3 shows quiver diagrams with the five nodes, and it is noted that the number of incoming arrows is equal to that of outgoing ones at each node and both diagrams have a $\mathbb{Z}_5$ cyclic symmetry among each node. As in Eq. (B.3.1) and in the left diagram of Fig. B.3, we have five left-handed fermions charged against $(U(1)_1, U(1)_2, U(1)_3, U(1)_4, U(1)_5)$. The divergences
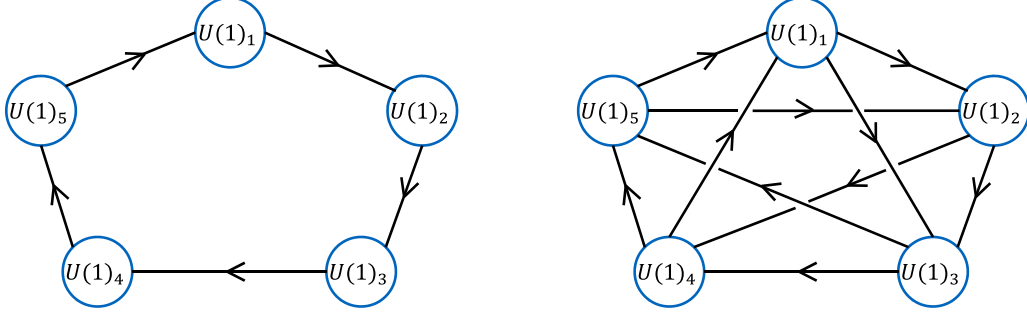
Figure B.3: Quiver diagrams with five nodes [AHT20]. Both diagrams have a $\mathbb{Z}_5$ cyclic symmetry among each node. In the right diagram, all nodes are connected with arrows.

of $U(1)^5$ chiral currents are given by

$$
\partial \cdot \begin{pmatrix} j^1 \\ j^2 \\ j^3 \\ j^4 \\ j^5 \end{pmatrix} = \begin{pmatrix} 0 & 1 & 0 & 0 & -1 \\ -1 & 0 & 1 & 0 & 0 \\ 0 & -1 & 0 & 1 & 0 \\ 0 & 0 & -1 & 0 & 1 \\ 1 & 0 & 0 & -1 & 0 \end{pmatrix} \begin{pmatrix} Q_1 \\ Q_2 \\ Q_3 \\ Q_4 \\ Q_5 \end{pmatrix}.
\tag{B.3.11}
$$

The number of anomaly-free $U(1)$'s is given by that of zero eigenvalues of this coefficient matrix, and we find only one zero eigenvalue in this model. The anomaly-free $U(1)$ is given by the corresponding eigenvector

$$
U(1)_{\text{anomaly-free}} = U(1)_1 + U(1)_2 + U(1)_3 + U(1)_4 + U(1)_5.
\tag{B.3.12}
$$

Thus all matters are again neutral under this anomaly-free $U(1)$ and this system will not simply be applied to the WGC. The situation is similar to the three quivers model in Section B.3.1.

The result is not changed by adding five chiral fermions to this model as in the right diagram of Fig. B.3. Then their action is additionally given by

$$
S = \sum_{j=1}^{5} \int d^4x \left[\overline{\psi}_{j,j+2} i\gamma^\mu \left(\partial_\mu + iA_\mu^{(j)} - iA_\mu^{(j+2)} \right) \psi_{j,j+2} + \cdots \right].
\tag{B.3.13}
$$

The anomaly coefficient matrix reads

$$
\begin{pmatrix} 0 & 1 & 1 & -1 & -1 \\ -1 & 0 & 1 & 1 & -1 \\ -1 & -1 & 0 & 1 & 1 \\ 1 & -1 & -1 & 0 & 1 \\ 1 & 1 & -1 & -1 & 0 \end{pmatrix}.
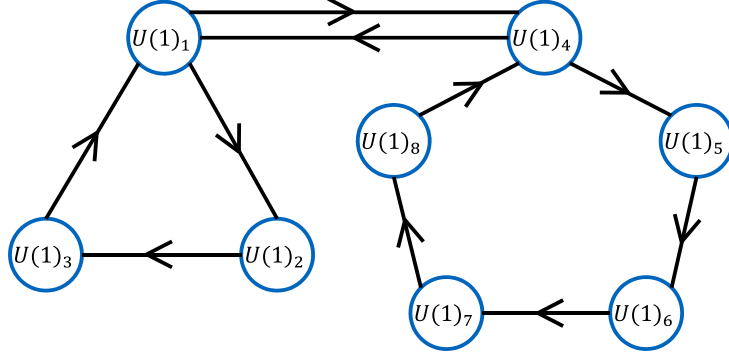\tag{B.3.14}
$$

Figure B.4: A quiver diagram of three nodes connected with five nodes by a pair of two arrows of vector-like matters [AHT20].

Thus, the anomaly-free $U(1)$ is similary given by Eq. (B.3.12).

So far we have discussed specific quiver models with three and five nodes, but the result can be simply extended to general models with odd number nodes as shown in Fig. B.1. Since the entries of the anomaly coefficient matrix are composed of the same number of 1 and -1 as above, the anomaly-free $U(1)$ is uniquely determined as

$$U(1)_{\text{anomaly-free}} = \sum_i^{2k-1} U(1)_i, \qquad (\text{B.3.15})$$

and the gauge coupling is given by

$$\frac{1}{e^2} = \sum_{i=1}^{2k-1} \frac{1}{g_i^2}. \qquad (\text{B.3.16})$$

In concrete models, these are easily verified and it is checked also that the result does not change for models with odd nodes and full diagonal lines that are similar to the right diagram of Fig. B.3. As noted previously, however, there exist no charged chiral matters for this anomaly-free $U(1)$.

$U(1)^{2k-1} \times U(1)^{2l-1}$ with vector-like matters

We shall consider quiver gauge theories with $U(1)^{2k-1} \times U(1)^{2l-1}$ in the presence of vector-like matters. As in Fig. B.4, the correspoinding diagram is composed of two diagrams with odd nodes which are connected by a pair of two arrows of vector-like matters. Action is given by two kinds of Eq. (B.3.1) showing $U(1)^{2k-1} \times U(1)^{2l-1}$ symmetry

147

and vector-like part of

$$S = \int d^4x \left[\overline{\psi}_{1,2k} i\gamma^\mu \left(\partial_\mu + iA_\mu^{(1)} - iA_\mu^{(2k)} \right) \psi_{1,2k} + \overline{\psi}_{2k,1} i\gamma^\mu \left(\partial_\mu - iA_\mu^{(1)} + iA_\mu^{(2k)} \right) \psi_{2k,1} \right.$$
$$\left. - m \overline{\psi}_{2k,1}^C \psi_{1,2k} + \text{h.c.} \right], \tag{B.3.17}$$

where we assume that the bi-fundamental vector-like matters are charged under the gauge groups of $U(1)_1 \times U(1)_{2k}$ and that the mass m remains non-zero in the weak gauge coupling limit. In this case, the discrete symmetry is explicitly broken since $\psi_{1,2k}$ is transformed to $\psi_{2,2k+1}$ that is originally absent. For instance, we focus on $U(1)^3 \times U(1)^5$ theory with vector-like matter, which is the case of $k = 2$ and $l = 3$. Since vector-like matter does not contribute to the chiral anomalies, we have two anomaly-free $U(1)$'s as mentioned above: one denotes $U(1)_X$ from $U(1)^3$ and another denotes $U(1)_{X'}$ from $U(1)^5$. Here,

$$U(1)_X = \sum_{i=1}^{3} U(1)_i, \qquad U(1)_{X'} = \sum_{i=4}^{8} U(1)_i, \tag{B.3.18}$$

hence charges of vector-like matters are $(+1, -1)$ and $(-1, +1)$ for $(U(1)_X, U(1)_{X'})$ and other chiral matters are neutral for them. The respective gauge couplings are given by

$$\frac{1}{e_X^2} = \sum_{i=1}^{3} \frac{1}{g_i^2}, \qquad \frac{1}{e_{X'}^2} = \sum_{i=4}^{8} \frac{1}{g_i^2}. \tag{B.3.19}$$

These can be weaker than the original gauge couplings of g_i's. Then the WGC for the vector-like matter reads[11]

$$e_X^2 + e_{X'}^2 \geq \frac{m^2}{2M_P^2}. \tag{B.3.20}$$

In the large limit of k and l with a given m and g_i's, we find

$$e_X^2 + e_{X'}^2 \sim \frac{g_i^2}{k} + \frac{g_i^2}{l} \to 0, \tag{B.3.21}$$

and then the WGC can be violated since the couplings becomes very weak as long as the mass m remains non-zero in the limit of $e_X \to 0$ and $e_{X'} \to 0$. Note that we now fix g_i's but change only k and l. This indicates that there exists an upper bounds on the numbers of $U(1)$ gauge groups, k and l as $k + l \lesssim (g_i \frac{M_P}{m})^2$ if the WGC is correct.

B.3.2 $U(1)^{2k}$

We consider quiver gauge theories with $U(1)^{2k}$ symmetry as shown in Fig. B.1. These types of models are also studied in D-brane models similarly to $U(1)^{2k-1}$ cases. As the

---

[11]In the $(U(1)_X, U(1)_{X'})$ theory, we need also additional $(+1, +1)$ and $(-1, -1)$ vector-like matters to satisfy the convex-hull condition so that extremal black holes with (Q, Q) charge can decay. This would imply that orientifold planes are required to cancel D-brane charges in the string theory. However, our conclusion does not change.
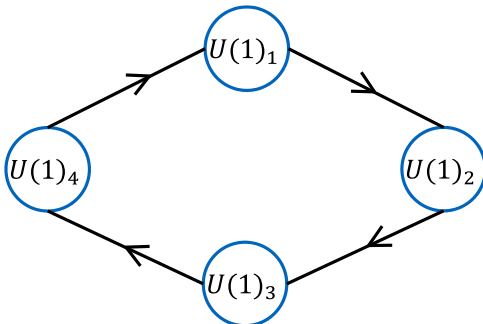
Figure B.5: The $\mathbb{Z}_4$ symmetric quiver diagram with four nodes [AHT20].

simplest model with chiral anomalies, we focus on $U(1)^4$ symmetry and this model has four left-handed fermions as in Fig. B.5. Divergences of each chiral current are given by

$$
\partial \cdot \begin{pmatrix} j^1 \\ j^2 \\ j^3 \\ j^4 \end{pmatrix} = \begin{pmatrix} 0 & 1 & 0 & -1 \\ -1 & 0 & 1 & 0 \\ 0 & -1 & 0 & 1 \\ 1 & 0 & -1 & 0 \end{pmatrix} \begin{pmatrix} Q_1 \\ Q_2 \\ Q_3 \\ Q_4 \end{pmatrix},
\tag{B.3.22}
$$

Since the anomaly coefficient matrix have two zero eigenstate, this model has two independent anomaly-free $U(1)$'s, which are represented by the eigenvectors $(1,0,1,0)$ and $(0,1,0,1)$. The former relates first node to third one, whereas the latter does second node to fourth one. The independent anomaly-free $U(1)$'s are generally given by

$$
U(1)_X = cU(1)_1 + U(1)_2 + cU(1)_3 + U(1)_4,
\tag{B.3.23}
$$

$$
U(1)_{X'} = -\frac{1}{c}U(1)_1 + U(1)_2 - \frac{1}{c}U(1)_3 + U(1)_4,
\tag{B.3.24}
$$

where c is a free parameter that depends on the D-brane configuration in concrete UV string models [AIQU00, AFI+01b, AFI+01a][12], and will be a rational number. Otherwise, there exists a global symmetry [BD88, BS11, HO21]. The result does not change even if we add bi-fundamental vector-like matters that are charged under only $U(1)_1 \times U(1)_3$ or only $U(1)_2 \times U(1)_4$. For $c = 0$, we find $U(1)_X = U(1)_2 + U(1)_4$ and $U(1)_{X'} = U(1)_1 + U(1)_3$. It is noted that for a general c a linear combination can violate the $\mathbb{Z}_4$ to $\mathbb{Z}_2^2$ exchanging $1 \leftrightarrow 3$ and $2 \leftrightarrow 4$. The gauge couplings relevant to the anomaly-free $U(1)$'s read

$$
\frac{1}{e_X^2} = \frac{c^2}{g_1^2} + \frac{1}{g_2^2} + \frac{c^2}{g_3^2} + \frac{1}{g_4^2},
\tag{B.3.25}
$$

---

[12] A gauge boson in one of the two $U(1)$'s could be massive in UV models. But, the behavior of gauge coupling will not change in the large k limit.
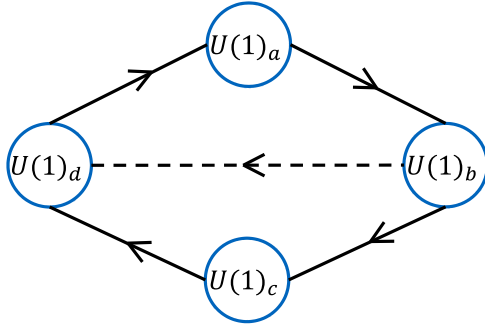
Figure B.6: A quiver diagram of $U(1)^4$ model including a complex scalar [AHT20].

$$\frac{1}{e_{X'}^2} = \frac{1/c^2}{g_1^2} + \frac{1}{g_2^2} + \frac{1/c^2}{g_3^2} + \frac{1}{g_4^2}. \tag{B.3.26}$$

In this model, the chiral fermions have non-trivial charges under these anomaly-free $U(1)$'s as shown in Table B.1. In the next section, we will numerically study the SWGC in this model by adding a complex scalar.

Extending this model to general theories with $U(1)^{2k}$ is simple, and we can verify that there exists at least two anomaly-free $U(1)$'s in a concrete model. So it is expected that in the large k limit with a given c and a fixed g_i, anomaly-free gauge couplings become very small as in cases of $U(1)^{2k-1} \times U(1)^{2l-1}$. Then there exists an upper bound on the number of abelian gauge groups if the WGC is correct and a fermion mass remains non-zero in the large k limit.

B.4 A $U(1)^4$ model and the SWGC

In this section, we discuss the detail of $U(1)^4$ quiver gauge theory shown in the previous section and its application to the SWGC at the tree level in the presence of a complex scalar field. The motivation for this is to study SWGC in a more realistic (or string-inspired) model with a scalar field. The SWGC shows numerically constraints of a smallness of gauge couplings against Yukawa couplings. We also study a UV completion of 5D orbifold model for it.

B.4.1 Constraints of the SWGC

Fig. B.6 shows a quiver diagram of $U(1)^4$ model in the presence of a complex scalar φ, whose charge is $(+1, -1)$ for $(U(1)_b, U(1)_d)$.[13] Due to this scalar field, we have Yukawa

---

[13]The direction of the dashed arrow shows the scalar charge same as chiral fermions. We changed the names of gauge groups from $U(1)_1 \times U(1)_2 \times U(1)_3 \times U(1)_4$ to $U(1)_a \times U(1)_b \times U(1)_c \times U(1)_d$ and

Fields	q_X	$q_{X'}$
ψ_{ab}	$-1+c$	$-1-1/c$
ψ_{da}	$1-c$	$1+1/c$
ψ_{bc}	$1-c$	$1+1/c$
ψ_{cd}	$-1+c$	$-1-1/c$
φ	0	0

Table B.1: The charges of fields for the anomaly-free $U(1)_X \times U(1)_{X'}$ group.

couplings of

$$\mathcal{L}_{\text{Yukawa}} = -y\varphi\overline{\psi_{ab}^C}\psi_{da} - y'\varphi^\dagger\overline{\psi_{bc}^C}\psi_{cd} + \text{h.c.} \tag{B.4.1}$$

This model is inspired by intersecting brane models [IMR01, CIM02a]. No $\mathbb{Z}_4$ symmetry exists. This is because φ can be written as φ_{bd} in the view point of the $U(1)$ charges and hence φ_{bd} is transformed to φ_{ca} that is originally absent. There could exist $\mathbb{Z}_2$ that simultaneously exchanges the labels as $a \leftrightarrow c$ and $b \leftrightarrow d$ for $y = y'$, if we can identify $\varphi_{bd} = \varphi_{db}^\dagger$. As seen in the previous section, two anomaly-free $U(1)$'s are given by

$$U(1)_X = cU(1)_a + U(1)_b + cU(1)_c + U(1)_d, \tag{B.4.2}$$

$$U(1)_{X'} = -\frac{1}{c}U(1)_a + U(1)_b - \frac{1}{c}U(1)_c + U(1)_d, \tag{B.4.3}$$

where a free parameter c is a rational number and can be fixed in concrete models by the brane configuration in the string theory. The charges of the fields are summarized in Table B.1.

The effective Lagrangian showing two anomaly-free $U(1)$'s may read

$$\mathcal{L} = \sum_{I=ab,bc,cd,da} i\overline{\psi}_I \not{D}\psi_I + |\partial_\mu\varphi|^2 - \frac{1}{4e_X^2}\left(F_{\mu\nu}^{(X)}\right)^2 - \frac{1}{4e_{X'}^2}\left(F_{\mu\nu}^{(X')}\right)^2$$
$$- \left[y\varphi\overline{\psi_{ab}^C}\psi_{da} + y'\varphi^\dagger\overline{\psi_{bc}^C}\psi_{cd} + \text{h.c.}\right] + \cdots, \tag{B.4.4}$$

where $D_\mu = \partial_\mu + iq_X A_\mu^{(X)} + iq_{X'}A_\mu^{(X')}$, gauge bosons relevant to two anomalous $U(1)$'s are neglected since they become massive if the Green-Schwarz mechanism works. Yukawa couplings between the complex scalar and chiral fermions are denoted by y and y', which are not the same in general. It is noted that vector-like pairs of $\psi_{ab} + \psi_{da}$ and $\psi_{bc} + \psi_{cd}$ will constitute the Dirac spinors.[14] Now scalar φ is neutral under anomaly-free $U(1)$'s

---

accordingly those of left-handed fermions from $(\psi_{1,2}, \psi_{2,3}, \psi_{3,4}, \psi_{4,1})$ to $(\psi_{ab}, \psi_{bc}, \psi_{cd}, \psi_{da})$ for the latter convenience.

[14]From the view point of the anomaly-free $U(1)$'s, there may exist Yukawa couplings including $\overline{\psi_{ab}^C}\psi_{bc}$ and $\overline{\psi_{cd}^C}\psi_{da}$, but they are supposed to be much smaller than y and y' here. Similarly, there may exist Dirac masses to these fermions because φ is singlet for the anomaly-free $U(1)$'s in the low energy, but the masses would be negligibly small against the Planck scale.

and will not be considered for the SWGC. The scalar potential will be neglected hereafter with an assumption that φ is sufficiently light at energy scales of our interest since the scalar potential will be model-dependent. To check strong SWGC [GIn19] for φ is an interesting issue, but this is left for future work and we focus on the SWGC for fermions with non-trivial anomaly-free gauge charges. Here the anomaly-free gauge couplings are given by

$$\frac{1}{e_X^2} = \frac{c^2}{g_a^2} + \frac{1}{g_b^2} + \frac{c^2}{g_c^2} + \frac{1}{g_d^2}, \tag{B.4.5}$$

$$\frac{1}{e_{X'}^2} = \frac{1/c^2}{g_a^2} + \frac{1}{g_b^2} + \frac{1/c^2}{g_c^2} + \frac{1}{g_d^2}. \tag{B.4.6}$$

In the presence of a very light φ, the SWGC can be expressed as

$$(-1+c)^2 e_X^2 + \left(1 + \frac{1}{c}\right)^2 e_{X'}^2 \geq \frac{M^2}{2M_P^2} + \frac{Y^2}{2}, \tag{B.4.7}$$

for a test fermion. Here, $Y = y$ and $M = y\mathrm{Re}(\varphi)$ for a Dirac fermion of $\psi_{ab} + \psi_{da}$, whereas $Y = y'$ and $M = y'\mathrm{Re}(\varphi)$ for $\psi_{bc} + \psi_{cd}$. A factor $Y^2/2$ is obtained because of the canonical normalization of $\mathrm{Re}(\varphi)$, and $\mathrm{Im}(\varphi)$ contributes to the spin-dependent interaction that is not $1/r^2$-force. If the scalar is sufficiently heavy, Y does not contribute to the SWGC condition owing to exponentially damping force and hence the WGC can be easily satisfied. To reduce the number of parameters, we will set $g_b = g_d =: g$ for simplicity. In the next subsection, we will study this situation realized in the 5D orbifold model. Thus this equation can be rewritten as

$$\frac{(1-c)^2}{c^2(g^2/g_a^2 + g^2/g_c^2) + 2} + \frac{(1+1/c)^2}{(1/c^2)(g^2/g_a^2 + g^2/g_c^2) + 2} \gtrsim \frac{1}{2}\left(\frac{Y}{g}\right)^2. \tag{B.4.8}$$

Here, the masses are neglected because $M/M_{\mathrm{Pl}} \ll 1$ is numerically expected in the effective field theory. Indeed, there is almost no change in appearance of the plots for $M/gM_{\mathrm{Pl}} \lesssim 0.1$, where gM_{Pl} is expected as a cutoff scale [AHMNV07], when the scalar is massless. It is noted also that a gauge boson in either $U(1)_X$ or $U(1)_{X'}$ may be massive owing to the Stückelberg coupling and then either e_X or $e_{X'}$ vanishes in Eq. (B.4.8).

In the top panels of Fig. B.7, we show the plots of the SWGC (B.4.8) in the $(X, Y/g)$-, $(c, Y/g)$- and (c, X)-planes, where $X := g^2/g_a^2 + g^2/g_c^2$. The each line saturates Eq. (B.4.8), hence the allowed region exists below them. In the presence of the mass, the SWGC is violated on each line. Note that these plots are symmetric under $c \to -1/c$ owing to the definition of the anomaly-free $U(1)$'s. A region for a large Yukawa coupling is excluded by the SWGC. For a large X, the constraint becomes tighter. In other words, a big discrepancy between gauge couplings is disfavored. It turns out that the constraint becomes stronger near $c = \pm1$ because either e_X or $e_{X'}$ vanishes then. We find also that the constraint is independent of c for special values of $X = 2$ and $Y/g = \sqrt{2}$. This is because for $X = 2$ the left hand side of Eq. (B.4.8) becomes unity and hence for $Y/g \geq \sqrt{2}$
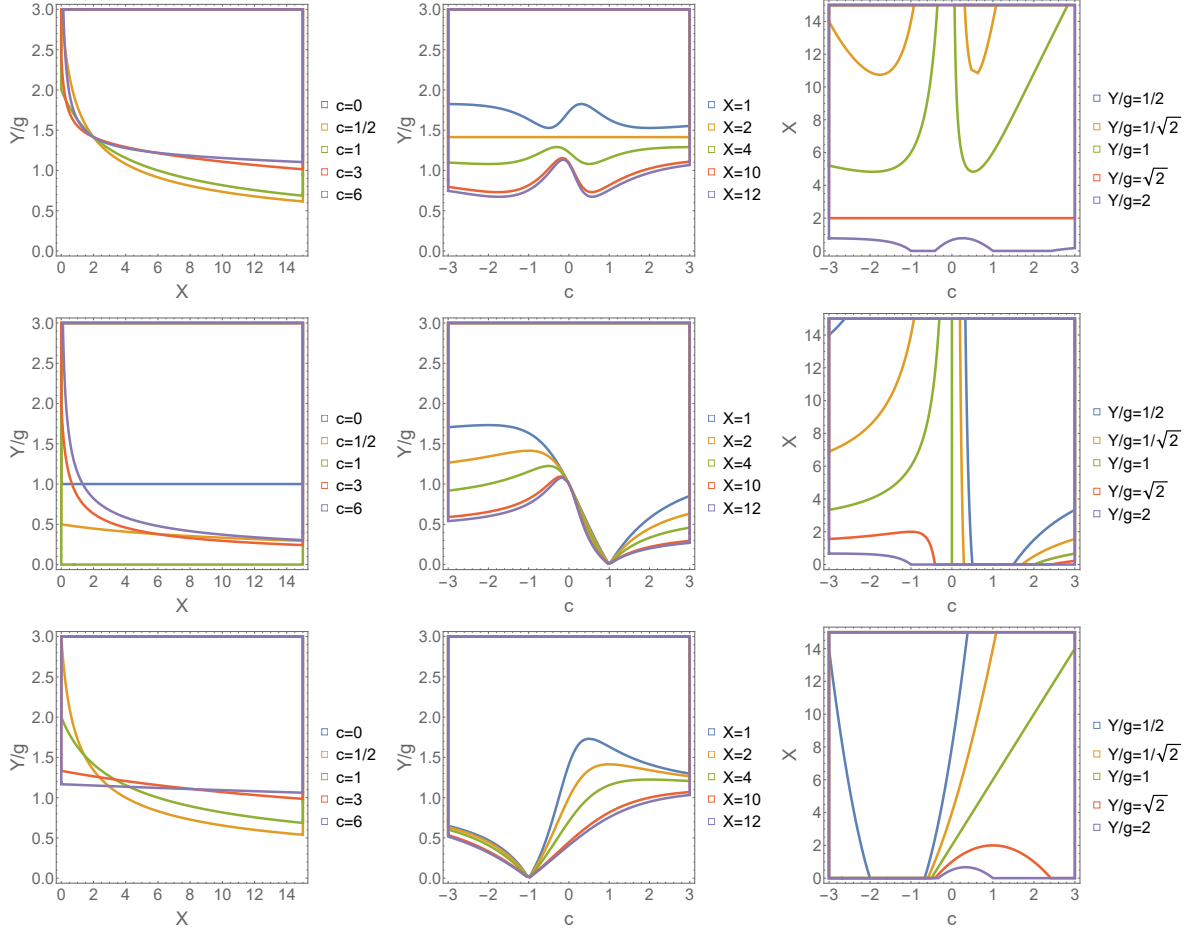
Figure B.7: Plots of the SWGC constraints in $(X, Y/g)$-, $(c, Y/g)$- and (c, X)-planes [AHT20]. The top panels plot the constraints of Eq. (B.4.8). The middle (bottom) figures show the similar plots with $e_{X'} = 0$ ($e_X = 0$), when $U(1)_X$ ($U(1)_{X'}$) gauge group survives in low energy limit. The condition is saturated on each lines, below which there exist an allowed region. In the presence of mass, the SWGC is violated on each line.

the SWGC is then violated in the presence of the mass term. We can find also that the constraint becomes weaker as the $c > 0$ increases in the top-left panel for $X > 2$, because either e_X or $e_{X'}$ gets stronger then whereas the constraint does not depend on c for $X \ll 1$. It is noted that in the string theory c depends on the D-brane configuration and the couplings depend on moduli fields with the fixed configuration. The middle (bottom) figures show the similar plots with $e_{X'} = 0$ ($e_X = 0$), when only a gauge boson of $U(1)_X$ ($U(1)_{X'}$) remains massless and mediates the long-range repulsive force. In these cases, the condition of the SWGC tends to give tighter constraints.

Fields	$U(2)$	$U(1)_a$	$U(1)_c$
A_M	adj	0	0
Ψ_a	$\mathbf{2}_{1/2}$	-1	0
Ψ_c	$\overline{\mathbf{2}}_{-1/2}$	0	$+1$
$A_M^{(a)}$	0	adj	0
$A_M^{(c)}$	0	0	adj

Table B.2: Table of the field contents and their charges in 5D model for realizing $U(1)^4$ gauge theory in 4D. Subscripts of $U(2)$ representation for fermions are $U(1)$ charges against the overall $U(1) \in U(2)$.

B.4.2   A $U(1)^4$ model from $S^1/\mathbb{Z}_2$ orbifold and the SWGC

We consider a 5D gauge theory with $U(2) \times U(1)_a \times U(1)_c$ on the $S^1/\mathbb{Z}_2$ orbifold for realizing chiral fermions. The purpose of this subsection is to give a concrete Yukawa coupling associated with the gauge coupling and a relation between gauge couplings as in the previous subsection via the symmetry breaking of $U(2) \to U(1)_b \times U(1)_d$ by an orbifold projection. The fields contents and their representations are exhibited in Table B.2. The 5D action is given by

$$S_{5D} = \int_{M_4 \times S^1/\mathbb{Z}_2} d^4 x\, dy\, \sqrt{-G_5} \left[-\frac{1}{2\kappa_5^2} \mathcal{R}_5 - \frac{1}{2\hat{g}_2^2} \mathrm{tr}(F_{MN})^2 - \frac{1}{4\hat{g}_a^2} \left(F_{MN}^{(a)}\right)^2 - \frac{1}{4\hat{g}_c^2} \left(F_{MN}^{(c)}\right)^2 \right.$$
$$\left. + \overline{\Psi}_a(i\slashed{D} - M_a)\Psi_a + \overline{\Psi}_c(i\slashed{D} - M_c)\Psi_c \right], \qquad (B.4.9)$$

where $M = 0, 1, 2, 3, y$, $D_M = \nabla_M + iA_M + i\hat{q}_a A_M^{(a)} + i\hat{q}_c A_M^{(c)}$ and $\hat{q}_a$ and $\hat{q}_c$ are the charges of $U(1)_a$ and $U(1)_c$ respectively. 5D Chern Simons terms associated with 4D Green-Schwarz mechanism is neglected as already noted. The field strengths are given by $F_{MN} = \partial_M A_N - \partial_N A_M + i[A_M, A_N]$ and $F_{MN}^{(a,c)} = \partial_M A_N^{(a,c)} - \partial_N A_M^{(a,c)}$ for the non-abelian gauge field and abelian gauge fields respectively. The normalization of generator of $U(2)$ is chosen as $\mathrm{tr}(T_a T_b) = \delta_{ab}/2$, hence the $U(2)$ gauge field is expanded as $A_M = \frac{\mathbb{1}_2}{2} A_M^{(0)} + \frac{\sigma^a}{2} A_M^{(a)}$, where $\mathbb{1}_2$ is 2×2 identity matrix and σ^a's ($a = 1, 2, 3$) are the Pauli matrices. Since the covariant derivative is acting on Ψ_a as $D_M \Psi_a \ni iA_M \Psi_a = i\frac{\mathbb{1}_2}{2} A_M^{(0)} \Psi_a + \cdots$, Ψ_a has 1/2 charge against the overall $U(1)$. This is similar to Ψ_c, which has the opposite $U(1)$ charge. Here, $\Psi_{a,c} = (\psi_{a,c1}, \psi_{a,c2})$ are doublets for the $SU(2)$ and $\psi_{a,c}$ are the 4D Dirac spinors. The metric of $M_4 \times S^1/\mathbb{Z}_2$ is written by $ds_5^2 = e^{-\sigma} g_{\mu\nu} dx^\mu dx^\nu + e^{2\sigma} dy^2$, where σ is the radion field, and gives 4D Einstein frame. The size of $S^1/\mathbb{Z}_2$ is assumed to be πL and we take $\langle \sigma \rangle = 0$ without loss of generality. The graviphoton $g_{\mu y}$ is dropped since it is parity odd while the 4D graviton $g_{\mu\nu}$ remains massless. Then, the massive graviphoton mediates the short-range force among particles which have the Kaluza-Klein (KK) charges, and does not contribute to the SWGC condition. On top of the usual periodic boundary condition

of S^1, the orbifold boundary conditon is given by

$$PA_M(x, -y)P^{-1} = \eta_A A_M(x, y), \quad A_M^{(a,c)}(x, -y) = \eta_A A_M^{(a,c)}(x, y), \tag{B.4.10}$$

$$P\Psi_{a,d}(x, -y) = \gamma_5 \Psi_{a,d}(x, y), \tag{B.4.11}$$

where $P = \mathrm{diag}(+1, -1) \in U(2)$, $\eta_A = 1$ for $M = \mu = 0, 1, 2, 3$ and $\eta_A = -1$ for $M = y$. Thus 4D massless modes read

$$A_\mu = \begin{pmatrix} A_\mu^{(b)} & \\ & A_\mu^{(d)} \end{pmatrix}, \quad A_y = \begin{pmatrix} & i\varphi/\sqrt{2} \\ -i\varphi^\dagger/\sqrt{2} & \end{pmatrix}, \quad A_\mu^{(a)}, \quad A_\mu^{(c)}, \tag{B.4.12}$$

$$\psi_{a1R}, \ \psi_{a2L}, \quad \psi_{c1R}, \ \psi_{c2L}. \tag{B.4.13}$$

where $A_\mu^{(b)} := \frac{1}{2}(A_\mu^{(0)} + A_\mu^{(3)})$, $A_\mu^{(d)} := \frac{1}{2}(A_\mu^{(0)} - A_\mu^{(3)})$, $\varphi = -(iA_y^{(1)} + A_y^{(2)})/\sqrt{2}$ is the complex scalar originating from the W-boson of y-direction[15], and the ψ_L (ψ_R) is the left-handed (right-handed) chiral fermion in 4D. It turns out that there exists the gauge symmetry of $U(1)_a \times U(1)_b \times U(1)_c \times U(1)_d$. As seen from the zero mode basis in the $U(2)$ gauge bosons, we find matter charges for the gauge symmetry: As for $(U(1)_a, U(1)_b, U(1)_c, U(1)_d)$, $\psi_{a1R}^C \equiv \psi_{ab} : (+1, -1, 0, 0)$, $\psi_{c1R}^C \equiv \psi_{bc} : (0, +1, -1, 0)$, $\psi_{c2L} \equiv \psi_{cd} : (0, 0, 1, -1)$, $\psi_{a2L} \equiv \psi_{da} : (-1, 0, 0, 1)$ and $\varphi : (0, 1, 0, -1)$. This is the same field content as in the previous subsection, hence φ is a neutral scalar under anomaly-free $U(1)$'s and will not be considered for the SWGC. The scalar potential will be neglected as previously noted since the scalar potential including radion will depend on the model and the radion stabilization. Deriving the scalar potential and checking the strong SWGC for this is left for future work.

The 4D parameters are given by the 5D parameters with an assumption of $\langle\sigma\rangle = 0$. For the details, see Appendix B.C. The 4D Planck mass is associated with the 5D gravitational coupling κ_5 as

$$M_P^2 = \frac{\pi L}{\kappa_5^2}, \tag{B.4.14}$$

and the gauge couplings in 4D are expressed by

$$\frac{2}{g_2^2} := \frac{1}{g_b^2} = \frac{1}{g_d^2} = \frac{2\pi L}{\hat{g}_2^2}, \qquad \frac{1}{g_a^2} := \frac{\pi L}{\hat{g}_a^2}, \quad \frac{1}{g_c^2} := \frac{\pi L}{\hat{g}_c^2}. \tag{B.4.15}$$

This is because we have the gauge kinetic term $\mathcal{L} = -2/4g_2^2 (F_{\mu\nu}^{(b)})^2 - 2/4g_2^2 (F_{\mu\nu}^{(d)})^2$ via the symmetry breaking of $U(2) \to U(1)_b \times U(1)_d$. With these, the anomaly-free couplings are defined as previously:

$$\frac{1}{e_X^2} = \frac{c^2}{g_a^2} + \frac{2}{g_2^2} + \frac{c^2}{g_c^2} + \frac{2}{g_2^2}, \tag{B.4.16}$$

---

[15]Here we define the complex scalar by multiplying the ordinary W^+-boson by $-i$ so that the effective Lagrangian of the zero modes reproduces Eq. (B.4.4) after this orbifold projection.

$$\frac{1}{e_{X'}^2} = \frac{1/c^2}{g_a^2} + \frac{2}{g_2^2} + \frac{1/c^2}{g_c^2} + \frac{2}{g_2^2}, \tag{B.4.17}$$

where a free parameter c is a rational number.

The Yukawa couplings between φ and ψ's are given by

$$y = y' = \frac{\hat{g}_2}{\sqrt{2\pi L}} = \frac{g_2}{\sqrt{2}}. \tag{B.4.18}$$

Here, y and y' are the same definition as in the previous subsection. This equation relates the Yukawa coupling to the gauge coupling. In the presence of a light $\mathrm{Re}(\varphi)$ and the radion, the SWGC inequality for zero mode fermions reads

$$(1-c)^2 e_X^2 + \left(1 + \frac{1}{c}\right)^2 e_{X'}^2 \geq \frac{y^2}{2} + \left(\frac{1}{2} + \frac{1}{6}\right) \frac{M^2}{M_P^2} \tag{B.4.19}$$

where M has the same definition as in the previous subsection[16] and $1/6$ comes from the radion exchange via $y e^{-\sigma_c/\sqrt{6}M_{\mathrm{Pl}}} \mathrm{Re}(\varphi) \overline{\psi}\psi$ with the canonically normalized radion $\sigma_c = \sqrt{3/2} M_{\mathrm{Pl}} \sigma$. We have neglected momentum-dependent terms induced by the radion exchange with terms of $\overline{\psi}\gamma^\mu \psi \partial_\mu \sigma$. If $\mathrm{Re}(\varphi)$ is sufficiently heavy, the yukawa interaction in this equation can be neglected and the WGC can be then easily satisfied. Gravitational interactions including radion exchange will be numerically neglected below as in the previous subsection owing to the Planck-suppressed interaction within the effective field theory. For $M/g_2 M_{\mathrm{Pl}} \lesssim 0.1$ and $p/g_2 M_{\mathrm{Pl}} \lesssim 0.1$, where p is the momentum of a test fermion, there are not significant differences compared to the plots shown below. Substituting the above couplings given by Eqs.(B.4.16)–(B.4.18) to Eq. (B.4.19), we then find the SWGC condition

$$\frac{(1-c)^2}{(c^2/2)(g_2^2/g_a^2 + g_2^2/g_c^2) + 2} + \frac{(1+1/c)^2}{(1/2c^2)(g_2^2/g_a^2 + g_2^2/g_c^2) + 2} \gtrsim \frac{1}{4}. \tag{B.4.20}$$

This is also obtained when the parameters in Eq. (B.4.8) are replaced as $g^2 \to g_2^2/2$ and $(Y/g)^2 \to 1/2$. This gives a constraint between c and $X := g_2^2/g_a^2 + g_2^2/g_c^2$.

As for the KK modes or the massive parity odd ones, a similar equation to Eq. (B.4.19) will be hold. It is noted that massive gauge bosons do not contribute to long-range forces and all bosons including scalar zero mode are neutral under anomaly-free $U(1)$'s and fermions with non-trivial gauge charges are considered for the SWGC. Parity odd fermions of ψ_{a1L}, ψ_{a2R}, ψ_{c1L} and ψ_{a2R} have opposite charges to zero mode fermions. KK modes of a field have the same charge as that of the lightest mode. Yukawa couplings that are invariant under $\mathbb{Z}_2$ projection are given by $\phi_{\mathrm{even}}\psi_{\mathrm{even}}\psi_{\mathrm{even}}$, $\phi_{\mathrm{even}}\psi_{\mathrm{odd}}\psi_{\mathrm{odd}}$, $\phi_{\mathrm{odd}}\psi_{\mathrm{odd}}\psi_{\mathrm{even}}$, where ϕ_{even} (ϕ_{odd}) is an even (odd) parity scalar and ψ_{even} (ψ_{odd}) is an even (odd) parity fermion. As massive scalars do not contribute to a long-range force, Yukawa couplings relevant to the SWGC are associated with φ: $\varphi\psi_{\mathrm{even}}\psi_{\mathrm{even}}$, $\varphi\psi_{\mathrm{odd}}\psi_{\mathrm{odd}}$. After integration

---

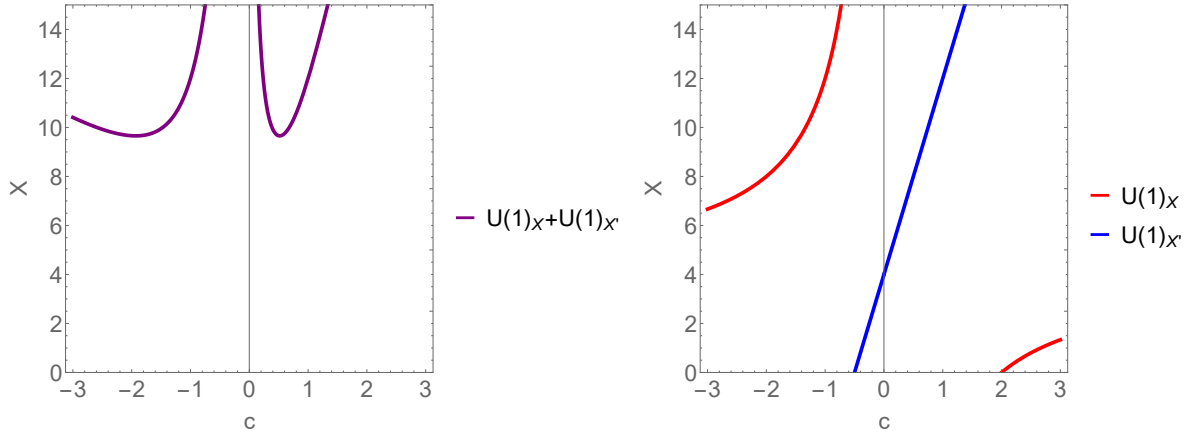[16]We have factored out the common radion dependence $e^{-\sigma}$.

Figure B.8: The left panel: Plots of the SWGC conditons (B.4.20) in the (c, X)-planes. The condition is saturated on each lines, below which there exist an allowed region. In the presence of mass, the SWGC is violated on each line. The right panel: A similar plot with only $U(1)_X$ (red) and one with only $U(1)_{X'}$ (blue). These figures are from Ref. [AHT20].

over the extra dimension, we will find Yukawa couplings of $y\varphi\psi'_n\psi_n$ in addition to KK mass terms $(n/L)\overline{\psi}_n\psi_n + (n/L)\overline{\psi}'_n\psi'_n$ for n-th KK modes with the canonically normalized kinetic terms (up to the radion dependence). Then n-th KK mass eigenstates will have mass $M^2 = (n/L \pm y\mathrm{Re}(\varphi))^2$. As the SWGC could be violated by heavy KK modes, it is necessary to check whether lighter modes including the zero modes satisfy the SWGC.

Fig. B.8 shows the plots of the SWGC (B.4.20) in the (c, X) plane. The each line saturates Eq. (B.4.20), hence the allowed region exists below them. In the presence of mass, the SWGC is violated on each line. The these plots are symmetric under $c \to -1/c$. The left panel shows the constraint when there exists two anomaly-free $U(1)$'s. This is very similar to the top-right one of Fig. B.7 for a small value of Yukawa. For a large X, not only $U(1)_b \times U(1)_d$ gauge coupling but also Yukawa coupling $\propto g_2$ become much stronger than g_a or g_c, and hence there exist an upper bound on X. It is noted that in the context of the string theory a large X may imply a big discrepancy among moduli VEVs. In the vicinty of $c = \pm 1$, matter becomes neutral against either one of the anomaly-free $U(1)$'s, then the constraint becomes tighter. In the right panel, plots show the SWGC constraint with $e_X = 0$ or $e_{X'} = 0$, when only the gauge boson of either $U(1)_X$ or $U(1)_{X'}$ remains massless owing to a Stückelberg coupling as often seen in concrete string models.

B.5   Summary

We have studied the (S)WGC in several types of quiver gauge theories with $U(1)^k$ gauge symmetry in the presence of bi-fundamental chiral fermions leading to the chiral anomalies, which is supposed to be canceled by the Green-Schwarz mechanism. The theories which we consider possesses a cyclic $\mathbb{Z}_k$ symmetry associated with a shift of

the label of the gauge groups. As a consequence of this, we can study anomalies in the models systematically and the (S)WGC constraints on the gauge couplings. We identified concretely the anomaly-free $U(1)$'s and their gauge couplings obtained via linear combinations of the original $U(1)$'s. Then, $\mathbb{Z}_k$ symmetry can be broken in general. In the large k limit, an anomaly-free gauge coupling becomes very weak as $e \sim k^{-1/2}$, and there exists an upper bound on k if the WGC is correct and the mass for a test particle remains in the large k limit. This may be regarded as an example of the weak coupling conjecture. For quiver theories with $U(1)^{2k-1}$, an unique anomaly-free $U(1)$ is proportional to $\sum_{i=1}^{2k-1} U(1)_i$ and all matters are neutral under the anomaly-free $U(1)$. There exist charged matters in the presence of vector-like pairs, and $\mathbb{Z}_{2k-1}$ symmetry is broken then. For quiver theories with $U(1)^{2k}$ gauge symmetry, there exist two anomaly-free $U(1)$'s and charged matters under these gauge groups, and $\mathbb{Z}_{2k}$ symmetry is broken in general. Even if the gauge couplings of the the anomaly-free $U(1)$'s receive quantum corrections, the IR couplings will remain very weak in the large k limit since $U(1)$ couplings are generally asymptotic non-free as far as the pertubation theory is valid.

We have numerically studied also the SWGC in $U(1)^4$ theory in the presence of a complex scalar field, and construct a similar model based on a 5D orbifold. It turns out that a much larger Yukawa coupling than gauge couplings is forbidden and also that a big discrepancy among gauge couplings is disfavored. A special linear combination for realizing the anomaly-free $U(1)$'s can be also be disfavored, since matter charge becomes small then.

So far, we neglected kinetic mixings $\chi_{ij} F^i_{\mu\nu} F^{j\mu\nu}$ among gauge fields. If we have such terms, we may have a kinetic mixing of $\chi F^X_{\mu\nu} F^{X'\mu\nu}$, where $\chi \sim \sum_{i,j}^k \chi_{ij} c_i c'_j$, for anomaly-free $U(1)_X = \sum_i c_i U(1)_i$ and $U(1)_{X'} = \sum_i c'_i U(1)_i$ with c_i's $= \mathcal{O}(1)$. If the mixing χ is at most of $\mathcal{O}(k^{3/2-\alpha})$ ($\alpha > 0$) in the large k limit, the WGC can still be violated as in Section B.3. This is because the canonically normalized mixing is given by $e_X e_{X'} \chi$ and hence an induced coupling of a fermion to an anomay-free gauge field is proportional to $e_X^2 e_{X'} \chi$ or $e_X e_{X'}^2 \chi$ that are scaling as $k^{-\alpha}$ then. However, if $\chi = \mathcal{O}(k^2)$ in the large k limit, the WGC can be satisfied.

In the Section B.4, the scalar φ is a singlet under the anomaly-free gauge groups, and we did not discuss the detail of the scalar potential in addition to the radion. Hence it may be an interesting challenge to check the strong SWGC within a fixed model. This is left for future work.

It will be worth to investigate the (S)WGC in theories with more general gauge groups. In actual string compactifications, the number of closed string axions is known to be finite and depends on the Hodge number of compactification manifold. Some of the axions play an important role to cancel anomalies through the Green-Schwarz mechanism. Hence, the number of anomalous $U(1)$ gauge theories, which is $k-1$ or $k-2$ in our cases, should be constrained by the number of such axions. If the anomalies are independent among the anomalous theories, the number of anomalous $U(1)$'s can be less than that of axions

for anomaly cancellation. Also in the string theory, the conjecture would constrain brane configuration and moduli values. If one starts with 10D super Yang-Mills theory, 4D effective action including an anomaly-free $U(1)$ may be given by [CIM03, CIM04]

$$\mathcal{L} = -c\frac{S}{4}(F_{\mu\nu})^2 - \frac{\vartheta(\tau)}{\sqrt{S}}\phi\overline{\psi}\psi + \cdots , \tag{B.5.1}$$

where S is the 4D dilaton, τ is a complex structure modulus, and a rational number c originates from a linear combination of $U(1)$'s depends on brane configuration of the number of branes and magnetic fluxes. The SWGC of $e^2 \gtrsim y^2$ (up to mass term) for matter fermion may read

$$c \lesssim \frac{1}{|\vartheta(\tau)|^2}. \tag{B.5.2}$$

However, it will be required a deep understanding of the string theory or concrete effective field theories including (non-abelian) Dirac-Born-Infeld action to study the SWGC constraints on moduli space for consistent gauge theories in the presence of the Green-Schwarz mechanism. This is also left for future works.

Appendix B.A   Anomalies in string-inspired (SUSY) gauge theories

We discuss anomaly-free $U(1)$'s in $U(N)^k$ quiver gauge theories inspired by the string theory. We focus only on certain types of quiver theories considered in Section B.3 in this section. Hereafter, N_a denotes the rank of the gauge group of $U(N_a)$ at the a-node, and n_{ab} shows the number of bi-fundamental matter fields which correspond to that of arrows connecting between a-node and b-node in the quiver diagram.

B.A.1 $U(N)^3$

We consider a $U(N)^3$ quiver gauge theory as shown in Fig. B.9, and identify an anomaly-free $U(1)$. To this end, we calculate chiral anomalies and mixed anomalies. Then, we find the constraints on the ranks of gauge groups and the numbers of generations. For a consistent theory, the non-abelian cubic anomalies $\mathcal{A}_{SU(N_{a,b,c})^3}$ give the following constraints,

$$\mathcal{A}_{SU(N_a)^3} \propto (n_{ab}N_b - n_{ca}N_c) \equiv 0, \tag{B.A.1}$$

$$\mathcal{A}_{SU(N_b)^3} \propto (n_{bc}N_c - n_{ab}N_a) \equiv 0, \tag{B.A.2}$$

$$\mathcal{A}_{SU(N_c)^3} \propto (n_{ca}N_a - n_{bc}N_b) \equiv 0. \tag{B.A.3}$$

With these equations, the ranks of the gauge groups are related as

$$N_a = \frac{n_{bc}}{n_{ab}}N_c \in \mathbb{N}, \quad N_b = \frac{n_{ca}}{n_{ab}}N_c \in \mathbb{N}. \tag{B.A.4}$$
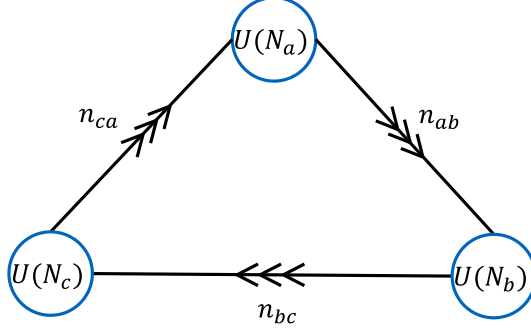
Figure B.9: A quiver diagram of $U(N)^3$ gauge theory [AHT20].

Thus, we find $N_a = N_b = N_c$ for $n_{ab} = n_{bc} = n_{ca}$. The divergences of the chiral currents $j^{a,b,c}$ for $U(1)_{a,b,c}$ are given by

$$\partial \cdot j^a = N_a(N_b n_{ab} Q_b - N_c n_{ac} Q_c) + N_a(n_{ab} N_b - n_{ca} N_c)Q_a + \mathcal{A}_{U(1)_a G^2}, \tag{B.A.5}$$

$$\partial \cdot j^b = N_b(N_c n_{bc} Q_c - N_a n_{ab} Q_a) + N_b(n_{bc} N_c - n_{ab} N_a)Q_b + \mathcal{A}_{U(1)_b G^2}, \tag{B.A.6}$$

$$\partial \cdot j^c = N_c(N_a n_{ca} Q_a - N_b n_{bc} Q_b) + N_c(n_{ca} N_a - n_{bc} N_b)Q_c + \mathcal{A}_{U(1)_c G^2}, \tag{B.A.7}$$

where $Q_x = Q^{U(1)x} + \frac{1}{N_x}Q^{SU(N_x)}$, $Q^{G_x} = \frac{1}{16\pi^2}\epsilon^{\mu\nu\rho\sigma}\mathrm{tr}(F^{(x)}_{\mu\nu}F^{(x)}_{\rho\sigma})$ for $x = a, b, c$, and $\mathrm{tr}(T^i T^j) = \delta^{ij}/2$ for $U(N)$ generators T^i's. These include anomalies of $U(1)^3$, $U(1)SU(N)^2$ and the mixed anomalies between the gravity and $U(1)$'s, which are denoted by $\mathcal{A}_{U(1)_{a,b,c}G^2}$. We impose that they are vanishing:

$$\mathcal{A}_{U(1)_a G^2} \propto N_a(n_{ab}N_b - n_{ca}N_c) \equiv 0, \tag{B.A.8}$$

$$\mathcal{A}_{U(1)_b G^2} \propto N_b(n_{bc}N_c - n_{ab}N_a) \equiv 0, \tag{B.A.9}$$

$$\mathcal{A}_{U(1)_c G^2} \propto N_c(n_{ca}N_a - n_{bc}N_b) \equiv 0. \tag{B.A.10}$$

This is the same condition as in the non-abelian anomalies. There are not exist charged fields under all $(U(1)_a, U(1)_b, U(1)_c)$, then the anomaly between $U(1)_a U(1)_b U(1)_c$ vanishes automatically. Then we find

$$\partial \cdot j^a \equiv N_a(N_b n_{ab} Q_b - N_c n_{ac} Q_c), \tag{B.A.11}$$

$$\partial \cdot j^b \equiv N_b(N_c n_{bc} Q_c - N_a n_{ab} Q_a), \tag{B.A.12}$$

$$\partial \cdot j^c \equiv N_c(N_a n_{ca} Q_a - N_b n_{bc} Q_b). \tag{B.A.13}$$

To identify the anomaly-free $U(1)$ we define it as

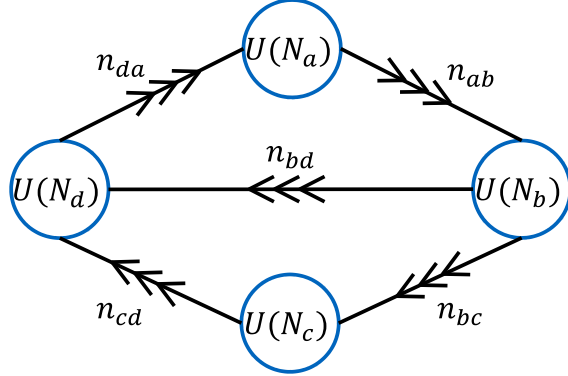$$U(1)_X := \frac{c_a}{N_a}U(1)_a + \frac{c_b}{N_b}U(1)_b + \frac{c_c}{N_c}U(1)_c, \tag{B.A.14}$$

Figure B.10: $U(N)^4$ quiver diagram [AHT20].

and we impose that the divergence of the current associated with $U(1)_X$ vanishes

$$\partial \cdot j^X = \sum_{x=a,b,c} \frac{c_x}{N_x} \partial \cdot j^x$$
$$= N_a(c_c n_{ca} - c_b n_{ab})Q_a + N_b(c_a n_{ab} - c_c n_{bc})Q_b + N_c(c_b n_{bc} - c_a n_{ca})Q_c \equiv 0.$$
(B.A.15)

From this equation, the coefficients satisfy the following conditions

$$c_a = \frac{n_{bc}}{n_{ab}} c_c, \quad c_b = \frac{n_{ca}}{n_{ab}} c_c.$$
(B.A.16)

We take $c_c = 1$ and use Eqs. (B.A.4) and (B.A.16), then the anomaly-free $U(1)$ is given by

$$U(1)_X = \frac{c_c}{N_c} \big(U(1)_a + U(1)_b + U(1)_c\big).$$
(B.A.17)

It is noted that all fields are neutral matter under this anomaly-free $U(1)$. The anomaly-free gauge coupling is given by

$$\frac{1}{e_X^2} = \frac{1}{g_a^2} + \frac{1}{g_b^2} + \frac{1}{g_c^2}.$$
(B.A.18)

B.A.2 $U(N)^4$

In this case, we impose that the anomaly coefficients of non-abelian cubic anomaly are vanishing:

$$\mathcal{A}_{SU(N_a)^3} \propto (n_{ab}N_b - n_{da}N_d) \equiv 0,$$
(B.A.19)

161

$$\mathcal{A}_{SU(N_b)^3} \propto (-n_{ab}N_a + n_{bc}N_c + n_{bd}N_d) \equiv 0, \tag{B.A.20}$$

$$\mathcal{A}_{SU(N_c)^3} \propto (-n_{bc}N_b + n_{cd}N_d) \equiv 0, \tag{B.A.21}$$

$$\mathcal{A}_{SU(N_d)^3} \propto (n_{da}N_a - n_{bd}N_b - n_{cd}N_c) \equiv 0. \tag{B.A.22}$$

Solving these equations, we find that the ranks of gauge groups and the numbers of generations have the following relations,

$$N_b = \frac{n_{da}}{n_{ab}}N_d \in \mathbb{N}, \quad N_c = \frac{n_{da}}{n_{cd}}\left[N_a - \left(\frac{n_{bd}}{n_{ab}}\right)N_d\right] \in \mathbb{N}, \quad \frac{n_{da}}{n_{ab}} = \frac{n_{cd}}{n_{bc}}. \tag{B.A.23}$$

The cancellation of the mixed anomaly between the gravity and $U(1)$'s imposes the same constraints as above:

$$\mathcal{A}_{U(1)_a G^2} \propto N_a(n_{ab}N_b - n_{da}N_d) \equiv 0, \tag{B.A.24}$$

$$\mathcal{A}_{U(1)_b G^2} \propto N_b(-n_{ab}N_a + n_{bc}N_c + n_{bd}N_d) \equiv 0, \tag{B.A.25}$$

$$\mathcal{A}_{U(1)_c G^2} \propto N_c(-n_{bc}N_b + n_{cd}N_d) \equiv 0, \tag{B.A.26}$$

$$\mathcal{A}_{U(1)_d G^2} \propto N_d(n_{da}N_a - n_{bd}N_b - n_{cd}N_c) \equiv 0. \tag{B.A.27}$$

The divergences of the $U(1)$ currents are expressed as

$$\partial \cdot j^a \equiv N_a(N_b n_{ab} Q_b - N_d n_{da} Q_d), \tag{B.A.28}$$

$$\partial \cdot j^b \equiv N_b(-N_a n_{ab} Q_a + N_b n_{bc} Q_c + N_d n_{bd} Q_d), \tag{B.A.29}$$

$$\partial \cdot j^c \equiv N_c(-N_b n_{bc} Q_b + N_d n_{cd} Q_d), \tag{B.A.30}$$

$$\partial \cdot j^d \equiv N_d(N_a n_{da} Q_a - N_b n_{bd} Q_b - N_c n_{cd} Q_c), \tag{B.A.31}$$

where we used vanishing conditions of non-abelian anomalies. We define the anomaly-free $U(1)$ by the following equation as in the previous subsection

$$U(1)_X := \frac{c_a}{N_a}U(1)_a + \frac{c_b}{N_b}U(1)_b + \frac{c_c}{N_c}U(1)_c + \frac{c_d}{N_d}U(1)_d, \tag{B.A.32}$$

and impose the current divergence associated with this $U(1)_X$ is vanishing

$$\sum_{x=a,b,c,d} \frac{c_x}{N_x}\partial \cdot j^x = N_a(-c_b n_{ab} + n_d n_{da})Q_a + N_b(c_a n_{ab} - c_c n_{bc} - c_d n_{bd})Q_b$$

$$+ N_c(c_b n_{bc} - c_d n_{cd})Q_c + N_d(-c_a n_{da} + c_b n_{bd} + c_c n_{cd})Q_d$$

$$\equiv 0. \tag{B.A.33}$$

Solving these equations for the coefficients c_x, we get the following relations

$$c_b = \frac{n_{da}}{n_{ab}}c_d, \quad c_c = \frac{n_{da}}{n_{cd}}\left[c_a - \left(\frac{n_{bd}}{n_{ab}}\right)c_d\right], \quad \frac{n_{da}}{n_{ab}} = \frac{n_{cd}}{n_{bc}}. \tag{B.A.34}$$

From Eqs. (B.A.23) and (B.A.34), the coefficient c_a (or c_b) is a free parameter. In oder to solve these equations, we shall impose some assumptions. Here we will list some examples satisfying these equations.

- $\forall\ N = 1$

  - $n_{bd} = 0$

    A solution is

    $$N_a = N_b = N_c = N_d = 1, \quad n_{ab} = n_{bc} = n_{cd} = n_{da}, \quad n_{bd} = 0. \tag{B.A.35}$$

    This is similar to the quiver gauge theory shown in Fig. B.5. The two indepen-dent anomaly-free $U(1)$'s are generally given by Eqs. (B.3.23) and (B.3.24), and the corresponding gauge couplings are expressed as Eq. (B.3.25) and (B.3.26).

  - $n_{bd} = 2$

    A solutions is given by

    $$N_a = N_b = N_c = N_d = 1, \quad n_{ab} = n_{da} = -n_{bc} = -n_{cd} = 1, \quad n_{bd} = 2. \tag{B.A.36}$$

    The minus sign represents the opposite arrow of Fig. B.10. The independent anomaly-free $U(1)$'s are defined by

    $$U(1)_X = cU(1)_a + U(1)_b + (2-c)U(1)_c + U(1)_d, \tag{B.A.37}$$

    $$U(1)_{X'} = \frac{c-3}{c-1}U(1)_a + U(1)_b + \frac{c+1}{c-1}U(1)_c + U(1)_d. \tag{B.A.38}$$

    For these anomaly-free $U(1)$'s, bd matters are neutral. The anomaly-free gauge couplings are given by

    $$\frac{1}{e_X^2} = \frac{c^2}{g_a^2} + \frac{1}{g_b^2} + \frac{(2-c)^2}{g_c^2} + \frac{1}{g_d^2}, \tag{B.A.39}$$

    $$\frac{1}{e_{X'}^2} = \left(\frac{c-3}{c-1}\right)^2 \frac{1}{g_a^2} + \frac{1}{g_b^2} + \left(\frac{c+1}{c-1}\right)^2 \frac{1}{g_c^2} + \frac{1}{g_d^2}. \tag{B.A.40}$$

- $\forall\ |n| = 1$

  A solution is given by

  $$N_b = N_d = 2, \quad N_a = N_c = 1, \quad n_{ab} = n_{da} = n_{bd} = -n_{bc} = -n_{cd} = 1. \tag{B.A.41}$$

  The independent anomaly-free $U(1)$'s for this solution is defined as

  $$U(1)_X = cU(1)_a + \frac{1}{2}U(1)_b + (1-c)U(1)_c + \frac{1}{2}U(1)_d, \tag{B.A.42}$$

  $$U(1)_{X'} = \frac{2c-3}{4c-2}U(1)_a + \frac{1}{2}U(1)_b + \frac{2c+1}{4c-2}U(1)_c + \frac{1}{2}U(1)_d. \tag{B.A.43}$$

  bd matter is neutral for these anomaly-free gauge groups. The gauge couplings are given by

  $$\frac{1}{e_X^2} = \frac{c^2}{g_a^2}\frac{1/2}{g_b^2} + \frac{(1-c)^2}{g_c^2} + \frac{1/2}{g_d^2}, \tag{B.A.44}$$

  $$\frac{1}{e_{X'}^2} = \left(\frac{2c-3}{4c-2}\right)^2 \frac{1}{g_a^2} + \frac{1/2}{g_b^2} + \left(\frac{2c+1}{4c-2}\right)^2 \frac{1}{g_c^2} + \frac{1/2}{g_d^2}. \tag{B.A.45}$$

  It is noted that a coefficient of $1/g_{b,d}^2$ is given by $1/2 = N_{b,d} \cdot (1/2)^2$ for $N_{b,d} = 2$.
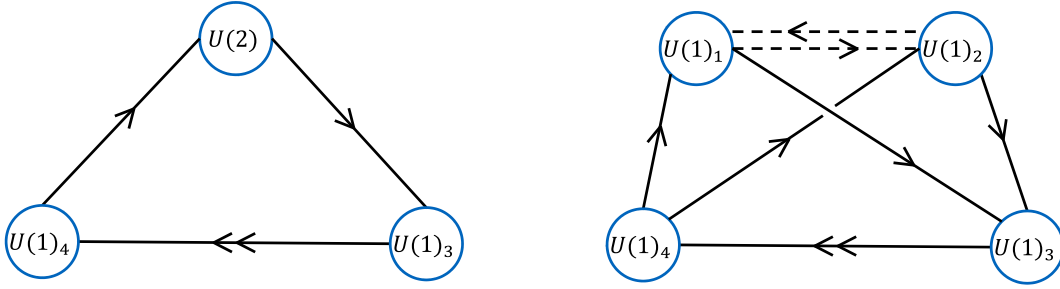
Figure B.11: The left panel: $U(2) \times U(1)_1 \times U(1)_2$ quiver diagram. The right panel: $U(1)_1 \times U(1)_2 \times U(1)_3 \times U(1)_4$ quiver diagram obtained from $U(2) \to U(1)_1 \times U(1)_2$ by the Higgs mechanism. The dashed quiver shows bi-fundamental scalars arising from this symmetry breaking. These figures are from Ref. [AHT20].
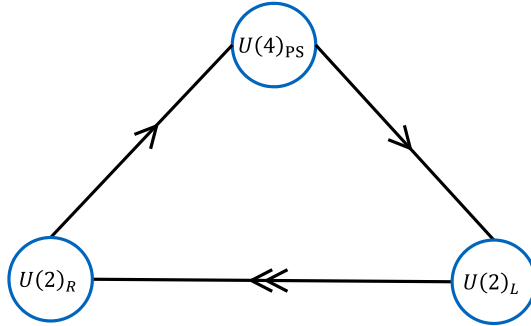

Figure B.12: A quiver diagram of left-right symmetric Pati-Salam model [AHT20].

Appendix B.B   Models inspired by the SM

We consider two quiver models with $U(1)^4$ and $U(1)^5$ symmetries inspired by the SM. These are different from the models exhibited in the Section B.3 in terms of chiral fermions. We show just that the anomaly-free gauge couplings are still given by a linear combination of the original couplings. The SM might not originate from a gauge symmetry that has too many $U(1)$'s.

B.B.1   A model inspired by Pati-Salam

We shall consider the $U(1)^4$ gauge theory shown in the right panel of Fig. B.11. It is noted that we have two left-handed fermions charged only under $U(1)_3 \times U(1)_4$, and

there exist six chiral fermions and two complex scalars. This model is obtained from three nodes model of $U(2) \times U(1)_3 \times U(1)_4$ in the left panel of Fig. B.11 by the Higgs mechanism of $U(2)$ complex adjoint scalar whose VEV is given by $\langle \Phi \rangle = \text{diag}(v, -v)$. This can be regard as a toy model of left-right symmetric theory obtained from the Pati-Salam model [PS74, MP75, SM75] as in Fig. B.12.

The $U(1)^4$ model has two anomaly-free $U(1)$'s and non-trivial charged matter fields, but we focus only on the relevant gauge couplings. The detail of the anomaly cancellation is discussed in Appendix B.A. The divergences of $U(1)$ currents are given by

$$\partial \cdot \begin{pmatrix} j^1 \\ j^2 \\ j^3 \\ j^4 \end{pmatrix} = \begin{pmatrix} 0 & 0 & 1 & -1 \\ 0 & 0 & 1 & -1 \\ -1 & -1 & 0 & 2 \\ 1 & 1 & -2 & 0 \end{pmatrix} \begin{pmatrix} Q_1 \\ Q_2 \\ Q_3 \\ Q_4 \end{pmatrix}, \tag{B.B.1}$$

and we define two independent anomaly-free $U(1)$'s with a free parameter c as

$$U(1)_X = cU(1)_1 + (2 - c)U(1)_2 + U(1)_3 + U(1)_4, \tag{B.B.2}$$

$$U(1)_{X'} = \frac{3-c}{1-c}U(1)_1 - \frac{1+c}{1-c}U(1)_2 + U(1)_3 + U(1)_4. \tag{B.B.3}$$

Two chiral fermions charged only under $U(1)_3 \times U(1)_4$ is still neutral but other fermions have non-trivial charges under these anomaly-free $U(1)$ gauge groups. The corresponding anomaly-free gauge couplings read

$$\frac{1}{e_X^2} = \frac{c^2}{g_1^2} + \frac{(2-c)^2}{g_2^2} + \frac{1}{g_3^2} + \frac{1}{g_4^2}, \tag{B.B.4}$$

$$\frac{1}{e_{X'}^2} = \left(\frac{3-c}{1-c}\right)^2 \frac{1}{g_1^2} + \left(\frac{1+c}{1-c}\right)^2 \frac{1}{g_2^2} + \frac{1}{g_3^2} + \frac{1}{g_4^2}. \tag{B.B.5}$$

These gauge couplings are given by linear combinations of the original ones, and when $U(1)_1 \times U(1)_2$ is unified to $U(2)$ we find $g_1 = g_2$.

B.B.2 A model inspired by the SM

Another example is a model in Fig. B.13 that is inspired by the SM-like model in Fig. B.14.[17] The divergences of chiral currents are given by

$$\partial \cdot \begin{pmatrix} j^1 \\ j^2 \\ j^3 \\ j^4 \\ j^5 \end{pmatrix} = \begin{pmatrix} 0 & -2 & 1 & 0 & 1 \\ 2 & 0 & -2 & 2 & -2 \\ -1 & 2 & 0 & -1 & 0 \\ 0 & -2 & 1 & 0 & 1 \\ -1 & 2 & 0 & -1 & 0 \end{pmatrix} \begin{pmatrix} Q_1 \\ Q_2 \\ Q_3 \\ Q_4 \\ Q_5 \end{pmatrix}. \tag{B.B.6}$$

---

[17]The authors of Ref. [VW07] discussed the world-volume theory on a stack of D3-branes reproducing the field content of the minimal supersymmetric standard model with extended Higgs sector in a quiver extension.
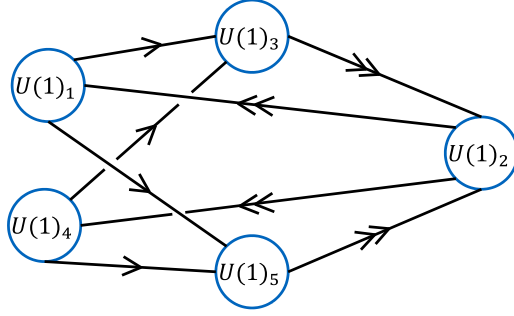
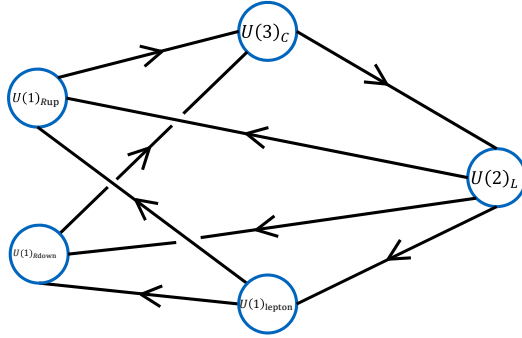Figure B.13: A diagram of quiver gauge theory inspired by the SM [AHT20].

Figure B.14: A quiver diagram of the SM-like model [VW07]. This figure is from Ref. [AHT20].

We find three anomaly-free $U(1)$'s and they can generally be written as

$$U(1)_X = c_1 U(1)_1 + U(1)_2 + c_2 U(1)_3 + (2 - c_1)U(1)_4 + (2 - c_2)U(1)_5, \qquad \text{(B.B.7)}$$

with two free parameters of c_1 and c_2 which will be a rational numbers. The parameters of c_i's are taken as a gauge group is orthognal to each other. Then the fermions have non-trivial charge in this anomaly-free $U(1)$'s, but we focus only on the gauge couplings. The relevant gauge coupling is given by

$$\frac{1}{e_X^2} = \frac{c_1^2}{g_1^2} + \frac{1}{g_2^2} + \frac{c_2^2}{g_3^2} + \frac{(2 - c_1)^2}{g_4^2} + \frac{(2 - c_2)^2}{g_5^2}. \qquad \text{(B.B.8)}$$

As mentioned earlier, an anomaly-free coupling can contain more of the original couplings as the number of $U(1)$'s in a theory increases.

Appendix B.C   Orbifold compactification

Let us dimensionally reduce the 5D action in Eq. (B.4.9) and show the gauge couplings and Yukawa couplings in 4D. The metric of $M_4 \times S^1/\mathbb{Z}_2$ is written by $ds_5^2 = e^{-\sigma} g_{\mu\nu} dx^\mu dx^\nu + e^{2\sigma} dy^2$. Thus, the vielbein is given as

$$
E^A{}_M = \begin{pmatrix} e^{-\sigma/2} e^a{}_\mu & \\ & e^\sigma \end{pmatrix}, \tag{B.C.1}
$$

where A and a represent 5D and 4D local Lorentz indices respectively, and $e^a{}_\mu$ is the 4D vielbein. The off-diagonal element of the vielbein is absent because the orbifold projection prohibits the graviphoton. It is noted that 5D fermion kinetic term is given by $\overline{\Psi} \Gamma^A E_A{}^M D_M \Psi$, where $E_A{}^M$ is the inverse matrix of $E^A{}_M$. Using these equations, we obtain 4D action for massless modes in Eqs. (B.4.12) and (B.4.13):

$$
\begin{aligned}
S_{4D} = \int d^4 x \sqrt{-g_4} \Bigg[& -\frac{\pi L}{2\kappa_5^2} \mathcal{R}_4 + \frac{3\pi L}{4\kappa_5^2} (\partial_\mu \sigma)^2 \\
& -\frac{1}{4} \frac{\pi L e^\sigma}{\hat{g}_a^2} (F_{\mu\nu}^{(a)})^2 - 2\frac{1}{4} \frac{\pi L e^\sigma}{\hat{g}_2^2} (F_{\mu\nu}^{(b)})^2 - \frac{1}{4} \frac{\pi L e^\sigma}{\hat{g}_c^2} (F_{\mu\nu}^{(c)})^2 - 2\frac{1}{4} \frac{\pi L e^\sigma}{\hat{g}_2^2} (F_{\mu\nu}^{(d)})^2 + \frac{\pi L e^{-2\sigma}}{\hat{g}_2^2} |D_\mu \varphi|^2 \\
& + \pi L e^{-\sigma/2} i \overline{\psi_{ab}} \slashed{D} \psi_{ab} + \pi L e^{-\sigma/2} i \overline{\psi_{da}} \slashed{D} \psi_{da} + \pi L e^{-\sigma/2} i \overline{\psi_{cd}} \slashed{D} \psi_{cd} + \pi L e^{-\sigma/2} i \overline{\psi_{bc}} \slashed{D} \psi_{bc} \\
& - \frac{\pi L e^{-2\sigma}}{\sqrt{2}} \varphi_R (\overline{\psi_{ab}^C} \psi_{da} + \overline{\psi_{da}} \psi_{ab}^C) - \frac{\pi L i e^{-2\sigma}}{\sqrt{2}} \varphi_I (\overline{\psi_{ab}^C} \psi_{da} - \overline{\psi_{da}} \psi_{ab}^C) \\
& - \frac{\pi L e^{-2\sigma}}{\sqrt{2}} \varphi_R (\overline{\psi_{bc}^C} \psi_{cd} + \overline{\psi_{cd}} \psi_{bc}^C) + \frac{\pi L i e^{-2\sigma}}{\sqrt{2}} \varphi_I (\overline{\psi_{bc}^C} \psi_{cd} - \overline{\psi_{cd}} \psi_{bc}^C) - V(\sigma, \varphi) \Bigg], \tag{B.C.2}
\end{aligned}
$$

where $D_\mu = \partial_\mu + i \sum_{j=a,b,c,d} q_\psi A_\mu^{(j)}$ is the covariant derivative associated with the gauge group $U(1)_a \times U(1)_b \times U(1)_c \times U(1)_d$, and the chiral fermions ψ_{ij} are defined in Section B.4.2. The four dimensional Ricci scalar is denoted by $\mathcal{R}_4$, and $\varphi = \varphi_R + i\varphi_I$ is the complex scalar. We introduce the scalar potential $V(\sigma, \varphi)$ formally.[18] Thus, the gauge couplings are given as in Eq. (B.4.15).

In order to find the relation between the Yukawa coupling and the gauge coupling, we canonically normalize the fermion and the complex scalar as

$$
\psi_{ij} \to \frac{e^{\sigma/4}}{\sqrt{\pi L}} \psi_{ij}, \quad \varphi \to \frac{\hat{g}_2 e^\sigma}{\sqrt{\pi L}} \varphi. \tag{B.C.3}
$$

Then, the kinetic term is rewritten as

$$
\pi L e^{-\sigma/2} i \overline{\psi_{ij}} \slashed{D} \psi_{ij} \to i \overline{\psi_{ij}} \slashed{D} \psi_{ij} - \frac{i}{2} \overline{\psi_{ij}} \gamma^\mu \psi_{ij} \partial_\mu \sigma. \tag{B.C.4}
$$

---

[18] At the classical level, the scalars σ and φ do not have potential due to the gauge symmetries, but the potential can be generated by the radiative corrections. In addition, we assume the radion field develops the VEV of $\langle \sigma \rangle = 0$ around the radius L.

Hereafter, we will ignore the derivative coupling of the radion to the fermions. The Yukawa interactions are expressed as

$$
\mathcal{L}_{\text{4D,Yukawa}} = -\frac{\hat{g}_2 e^{-\sigma/2}}{\sqrt{2\pi L}} \varphi_R (\overline{\psi_{ab}^C} \psi_{da} + \overline{\psi_{da}} \psi_{ab}^C) - \frac{\hat{g}_2 i e^{-\sigma/2}}{\sqrt{2\pi L}} \varphi_I (\overline{\psi_{ab}^C} \psi_{da} - \overline{\psi_{da}} \psi_{ab}^C)
$$
$$
- \frac{\hat{g}_2 e^{-\sigma/2}}{\sqrt{2\pi L}} \varphi_R (\overline{\psi_{bc}^C} \psi_{cd} + \overline{\psi_{cd}} \psi_{bc}^C) + \frac{\hat{g}_2 i e^{-\sigma/2}}{\sqrt{2\pi L}} \varphi_I (\overline{\psi_{bc}^C} \psi_{cd} - \overline{\psi_{cd}} \psi_{bc}^C).
$$

$$(\text{B.C.5})$$

We introduce the Dirac fermions as

$$
\psi_a = \begin{pmatrix} \psi_{da} \\ \psi_{ab}^C \end{pmatrix}, \quad \psi_c = \begin{pmatrix} \psi_{cd} \\ \psi_{bc}^C \end{pmatrix}.
$$

$$(\text{B.C.6})$$

With these Dirac fermions, the kinetic terms of the anomaly-free sector read

$$
\mathcal{L}_{\text{4D,KT}} = -\frac{1}{4e_X^2} \left(F_{\mu\nu}^{(X)}\right)^2 - \frac{1}{4e_{X'}^2} \left(F_{\mu\nu}^{(X')}\right)^2 + (\partial_\mu \varphi_R)^2 + (\partial_\mu \varphi_I)^2
$$
$$
+ i\overline{\psi_a}\slashed{D}\psi_a + i\overline{\psi_c}\slashed{D}\psi_c,
$$

$$(\text{B.C.7})$$

where we neglected gauge bosons in anomalous $U(1)$'s, the anomaly-free gauge couplings are defined by Eqs. (B.4.16) and (B.4.17). As shown in Table B.1, the covariant derivatives of the Dirac fermions associated with anomaly-free $U(1)$'s are expressed as

$$
\mathcal{D}_\mu \psi_a = \left[\partial_\mu + i(-1+c)A_\mu^{(X)} - i\left(1 + \frac{1}{c}\right)A_\mu^{(X')}\right]\psi_a,
$$

$$(\text{B.C.8})$$

$$
\mathcal{D}_\mu \psi_c = \left[\partial_\mu - i(-1+c)A_\mu^{(X)} + i\left(1 + \frac{1}{c}\right)A_\mu^{(X')}\right]\psi_c.
$$

$$(\text{B.C.9})$$

The charges of ψ_a and ψ_c under $U(1)_X$ and $U(1)_{X'}$ are opposite to each other due to the 4D anomaly-free conditions. With the Dirac spinor, the Yukawa terms in this Lagrangian are rewritten as below:

$$
\mathcal{L}_{\text{4D,Yukawa}} = -ye^{-\sigma/2}\varphi_R \overline{\psi_a}\psi_a - iye^{-\sigma/2}\varphi_I \overline{\psi_a}\gamma_5 \psi_a
$$
$$
- ye^{-\sigma/2}\varphi_R \overline{\psi_c}\psi_c + iye^{-\sigma/2}\varphi_I \overline{\psi_c}\gamma_5 \psi_c,
$$

$$(\text{B.C.10})$$

where the 4D Yukawa coupling is defined as

$$
y = \frac{\hat{g}_2}{\sqrt{2\pi L}}.
$$

$$(\text{B.C.11})$$

Appendix C

Leptonic CP asymmetry and Light flavored scalar

C.1 Matter-antimatter asymmetry and type-I seesaw model with flavored scalar

The Standard Model of particle physics and cosmology still have some mysteries, e.g., the nature of dark matter, the source of matter-antimatter asymmetry, the origin of neutrino masses, and so on. An attractive idea to realize tiny neutrino masses is the seesaw mechanism with Majorana right-handed neutrinos [Min77, Yan79, GMRS79], called the type I seesaw. The additional Majorana fermions can also be the origin of matter-antimatter asymmetry via their decay, the scenario called leptogenesis [FY86].

The baryon asymmetry in the present universe is measured by the cosmic microwave background observation [A$^+$20a] as

$$Y_{\Delta B} = \frac{n_{\Delta B}}{s} = (0.852 - 0.888) \times 10^{-10}, \tag{C.1.1}$$

with the number density $n_{\Delta B}$ and the entropy density s. In the leptogenesis scenario, the right-handed neutrinos generate the lepton asymmetry, which is then converted to the baryon asymmetry [KRS85] via the sphaleron process [KM84]. In the simplest leptogenesis, the interference between the tree-level and one-loop level right-handed neutrino two-body decays gives a source of the asymmetry, which is determined by neutrino Yukawa couplings. On the other hand, Refs. [AS98, Ham02, DBDKZ20, AKS20, BDM20, LDR14] also discuss possibilities of tree-level leptogenesis by considering various extensions of the neutrino sector.

In this chapter, we focus on a possibility of flavorful light scalar for the lepton asymmetry generation. This is a minimal scalar extension of the type-I seesaw model by introducing a SM singlet scalar interacting with the right-handed neutrinos. This kind of scalar may be motivated by some dynamical origin of Majorana neutrino mass scale, but in this work we do not specify it and investigate the general form of scalar interaction

to the right-handed neutrinos. In this setup, we study the tree-level leptogenesis via the right-handed neutrino three-body decays with this flavorful scalar field.

This chapter is based on Ref. [AIY21] and the rest parts are organized as follows. In Section C.2, the model we focus on is introduced and we derive the decay widths and the asymmetry parameters of the two-body decay processes. In Section C.3, the three-body decay widths and the asymmetry parameter are evaluated and we give their approximation formulae. In Section C.4, we discuss the behaviors of the lepton asymmetry and its approximated relic value by solving the Boltzmann equations, and show the allowed parameter spaces of this model. We also give some comments on the dynamics of the additional singlet scalar field and its realization in some phenomenological models. Section C.5 is devoted to the summary of this chapter.

C.2   Lagrangian and two-body decay

In this work, we denote the right-handed neutrinos as N_i in the mass diagonal basis. They are the Majorana fermions with the Majorana masses m_{N_i}. An SM gauge singlet scalar χ is introduced and assumed to have the coupling to the right-handed neutrinos. The lagrangian we consider is

$$\mathcal{L} = \mathcal{L}_{\text{SM}} + \frac{1}{2}\overline{N_i}(i\slashed{\partial} - m_{N_i})N_i - y_{ij}^\nu \tilde{H}^\dagger \overline{N_i} P_L L_j + \text{h.c.} - \frac{1}{2}\chi \overline{N_i}\big(\xi_{ij} P_R + \xi_{ij}^* P_L\big)N_j. \quad \text{(C.2.1)}$$

The coupling constants ξ_{ij} are i, j symmetric and generally complex-valued. They can be decomposed into the scalar (real part) and pseudo-scalar (imaginary part) couplings to N_i. As discussed in Ref. [CI01], with the seesaw relation, the neutrino Yukawa coupling y^ν can be generally parameterized as

$$y^\nu = \frac{\sqrt{2}i}{v}\sqrt{M_N}R\sqrt{m_\nu}U_{\text{MNS}}^\dagger, \quad \text{(C.2.2)}$$

with the Majorana mass matrix $M_N = \text{diag}(m_{N_1}, m_{N_2}, m_{N_3})$ and the neutrino mass matrix $m_\nu = \text{diag}(m_{\nu_1}, m_{\nu_2}, m_{\nu_3})$, and the neutrino flavor mixing matrix U_{MNS}. $v \approx 246$ GeV is the electroweak scale. For the neutrino masses and mixing angles, we use the experimentally observed values summarized in Ref. [Z+20]. R is an arbitrary complex orthogonal matrix describing the degrees of freedom of neutrino Yukawa couplings which cannot be reached with the seesaw relation. We parameterize R as

$$R = \begin{pmatrix} 1 & 0 & 0 \\ 0 & \cos\omega_{23} & \sin\omega_{23} \\ 0 & -\sin\omega_{23} & \cos\omega_{23} \end{pmatrix} \begin{pmatrix} \cos\omega_{13} & 0 & \sin\omega_{13} \\ 0 & 1 & 0 \\ -\sin\omega_{13} & 0 & \cos\omega_{13} \end{pmatrix} \begin{pmatrix} \cos\omega_{12} & \sin\omega_{12} & 0 \\ -\sin\omega_{12} & \cos\omega_{12} & 0 \\ 0 & 0 & 1 \end{pmatrix},$$
$$\text{(C.2.3)}$$

introducing the complex angles ω_{ij} (called the Casas-Ibarra (CI) parameters in the following).

Through the neutrino Yukawa coupling, the right-handed neutrinos interact with the SM thermal bath. For the two-body decay of N_i to the SM particles, the partial widths at tree level are given by

$$\Gamma_{N_i \to L_j H} = \Gamma_{N_i \to \bar{L}_j \bar{H}} = \frac{y^\nu_{ij} y^{\nu\dagger}_{ji}}{16\pi} m_{N_i}, \tag{C.2.4}$$

where $\bar{L}$, $\bar{H}$ means the corresponding anti-particles. We denote the total width of the two-body decay via neutrino Yukawa coupling as

$$\tilde{\Gamma}_i = \sum_j \left(\Gamma_{N_i \to L_j H} + \Gamma_{N_i \to \bar{L}_j \bar{H}} \right). \tag{C.2.5}$$

When $m_{N_2} > m_{N_1} + m_\chi$, a heavier mode N_2 can also decay to N_1 and χ via the off-diagonal coupling ξ_{12} and its width is evaluated as

$$\Gamma_{N_2 \to N_1 \chi} = \frac{m_{N_2}}{16\pi} \frac{\sqrt{\lambda(m^2_{N_2}, m^2_{N_1}, m^2_\chi)}}{m^2_{N_2}} \left\{ \left[\left(1 - \frac{m_{N_1}}{m_{N_2}} \right)^2 - \frac{m^2_\chi}{m^2_{N_2}} \right] (\text{Im}\,\xi_{12})^2 \right.$$
$$\left. + \left[\left(1 + \frac{m_{N_1}}{m_{N_2}} \right)^2 - \frac{m^2_\chi}{m^2_{N_2}} \right] (\text{Re}\,\xi_{12})^2 \right\}, \tag{C.2.6}$$

with the kinematic function $\lambda(x, y, z) = x^2 + y^2 + z^2 - 2xy - 2yz - 2zx$.

As we will see in the following, the decay of the lightest N_1 is dominated by the two-body decay, but for a heavier mode the resonant contribution of three-body decay is comparable to that of $N_2 \to N_1 \chi$. Then the total decay widths Γ_{N_i} of the lightest and heavier right-handed neutrinos are generally written by

$$\Gamma_{N_1} \approx \tilde{\Gamma}_1, \qquad \Gamma_{N_2} = \tilde{\Gamma}_2 + \Gamma_{N_2 \to N_1 \chi} + \Gamma_2, \tag{C.2.7}$$

where Γ_i are the three-body decay widths of N_i and will be described in the next section.

The CP asymmetry in the ordinary leptogenesis comes from the interference of the right-handed neutrino's two-body decays (the tree-level and the right two diagrams in Fig. C.1), where the phases of neutrino Yukawa couplings play an important role. The asymmetry parameters $\tilde{\epsilon}^{(LH)}_i$ associated with this interference is evaluated as (for a review [DNN08]),

$$\tilde{\epsilon}^{(LH)}_i = \frac{\Gamma_{N_i \to LH} - \Gamma_{N_i \to \bar{L}\bar{H}}}{\Gamma_{N_i \to LH} + \Gamma_{N_i \to \bar{L}\bar{H}}} = \frac{1}{8\pi (y^\nu y^{\nu\dagger})_{ii}} \sum_j \text{Im}\left[(y^\nu y^{\nu\dagger})_{ji} \right]^2 \text{g}(m^2_{N_j}/m^2_{N_i}), \tag{C.2.8}$$

where g(x) in the SM is given by g$(x) = \sqrt{x}\left[\frac{2-x}{1-x} - (1+x)\log\left(\frac{1+x}{x}\right) \right]$. It is noticed that, when ω_{ij} are real or pure imaginary, $\tilde{\epsilon}^{(LH)}_i$ vanish and the two-body decay via the neutrino Yukawa loop does not generate the CP asymmetry.

In addition to the SM particle loops, lighter right-handed neutrinos and the scalar field χ give an additional asymmetry in the two-body decay of heavier right-handed neutrinos.
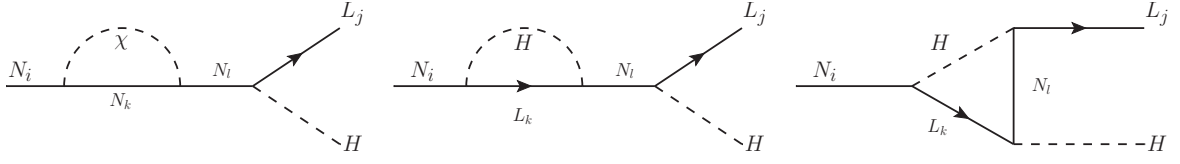
Figure C.1: The one-loop two-body decays of a right-handed neutrino N_i to the SM fields. (Left) from lighter right-handed neutrinos and the scalar χ. (Middle and Right) from the SM loops.

The left diagram in Fig. C.1 shows the relevant one-loop contribution to the N_i decay. The asymmetry reads from the difference between the decay widths to particles and anti-particles,

$$\Delta\Gamma_{N\chi} = \left|\mathcal{M}_0 + \mathcal{M}_1\right|^2 - \left|\mathcal{M}_0^C + \mathcal{M}_1^C\right|^2, \tag{C.2.9}$$

where $\mathcal{M}_0^{(C)}$ denotes the amplitude of the tree-level decay to the (anti-)particles and $\mathcal{M}_1^{(C)}$ that of the one-loop diagram including χ, respectively. This is evaluated as

$$\Delta\Gamma_{N\chi} = \frac{m_{N_i}^4}{4\pi^2} \sum_{k,l} \frac{1}{m_{N_l}^2 - m_{N_i}^2} \int_0^1 dx \, \mathrm{Im}\left(\log \Delta_{N_k\chi}^2\right) \mathrm{Im}\left[f_{li}(x)(y^\nu y^{\nu\dagger})_{il}\right], \tag{C.2.10}$$

where

$$\Delta_{N_k\chi}^2 = x(x-1)m_{N_i}^2 + (1-x)m_{N_k}^2 + xm_\chi^2, \tag{C.2.11}$$

$$f_{li}(x) = \left(\xi_{lk}^*\xi_{ki} + \xi_{lk}\xi_{ki}^* \frac{m_{N_l}}{m_{N_i}}\right)x + \xi_{lk}^*\xi_{ki}^* \frac{m_{N_k}}{m_{N_i}} + \xi_{lk}\xi_{ki}\frac{m_{N_k}m_{N_l}}{m_{N_i}^2}. \tag{C.2.12}$$

In order to produce non-trivial asymmetry, the conditions $i \neq k$ for the interference and $\Delta_{N_k\chi}^2 < 0$ are needed. The latter condition is satisfied if the internal loop particles N_k and χ are lighter than the parent particle N_i, and then only the case of $i = 2$, $k = l = 1$ gives a non-vanishing asymmetry parameter. As a result, we obtain the N-χ loop contribution to asymmetry parameter

$$\tilde{\epsilon}_2^{(N\chi)} = \frac{-m_{N_2}}{64\pi^2\tilde{\Gamma}_2} \int_{x_-}^{x_+} dx \, \mathrm{Im}\left[f_{12}(x)(y^\nu y^{\nu\dagger})_{21}\right] \approx \frac{1}{16\pi(y^\nu y^{\nu\dagger})_{22}} \mathrm{Im}\left[\xi_{11}\xi_{12}^*(y^\nu y^{\nu\dagger})_{12}\right], \tag{C.2.13}$$

where $x_\pm$ are the solutions for $\Delta_{N_1\chi}^2 = 0$. In the latter approximation, we have assumed the hierarchy $m_{N_1} \ll m_{N_2}$. The total CP asymmetry from two-body decay of the lightest and heavier right-handed neutrinos are given by

$$\tilde{\epsilon}_1 = \tilde{\epsilon}_1^{(LH)}, \qquad \tilde{\epsilon}_2 = \tilde{\epsilon}_2^{(LH)} + \tilde{\epsilon}_2^{(N\chi)}. \tag{C.2.14}$$

With general complex phases of neutrino Yukawa couplings, $\tilde{\epsilon}_i^{(LH)}$ are not necessarily vanishing simultaneously. In the following analysis, we simply assume that the CI parameters are real or pure imaginary to examine the CP asymmetry effect of the flavorful scalar χ.
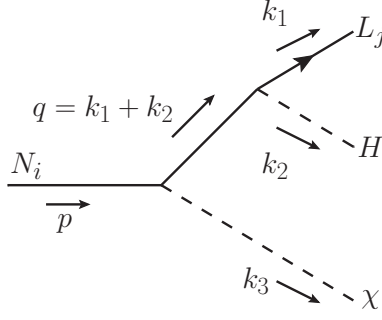
Figure C.2: The three-body decay of a right-handed neutrino N_i at tree level including the scalar χ.

C.3   Three-body decay for asymmetry

When there exist a scalar χ and its (pseudo-) scalar coupling to the right-handed neutrinos N, non-trivial CP asymmetry can be generated at the three-body decay $N \rightarrow LH\chi$ (Fig. C.2). Its amplitude is

$$\mathcal{M}_{N_i \rightarrow L_j H\chi} = -\sum_k \overline{u_{L_j}}(k_1) y_{jk}^{\nu\dagger} P_R \frac{1}{\slashed{q} - \bar{m}_{N_k}} (\xi_{ki} P_R + \xi_{ki}^* P_L) u_{N_i}(p), \tag{C.3.1}$$

where $\bar{m}_{N_k} = m_{N_k} - i\Gamma_{N_k}/2$. The initial and final state momenta p, k_i are shown in the figure ($q = k_1 + k_2$). The renormalized mass parameters are $m_{N_i}^{r\,2} = m_{N_i}^2 - \Gamma_{N_i}^2/4$ for Γ_{N_i} being the width of the resonance N_i, but we quantitatively drop any difference of $\mathcal{O}((\Gamma/m_N)^2)$ throughout this chapter. Summing up the final charged-lepton flavor and gauge charge, the three-body decay width becomes

$$\Gamma_{N_i \rightarrow LH\chi} = \sum_{k,l} \frac{(y^\nu y^{\nu\dagger})_{lk}}{256\pi^3 m_{N_i}^3} \int_0^{(m_{N_i}-m_\chi)^2} dm_{12}^2 \int_{[m_{23}^2]_-}^{[m_{23}^2]_+} dm_{23}^2 \frac{1}{(m_{12}^2 - \bar{m}_{N_l}^{*2})(m_{12}^2 - \bar{m}_{N_k}^2)}$$
$$\times \Big[\xi_{il}\xi_{ki}^* m_{12}^2 (m_{12}^2 + m_{23}^2 - m_\chi^2) + (\xi_{il}\xi_{ki}\bar{m}_{N_k} + \xi_{il}^*\xi_{ki}^*\bar{m}_{N_l}^*)m_{N_i} m_{12}^2$$
$$+ \xi_{il}^*\xi_{ki}\bar{m}_{N_l}^*\bar{m}_{N_k}(m_{N_i}^2 - m_{23}^2) \Big]. \tag{C.3.2}$$

The invariant mass parameters are defined by $m_{12}^2 = (k_1 + k_2)^2$, $m_{23}^2 = (k_2 + k_3)^2$, and the maximum and minimum values of m_{23}^2 with a fixed s are given by [Kum69, Z+20]

$$[m_{23}^2]_\pm = \frac{1}{2} \left[m_{N_i}^2 + m_\chi^2 - m_{12}^2 \pm \sqrt{\lambda(m_{N_i}^2, m_\chi^2, m_{12}^2)} \right]. \tag{C.3.3}$$

The three-body decay to the anti-particles $\Gamma_{N_i \rightarrow \bar{L}\bar{H}\chi}$ is evaluated in the same manner. The total decay width and the CP asymmetry parameter for the three-body decay are defined by

$$\Gamma_i = \Gamma_{N_i \rightarrow LH\chi} + \Gamma_{N_i \rightarrow \bar{L}\bar{H}\chi}, \qquad \epsilon_i = \frac{\Gamma_{N_i \rightarrow LH\chi} - \Gamma_{N_i \rightarrow \bar{L}\bar{H}\chi}}{\Gamma_{N_i \rightarrow LH\chi} + \Gamma_{N_i \rightarrow \bar{L}\bar{H}\chi}}. \tag{C.3.4}$$

In the following, we will discuss dominant contributions to the widths and asymmetry parameters and their approximate forms.

C.3.1   The lightest mode

Among the intermediate states N_k, the lightest one N_1 generally gives the dominant contribution to the N_1 three-body decay, i.e., the $i = k = l = 1$ part in (C.3.2). For a typical hierarchy of mass parameters, $m_\chi \ll m_{N_1} \ll m_{N_2}$, the N_1 decay width reduces to

$$\Gamma_1^{(11)} \approx \frac{m_{N_1}}{64\pi^3}(y^\nu y^{\nu\dagger})_{11}\left[|\xi_{11}|^2 + \mathrm{Re}(\xi_{11}^2)\right]\log\left(\frac{m_{N_1}}{m_\chi}\right), \tag{C.3.5}$$

which is mainly determined by the diagonal coupling ξ_{11}. Compared with the two-body decay $N_1 \to LH$, the width is multiplied by a factor $\sim (\xi_{11})^2/4\pi \log(m_{N_1}/m_\chi)$, which can be of order one. If ξ_{11} is negligibly small, the width is instead given by the $k = l = 2$ part,

$$\Gamma_1^{(22)} \approx \frac{m_{N_1}^3}{384\pi^3 m_{N_2}^2}(y^\nu y^{\nu\dagger})_{22}|\xi_{12}|^2. \tag{C.3.6}$$

The CP asymmetry, the difference between the decay widths to particles and anti-particles, is usually described by the quantum interference of processes with different intermediate states. For the current three-body decay, such interference occurs from the diagrams with different intermediate neutrinos $N_{k,l}$ ($k \neq l$), that is, the cross terms in the amplitude squared. It is important that, in addition to this usual asymmetry, the present model induces CP asymmetry from a single diagram with one intermediate state. For example, we find the N_1 three-body decay with virtual N_1 generates a nonzero CP asymmetry parameter

$$\epsilon_1^{(11)} \approx \frac{\mathrm{Im}(\xi_{11}^2)}{|\xi_{11}|^2 + \mathrm{Re}(\xi_{11}^2)}\frac{\Gamma_{N_1}}{2m_{N_1}}, \tag{C.3.7}$$

which is irrelevant to the N_2 physics at the leading order. (This is the approximate formula for $m_\chi \ll m_{N_1} \ll m_{N_2}$. The exact form of asymmetry parameter is found in Appendix C.B.)

The non-vanishing "interference" from a single diagram (C.3.7) is a characteristic feature of the present decay mode and its origin is understood by the amplitude form. The three-body decay amplitude (C.3.1) contains the factor $P_R(\slashed{q} + \bar{m}_N)(\xi P_R + \xi^* P_L)$ between the initial and final spinor wavefunctions. The first projection P_R comes from the Yukawa (chirality-violating) vertex, the second factor $(\slashed{q} + \bar{m}_N)$ the propagator of heavy unstable fermion, and the third one $(\xi P_R + \xi^* P_L)$ means the Majorana fermion vertex. The chirality structure implies this factor is divided into two pieces $\bar{m}_N\xi$ and $\slashed{q}\xi^*$, and hence the squared amplitude generally contains a cross term of these two pieces (Fig. C.3). Further the corresponding decay width to anti-particles is obtained by the replacement of couplings $\xi \leftrightarrow \xi^*$ (and $y^\nu \leftrightarrow y^{\nu*}$, $P_R \leftrightarrow P_L$). In the end, the interference of these two pieces leads to the CP asymmetry proportional to $\mathrm{Im}(\xi^2)\,\mathrm{Im}(\bar{m})$, appearing in the numerator of (C.3.7). We thus find that this CP asymmetry from a single decay
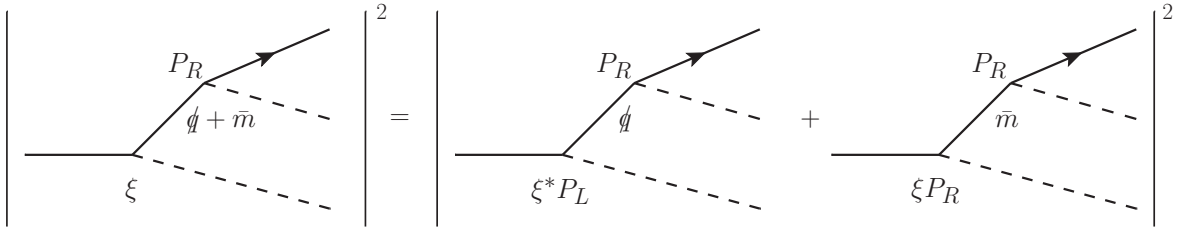
Figure C.3: CP asymmetry (cross term) from a single amplitude squared.

process is generated in the presence of a chiral vertex, a unstable intermediate state, and a complex decay coupling. The three-body decay of a right-handed neutrino to the SM particles plus scalar is an interesting realization of all these criteria satisfied.

The interference of different intermediate states also contributes to the CP asymmetry as usual, and its approximate form is found

$$\epsilon_1^{(12)} \approx \frac{m_{N_1}\Gamma_{N_2}}{8m_{N_2}^2} \frac{\text{Im}\big[(y^\nu y^{\nu\dagger})_{12}\xi_{12}(2\xi_{11}+3\xi_{11}^*)\big]}{(y^\nu y^{\nu\dagger})_{11}\big[|\xi_{11}|^2+\text{Re}(\xi_{11}^2)\big]\log\big(\frac{m_{N_1}}{m_\chi}\big)}. \tag{C.3.8}$$

Which contribution (C.3.7) or (C.3.8) is the dominant CP asymmetry depends on the model parameters.

The $k=l=2$ part in the N_1 decay width only gives a subdominant CP asymmetry in almost case due to the large m_{N_2} suppression.

C.3.2 Heavier modes

A heavier right-handed neutrino than N_1 can also generate CP asymmetry at its three-body decay. A lighter intermediate state, e.g., N_1 meets the resonance around its mass $m_{12}^2 \sim m_{N_1}^2$ and then the amplitude is largely enhanced. There are two types of enhancement in the decay width (C.3.2), the $k=l=1$ and cross terms. The enhanced contributions to the decay width are evaluated with the narrow width approximation. For the $k=l=1$ part, we obtain

$$\Gamma_2^{(11)} = \frac{m_{N_1}}{128\pi^3 m_{N_2}^3 \Gamma_{N_1}}(y^\nu y^{\nu\dagger})_{11}\sqrt{\lambda(m_{N_1}^2, m_{N_2}^2, m_\chi^2)}$$
$$\times \big[|\xi_{12}|^2(m_{N_1}^2+m_{N_2}^2-m_\chi^2)+2\,\text{Re}(\xi_{12}^2)m_{N_1}m_{N_2}\big], \tag{C.3.9}$$

where we have neglected $\mathcal{O}\big((\Gamma_{N_1})^2\big)$ terms. In the limit $m_\chi \ll m_{N_1} \ll m_{N_2}$ and $\Gamma_{N_1} \approx \tilde{\Gamma}_1$, the N_1 resonant contribution (C.3.9) is equal to $\frac{1}{2}\Gamma_{N_2\to N_1\chi}$. (The prefactor $\frac{1}{2}$ implies $\tilde{\Gamma}_1$ contains the decays both to particles and anti-particles.) We also find the cross-term contribution is relatively suppressed than the $k=l=1$ one. The enhanced on-shell decay (C.3.9) is controlled by the off-diagonal coupling ξ_{12}. When ξ_{12} is negligibly small, the N_2 three-body decay width is dominantly given by the non-resonant $k=l=2$ part and its approximate form is

$$\Gamma_2^{(22)} \approx \frac{m_{N_2}}{64\pi^3}(y^\nu y^{\nu\dagger})_{22}\big[|\xi_{22}|^2+\text{Re}(\xi_{22}^2)\big]\log\Big(\frac{m_{N_2}}{m_\chi}\Big). \tag{C.3.10}$$

The CP asymmetry of N_2 three-body decay is also generated by the resonant and non-resonant parts. The asymmetry from the N_1 resonant part comes from the last term in (C.3.9) and reads

$$\epsilon_2^{(11)} = \frac{m_{N_1}}{128\pi^2 m_{N_2}^2 \Gamma_2} (y^\nu y^{\nu\dagger})_{11} \sqrt{\lambda(m_{N_1}^2, m_{N_2}^2, m_\chi^2)} \, \text{Im}(\xi_{12})^2. \tag{C.3.11}$$

The usual interference of different diagrams also contributes to the asymmetry and is approximately found

$$\epsilon_2^{(12)} \approx \frac{-m_{N_1}}{128\pi^2 \Gamma_2} \, \text{Im}\left[(y^\nu y^{\nu\dagger})_{21} \xi_{22}^* \xi_{12}\right] \tag{C.3.12}$$

in the limit $m_{N_1} \ll m_{N_2}$. This usual cross-term part gives a tiny contribution to the decay width as mentioned above, but a possibly large one to the CP asymmetry parameter. The exact form of asymmetry parameters from the resonant contribution is found in Appendix C.B.

Similar to the N_1 decay, there is the CP asymmetry from a single diagram where the unstable N_2 is the intermediate state. In this case, the difference of the decay widths to particles and anti-particles is the same form as in the N_1 decay, but the total three-body decay width has several possibilities as described above. The resultant asymmetry parameter from the N_2-intermediate diagram becomes

$$\epsilon_2^{(22)} \approx \frac{\Gamma_{N_2}}{128\pi^3 \Gamma_2} (y^\nu y^{\nu\dagger})_{22} \, \text{Im}(\xi_{22}^2) \log\left(\frac{m_{N_2}}{m_\chi}\right) \tag{C.3.13}$$

Among the above 3 types of ϵ_2, the leading contribution is generally given by the non-resonant part (C.3.13) except for a tiny ξ_{22} (see Fig. C.4). We thus find for the N_2 three-body decay that the width is determined by the diagonal $k = l = 1$ or $k = l = 2$ part, and the CP asymmetry is governed by the non-resonant $k = l = 2$ part.

C.4 Lepton asymmetry with χ scalar

C.4.1 Boltzmann equations

In this section, solving the Boltzmann equations in the present system, we discuss the time evolution of yields and the washout effect of asymmetry.

In the following analysis, we apply for simplicity the single flavor approximation to the lepton asymmetry, and write the yields of leptons and anti-leptons as

$$Y_L = Y_L^{\text{eq}} + \frac{1}{2} Y_{\Delta L}, \qquad Y_{\bar{L}} = Y_L^{\text{eq}} - \frac{1}{2} Y_{\Delta L}, \tag{C.4.1}$$

where $Y_{\Delta L}$ denotes the yield of the lepton asymmetry. If one would like to include flavor-dependent effects, a further detailed analysis with, e.g., the density matrix formalism, is needed [GMP21], but that is beyond the purpose of this work. The SM particles including
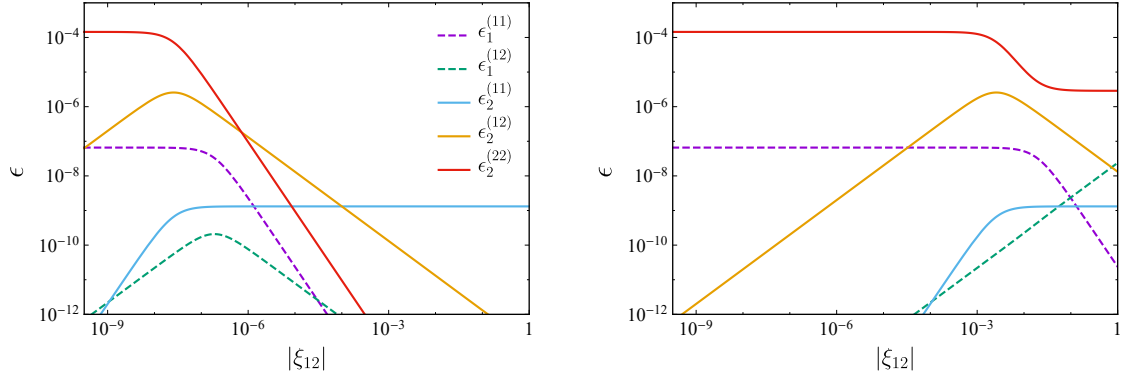
Figure C.4: A typical comparison of various asymmetry parameters. The approximate formulae of these parameters are given in the text. (Left) $|\xi_{11}| = |\xi_{22}| = 10^{-5}$. (Right) $|\xi_{11}| = |\xi_{22}| = 1$. In these figures, the neutrino Yukawa couplings are roughly replaced by the mass eigenvalues of neutrinos as $(y^\nu y^{\nu\dagger})_{ij} \sim (m_{N_i} m_{N_j} m_{\nu_i} m_{\nu_j})^{1/2}/v^2$, and the complex phases of couplings are assumed such that the asymmetry parameters take their maximal values.

the leptons and the Higgs field are assumed to be in the thermal bath. In this setup, the Boltzmann equations needed for the lepton asymmetry are given by

$$
Hx\frac{dY_{N_1}}{dx} \approx \frac{K_1(m_{N_1}/T)}{K_2(m_{N_1}/T)}Y_{N_1}^{\rm eq}\left[\tilde{\Gamma}_1\left(1 - \frac{Y_{N_1}}{Y_{N_1}^{\rm eq}}\right) - \frac{1}{2}\tilde{\Gamma}_1\tilde{\epsilon}_1\frac{Y_{\Delta L}}{Y_L^{\rm eq}} + \Gamma_1\left(-\frac{Y_{N_1}}{Y_{N_1}^{\rm eq}} + \frac{Y_\chi}{Y_\chi^{\rm eq}}\right)\right.
$$
$$
\left. - \frac{1}{2}\Gamma_1\epsilon_1\frac{Y_\chi}{Y_\chi^{\rm eq}}\frac{Y_{\Delta L}}{Y_L^{\rm eq}}\right] + \frac{K_1(m_{N_2}/T)}{K_2(m_{N_2}/T)}Y_{N_2}^{\rm eq}\Gamma_{N_2\to N_1\chi}\left(\frac{Y_{N_2}}{Y_{N_2}^{\rm eq}} - \frac{Y_{N_1}}{Y_{N_1}^{\rm eq}}\frac{Y_\chi}{Y_\chi^{\rm eq}}\right), \quad \text{(C.4.2)}
$$

$$
Hx\frac{dY_{N_2}}{dx} \approx \frac{K_1(m_{N_2}/T)}{K_2(m_{N_2}/T)}Y_{N_2}^{\rm eq}\left[\tilde{\Gamma}_2\left(1 - \frac{Y_{N_2}}{Y_{N_2}^{\rm eq}}\right) - \frac{1}{2}\tilde{\Gamma}_2\tilde{\epsilon}_2\frac{Y_{\Delta L}}{Y_L^{\rm eq}} + \Gamma_2\left(-\frac{Y_{N_2}}{Y_{N_2}^{\rm eq}} + \frac{Y_\chi}{Y_\chi^{\rm eq}}\right)\right.
$$
$$
\left. - \frac{1}{2}\Gamma_2\epsilon_2\frac{Y_\chi}{Y_\chi^{\rm eq}}\frac{Y_{\Delta L}}{Y_L^{\rm eq}} - \Gamma_{N_2\to N_1\chi}\left(\frac{Y_{N_2}}{Y_{N_2}^{\rm eq}} - \frac{Y_{N_1}}{Y_{N_1}^{\rm eq}}\frac{Y_\chi}{Y_\chi^{\rm eq}}\right)\right], \quad \text{(C.4.3)}
$$

$$
Hx\frac{dY_{\Delta L}}{dx} \approx \sum_i \frac{K_1(m_{N_i}/T)}{K_2(m_{N_i}/T)}Y_{N_i}^{\rm eq}\left[\tilde{\Gamma}_i\tilde{\epsilon}_i\left(\frac{Y_{N_i}}{Y_{N_i}^{\rm eq}} - 1\right) - \frac{1}{2}\tilde{\Gamma}_i\frac{Y_{\Delta L}}{Y_L^{\rm eq}}\right.
$$
$$
\left. + \Gamma_i\epsilon_i\left(\frac{Y_{N_i}}{Y_{N_i}^{\rm eq}} - \frac{Y_\chi}{Y_\chi^{\rm eq}}\right) - \frac{1}{2}\Gamma_i\frac{Y_\chi}{Y_\chi^{\rm eq}}\frac{Y_{\Delta L}}{Y_L^{\rm eq}}\right], \quad \text{(C.4.4)}
$$

$$
Hx\frac{dY_\chi}{dx} \approx \sum_i \frac{K_1(m_{N_i}/T)}{K_2(m_{N_i}/T)}Y_{N_i}^{\rm eq}\left[\Gamma_i\left(\frac{Y_{N_i}}{Y_{N_i}^{\rm eq}} - \frac{Y_\chi}{Y_\chi^{\rm eq}}\right) + \frac{1}{2}\Gamma_i\epsilon_i\frac{Y_\chi}{Y_\chi^{\rm eq}}\frac{Y_{\Delta L}}{Y_L^{\rm eq}}\right]
$$
$$
+ Y_{N_2}^{\rm eq}\frac{K_1(m_{N_2}/T)}{K_2(m_{N_2}/T)}\Gamma_{N_2\to N_1\chi}\left(\frac{Y_{N_2}}{Y_{N_2}^{\rm eq}} - \frac{Y_{N_1}}{Y_{N_1}^{\rm eq}}\frac{Y_\chi}{Y_\chi^{\rm eq}}\right), \quad \text{(C.4.5)}
$$

where the dimensionless parameter x is introduced by $x = m_{N_1}/T$, $K_n(z)$ denotes the modified Bessel function of second kind, and off-shell scattering contributions are dropped

	N_2 decay dominant	N_1 decay dominant
weak washout	$\mathcal{Y}_{\Delta L}^{\mathrm{FI}}(z_1)$	$Y_{\Delta L}^{\mathrm{FI}}(\infty)$
strong washout	——	$\mathcal{Y}_{\Delta L}^{\mathrm{WO}}(\infty)$

Table C.1: Four possible patterns of dominant contributions to the lepton asymmetry.

for simplifying the analysis. For the three-body decay process, the on-shell contributions of right-handed neutrinos are deducted in order to avoid the double counting when deriving the Boltzmann equations (C.4.2)–(C.4.5).

The right-handed neutrinos are first generated by their interactions to the thermal bath, and the lepton asymmetry and the scalar χ are produced via the right-handed neutrino decays. While the total amounts of the lepton asymmetry and χ are related, the washout (inverse decay) effect via the neutrino Yukawa couplings deduces only the asymmetry. The Boltzmann equation for the lepton asymmetry approximately becomes

$$\frac{dY_{\Delta L}}{dx} \approx \sum_i \frac{1}{Hx} \frac{K_1(m_{N_i}x/m_{N_1})}{K_2(m_{N_i}x/m_{N_1})} \left[\Gamma_i \epsilon_i \left(Y_{N_i} - \frac{Y_{N_i}^{\mathrm{eq}} Y_\chi}{Y_\chi^{\mathrm{eq}}} \right) - \frac{1}{2} \left(\tilde{\Gamma}_i + \Gamma_i \frac{Y_\chi}{Y_\chi^{\mathrm{eq}}} \right) \frac{Y_{N_i}^{\mathrm{eq}}}{Y_L^{\mathrm{eq}}} Y_{\Delta L} \right],$$

where the $\tilde{\epsilon}_i$ terms have been dropped since we are interested in the asymmetry produced by the three-body decay process. The first term of rhs produces the asymmetry via the N_i decay and the second term denotes the washout term. Depending on the N_1 or N_2 decay process being dominant to the production and the washout effect being strong or weak, there are four possibilities of the main lepton asymmetry as listed in Table C.1. We also show in Fig. C.5 the typical time evolution of the yields corresponding to these four patterns, respectively. The top panels in Fig. C.5 are the results for the weak washout, and the bottom panels are for the strong one. Further, the N_2 decay process is the main contribution to the asymmetry in the left panels in Fig. C.5 and the N_1 process is dominant in the right panels. Roughly speaking, the relic of lepton asymmetry in the bottom line is given by that in the top line times the washout suppression factor.

In the case that the freeze-in production from N_2 is dominant (top-left panel), we have to take the washout effect into account (for the detail, see Appendix C.C.2). The lepton asymmetry of this case is evaluated by

$$\mathcal{Y}_{\Delta L}^{\mathrm{FI}}(z_1) = \int_0^{z_1} dx' \, \mathcal{F}_2(x') \exp\left[- \int_{x'}^{z_1} dx'' \, W_2(x'') \right], \tag{C.4.6}$$

where

$$W_2 := \frac{1}{2Hx} \frac{K_1(m_{N_2}x/m_{N_1})}{K_2(m_{N_2}x/m_{N_1})} \left(\tilde{\Gamma}_2 + \Gamma_2 \frac{\boldsymbol{Y}_\chi}{Y_\chi^{\mathrm{eq}}} \right) \frac{Y_{N_2}^{\mathrm{eq}}}{Y_L^{\mathrm{eq}}} + \frac{1}{2Hx} \frac{K_1(x)}{K_2(x)} \left(\tilde{\Gamma}_1 + \Gamma_1 \frac{\boldsymbol{Y}_\chi}{Y_\chi^{\mathrm{eq}}} \right) \frac{Y_{N_2}^{\mathrm{eq}}}{Y_L^{\mathrm{eq}}}, \tag{C.4.7}$$

$$\mathcal{F}_2 = \frac{1}{Hx} \frac{K_1(m_{N_2}x/m_{N_1})}{K_2(m_{N_2}x/m_{N_1})} \Gamma_2 \epsilon_2 \left(\boldsymbol{Y}_{N_2} - \frac{Y_{N_2}^{\mathrm{eq}}}{Y_\chi^{\mathrm{eq}}} \boldsymbol{Y}_\chi \right) + \frac{1}{Hx} \frac{K_1(x)}{K_2(x)} \Gamma_1 \epsilon_1 \left(\boldsymbol{Y}_{N_1} - \frac{Y_{N_1}^{\mathrm{eq}}}{Y_\chi^{\mathrm{eq}}} \boldsymbol{Y}_\chi \right). \tag{C.4.8}$$
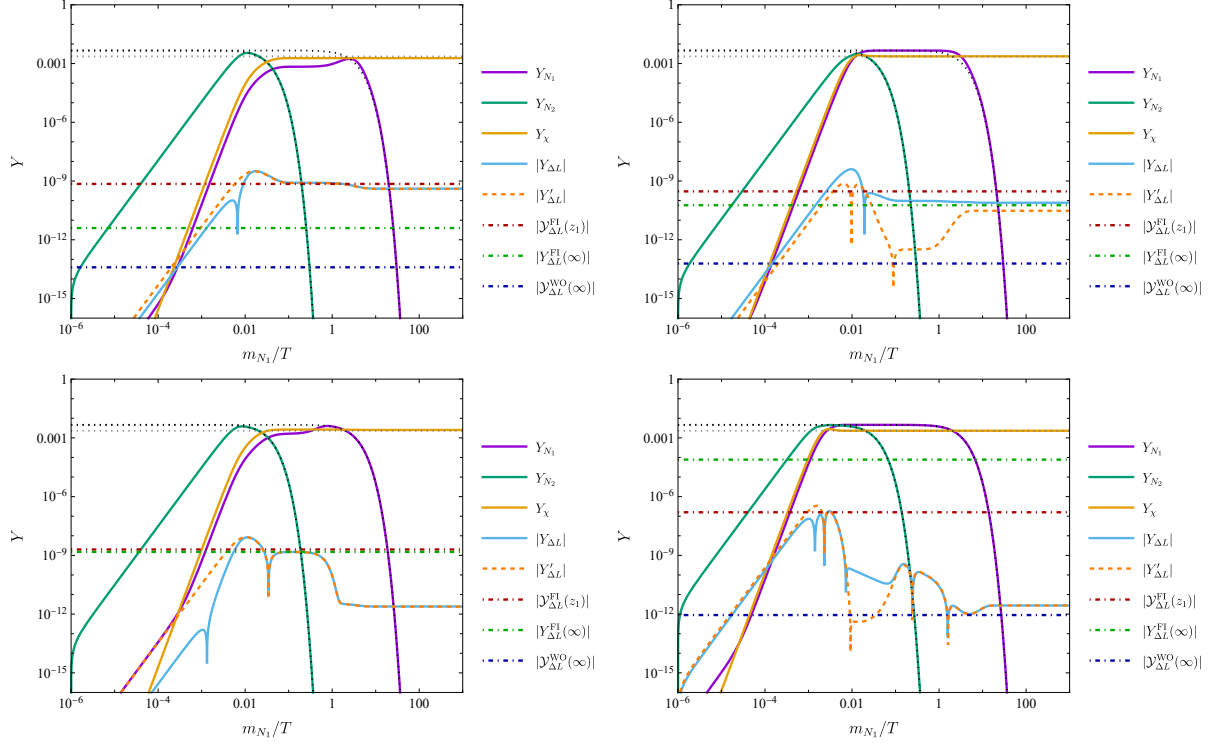
Figure C.5: The time evolution of the yields. In the top panels, the washout effect is weak and the asymmetry is produced by the freeze-in mechanism of the right-handed neutrino decays. The washout works well in the bottom panels. In the left panels, the N_2 decay is the dominant production channels and N_1 dominant in the right panels. The solid lines are numerical solutions of the Boltzmann equations [Eqs. (C.4.2)–(C.4.5)]. The orange dashed line is evaluated by solving the Boltzmann equations of N_1, χ and ΔL with $Y_{N_2} = Y_{N_2}^{\mathrm{eq}}$. The dot-dashed dark red, dark green and dark blue lines are given by Eqs. (C.4.6), (C.4.13) and (C.4.14), respectively.

$$\boldsymbol{Y}_{N_2} = \frac{45\sqrt{10}}{2\pi^5 g_*^{1/2} g_*^S} \frac{M_P m_{N_2} \tilde{\Gamma}_2}{m_{N_1}^3} x^3, \tag{C.4.9}$$

$$\boldsymbol{Y}_\chi = \frac{135}{2\pi^6 g_* g_*^S} \frac{M_P^2 m_{N_2}^2 \tilde{\Gamma}_2 (\Gamma_{N_2 \to N_1 \chi} + \Gamma_2)}{m_{N_1}^6} x^6, \tag{C.4.10}$$

$$\boldsymbol{Y}_{N_1} = \frac{45\sqrt{10}}{2\pi^5 g_*^{1/2} g_*^S} \frac{M_P \tilde{\Gamma}_1}{m_{N_1}^2} x^3 + \frac{135}{2\pi^6 g_* g_*^S} \frac{M_P^2 m_{N_2}^2 \tilde{\Gamma}_2 (\Gamma_{N_2 \to N_1 \chi} + \Gamma_2)}{m_{N_1}^6} x^6. \tag{C.4.11}$$

z_1 is given by using these $\boldsymbol{Y}_{N_2}$ and $\boldsymbol{Y}_\chi$ as

$$z_1 = \min(z_{N_2}, z_\chi), \quad \boldsymbol{Y}_{N_2}(z_{N_2}) = \frac{45}{\pi^4 g_*^S}, \quad \boldsymbol{Y}_\chi(z_\chi) = \frac{45}{2\pi^4 g_*^S}, \tag{C.4.12}$$

and z_{N_2} (z_χ) is regarded as the time of N_2 (χ) being close to the thermal equilibrium. The washout gives the exponential suppression through $e^{-\int dx' W_2(x')}$. On the other hand, if the N_1 process is dominant, the asymmetry is mainly produced by the ordinary freeze-in

mechanism via N_1 decay such as the FIMP dark matter [HJMRW10] (top-right panel in Fig. C.5). The relic of the lepton asymmetry is written as

$$Y_{\Delta L}^{\text{FI}}(\infty) \approx \frac{135\sqrt{10}}{2\pi^5 g_*^{1/2} g_*^S} \frac{M_P \Gamma_1 \epsilon_1}{m_{N_1}^2} \int_0^\infty dx\, x^3 K_1(x) = \frac{405\sqrt{10}}{4\pi^4 g_*^{1/2} g_*^S} \frac{M_P \Gamma_1 \epsilon_1}{m_{N_1}^2}. \qquad \text{(C.4.13)}$$

If the washout is strong and dilutes the relic from the N_1 decay (bottom right panel in Fig. C.5), the lepton asymmetry is evaluated as

$$\mathcal{Y}_{\Delta L}^{\text{WO}}(\infty) = \int_0^\infty dx'\, \mathcal{F}_1(x') \exp\left[-\int_{x'}^\infty dx''\, W_1(x'')\right], \qquad \text{(C.4.14)}$$

where the washout function of this case is given by

$$W_1 := \frac{1}{2Hx} \frac{K_1(m_{N_2} x/m_{N_1})}{K_2(m_{N_2} x/m_{N_1})}(\tilde{\Gamma}_2 + \Gamma_2)\frac{Y_{N_2}^{\text{eq}}}{Y_L^{\text{eq}}} + \frac{1}{2Hx} \frac{K_1(x)}{K_2(x)}(\tilde{\Gamma}_1 + \Gamma_1)\frac{Y_{N_1}^{\text{eq}}}{Y_L^{\text{eq}}}, \qquad \text{(C.4.15)}$$

and we introduce the following function

$$\mathcal{F}_1 := \frac{1}{Hx} \frac{K_1(m_{N_2} x/m_{N_1})}{K_2(m_{N_2} x/m_{N_1})}\Gamma_2 \epsilon_2 \left(\frac{\tilde{\Gamma}_2 + \Gamma_2}{m_{N_2}}\right) Y_{N_2}^{\text{eq}} + \frac{1}{Hx} \frac{K_1(x)}{K_2(x)}\Gamma_1 \epsilon_1 \left(\frac{\tilde{\Gamma}_1 + \Gamma_1}{m_{N_1}}\right) Y_{N_1}^{\text{eq}}. \qquad \text{(C.4.16)}$$

C.4.2 Parameter space

Based on the analysis of the Boltzmann equations in the previous subsection, we discuss the parameter spaces of the model where the lepton asymmetry is properly generated. The Majorana masses of the right-handed neutrinos are fixed to $m_{N_1} = 10^{10}$ GeV, $m_{N_2} = 10^{12}$ GeV, and $m_{N_3} = 10^{14}$ GeV. N_3 is heavy so that it is assumed not to join the initial and final states of our considering processes. The scalar χ is light and its mass is assumed in this work to be $m_\chi = 10^{-3}$ GeV, but its detailed value does not largely affect the asymmetry. As for the CI parameters (the degrees of freedom of neutrino Yukawa couplings), we consider the following two typical patterns of parameters:

(I) Real CI parameters

$$\omega_{12} = \frac{1}{4}, \quad \omega_{23} = \frac{3}{7}, \quad \omega_{13} = 0 \qquad \text{(C.4.17)}$$

(II) Pure imaginary CI parameters

$$\omega_{12} = 2i, \quad \omega_{23} = i, \quad \omega_{13} = 0. \qquad \text{(C.4.18)}$$

With these parameter sets, the asymmetry from the SM particle loops vanish, $\tilde{\epsilon}_i^{(LH)} = 0$, found from Eq. (C.2.8).

Fig. C.6 shows the relic of the lepton asymmetry $Y_{\Delta L}(\infty)$ for

$$\text{Re}\,\xi = \begin{pmatrix} \frac{1}{20} & \text{Re}\,\xi_{12} \\ \text{Re}\,\xi_{12} & \frac{1}{10} \end{pmatrix}, \quad \text{Im}\,\xi = \begin{pmatrix} \frac{1}{2} & \text{Im}\,\xi_{12} \\ \text{Im}\,\xi_{12} & 1 \end{pmatrix}. \qquad \text{(C.4.19)}$$
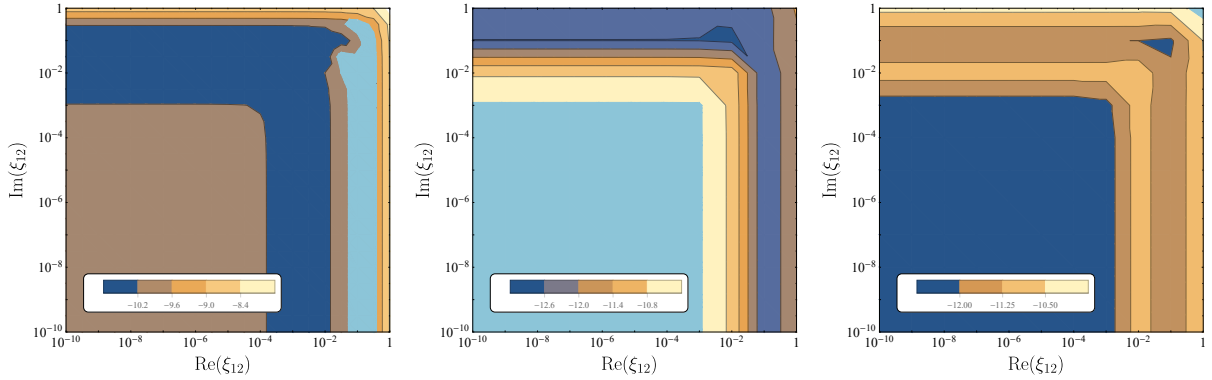
Figure C.6: The density plots of the lepton asymmetry in the $(\mathrm{Re}\,\xi_{12}, \mathrm{Im}\,\xi_{12})$ plane. The left panel is the parameter space for the normal mass hierarchy and all the CI parameters real-valued. In other two panels, the inverted mass hierarchy is assumed and the middle (right) panel shows the parameter space with all the CI parameters being real (pure imaginary). The light blue regions properly produce the observed baryon asymmetry in the universe.

The light blue regions properly produce the observed baryon asymmetry. The CP asymmetry parameters Eqs. (C.3.7), (C.3.8) and (C.3.11)–(C.3.13) are roughly determined by the large values in ξ^2, which then lead to the contours seen in Fig. C.6.

The left panel of Fig. C.6 is the parameter space for the normal mass hierarchy of neutrinos and real CI parameters, where the washout effect is less dominant. In this case, larger values of couplings lead larger lepton asymmetry through the freeze-in like production of N_1. Then the lepton asymmetry reduces due to weaker couplings, but the asymmetry becomes large again when ξ_{12} is small enough. This is because the freeze-in like production of N_2 is dominant. If the washout effect works well as in the inverted mass hierarchy, the lepton asymmetry is suppressed as shown in the middle and right panels of Fig. C.6. When the CI parameters are real, the final value of the lepton asymmetry tends to converge to a value slightly smaller than 10^{-10} if ξ are feeble couplings, which means the relic asymmetry is determined by the neutrino Yukawa couplings. However the washout is relatively stronger if ξ is larger, and the relic is more suppressed. On the other hand, the washout effect of neutrino Yukawa couplings works well and the lepton asymmetry can only take a tiny value. In this case, an enough large coupling is needed for a large amount of $Y_{\Delta L}$ produced in the early universe to explain the observed asymmetry even when it is washed out. From these observations, the tree-level leptogenesis from the three-body decay of right-handed neutrinos with a flavorful scalar does not favor the inverted mass hierarchy of neutrinos.

We now discuss a singlet scalar χ and its general form of couplings to the right-handed neutrinos. If χ is something like a pNGB associated with the lepton number symmetry, the imaginary parts of the diagonal couplings ξ_{ii} tend to be dominant. Keeping in mind
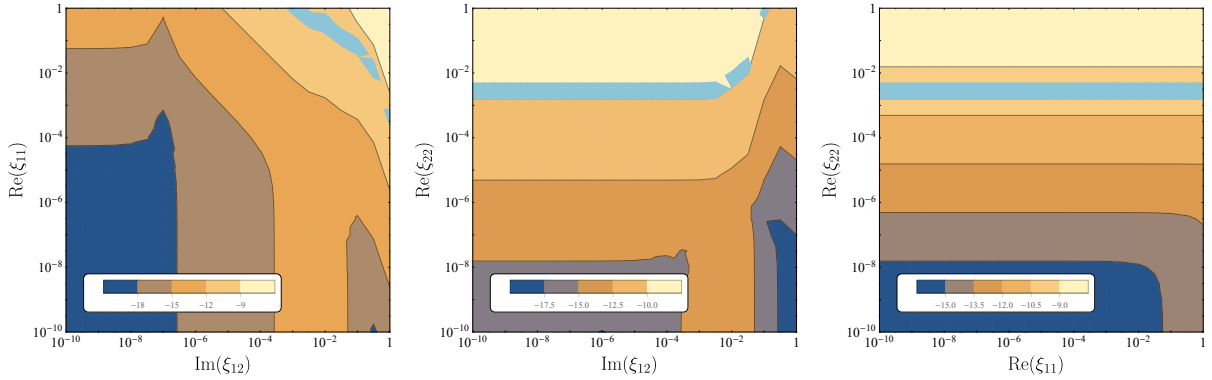
Figure C.7: The density plots of the lepton asymmetry in the $(\text{Im}\,\xi_{12}, \text{Re}\,\xi_{11})$, $(\text{Im}\,\xi_{12}, \text{Re}\,\xi_{22})$ and $(\text{Re}\,\xi_{11}, \text{Re}\,\xi_{22})$ planes with the parameterization (C.4.20). The normal mass hierarchy and real CI parameters are adopted for realizing $Y_{\Delta L}(\infty) \sim 10^{-10}$.

this fact, we take the coupling ξ as

$$\text{Re}\,\xi = \begin{pmatrix} \text{Re}\,\xi_{11} & 0 \\ 0 & \text{Re}\,\xi_{22} \end{pmatrix}, \qquad \text{Im}\,\xi = \begin{pmatrix} 10^{-2} & \text{Im}\,\xi_{12} \\ \text{Im}\,\xi_{12} & 1 \end{pmatrix}. \tag{C.4.20}$$

The parameter spaces are shown in Fig. C.7 when $\text{Re}\,\xi_{11}$, $\text{Re}\,\xi_{22}$ and $\text{Im}\,\xi_{12}$ are assumed to be the modifications to the imaginary diagonal elements. In this situation, the lepton asymmetry is produced by the freeze-in mechanism of N_1 or N_2 as shown in the top panels of Fig. C.5, and there exist the allowed regions between the parameter spaces of over- and under-productions of the asymmetry.

On the other hand, the parameter spaces of the imaginary diagonal elements are shown in Fig. C.8. For evaluating the lepton asymmetry in these planes, $\text{Im}\,\xi_{12}$ and one of $\text{Im}\,\xi_{12}$ or $\text{Re}\,\xi_{22}$ are fixed to 10^{-1} or 10^{-5}, and the normal mass hierarchy for the neutrino masses is assumed. As seen from these figures, larger couplings lead to larger relic asymmetry, similar to the above cases of the normal mass hierarchy, and $\text{Im}\,\xi_{11}$, $\text{Im}\,\xi_{22} \sim 10^{-(1-2)}$ are favored.

C.4.3 Property of χ scalar

In the present work, the scalar field χ has two important property that (i) it has the complex coupling ξ_{ij} to the parent decay particles and (ii) its remnant Y_χ in the present universe is large. That is a general result to have an appropriate order of baryon asymmetry generated from the three-body decay including χ.

Let us first discuss about the coupling ξ_{ij}. The analysis in the above shows that ξ_{ij} should be complex-valued so that the CP asymmetry is properly produced through the three-body decay. Further the flavor-changing components ξ_{ij} $(i \neq j)$ can play an important role for the leptogenesis. These nature of couplings put some constraint on the property of the field χ, for example, a dynamical completion in high-energy regime.
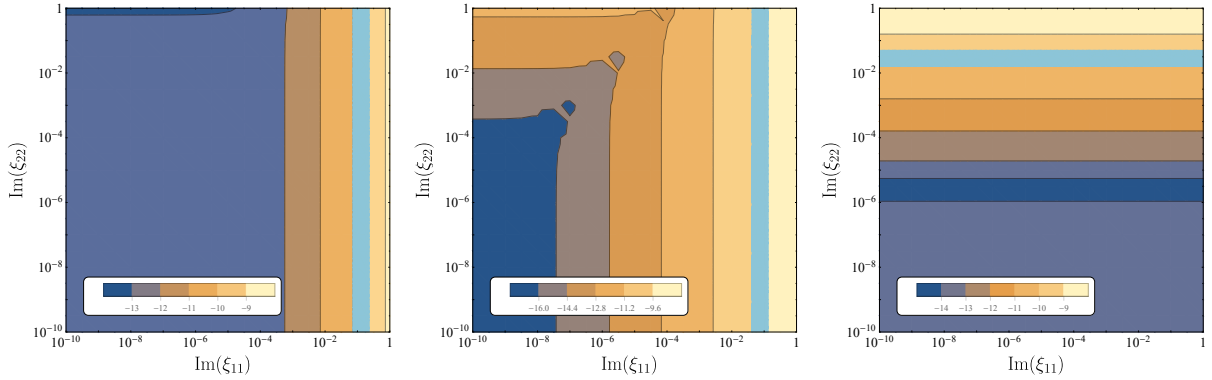
Figure C.8: The density plots of the lepton asymmetry in the $(\mathrm{Im}\,\xi_{11}, \mathrm{Im}\,\xi_{22})$ plane for the normal mass hierarchy. (Left) $\mathrm{Im}\,\xi_{12} = 10^{-1}$, $\mathrm{Re}\,\xi_{12} = 10^{-1}$. (Middle) $\mathrm{Im}\,\xi_{12} = 10^{-5}$, $\mathrm{Re}\,\xi_{12} = 10^{-1}$. (Right) $\mathrm{Im}\,\xi_{12} = 10^{-5}$, $\mathrm{Re}\,\xi_{22} = 10^{-1}$.

- NGB :

    A simple example for scalar couplings to neutrinos is the one whose VEV gives the masses of right-handed neutrinos N_i. If such a scalar is complex, the coupling has the lepton number symmetry (the chiral rotation of N_i) and the scalar VEV breaks it. As a result of symmetry breaking, a NGB appears [CMP80, CMP81, GR81], which couples to N_i and can be identified to χ. This is a typical and the simplest dynamical realization of the present model. It is however noticed that, if the NGB nature is exact, χ is massless and its couplings to N_i are real and flavor diagonal, i.e., $\xi_{ij} = c_i\,\delta_{ij}$, $c_i \in \mathbb{R}$. As mentioned above, such a too simple form of scalar couplings is not suitable for generating the asymmetry.

- Flavor-dependent interaction :

    There are several ways to ameliorate the NGB problem, too simple ξ_{ij}, found in the above simplest setup. The first is to introduce multi scalars which couple to the right-handed neutrinos N_i. These scalars generally couple to each other and develop nonzero VEVs. The resultant NGB, which is identified to χ, is a linear combination of (the phases of) these scalars. As a result, the flavor structure becomes different between the masses and the scalar couplings of right-handed neutrinos.

    A more interesting realization is to assign generation-dependent charges to leptons under some flavor symmetry. The assignment is chosen so that the masses (and Yukawa couplings) are forbidden and then induced by some VEV of complex scalar, charged under the same flavor symmetry [FN79]. In this case, χ is possibly the NGB of flavor symmetry and its coupling to leptons is determined by the flavor structure of lepton masses and symmetry charges. Unless the masses and charges have exactly the same structure, the χ couplings are generally flavor dependent [DW82, Wil82] (and complex valued). Typical examples may be constructed with flavor $U(1)$ symmetry for fermion mass hierarchy, and non-universal anomaly-free lepton numbers

such as $L_\mu - L_\tau$ and others [BV91, MS15].

- Radiative corrections :

  The NGB property is not exactly hold if the original symmetry is somehow violated via explicit breaking terms. A well-known example is the scalar mass term which does not respect (global) symmetry, and hence the NGB acuires its nonzero mass (the "pion" mass) at classical level. With such explicit breaking, one generally expects to have non-vanishing radiative corrections to unusual NGB couplings and resolve the NGB problem mentioned above. There are phenomenological analysis for large breaking, e.g., a heavy NGB of the lepton number symmetry [AHO+20, MY10], where suitably size of corrections might be obtained.

The large remnant of χ is another characteristic result of the model. We here discuss two approaches to this issue: (i) additional scalar interactions. (ii) a very light χ. The first resolution is to introduce additional interaction such that it suppresses the scalar abundance somewhere in the thermal history. However, when χ is the NGB of high-scale symmetry, its large decay constant generally suppresses the χ couplings to the SM fields and cannot give an enough suppression to the χ abundance. For example, when χ is the NGB of lepton number symmetry which couples to the right-handed neutrinos, a typical ratio $\Gamma/H(T = m_\chi)$ is $10^{-20}\xi^2(m_\chi/\text{GeV})$. We are therefore lead to the situation that the scalar including three-body decay is not a NGB-like pseudo-scalar χ but some heavy real scalar ρ (heavier than the electroweak scale). As long as ρ is rather lighter than N_i, the analysis of leptogenesis from three-body decay discussed in this chapter is unchanged even for $N_i \to L_j H \rho$. Dynamical examples of ρ are a partner of NGB (a radial fluctuation around a VEV), a massive scalar in the multi scalar scenario, and so on. A main difference between χ and ρ is the interaction to other (SM) fields. In particular, for the Higgs portal interaction, ρ interacts with the portal quartic coupling λ, but χ has a suppressed amplitude given by $\lambda E^2/(\text{VEV})^2$ where E is the energy scale considered. Upon the decoupling $E \sim m_\rho$ or m_χ, the latter interaction (for χ) is too tiny to reduce the abundance, and the former one (for ρ) can be used for the suppression. Whether ρ is the dark matter component in the universe or not depends on the model parameters, though both are possible to realize.

The second option is to assume that χ is very light and does not contribute much to the mass density of the present universe. The relic abundance of χ is given by $\Omega_\chi h^2 = m_\chi s_0 Y_{\chi,0}/(\varepsilon_{c,0}/h^2)$ with the today entropy and critical energy densities, $s_0 = 2891$ cm^{-3} and $\varepsilon_{c,0} = 5.16(h/0.7)^2$ GeV/m^3. If this abundance is required to be less than the observed dark matter density times a small ratio δ, that implies the upper bound on m_χ,

$$m_\chi < \delta \frac{\Omega_{\text{DM}}\varepsilon_{c,0}}{s_0 Y_\chi^{\text{eq}}} = 1.89 \times 10^{-7}\,\delta\ [\text{GeV}] \qquad (\text{C.4.21})$$

where we have assumed $Y_{\chi,0}$ is equal to the equilibrium value Y_χ^{eq}. For example, χ has a sub-eV mass for $\delta = 10^{-3}$ but weighs more than the current temperature. Furthermore

the interaction of χ to the SM sector is generally suppressed by $\mathcal{O}(m_\nu)$. Such a very light and feebly-interacting scalar may be harmlessly floating in the present universe.

C.5   Summary

We have studied the lepton asymmetry produced by the tree-level right-handed neutrino three-body decays with a singlet scalar field. In order to cover the general case, we considered the scalar and pseudo-scalar couplings between the scalar field and right-handed neutrinos. We evaluated the right-handed neutrino two-body and three-body decay widths with the scalar field and the asymmetry parameters. For the decay widths, the $k = l = 1$ contribution tends to be dominant in the lightest N_1 decay, and the contribution of the resonant $k = l = 1$ or the non-resonant $k = l = 2$ is dominant depending on ξ in the heavier N_2 decay. For the asymmetry parameters, not only usual cross terms but also the $k = l = 1$ can be dominant to ϵ_1, and the $k = l = 2$ term is the leading contribution to ϵ_2. In the latter two contributions, the CP asymmetry comes from a single decay process, which is characteristic of the existence of the flavorful scalar. We derived the Boltzmann equations and discussed there are four typical patterns of the lepton asymmetry production depending on the N_1 or N_2 decay process being dominant to the production and the washout effect being strong or weak. Based on these analyses, we show the parameter space of the model where the lepton asymmetry is properly generated. For example, we find the tree-level leptogenesis via the three-body decay with the flavorful scalar does not favor the inverted mass hierarchy due to the strong washout suppression, without a help of the two-body decay asymmetry.

In this chapter, we consider a simplified model with a single flavorful scalar coupling to the right-handed neutrinos and investigate the possibility of the leptogenesis via the three-body decay with specific values of couplings. Pursuing the UV origin of this additional scalar such as a pNGB and a more detailed analysis of flavor dynamics are important and left for future study.

Appendix C.A   Three-body decay widths

We consider for simplicity the two-generation case $N_{1,2}$. The generalization to more generations is straightforward. We assume $m_\chi \ll m_{N_i}$ and no large hierarchy among m_{N_i}. The masses of charged leptons and Higgs boson are dropped in the following formulae. The three-body decay width of the lightest right-handed neturino N_1 is found from the full form (C.3.2) after the phase space integral as

$$\Gamma_{N_1 \to L_j H \chi} = \sum_{k,l} y^\nu_{lj} y^{\nu*}_{kj} \left(\xi^*_{1l} \xi_{1k} G^A_{kl} + \xi_{1l} \xi^*_{1k} G^B_{kl} + \xi^*_{1l} \xi^*_{1k} G^C_{kl} + \xi_{1l} \xi_{1k} G^D_{kl} \right) = \sum_{k,l} \Gamma^{(kl)}_1,$$

$$\text{(C.A.1)}$$

where k, l indicate the contributions to the amplitudes which contain the intermediate states are $N_{k,l}$, respectively. For example, $k \neq l$ means the cross term in the amplitude squared. Each piece $G^{A,B,C,D}$ reads from the full form (C.3.2) and not explicitly given here. We instead show the exact form of $\Gamma_1^{(kl)}$, corresponding $\mathcal{M}_k^* \mathcal{M}_l$, where $\mathcal{M}_m$ is the N_1 three-body decay amplitude with the intermediate state N_m. The result is found in the limit of light m_χ as

$$\Gamma_1^{(11)} = \frac{1}{128\pi^3} y_{1j}^\nu y_{1j}^{\nu*} \left[|\xi_{11}|^2 m_{N_1} + \mathrm{Re}(\xi_{11}^2 \bar{m}_{N_1}) \right] \log\left(\frac{m_{N_1}}{m_\chi}\right), \tag{C.A.2}$$

$$\Gamma_1^{(12)} = \frac{1}{512\pi^3 m_{N_1}^3} y_{2j}^\nu y_{1j}^{\nu*} \left[\xi_{11} \xi_{12}^* \bar{m}_{N_1} \bar{m}_{N_2}^* \left[\left(m_{N_1}^2 + m_{N_2}^2 \right) \log\left(\frac{m_{N_2}^2}{m_{N_2}^2 - m_{N_1}^2}\right) - m_{N_1}^2 \right] \right.$$

$$+ 2m_{N_1}(\xi_{11}\xi_{12}\bar{m}_{N_1} + \xi_{11}^*\xi_{12}^*\bar{m}_{N_2}^*) \left[m_{N_2}^2 \log\left(\frac{m_{N_2}^2}{m_{N_2}^2 - m_{N_1}^2}\right) - m_{N_1}^2 \right]$$

$$\left. + \xi_{11}^*\xi_{12} \left[m_{N_2}^2(m_{N_1}^2 + m_{N_2}^2) \log\left(\frac{m_{N_2}^2}{m_{N_2}^2 - m_{N_1}^2}\right) - m_{N_1}^2 m_{N_2}^2 - \frac{3}{2} m_{N_1}^4 \right] \right], \tag{C.A.3}$$

$$\Gamma_1^{(21)} = \Gamma_1^{(12)*}, \tag{C.A.4}$$

$$\Gamma_1^{(22)} = \frac{1}{512\pi^3 m_{N_1}^3} y_{2j}^\nu y_{2j}^{\nu*} \left[|\xi_{12}|^2 \left[(5m_{N_2}^4 - m_{N_1}^4) \log\left(\frac{m_{N_2}^2}{m_{N_2}^2 - m_{N_1}^2}\right) - 5m_{N_1}^2 m_{N_2}^2 - \frac{5}{2} m_{N_1}^4 \right] \right.$$

$$\left. + 4\,\mathrm{Re}(\xi_{12}^2 \bar{m}_{N_2}) m_{N_1} \left[(2m_{N_2}^2 - m_{N_1}^2) \log\left(\frac{m_{N_2}^2}{m_{N_2}^2 - m_{N_1}^2}\right) - 2m_{N_1}^2 \right] \right]. \tag{C.A.5}$$

When N_2 is much heavier than N_1, the expressions are reduced to

$$\Gamma_1^{(12)} = \Gamma_1^{(21)*} \approx \frac{m_{N_1} \bar{m}_{N_2}^*}{1024\pi^3 m_{N_2}^2} y_{2j}^\nu y_{1j}^{\nu*} \, \xi_{12}^* (3\xi_{11}\bar{m}_{N_1} + 2\xi_{11}^* m_{N_1}), \tag{C.A.6}$$

$$\Gamma_1^{(22)} \approx \frac{m_{N_1}^3}{768\pi^3 m_{N_2}^2} y_{2j}^\nu y_{2j}^{\nu*} |\xi_{12}|^2. \tag{C.A.7}$$

The last equation implies that the $k = l = 2$ mode does not induce CP asymmetry at the leading order and then highly suppressed for the N_1 decay.

For a heavier right-handed neutrino, its three-body decay can meet the resonance around the mass of a lighter intermediate state, and then the width is largely enhanced. In the present case, the N_2 decay width $\Gamma_{N_2 \to L_j H \chi}$ has the enhancement both for $k = l = 1$ and the sum of cross terms, namely, $\Gamma_2^{(11)}$ and $\Gamma_2^{(12)} + \Gamma_2^{(21)}$ in the similar notation as (C.A.1). These on-shell contributions to the decay width are evaluated from the full form (C.3.2) with the narrow width approximation. For the $k = l = 1$ part, we obtain

$$\Gamma_2^{(11)} = \frac{m_{N_1}}{256\pi^2} \frac{m_{N_2}^2 - m_{N_1}^2}{m_{N_2}^3 \Gamma_{N_1}} y_{1j}^\nu y_{1j}^{\nu*} \left[|\xi_{12}|^2 (m_{N_1}^2 + m_{N_2}^2) + 2\,\mathrm{Re}(\xi_{12}^2 \bar{m}_{N_1}) m_{N_2} \right], \tag{C.A.8}$$

where Γ_{N_1} in the denominator indicates N_1 is the real intermediate state. Compared with the decay width for $N_2 \to N_1 \chi$ given in (C.2.6), the on-shell $k = l = 1$ contribution is found

$$\Gamma_2^{(11)} \approx \frac{m_{N_1}}{16\pi \Gamma_{N_1}} y_{1j}^\nu y_{1j}^{\nu*} \, \Gamma_{N_2 \to N_1 \chi} \approx \frac{1}{2} \Gamma_{N_2 \to N_1 \chi}. \tag{C.A.9}$$

186

For the cross-term part, a similar evaluation leads to the on-shell resonant contribution,

$$
\Gamma_2^{(12)} + \Gamma_2^{(21)} = \frac{m_{N_1}}{256\pi^2 m_{N_2}^3 (m_{N_2}^2 - m_{N_1}^2)} \left[\Gamma_{N_2} \left[\tfrac{1}{2} \operatorname{Re}(y_{2j}^\nu y_{1j}^{\nu *} \xi_{22}^* \xi_{12})(m_{N_1}^2 + m_{N_2}^2)^2 \right. \right.
$$
$$
- 4 \operatorname{Im}(y_{2j}^\nu y_{1j}^{\nu *} \xi_{12}^*) \operatorname{Im}(\xi_{22}) m_{N_1} m_{N_2} (m_{N_1}^2 + m_{N_2}^2) + 2 \operatorname{Re}(y_{2j}^\nu y_{1j}^{\nu *} \xi_{22} \xi_{12}) m_{N_1}^2 m_{N_2}^2 \Big]
$$
$$
- \left[\operatorname{Im}(y_{2j}^\nu y_{1j}^{\nu *} \xi_{22} \xi_{12}^*) m_{N_1} + \operatorname{Im}(y_{2j}^\nu y_{1j}^{\nu *} \xi_{22}^* \xi_{12}) m_{N_2} \right] (m_{N_2}^4 - m_{N_1}^4)
$$
$$
\left. - 2 \left[\operatorname{Im}(y_{2j}^\nu y_{1j}^{\nu *} \xi_{22} \xi_{12}) m_{N_1} + \operatorname{Im}(y_{2j}^\nu y_{1j}^{\nu *} \xi_{22}^* \xi_{12}^*) m_{N_2} \right] m_{N_1} m_{N_2} (m_{N_2}^2 - m_{N_1}^2) \right].
$$

$$ \text{(C.A.10)} $$

Finally the non-resonant part, $k = l = 2$, gives

$$
\Gamma_2^{(22)} = \frac{1}{128\pi^3} y_{2j}^\nu y_{2j}^{\nu *} \left[|\xi_{22}|^2 m_{N_2} + \operatorname{Re}(\xi_{22}^2 \bar{m}_{N_2}) \right] \log\left(\frac{m_{N_2}}{m_\chi}\right). \tag{C.A.11}
$$

Appendix C.B   CP asymmetry (width differences)

For a real particle (a real scalar, a Majorana fermion, etc), the decay to anti-particle final states is obtained by replacing all coupling constants with their complex conjugates in the corresponding decay amplitude to particle final states. In the present case, the three-body decay of N_i to the anti-lepton $\bar{L}_j$, the conjugate of Higgs boson $\bar{H}$, and the real scalar χ is described by $y^\nu \leftrightarrow y^{\nu *}$ and $\xi \leftrightarrow \xi^*$ (and $P_R \leftrightarrow P_L$) everywhere in the amplitude. The CP asymmetry is induced at the decay, proportionally to the difference of decay widths to particles and corresponding anti-particles. As a result, the asymmetry is originated from the pieces in the decay widths which are not real with respect to coupling constants.

The decay width to anti-particles is defined in a similar way to the decay to particles discussed in the previous section, namely,

$$
\Gamma_{N_1 \to L_j^c H^\dagger \chi} = \sum_{k,l} \bar{\Gamma}_1^{(kl)}. \tag{C.B.1}
$$

The differences of partial widths are written as $\Delta\Gamma_1^{(kl)} = \Gamma_1^{(kl)} - \bar{\Gamma}_1^{(kl)}$. From the explicit forms for $\Gamma_1^{(kl)}$ and the replacement rule mentioned above, we obtain

$$
\Delta\Gamma_1^{(11)} = \frac{\Gamma_{N_1}}{128\pi^3} y_{1j}^\nu y_{1j}^{\nu *} \operatorname{Im}(\xi_{11}^2) \log\left(\frac{m_{N_1}}{m_\chi}\right), \tag{C.B.2}
$$

$$
\Delta\Gamma_1^{(12)} + \Delta\Gamma_1^{(21)} = \frac{1}{256\pi^3 m_{N_1}^3} \left[\operatorname{Im}(y_{2j}^\nu y_{1j}^{\nu *} \xi_{11} \xi_{12}^*)(\Gamma_{N_1} m_{N_2} - \Gamma_{N_2} m_{N_1}) \right.
$$
$$
\times \left[\left(m_{N_1}^2 + m_{N_2}^2 \right) \log\left(\frac{m_{N_2}^2}{m_{N_2}^2 - m_{N_1}^2}\right) - m_{N_1}^2 \right]
$$
$$
\left. + m_{N_1} \left[\operatorname{Im}(y_{2j}^\nu y_{1j}^{\nu *} \xi_{11} \xi_{12}) \Gamma_{N_1} - \operatorname{Im}(y_{2j}^\nu y_{1j}^{\nu *} \xi_{11}^* \xi_{12}^*) \Gamma_{N_2} \right] \right.
$$

$$\times \left[m_{N_2}^2 \log\left(\frac{m_{N_2}^2}{m_{N_2}^2 - m_{N_1}^2}\right) - m_{N_1}^2 \right] \Bigg], \tag{C.B.3}$$

$$\Delta\Gamma_1^{(22)} = \frac{\Gamma_{N_2}}{128\pi^3 m_{N_1}^2} y_{2j}^\nu y_{2j}^{\nu*} \operatorname{Im}(\xi_{12}^2) \left[(2m_{N_2}^2 - m_{N_1}^2) \log\left(\frac{m_{N_2}^2}{m_{N_2}^2 - m_{N_1}^2}\right) - 2m_{N_1}^2 \right]. \tag{C.B.4}$$

When N_2 is much heavier than N_1, the expressions are reduced to

$$\Delta\Gamma_1^{(12)} + \Delta\Gamma_1^{(21)} \approx \frac{-m_{N_1}^2 \Gamma_{N_2}}{512\pi^3 m_{N_2}^2} \operatorname{Im}\left[y_{2j}^\nu y_{1j}^{\nu*} \xi_{12}^* (3\xi_{11} + 2\xi_{11}^*) \right], \tag{C.B.5}$$

$$\Delta\Gamma_1^{(22)} \approx \frac{m_{N_1}^4 \Gamma_{N_2}}{768\pi^3 m_{N_2}^4} y_{2j}^\nu y_{2j}^{\nu*} \operatorname{Im}(\xi_{12}^2). \tag{C.B.6}$$

In a similar way, we have the width differences for the N_2 resonant and non-resonant three-body decay,

$$\Delta\Gamma_2^{(11)} = \frac{m_{N_1}}{128\pi^2} \frac{m_{N_2}^2 - m_{N_1}^2}{m_{N_2}^2} y_{1j}^\nu y_{1j}^{\nu*} \operatorname{Im}(\xi_{12}^2), \tag{C.B.7}$$

$$\Delta\Gamma_2^{(12)} + \Delta\Gamma_2^{(21)} = \frac{-m_{N_1}}{128\pi^2 m_{N_2}^3} \Bigg[\left[\operatorname{Im}(y_{2j}^\nu y_{1j}^{\nu*} \xi_{22} \xi_{12}^*) m_{N_1} + \operatorname{Im}(y_{2j}^\nu y_{1j}^{\nu*} \xi_{22}^* \xi_{12}) m_{N_2} \right] (m_{N_1}^2 + m_{N_2}^2)$$

$$+ 2 \left[\operatorname{Im}(y_{2j}^\nu y_{1j}^{\nu*} \xi_{22} \xi_{12}) m_{N_1} + \operatorname{Im}(y_{2j}^\nu y_{1j}^{\nu*} \xi_{22}^* \xi_{12}^*) m_{N_2} \right] m_{N_1} m_{N_2} \Bigg], \tag{C.B.8}$$

$$\Delta\Gamma_2^{(22)} = \frac{\Gamma_{N_2}}{128\pi^3} y_{2j}^\nu y_{2j}^{\nu*} \operatorname{Im}(\xi_{22}^2) \log\left(\frac{m_{N_2}}{m_\chi}\right). \tag{C.B.9}$$

Appendix C.C   Boltzmann equations and asymmetry formulae

C.C.1   Boltzmann equations

The Boltzmann equations for the system of Eq. (C.2.1) are given by

$$Hx\frac{dY_{N_1}}{dx} = \frac{K_1(m_{N_1}/T)}{K_2(m_{N_1}/T)} Y_{N_1}^{\text{eq}} \Bigg[\sum_j \tilde\Gamma_{1j}\left(1 - \frac{Y_{N_1}}{Y_{N_1}^{\text{eq}}}\right) - \frac{1}{2}\sum_j \tilde\Gamma_{1j}\tilde\epsilon_{1j}\frac{Y_{\Delta L_j}}{Y_L^{\text{eq}}}$$

$$+ \sum_j \Gamma_{1j}\left(\frac{Y_\chi}{Y_\chi^{\text{eq}}} - \frac{Y_{N_1}}{Y_{N_1}^{\text{eq}}}\right) - \frac{1}{2}\sum_j \Gamma_{1j}\epsilon_{1j}\frac{Y_\chi}{Y_\chi^{\text{eq}}}\frac{Y_{\Delta L_j}}{Y_L^{\text{eq}}} \Bigg]$$

$$+ \frac{K_1(m_{N_2}/T)}{K_2(m_{N_2}/T)} Y_{N_2}^{\text{eq}} \Gamma_{N_2 \to N_1 \chi}\left(\frac{Y_{N_2}}{Y_{N_2}^{\text{eq}}} - \frac{Y_{N_1}}{Y_{N_1}^{\text{eq}}}\frac{Y_\chi}{Y_\chi^{\text{eq}}}\right) + C_{\text{scat.}}, \tag{C.C.1}$$

$$Hx\frac{dY_{N_2}}{dx} = \frac{K_1(m_{N_2}/T)}{K_2(m_{N_2}/T)} Y_{N_2}^{\text{eq}} \Bigg[\sum_j \tilde\Gamma_{2j}\left(1 - \frac{Y_{N_2}}{Y_{N_2}^{\text{eq}}}\right) - \frac{1}{2}\sum_j \tilde\Gamma_{2j}\tilde\epsilon_{2j}\frac{Y_{\Delta L_j}}{Y_L^{\text{eq}}}$$

$$+ \sum_j \Gamma_{2j}\left(\frac{Y_\chi}{Y_\chi^{\text{eq}}} - \frac{Y_{N_2}}{Y_{N_2}^{\text{eq}}}\right) - \frac{1}{2}\sum_j \Gamma_{2j}\epsilon_{2j}\frac{Y_\chi}{Y_\chi^{\text{eq}}}\frac{Y_{\Delta L_j}}{Y_L^{\text{eq}}}$$

$$- \Gamma_{N_2 \to N_1 \chi} \left(\frac{Y_{N_2}}{Y_{N_2}^{\text{eq}}} - \frac{Y_{N_1}}{Y_{N_1}^{\text{eq}}} \frac{Y_\chi}{Y_\chi^{\text{eq}}} \right) \Bigg] + C_{\text{scat.}}, \tag{C.C.2}$$

$$Hx\frac{dY_{\Delta L_i}}{dx} = \sum_j \frac{K_1(m_{N_j}/T)}{K_2(m_{N_j}/T)} Y_{N_j}^{\text{eq}} \Bigg[\tilde{\Gamma}_{ji}\tilde{\epsilon}_{ji}\left(\frac{Y_{N_j}}{Y_{N_j}^{\text{eq}}} - 1 \right) - \frac{1}{2}\tilde{\Gamma}_{ji}\frac{Y_{\Delta L_i}}{Y_L^{\text{eq}}}$$

$$+ \Gamma_{ji}\epsilon_{ji}\left(\frac{Y_{N_j}}{Y_{N_j}^{\text{eq}}} - \frac{Y_\chi}{Y_\chi^{\text{eq}}} \right) - \frac{1}{2}\Gamma_{ji}\frac{Y_\chi}{Y_\chi^{\text{eq}}}\frac{Y_{\Delta L_j}}{Y_L^{\text{eq}}} \Bigg]$$

$$+ C_{\text{scat.}}, \tag{C.C.3}$$

$$Hx\frac{dY_\chi}{dx} = \sum_{i,j} \frac{K_1(m_{N_i}/T)}{K_2(m_{N_i}/T)} Y_{N_i}^{\text{eq}} \Bigg[\Gamma_{ij}\left(\frac{Y_{N_i}}{Y_{N_i}^{\text{eq}}} - \frac{Y_\chi}{Y_\chi^{\text{eq}}} \right) + \frac{1}{2}\Gamma_{ij}\epsilon_{ij}\frac{Y_\chi}{Y_\chi^{\text{eq}}}\frac{Y_{\Delta L}}{Y_L^{\text{eq}}} \Bigg]$$

$$+ \frac{K_1(m_{N_2}/T)}{K_2(m_{N_2}/T)} Y_{N_2}^{\text{eq}} \Gamma_{N_2 \to N_1 \chi} \left(\frac{Y_{N_2}}{Y_{N_2}^{\text{eq}}} - \frac{Y_{N_1}}{Y_{N_1}^{\text{eq}}} \frac{Y_\chi}{Y_\chi^{\text{eq}}} \right) + C_{\text{scat.}}. \tag{C.C.4}$$

$C_{\text{scat.}}$ denotes the collision terms of the scattering divided by the entropy density with the on-shell contribution removed. In deriving these equations, the SM particles, in particular the leptons and the Higgs bosons, are assumed to be in thermal equilibrium:

$$Y_{L_j} = Y_L^{\text{eq}} + \frac{1}{2}Y_{\Delta L_j}, \quad Y_{\bar{L}_j} = Y_L^{\text{eq}} - \frac{1}{2}Y_{\Delta L_j}, \quad Y_H = Y_{\bar{H}} = Y_H^{\text{eq}}, \tag{C.C.5}$$

with the lepton asymmetry of j-th generation $Y_{\Delta L_j}$. In this paper, we analyze the Boltzmann equations with the single-flavored approximation. The total lepton asymmetry is defined by

$$Y_{\Delta L} \coloneqq \sum_i Y_{\Delta L_i}, \tag{C.C.6}$$

and the collision terms are approximated as in the following forms:

$$\sum_i \Gamma_{ji}\frac{Y_{\Delta L_i}}{Y_{L_i}^{\text{eq}}} \sim \Gamma_j\frac{Y_{\Delta L}}{Y_L^{\text{eq}}}, \quad \sum_i \Gamma_{ji}\epsilon_{ji}\frac{Y_{\Delta L_i}}{Y_{L_i}^{\text{eq}}} \sim \Gamma_j\epsilon_j\frac{Y_{\Delta L}}{Y_L^{\text{eq}}}, \tag{C.C.7}$$

$$\sum_i \tilde{\Gamma}_{ji}\frac{Y_{\Delta L_i}}{Y_{L_i}^{\text{eq}}} \sim \tilde{\Gamma}_j\frac{Y_{\Delta L}}{Y_L^{\text{eq}}}, \quad \sum_i \tilde{\Gamma}_{ji}\tilde{\epsilon}_{ji}\frac{Y_{\Delta L_i}}{Y_{L_i}^{\text{eq}}} \sim \tilde{\Gamma}_j\tilde{\epsilon}_j\frac{Y_{\Delta L}}{Y_L^{\text{eq}}}. \tag{C.C.8}$$

Using these equations, the Boltzmann equations (C.C.1)–(C.C.4) are rewritten as

$$Hx\frac{dY_{N_1}}{dx} \approx \frac{K_1(m_{N_1}/T)}{K_2(m_{N_1}/T)} Y_{N_1}^{\text{eq}} \Bigg[\tilde{\Gamma}_1\left(1 - \frac{Y_{N_1}}{Y_{N_1}^{\text{eq}}} \right) - \frac{1}{2}\tilde{\Gamma}_1\tilde{\epsilon}_1\frac{Y_{\Delta L}}{Y_L^{\text{eq}}} + \Gamma_1\left(-\frac{Y_{N_1}}{Y_{N_1}^{\text{eq}}} + \frac{Y_\chi}{Y_\chi^{\text{eq}}} \right)$$

$$- \frac{1}{2}\Gamma_1\epsilon_1\frac{Y_\chi}{Y_\chi^{\text{eq}}}\frac{Y_{\Delta L}}{Y_L^{\text{eq}}} \Bigg] + \frac{K_1(m_{N_2}/T)}{K_2(m_{N_2}/T)} Y_{N_2}^{\text{eq}} \Gamma_{N_2 \to N_1 \chi} \left(\frac{Y_{N_2}}{Y_{N_2}^{\text{eq}}} - \frac{Y_{N_1}}{Y_{N_1}^{\text{eq}}} \frac{Y_\chi}{Y_\chi^{\text{eq}}} \right) + C_{\text{scat.}},$$

$$\tag{C.4.2}$$

$$Hx\frac{dY_{N_2}}{dx} \approx \frac{K_1(m_{N_2}/T)}{K_2(m_{N_2}/T)} Y_{N_2}^{\text{eq}} \Bigg[\tilde{\Gamma}_2\left(1 - \frac{Y_{N_2}}{Y_{N_2}^{\text{eq}}} \right) - \frac{1}{2}\tilde{\Gamma}_2\tilde{\epsilon}_2\frac{Y_{\Delta L}}{Y_L^{\text{eq}}} + \Gamma_2\left(-\frac{Y_{N_2}}{Y_{N_2}^{\text{eq}}} + \frac{Y_\chi}{Y_\chi^{\text{eq}}} \right)$$

$$- \frac{1}{2}\Gamma_2\epsilon_2\frac{Y_\chi}{Y_\chi^{\rm eq}}\frac{Y_{\Delta L}}{Y_L^{\rm eq}} - \Gamma_{N_2\to N_1\chi}\left(\frac{Y_{N_2}}{Y_{N_2}^{\rm eq}} - \frac{Y_{N_1}}{Y_{N_1}^{\rm eq}}\frac{Y_\chi}{Y_\chi^{\rm eq}}\right)\Bigg] + C_{\rm scat.}, \tag{C.4.3}$$

$$Hx\frac{dY_{\Delta L}}{dx} \approx \sum_i \frac{K_1(m_{N_i}/T)}{K_2(m_{N_i}/T)}Y_{N_i}^{\rm eq}\Bigg[\tilde{\Gamma}_i\tilde{\epsilon}_i\left(\frac{Y_{N_i}}{Y_{N_i}^{\rm eq}} - 1\right) - \frac{1}{2}\tilde{\Gamma}_i\frac{Y_{\Delta L}}{Y_L^{\rm eq}}$$
$$+ \Gamma_i\epsilon_i\left(\frac{Y_{N_i}}{Y_{N_i}^{\rm eq}} - \frac{Y_\chi}{Y_\chi^{\rm eq}}\right) - \frac{1}{2}\Gamma_i\frac{Y_\chi}{Y_\chi^{\rm eq}}\frac{Y_{\Delta L}}{Y_L^{\rm eq}}\Bigg] + C_{\rm scat.}, \tag{C.4.4}$$

$$Hx\frac{dY_\chi}{dx} \approx \sum_i \frac{K_1(m_{N_i}/T)}{K_2(m_{N_i}/T)}Y_{N_i}^{\rm eq}\Bigg[\Gamma_i\left(\frac{Y_{N_i}}{Y_{N_i}^{\rm eq}} - \frac{Y_\chi}{Y_\chi^{\rm eq}}\right) + \frac{1}{2}\Gamma_i\epsilon_i\frac{Y_\chi}{Y_\chi^{\rm eq}}\frac{Y_{\Delta L}}{Y_L^{\rm eq}}\Bigg]$$
$$+ Y_{N_2}^{\rm eq}\frac{K_1(m_{N_2}/T)}{K_2(m_{N_2}/T)}\Gamma_{N_2\to N_1\chi}\left(\frac{Y_{N_2}}{Y_{N_2}^{\rm eq}} - \frac{Y_{N_1}}{Y_{N_1}^{\rm eq}}\frac{Y_\chi}{Y_\chi^{\rm eq}}\right) + C_{\rm scat.}. \tag{C.4.5}$$

C.C.2 Phenomenological formulae for lepton asymmetry

The Boltzmann equation of the lepton asymmetry (e.g. Eq. (C.4.4)) has following form:

$$\frac{dY_{\Delta L}(x)}{dx} = \mathcal{F}(x) - W(x)Y_{\Delta L}(x), \tag{C.C.9}$$

where $\mathcal{F}(x)$ is the $Y_{\Delta L}$ independent function describing the asymmetry production from decays and scatterings of N_i and $W(x)$ is the washout function. As discussed in Refs. [BCST00, BDBP04, DNN08], the solution of this equation can be expressed by

$$Y_{\Delta L}(x) = \int_{x_i}^x dx'\,\mathcal{F}(x')\exp\left[-\int_{x'}^x dx''\,W(x'')\right] + Y_{\Delta L}(x_i)\exp\left[-\int_{x_i}^x dx''\,W(x'')\right]. \tag{C.C.10}$$

Intuitively, the integral of $\mathcal{F}$ means the freeze-in like production [HJMRW10] and $e^{-\int dx'W(x')}$ denotes the washout suppression. Using this equation, we will show the approximated values of the lepton asymmetry, $\mathcal{Y}_{\Delta L}^{\rm FI}(z_1)$ and $\mathcal{Y}_{\Delta L}^{\rm WO}(\infty)$ in the following part of this section.

Case for freeze-in from N_2

N_2 is mainly produced by the first term of the rhs in Eq. (C.4.3). Using the approximation for the modified Bessel function

$$K_n(x) \underset{x\sim 0}{\sim} \frac{(n-1)!}{2}\left(\frac{x}{2}\right)^{-n}, \tag{C.C.11}$$

the Boltzmann equation is approximately written as

$$\frac{dY_{N_2}}{dx} \approx \frac{1}{Hx}\frac{K_1\left(\frac{m_{N_2}}{m_{N_1}}x\right)}{K_2\left(\frac{m_{N_2}}{m_{N_1}}x\right)}\tilde{\Gamma}_2 Y_{N_2}^{\rm eq} \sim \frac{135\sqrt{10}}{2\pi^5 g_*^{1/2}g_*^S}\frac{M_P m_{N_2}\tilde{\Gamma}_2}{m_{N_1}^3}x^2, \tag{C.C.12}$$

and the yield of N_2 is scaled by

$$Y_{N_2} = \frac{45\sqrt{10}}{2\pi^5 g_*^{1/2} g_*^S} \frac{M_P m_{N_2} \tilde{\Gamma}_2}{m_{N_1}^3} x^3. \tag{C.C.13}$$

This N_2 produces χ and N_1 via $N_2 \to N_1 \chi$ process, and their yields are also written as

$$Y_\chi = \frac{135}{2\pi^6 g_* g_*^S} \frac{M_P^2 m_{N_2}^2 \tilde{\Gamma}_2 (\Gamma_{N_2 \to N_1\chi} + \Gamma_2)}{m_{N_1}^6} x^6, \tag{C.C.14}$$

$$Y_{N_1} = \frac{45\sqrt{10}}{2\pi^5 g_*^{1/2} g_*^S} \frac{M_P \tilde{\Gamma}_1}{m_{N_1}^2} x^3 + \frac{135}{2\pi^6 g_* g_*^S} \frac{M_P^2 m_{N_2}^2 \tilde{\Gamma}_2 (\Gamma_{N_2 \to N_1\chi} + \Gamma_2)}{m_{N_1}^6} x^6. \tag{C.C.15}$$

where the contribution of the first term of the rhs in Eq. (C.4.2) is included, which is scaled by x^3 as in the same way to N_2. Using these functions, we will evaluate the lepton asymmetry. From Eq. (C.4.4), The washout function

$$W_2 := \frac{1}{2Hx} \frac{K_1(m_{N_2} x/m_{N_1})}{K_2(m_{N_2} x/m_{N_1})} \left(\tilde{\Gamma}_2 + \Gamma_2 \frac{Y_\chi}{Y_\chi^{eq}}\right) \frac{Y_{N_2}^{eq}}{Y_L^{eq}} + \frac{1}{2Hx} \frac{K_1(x)}{K_2(x)} \left(\tilde{\Gamma}_1 + \Gamma_1 \frac{Y_\chi}{Y_\chi^{eq}}\right) \frac{Y_{N_2}^{eq}}{Y_L^{eq}}, \tag{C.C.16}$$

is read, and the yield is evaluated by using (C.C.10) as

$$\mathcal{Y}_{\Delta L}^{FI}(x) = \int_0^x dx' \, \mathcal{F}_2(x') \exp\left[-\int_{x'}^x dx'' \, W_2(x'')\right], \tag{C.C.17}$$

with

$$\mathcal{F}_2 = \frac{1}{Hx} \frac{K_1(m_{N_2} x/m_{N_1})}{K_2(m_{N_2} x/m_{N_1})} \Gamma_2 \epsilon_2 \left(Y_{N_2} - \frac{Y_{N_2}^{eq}}{Y_\chi^{eq}} Y_\chi\right) + \frac{1}{Hx} \frac{K_1(x)}{K_2(x)} \Gamma_1 \epsilon_1 \left(Y_{N_1} - \frac{Y_{N_1}^{eq}}{Y_\chi^{eq}} Y_\chi\right). \tag{C.C.18}$$

If the washout suppression is weak enough, which is the case of the neutrino Yukawa couplings being small, the lepton asymmetry is mainly produced by the right-handed neutrinos before getting into the thermal bath and the total amount is evaluated as

$$Y_{\Delta L} \approx \mathcal{Y}_{\Delta L}^{FI}(z_1), \tag{C.C.19}$$

where

$$z_1 = \min(z_{N_2}, z_\chi), \quad Y_{N_2}(z_{N_2}) = \frac{45}{\pi^4 g_*^S}, \quad Y_\chi(z_\chi) = \frac{45}{2\pi^4 g_*^S}. \tag{C.C.20}$$

This is regarded as the asymmetry by the freeze-in production including the weak washout effects.

Case for strong N_1 washout

If the washout of N_1 is strong, the lepton asymmetry is mainly determined by this, and the contribution from $\mathcal{Y}_{\Delta L}^{\mathrm{FI}}(z_1)$ is exponentially suppressed. The washout function of this case is given by

$$W_1 := \frac{1}{2Hx} \frac{K_1(m_{N_2}x/m_{N_1})}{K_2(m_{N_2}x/m_{N_1})}(\tilde{\Gamma}_2 + \Gamma_2)\frac{Y_{N_2}^{\mathrm{eq}}}{Y_L^{\mathrm{eq}}} + \frac{1}{2Hx} \frac{K_1(x)}{K_2(x)}(\tilde{\Gamma}_1 + \Gamma_1)\frac{Y_{N_1}^{\mathrm{eq}}}{Y_L^{\mathrm{eq}}}, \qquad \text{(C.C.21)}$$

where $Y_\chi \approx Y_\chi^{\mathrm{eq}}$ is assumed. Then, the lepton asymmetry is written as

$$\mathcal{Y}_{\Delta L}^{\mathrm{WO}} = \int_0^x dx' \, \mathcal{F}_1(x') \exp\left[-\int_{x'}^x dx'' \, W_1(x'')\right], \qquad \text{(C.C.22)}$$

where we introduce the following function

$$\mathcal{F}_1 := \frac{1}{Hx} \frac{K_1(m_{N_2}x/m_{N_1})}{K_2(m_{N_2}x/m_{N_1})}\Gamma_2\epsilon_2\left(\frac{\tilde{\Gamma}_2 + \Gamma_2}{m_{N_2}}\right)Y_{N_2}^{\mathrm{eq}} + \frac{1}{Hx} \frac{K_1(x)}{K_2(x)}\Gamma_1\epsilon_1\left(\frac{\tilde{\Gamma}_1 + \Gamma_1}{m_{N_1}}\right)Y_{N_1}^{\mathrm{eq}}. \quad \text{(C.C.23)}$$

Using these functions, the lepton asymmetry is given by

$$Y_{\Delta L} \approx \mathcal{Y}_{\Delta L}^{\mathrm{WO}}(\infty). \qquad \text{(C.C.24)}$$

Appendix C.D Feynman rules for Majorana fermions

Let us briefly summarize the Feynman rules for the Majorana fermion $N = N^C$. The kinetic term is the standard form:

$$\mathcal{L}_{\mathrm{kin.}} = \frac{i}{2}N\slashed{\partial}N - \frac{M}{2}\overline{N}N. \qquad \text{(C.D.1)}$$

- For the propagator, we will use

$$\langle N\overline{N}\rangle = \frac{i(\slashed{p} + M)}{p^2 - m^2}, \qquad \text{(C.D.2)}$$

which is the standard propagator of the Dirac fermion [PS95]. [1] However, in addition to

$$\overset{\frown}{N\,N} \qquad \text{(C.D.5)}$$

---

[1] We will give some comments on the propagator [DEHK92]. For a Dirac fermion ψ, we introduce the propagator by

$$\langle\psi\overline{\psi}\rangle \to \frac{i}{\slashed{p} - m} = \frac{i(\slashed{p} + m)}{p^2 - m^2} = S(p). \qquad \text{(C.D.3)}$$

The charge conjugation of this Dirac propagator is given by

$$\langle\psi^C\overline{\psi^C}\rangle = C^{\,\mathrm{t}}(\langle\psi\overline{\psi}\rangle)C^{-1} \to C^{\,\mathrm{t}}S(p)C^{-1} = \frac{i}{-\slashed{p} - m} = S(-p) =: S'(p). \qquad \text{(C.D.4)}$$

the all possible contraction should be considered due to the Majorana fermion such as

$$\overset{\frown}{NN} \quad \overset{\frown}{NN}. \tag{C.D.6}$$

- For the interaction vertex, we will use the standard Feynman rules from the expansion of the partition function

$$\int \mathcal{D}N \, e^{iS_{\mathrm{kin}}} e^{iS_{\mathrm{int}}} \approx \int \mathcal{D}N \, e^{iS_{\mathrm{kin}}} \sum_{n=0} \frac{(iS_{\mathrm{int}})^n}{n!}. \tag{C.D.7}$$

In this calculation, We havue to consider the following possible contractions

$$\overset{\frown}{N\overline{N}} \quad \overset{\frown}{NN} \quad \overset{\frown}{\overline{N}N}.$$

For the interaction Lagrangian such as $\overline{\chi}\mathcal{O}_A\psi$, we determine to use $\overset{\frown}{N\overline{N}}$ as the propagator, and other rules are constructed so that they are consistent with this propagator rule. In order to pursue this method, we will rewrite the interaction Lagrangian in the $\overline{\psi^C}\epsilon_A \, {}^t\mathcal{O}_A\chi^C$ form by using the following flip formula:

$$\overline{\chi}\mathcal{O}_A\psi = \overline{\psi^C}C \, {}^t\mathcal{O}_A C^{-1}\chi^C. \tag{C.D.8}$$

In particular, the transformation rule of the basis of the spinor bi-linear is given by

$$\overline{\chi}\mathcal{O}_A\psi = \epsilon_A\overline{\psi^C}\mathcal{O}_A\chi^C,$$

$$\epsilon_A = \begin{cases} +1 & : \mathcal{O}_A = \mathbb{1}, \ \gamma_5, \ i\gamma_5\gamma_\mu \\ -1 & : \mathcal{O}_A = \gamma_\mu, \ \sigma_{\mu\nu} \end{cases}. \tag{C.D.9}$$

The point is that the signature is controlled by γ-matrices and other terms are rewritten as ${}^t\mathcal{O}_A$.

- For the outline spinor, we will use the standard wavefunction:

  – Dirac fermion: The mode expansion is given by

$$\psi(x) = \int \frac{d^3p}{(2\pi)^3 2E_{\boldsymbol{p}}} \sum_s \left[b_{\boldsymbol{p}}^s u^s(p)e^{-ip\cdot x} + d_{\boldsymbol{p}}^{s\dagger} v^s(p)e^{ip\cdot x} \right], \tag{C.D.10}$$

$$\overline{\psi}(x) = \int \frac{d^3p}{(2\pi)^3 2E_{\boldsymbol{p}}} \sum_s \left[b_{\boldsymbol{p}}^{s\dagger}\overline{u^s}(p)e^{ip\cdot x} + d_{\boldsymbol{p}}^s\overline{v^s}(p)e^{-ip\cdot x} \right], \tag{C.D.11}$$

  then we get the following relations:

$$\overset{\frown}{\psi b_{\boldsymbol{p}}^{s\dagger}} \to u^s(p), \quad \overset{\frown}{b_{\boldsymbol{p}}^s\overline{\psi}} \to \overline{u^s}(p), \quad \overset{\frown}{\overline{\psi}d_{\boldsymbol{p}}^{s\dagger}} \to \overline{v^s}(p), \quad \overset{\frown}{d_{\boldsymbol{p}}^s\psi} \to v^s(p) \tag{C.D.12}$$

– ψ^C: the charge conjugation of ψ is given by

$$\psi^C = C\,{}^{\mathrm{t}}\overline{\psi}, \quad \overline{\psi^C} = -\,{}^{\mathrm{t}}\psi C^{-1}, \tag{C.D.13}$$

where C satisfies

$$C^\dagger = C^{-1}, \quad {}^{\mathrm{t}}C = -C, \quad C^{-1}\gamma^\mu C = -\,{}^{\mathrm{t}}\gamma^\mu. \tag{C.D.14}$$

We note that the wavefunctions satisfy

$$u^s(p) = C\,{}^{\mathrm{t}}\overline{v^s}(p), \quad v^s(p) = C\,{}^{\mathrm{t}}\overline{u^s}(p). \tag{C.D.15}$$

The mode expansion of the fermion is

$$\psi^C = \int \frac{d^3 p}{(2\pi)^3 2E_{\boldsymbol{p}}} \sum_s \left[b_{\boldsymbol{p}}^{s\dagger} v^s(p) e^{ip\cdot x} + d_{\boldsymbol{p}}^s u^s(p) e^{-ip\cdot x} \right], \tag{C.D.16}$$

$$\overline{\psi^C} = \int \frac{d^3 p}{(2\pi)^3 2E_{\boldsymbol{p}}} \sum_s \left[b_{\boldsymbol{p}}^s \overline{v^s}(p) e^{-ip\cdot x} + d_{\boldsymbol{p}}^{s\dagger} \overline{u^s}(p) e^{ip\cdot x} \right], \tag{C.D.17}$$

then the following relations are read:

$$\overbrace{\psi^C d_{\boldsymbol{p}}^{s\dagger}} \to u^s(p), \quad \overbrace{d_{\boldsymbol{p}}^s \overline{\psi^C}} \to \overline{u^s}(p), \quad \overbrace{\overline{\psi^C} b_{\boldsymbol{p}}^{s\dagger}} \to \overline{v^s}(p), \quad \overbrace{b_{\boldsymbol{p}}^s \psi^C} \to v^s(p) \tag{C.D.18}$$

Example

Let us the following neutrino Yukawa interaction:

$$\mathcal{L}_{\text{int.}} = -\overline{N} y \tilde{H}^\dagger P_L L - \overline{L} y^\dagger \tilde{H} P_R N. \tag{C.D.19}$$

The amplitude contributing to the see-saw diagram is evaluated as

$$\begin{aligned}
i\mathcal{M} &= \frac{1}{2!} \left[-i\overline{N} y \tilde{H}^\dagger P_L L \right] \left[-i\overline{N} y \tilde{H}^\dagger P_L L \right] \\
&= \frac{1}{2!} \left[-i\overline{L^C}\,{}^{\mathrm{t}}(y\tilde{H}^\dagger P_L) N \right] \left[-i\overline{N} y \tilde{H}^\dagger P_L L \right] \\
&\sim -\frac{1}{2}\overline{u_L} \frac{{}^{\mathrm{t}} yy v^2}{2} P_L \frac{i(\slashed{q} + M)}{q^2 - M^2} P_L u_L \tag{C.D.20} \\
&= -\frac{1}{2}\overline{u_L} \frac{{}^{\mathrm{t}} yy v^2}{2} \frac{iM}{q^2 - M^2} P_L u_L. \tag{C.D.21}
\end{aligned}$$

References

[A+12]   **ATLAS** Collaboration, G. Aad *et al.*, *Observation of a new particle in the search for the Standard Model Higgs boson with the ATLAS detector at the LHC*, Phys. Lett. B **716** (2012) 1–29 [arXiv:1207.7214 [hep-ex]].

[A+16]   **ATLAS, CMS** Collaboration, G. Aad *et al.*, *Measurements of the Higgs boson production and decay rates and constraints on its couplings from a combined ATLAS and CMS analysis of the LHC pp collision data at $\sqrt{s} = 7$ and 8 TeV*, JHEP **08** (2016) 045 [arXiv:1606.02266 [hep-ex]].

[A+17a]   **LUX** Collaboration, D. S. Akerib *et al.*, *Limits on spin-dependent WIMP-nucleon cross section obtained from the complete LUX exposure*, Phys. Rev. Lett. **118** no. 25, (2017) 251302 [arXiv:1705.03380 [astro-ph.CO]].

[A+17b]   **Fermi-LAT, DES** Collaboration, A. Albert *et al.*, *Searching for Dark Matter Annihilation in Recently Discovered Milky Way Satellites with Fermi-LAT*, Astrophys. J. **834** no. 2, (2017) 110 [arXiv:1611.03184 [astro-ph.HE]].

[A+18]   **XENON** Collaboration, E. Aprile *et al.*, *Dark Matter Search Results from a One Ton-Year Exposure of XENON1T*, Phys. Rev. Lett. **121** no. 11, (2018) 111302 [arXiv:1805.12562 [astro-ph.CO]].

[A+19a]   **ATLAS** Collaboration, M. Aaboud *et al.*, *Combination of searches for invisible Higgs boson decays with the ATLAS experiment*, Phys. Rev. Lett. **122** no. 23, (2019) 231801 [arXiv:1904.05105 [hep-ex]].

[A+19b]   **IceCube** Collaboration, M. G. Aartsen *et al.*, *Neutrino astronomy with the next generation IceCube Neutrino Observatory*, arXiv:1911.02561 [astro-ph.HE].

[A+20a]   **Planck** Collaboration, N. Aghanim *et al.*, *Planck 2018 results. VI. Cosmological parameters*, Astron. Astrophys. **641** (2020) A6 [arXiv:1807.06209 [astro-ph.CO]]. [Erratum: Astron.Astrophys. 652, C4 (2021)].

[A⁺20b]   **Planck** Collaboration, N. Aghanim *et al.*, *Planck 2018 results. VI. Cosmological parameters*, Astron. Astrophys. **641** (2020) A6 [arXiv:1807.06209 [astro-ph.CO]]. [Erratum: Astron.Astrophys. 652, C4 (2021)].

[A⁺20c]   **Planck** Collaboration, Y. Akrami *et al.*, *Planck 2018 results. X. Constraints on inflation*, Astron. Astrophys. **641** (2020) A10 [arXiv:1807.06211 [astro-ph.CO]].

[A⁺20d]   **XENON** Collaboration, E. Aprile *et al.*, *Projected WIMP sensitivity of the XENONnT dark matter experiment*, JCAP **11** (2020) 031 [arXiv:2007.08796 [physics.ins-det]].

[A⁺21]   **Muon g-2** Collaboration, T. Albahri *et al.*, *Measurement of the anomalous precession frequency of the muon in the Fermilab Muon $g-2$ Experiment*, Phys. Rev. D **103** no. 7, (2021) 072002 [arXiv:2104.03247 [hep-ex]].

[ABC⁺90] M. G. Alford, K. Benson, S. R. Coleman, J. March-Russell, and F. Wilczek, *The Interactions and Excitations of Nonabelian Vortices*, Phys. Rev. Lett. **64** (1990) 1632. [Erratum: Phys.Rev.Lett. 65, 668 (1990)].

[ABC⁺91] M. G. Alford, K. Benson, S. R. Coleman, J. March-Russell, and F. Wilczek, *Zero modes of nonabelian vortices*, Nucl. Phys. B **349** (1991) 414–438.

[ABD⁺20] C. Arina, A. Beniwal, C. Degrande, J. Heisig, and A. Scaffidi, *Global fit of pseudo-Nambu-Goldstone Dark Matter*, JHEP **04** (2020) 015 [arXiv:1912.04008 [hep-ph]].

[ABDK06] P. Anastasopoulos, M. Bianchi, E. Dudas, and E. Kiritsis, *Anomalies, anomalous U(1)'s and generalized Chern-Simons terms*, JHEP **11** (2006) 057 [arXiv:hep-th/0605225].

[Abe20]   T. Abe, *Effect of the early kinetic decoupling in a fermionic dark matter model*, Phys. Rev. D **102** no. 3, (2020) 035018 [arXiv:2004.10041 [hep-ph]].

[ABM⁺04] C. S. Aulakh, B. Bajc, A. Melfo, G. Senjanovic, and F. Vissani, *The Minimal supersymmetric grand unified theory*, Phys. Lett. B **588** (2004) 196–202 [arXiv:hep-ph/0306242].

[Abr57]   A. A. Abrikosov, *On the Magnetic properties of superconductors of the second group*, Sov. Phys. JETP **5** (1957) 1174–1182.

[ACE20]   D. Andriot, N. Cribiori, and D. Erkinger, *The web of swampland conjectures and the TCC bound*, JHEP **07** (2020) 162 [arXiv:2004.00030 [hep-th]].

[ADD+10]   A. Arvanitaki, S. Dimopoulos, S. Dubovsky, N. Kaloper, and J. March-Russell, *String Axiverse*, Phys. Rev. D **81** (2010) 123530 [arXiv:0905.4720 [hep-th]].

[ADG+19]   D. Azevedo, M. Duch, B. Grzadkowski, D. Huang, M. Iglicki, and R. Santos, *One-loop contribution to dark-matter-nucleon scattering in the pseudo-scalar dark matter model*, JHEP **01** (2019) 138 [arXiv:1810.06105 [hep-ph]].

[AFH19]   T. Abe, M. Fujiwara, and J. Hisano, *Loop corrections to dark matter direct detection in a pseudoscalar mediator dark matter model*, JHEP **02** (2019) 028 [arXiv:1810.01039 [hep-ph]].

[AFHS20]   T. Abe, M. Fujiwara, J. Hisano, and Y. Shoji, *Maximum value of the spin-independent cross section in the 2HDM+a*, JHEP **01** (2020) 114 [arXiv:1910.09771 [hep-ph]].

[AFI+01a]   G. Aldazabal, S. Franco, L. E. Ibanez, R. Rabadan, and A. M. Uranga, *D = 4 chiral string compactifications from intersecting branes*, J. Math. Phys. **42** (2001) 3103–3126 [arXiv:hep-th/0011073].

[AFI+01b]   G. Aldazabal, S. Franco, L. E. Ibanez, R. Rabadan, and A. M. Uranga, *Intersecting brane worlds*, JHEP **02** (2001) 047 [arXiv:hep-ph/0011132].

[AHCG01]   N. Arkani-Hamed, A. G. Cohen, and H. Georgi, *(De)constructing dimensions*, Phys. Rev. Lett. **86** (2001) 4757–4761 [arXiv:hep-th/0104005].

[AHMNV07]   N. Arkani-Hamed, L. Motl, A. Nicolis, and C. Vafa, *The String landscape, black holes and gravity as the weakest force*, JHEP **06** (2007) 060 [arXiv:hep-th/0601001].

[AHO+20]   Y. Abe, Y. Hamada, T. Ohata, K. Suzuki, and K. Yoshioka, *TeV-scale Majorogenesis*, JHEP **07** no. 07, (2020) 105 [arXiv:2004.00599 [hep-ph]].

[AHT20]   Y. Abe, T. Higaki, and R. Takahashi, *Implications of the weak gravity conjecture in anomalous quiver gauge theories*, Phys. Rev. D **102** no. 6, (2020) 065004 [arXiv:2004.14917 [hep-th]].

[AHY21]   Y. Abe, Y. Hamada, and K. Yoshioka, *Electroweak axion string and superconductivity*, JHEP **06** (2021) 172 [arXiv:2010.02834 [hep-ph]].

[AIM06]   T. Asaka, K. Ishiwata, and T. Moroi, *Right-handed sneutrino as cold dark matter*, Phys. Rev. D **73** (2006) 051301 [arXiv:hep-ph/0512118].

[AIM07]   T. Asaka, K. Ishiwata, and T. Moroi, *Right-handed sneutrino as cold dark matter of the universe*, Phys. Rev. D **75** (2007) 065001 [arXiv:hep-ph/0612211].

[AIQU00]   G. Aldazabal, L. E. Ibanez, F. Quevedo, and A. M. Uranga, *D-branes at singularities: A Bottom up approach to the string embedding of the standard model*, JHEP **08** (2000) 002 [arXiv:hep-th/0005067].

[AIY21]   Y. Abe, T. Ito, and K. Yoshioka, *Leptonic CP asymmetry and Light flavored scalar*, arXiv:2110.11096 [hep-ph].

[AKMY03]   H. Abe, T. Kobayashi, N. Maru, and K. Yoshioka, *Field localization in warped gauge theories*, Phys. Rev. D **67** (2003) 045019 [arXiv:hep-ph/0205344].

[AKS20]   W. Abdallah, A. Kumar, and A. K. Saha, *Soft leptogenesis in the NMSSM with a singlet right-handed neutrino superfield*, JHEP **04** (2020) 065 [arXiv:1911.03363 [hep-ph]].

[ALQ$^+$18] G. Arcadi, M. Lindner, F. S. Queiroz, W. Rodejohann, and S. Vogl, *Pseudoscalar Mediators: A WIMP model at the Neutrino Floor*, JCAP **03** (2018) 042 [arXiv:1711.02110 [hep-ph]].

[AM83]   C. S. Aulakh and R. N. Mohapatra, *Implications of Supersymmetric SO(10) Grand Unification*, Phys. Rev. D **28** (1983) 217.

[AM13]   G. Altarelli and D. Meloni, *A non supersymmetric SO(10) grand unified model for all the physics below M_{GUT}*, JHEP **08** (2013) 021 [arXiv:1305.1001 [hep-ph]].

[AO90a]   J. Ambjorn and P. Olesen, *A Condensate Solution of the Electroweak Theory Which Interpolates Between the Broken and the Symmetric Phase*, Nucl. Phys. B **330** (1990) 193–204.

[AO90b]   J. Ambjorn and P. Olesen, *Electroweak Magnetism: Theory and Application*, Int. J. Mod. Phys. A **5** (1990) 4525–4558.

[AO92]   J. Ambjorn and P. Olesen, *Electroweak magnetism, W condensation and antiscreening*, in 4th Hellenic School on Elementary Particle Physics, pp. 396–406. 9, 1992. arXiv:hep-ph/9304220.

[AS83]   L. F. Abbott and P. Sikivie, *A Cosmological Bound on the Invisible Axion*, Phys. Lett. B **120** (1983) 133–136.

[AS98]   R. Adhikari and U. Sarkar, *Baryogenesis in a supersymmetric model without R-parity*, Phys. Lett. B **427** (1998) 59–64 [arXiv:hep-ph/9610221].

[AT21]   Y. Abe and T. Toma, *Direct detection of pseudo-Nambu-Goldstone dark matter with light mediator*, Phys. Lett. B **822** (2021) 136639 [arXiv:2108.10647 [hep-ph]].

[ATT20]   Y. Abe, T. Toma, and K. Tsumura, *Pseudo-Nambu-Goldstone dark matter from gauged $U(1)_{B-L}$ symmetry*, JHEP **05** (2020) 057 [arXiv:2001.03954 [hep-ph]].

[ATTY21]   Y. Abe, T. Toma, K. Tsumura, and N. Yamatsu, *Pseudo-Nambu-Goldstone dark matter model inspired by grand unification*, Phys. Rev. D **104** no. 3, (2021) 035011 [arXiv:2104.13523 [hep-ph]].

[ATY21]   Y. Abe, T. Toma, and K. Yoshioka, *Non-thermal Production of PNGB Dark Matter and Inflation*, JHEP **03** (2021) 130 [arXiv:2012.10286 [hep-ph]].

[AV00]   A. Achucarro and T. Vachaspati, *Semilocal and electroweak strings*, Phys. Rept. **327** (2000) 347–426 [arXiv:hep-ph/9904229].

[B+06]   C. A. Baker *et al.*, *An Improved experimental limit on the electric dipole moment of the neutron*, Phys. Rev. Lett. **97** (2006) 131801 [arXiv:hep-ex/0602020].

[B+19]   X. Bai *et al.*, *The Large High Altitude Air Shower Observatory (LHAASO) Science White Paper*, arXiv:1905.02773 [astro-ph.HE].

[Bar95]   M. Barriola, *Electroweak strings that produce baryons*, Phys. Rev. D **51** (1995) 300–304 [arXiv:hep-ph/9403323].

[BBD+17]   D. Barducci, A. Bharucha, N. Desai, M. Frigerio, B. Fuks, A. Goudelis, S. Kulkarni, G. Polesello, and D. Sengupta, *Monojet searches for momentum-dependent dark matter interactions*, JHEP **01** (2017) 078 [arXiv:1609.07490 [hep-ph]].

[BBDR18]   T. Bandyopadhyay, G. Bhattacharyya, D. Das, and A. Raychaudhuri, *Reappraisal of constraints on Z' models from unitarity and direct searches at the LHC*, Phys. Rev. D **98** no. 3, (2018) 035027 [arXiv:1803.07989 [hep-ph]].

[BBG+18a] G. Bélanger, F. Boudjema, A. Goudelis, A. Pukhov, and B. Zaldivar, *micrOMEGAs5.0 : Freeze-in*, Comput. Phys. Commun. **231** (2018) 173–186 [arXiv:1801.03509 [hep-ph]].

[BBG⁺18b] G. Bélanger, F. Boudjema, A. Goudelis, A. Pukhov, and B. Zaldivar, *microOMEGAs5.0 : Freeze-in*, Comput. Phys. Commun. **231** (2018) 173–186 [arXiv:1801.03509 [hep-ph]].

[BBGH17] T. Binder, T. Bringmann, M. Gustafsson, and A. Hryczuk, *Early kinetic decoupling of dark matter: when the standard way of calculating the thermal relic density fails*, Phys. Rev. D **96** no. 11, (2017) 115010 [arXiv:1706.07433 [astro-ph.CO]]. [Erratum: Phys.Rev.D 101, 099901 (2020)].

[BBLM20] K. Benakli, C. Branchina, and G. Lafforgue-Marmet, *Revisiting the scalar weak gravity conjecture*, Eur. Phys. J. C **80** no. 8, (2020) 742 [arXiv:2004.12476 [hep-th]].

[BBP11] R. A. Battye, G. D. Brawn, and A. Pilaftsis, *Vacuum Topology of the Two Higgs Doublet Model*, JHEP **08** (2011) 020 [arXiv:1106.3482 [hep-ph]].

[BBS18] N. F. Bell, G. Busoni, and I. W. Sanderson, *Loop Effects in Direct Detection*, JCAP **08** (2018) 017 [arXiv:1803.01574 [hep-ph]]. [Erratum: JCAP 01, E01 (2019)].

[BCM⁺09] N. Bevis, E. J. Copeland, P.-Y. Martin, G. Niz, A. Pourtsidou, P. M. Saffin, and D. A. Steer, *Evolution and stability of cosmic string loops with Y-junctions*, Phys. Rev. D **80** (2009) 125030 [arXiv:0904.2127 [hep-th]].

[BCMU20] G. Buratti, J. Calderon, A. Mininno, and A. M. Uranga, *Discrete Symmetries, Weak Coupling Conjecture and Scale Separation in AdS Vacua*, JHEP **06** (2020) 083 [arXiv:2003.09740 [hep-th]].

[BCP13] A. Belyaev, N. D. Christensen, and A. Pukhov, *CalcHEP 3.4 for collider physics within and beyond the Standard Model*, Comput. Phys. Commun. **184** (2013) 1729–1769 [arXiv:1207.6082 [hep-ph]].

[BCST00] R. Barbieri, P. Creminelli, A. Strumia, and N. Tetradis, *Baryogenesis through leptogenesis*, Nucl. Phys. B **575** (2000) 61–77 [arXiv:hep-ph/9911315].

[BD88] T. Banks and L. J. Dixon, *Constraints on String Vacua with Space-Time Supersymmetry*, Nucl. Phys. B **307** (1988) 93–108.

[BDBP04] W. Buchmuller, P. Di Bari, and M. Plumacher, *Some aspects of thermal leptogenesis*, New J. Phys. **6** (2004) 105 [arXiv:hep-ph/0406014].

[BDLM09] S. Bertolini, L. Di Luzio, and M. Malinsky, *Intermediate mass scales in the non-supersymmetric SO(10) grand unification: A Reappraisal*, Phys. Rev. D **80** (2009) 015013 [arXiv:0903.4049 [hep-ph]].

[BDM20]   D. Borah, A. Dasgupta, and D. Mahanta, *Dark Sector Assisted Low Scale Leptogenesis from Three Body Decay*, arXiv:2008.10627 [hep-ph].

[BGM+16]   I. Brivio, M. B. Gavela, L. Merlo, K. Mimasu, J. M. No, R. del Rey, and V. Sanz, *Non-linear Higgs portal to Dark Matter*, JHEP **04** (2016) 141 [arXiv:1511.01099 [hep-ph]].

[BGQS16]   M. G. Baring, T. Ghosh, F. S. Queiroz, and K. Sinha, *New Limits on the Dark Matter Lifetime from Dwarf Spheroidal Galaxies using Fermi-LAT*, Phys. Rev. D **93** no. 10, (2016) 103009 [arXiv:1510.00389 [hep-ph]].

[BHW05]   R. Blumenhagen, G. Honecker, and T. Weigand, *Supersymmetric (non-)Abelian bundles in the Type I and SO(32) heterotic string*, JHEP **08** (2005) 009 [arXiv:hep-th/0507041].

[BK94]   L. M. A. Bettencourt and T. W. B. Kibble, *Nonintercommuting configurations in the collisions of type I U(1) cosmic strings*, Phys. Lett. B **332** (1994) 297–304 [arXiv:hep-ph/9405221].

[BK15]   K. S. Babu and S. Khan, *Minimal nonsupersymmetric SO*(10) *model: Gauge coupling unification, proton decay, and fermion masses*, Phys. Rev. D **92** no. 7, (2015) 075018 [arXiv:1507.06712 [hep-ph]].

[BKLS07]   R. Blumenhagen, B. Kors, D. Lust, and S. Stieberger, *Four-dimensional String Compactifications with D-Branes, Orientifolds and Fluxes*, Phys. Rept. **445** (2007) 1–193 [arXiv:hep-th/0610327].

[BL94]   G. Bimonte and G. Lozano, *Vortex solutions in two Higgs doublet systems*, Phys. Lett. B **326** (1994) 270–275 [arXiv:hep-ph/9401313].

[BLM97]   L. M. A. Bettencourt, P. Laguna, and R. A. Matzner, *Nonintercommuting cosmic strings*, Phys. Rev. Lett. **78** (1997) 2066–2069 [arXiv:hep-ph/9612350].

[BLPZ06]   B. A. Burrington, J. T. Liu, and L. A. Pando Zayas, *Finite Heisenberg groups in quiver gauge theories*, Nucl. Phys. B **747** (2006) 436–454 [arXiv:hep-th/0602094].

[BLS03]   R. Blumenhagen, D. Lust, and S. Stieberger, *Gauge unification in supersymmetric intersecting brane worlds*, JHEP **07** (2003) 036 [arXiv:hep-th/0305146].

[BM93]   K. S. Babu and R. N. Mohapatra, *Predictive neutrino spectrum in minimal SO(10) grand unification*, Phys. Rev. Lett. **70** (1993) 2845–2848 [arXiv:hep-ph/9209215].

[BMS10]   V. Barger, M. McCaskey, and G. Shaughnessy, *Complex Scalar Dark Matter vis-\'a-vis CoGeNT, DAMA/LIBRA and XENON100*, Phys. Rev. D **82** (2010) 035019 [arXiv:1005.3328 [hep-ph]].

[BMSV06]   B. Bajc, A. Melfo, G. Senjanovic, and F. Vissani, *Yukawa sector in non-supersymmetric renormalizable SO(10)*, Phys. Rev. D **73** (2006) 055001 [arXiv:hep-ph/0510139].

[BMSV14]   S. M. Boucenna, S. Morisi, Q. Shafi, and J. W. F. Valle, *Inflation and majoron dark matter in the seesaw mechanism*, Phys. Rev. D **90** no. 5, (2014) 055023 [arXiv:1404.3198 [hep-ph]].

[Bor00]   B. Borasoy, *The Electric dipole moment of the neutron in chiral perturbation theory*, Phys. Rev. D **61** (2000) 114017 [arXiv:hep-ph/0004011].

[BRSW17]   R. Balkin, M. Ruhdorfer, E. Salvioni, and A. Weiler, *Charged Composite Scalar Dark Matter*, JHEP **11** (2017) 094 [arXiv:1707.07685 [hep-ph]].

[BRSW18]   R. Balkin, M. Ruhdorfer, E. Salvioni, and A. Weiler, *Dark matter shifts away from direct detection*, JCAP **11** (2018) 050 [arXiv:1809.09106 [hep-ph]].

[BRT99]   C. Bachas, B. Rai, and T. N. Tomaras, *New string excitations in the two Higgs standard model*, Phys. Rev. Lett. **82** (1999) 2443–2446 [arXiv:hep-ph/9801263].

[BS08a]   N. Bevis and P. M. Saffin, *Cosmic string Y-junctions: A Comparison between field theoretic and Nambu-Goto dynamics*, Phys. Rev. D **78** (2008) 023503 [arXiv:0804.0200 [hep-th]].

[BS08b]   F. L. Bezrukov and M. Shaposhnikov, *The Standard Model Higgs boson as the inflaton*, Phys. Lett. B **659** (2008) 703–706 [arXiv:0710.3755 [hep-th]].

[BS11]   T. Banks and N. Seiberg, *Symmetries and Strings in Field Theory and Gravity*, Phys. Rev. D **83** (2011) 084019 [arXiv:1011.5120 [hep-th]].

[BV91]   L. Bento and J. W. F. Valle, *The Simplest model for the 17-KeV neutrino and the MSW effect*, Phys. Lett. B **264** (1991) 373–380.

[BVB94]   M. Barriola, T. Vachaspati, and M. Bucher, *Embedded defects*, Phys. Rev. D **50** (1994) 2819–2825 [arXiv:hep-th/9306120].

[C+12]   **CMS** Collaboration, S. Chatrchyan *et al.*, *Observation of a New Boson at a Mass of 125 GeV with the CMS Experiment at the LHC*, Phys. Lett. B **716** (2012) 30–61 [arXiv:1207.7235 [hep-ex]].

[C+16]   **CTA** Collaboration, J. Carr *et al.*, *Prospects for Indirect Dark Matter Searches with the Cherenkov Telescope Array (CTA)*, PoS **ICRC2015** (2016) 1203 [arXiv:1508.06128 [astro-ph.HE]].

[C+17]   **PandaX-II** Collaboration, X. Cui *et al.*, *Dark Matter Results From 54-Ton-Day Exposure of PandaX-II Experiment*, Phys. Rev. Lett. **119** no. 18, (2017) 181302 [arXiv:1708.06917 [astro-ph.CO]].

[CACM16]   T. Charnock, A. Avgoustidis, E. J. Copeland, and A. Moss, *CMB constraints on cosmic strings and superstrings*, Phys. Rev. D **93** no. 12, (2016) 123503 [arXiv:1603.01275 [astro-ph.CO]].

[CDF20]   D. B. Costa, B. A. Dobrescu, and P. J. Fox, *Chiral Abelian gauge theories with few fermions*, Phys. Rev. D **101** no. 9, (2020) 095032 [arXiv:2001.11991 [hep-ph]].

[CDL15]   C.-Y. Chen, S. Dawson, and I. M. Lewis, *Exploring resonant di-Higgs boson production in the Higgs singlet model*, Phys. Rev. D **91** no. 3, (2015) 035015 [arXiv:1410.5488 [hep-ph]].

[CGGK19]   N. Craig, I. Garcia Garcia, and S. Koren, *Discrete Gauge Symmetries and the Weak Gravity Conjecture*, JHEP **05** (2019) 140 [arXiv:1812.08181 [hep-th]].

[CGGK20]   N. Craig, I. Garcia Garcia, and G. D. Kribs, *The UV fate of anomalous U(1)s and the Swampland*, JHEP **11** (2020) 063 [arXiv:1912.10054 [hep-ph]].

[CGIT10]   L. Covi, M. Grefe, A. Ibarra, and D. Tran, *Neutrino Signals from Dark Matter Decay*, JCAP **04** (2010) 017 [arXiv:0912.3521 [hep-ph]].

[CGN20]   P. Cox, T. Gherghetta, and M. D. Nguyen, *A Holographic Perspective on the Axion Quality Problem*, JHEP **01** (2020) 188 [arXiv:1911.09385 [hep-ph]].

[CGR12]   M. Cicoli, M. Goodsell, and A. Ringwald, *The type IIB string axiverse and its low-energy phenomenology*, JHEP **10** (2012) 146 [arXiv:1206.0819 [hep-th]].

[CH85]   C. G. Callan, Jr. and J. A. Harvey, *Anomalies and Fermion Zero Modes on Strings and Domain Walls*, Nucl. Phys. B **250** (1985) 427–436.

[CHN20]   C. Chatterjee, T. Higaki, and M. Nitta, *Note on a solution to domain wall problem with the Lazarides-Shafi mechanism in axion dark matter models*, Phys. Rev. D **101** no. 7, (2020) 075026 [arXiv:1903.11753 [hep-ph]].

[CHR09]   M. Cvetic, J. Halverson, and R. Richter, *Realistic Yukawa structures from orientifold compactifications*, JHEP **12** (2009) 063 [arXiv:0905.3379 [hep-th]].

[CHS99]   S. Chang, C. Hagmann, and P. Sikivie, *Studies of the motion and decay of axion walls bounded by strings*, Phys. Rev. D **59** (1999) 023505 [arXiv:hep-ph/9807374].

[CI01]   J. A. Casas and A. Ibarra, *Oscillating neutrinos and $\mu \to e, \gamma$*, Nucl. Phys. B **618** (2001) 171–204 [arXiv:hep-ph/0103065].

[CIM02a]   D. Cremades, L. E. Ibanez, and F. Marchesano, *Intersecting brane models of particle physics and the Higgs mechanism*, JHEP **07** (2002) 022 [arXiv:hep-th/0203160].

[CIM02b]   D. Cremades, L. E. Ibanez, and F. Marchesano, *SUSY quivers, intersecting branes and the modest hierarchy problem*, JHEP **07** (2002) 009 [arXiv:hep-th/0201205].

[CIM03]   D. Cremades, L. E. Ibanez, and F. Marchesano, *Yukawa couplings in intersecting D-brane models*, JHEP **07** (2003) 038 [arXiv:hep-th/0302105].

[CIM04]   D. Cremades, L. E. Ibanez, and F. Marchesano, *Computing Yukawa couplings from magnetized extra dimensions*, JHEP **05** (2004) 079 [arXiv:hep-th/0404229].

[CK86]   D. Chang and A. Kumar, *Symmetry Breaking of SO(10) by 210-dimensional Higgs Boson and the Michel's Conjecture*, Phys. Rev. D **33** (1986) 2695.

[CKS06]   E. J. Copeland, T. W. B. Kibble, and D. A. Steer, *Collisions of strings with Y junctions*, Phys. Rev. Lett. **97** (2006) 021602 [arXiv:hep-th/0601153].

[CKS07]   E. J. Copeland, T. W. B. Kibble, and D. A. Steer, *Constraints on string networks with junctions*, Phys. Rev. D **75** (2007) 065024 [arXiv:hep-th/0611243].

[CMG+85]   D. Chang, R. N. Mohapatra, J. Gipson, R. E. Marshak, and M. K. Parida, *Experimental Tests of New SO(10) Grand Unification*, Phys. Rev. D **31** (1985) 1718.

[CMK19]   J. Chakrabortty, R. Maji, and S. F. King, *Unification, Proton Decay and Topological Defects in non-SUSY GUTs with Thresholds*, Phys. Rev. D **99** no. 9, (2019) 095008 [arXiv:1901.05867 [hep-ph]].

[CMP80]   Y. Chikashige, R. N. Mohapatra, and R. D. Peccei, *Spontaneously Broken Lepton Number and Cosmological Constraints on the Neutrino Mass Spectrum*, Phys. Rev. Lett. **45** (1980) 1926.

[CMP81]   Y. Chikashige, R. N. Mohapatra, and R. D. Peccei, *Are There Real Goldstone Bosons Associated with Broken Lepton Number?*, Phys. Lett. B **98** (1981) 265–268.

[CMP84a]   D. Chang, R. N. Mohapatra, and M. K. Parida, *A New Approach to Left-Right Symmetry Breaking in Unified Gauge Theories*, Phys. Rev. D **30** (1984) 1052.

[CMP84b]   D. Chang, R. N. Mohapatra, and M. K. Parida, *Decoupling Parity and SU(2)-R Breaking Scales: A New Approach to Left-Right Symmetric Models*, Phys. Rev. Lett. **52** (1984) 1072.

[CPS20]   M. Chakraborty, M. K. Parida, and B. Sahoo, *Triplet Leptogenesis, Type-II Seesaw Dominance, Intrinsic Dark Matter, Vacuum Stability and Proton Decay in Minimal SO(10) Breakings*, JCAP **01** (2020) 049 [arXiv:1906.05601 [hep-ph]].

[CR14]   C. Cheung and G. N. Remmen, *Naturalness and the Weak Gravity Conjecture*, Phys. Rev. Lett. **113** (2014) 051601 [arXiv:1402.2287 [hep-ph]].

[CS00]   E. Corbelli and P. Salucci, *The Extended Rotation Curve and the Dark Matter Halo of M33*, Mon. Not. Roy. Astron. Soc. **311** (2000) 441–447 [arXiv:astro-ph/9909252].

[CT86]   E. J. Copeland and N. Turok, *Cosmic String Interactions*,.

[CT19]   J. M. Cline and T. Toma, *Pseudo-Goldstone dark matter confronts cosmic ray and collider anomalies*, Phys. Rev. D **100** no. 3, (2019) 035023 [arXiv:1906.02175 [hep-ph]].

[Dav86]   R. L. Davis, *Cosmic Axions from Cosmic Strings*, Phys. Lett. B **180** (1986) 225–230.

[DBDKZ20]   A. Dasgupta, P. S. Bhupal Dev, S. K. Kang, and Y. Zhang, *New mechanism for matter-antimatter asymmetry and connection with dark matter*, Phys. Rev. D **102** no. 5, (2020) 055009 [arXiv:1911.03013 [hep-ph]].

[DEHK92]   A. Denner, H. Eck, O. Hahn, and J. Kublbeck, *Feynman rules for fermion number violating interactions*, Nucl. Phys. B **387** (1992) 467–481.

[DF83] M. Dine and W. Fischler, *The Not So Harmless Axion*, Phys. Lett. B **120** (1983) 137–141.

[DFG⁺16] I. Doršner, S. Fajfer, A. Greljo, J. F. Kamenik, and N. Košnik, *Physics of leptoquarks in precision experiments and at particle colliders*, Phys. Rept. **641** (2016) 1–68 [arXiv:1603.04993 [hep-ph]].

[DFS81] M. Dine, W. Fischler, and M. Srednicki, *A Simple Solution to the Strong CP Problem with a Harmless Axion*, Phys. Lett. B **104** (1981) 199–202.

[DJ74] L. Dolan and R. Jackiw, *Symmetry Behavior at Finite Temperature*, Phys. Rev. D **9** (1974) 3320–3341.

[DK07] M. R. Douglas and S. Kachru, *Flux compactification*, Rev. Mod. Phys. **79** (2007) 733–796 [arXiv:hep-th/0610102].

[DKP93a] N. G. Deshpande, E. Keith, and P. B. Pal, *Implications of LEP results for SO(10) grand unification*, Phys. Rev. D **46** (1993) 2261–2264.

[DKP93b] N. G. Deshpande, E. Keith, and P. B. Pal, *Implications of LEP results for SO(10) grand unification with two intermediate stages*, Phys. Rev. D **47** (1993) 2892–2896 [arXiv:hep-ph/9211232].

[DKQ11] M. J. Dolan, S. Krippendorf, and F. Quevedo, *Towards a Systematic Construction of Realistic D-brane Models on a del Pezzo Singularity*, JHEP **10** (2011) 024 [arXiv:1106.6039 [hep-th]].

[DM96] M. R. Douglas and G. W. Moore, *D-branes, quivers, and ALE instantons*, arXiv:hep-th/9603167.

[DN13] R. Durrer and A. Neronov, *Cosmological Magnetic Fields: Their Generation, Evolution and Observation*, Astron. Astrophys. Rev. **21** (2013) 62 [arXiv:1303.7121 [astro-ph.CO]].

[DNN08] S. Davidson, E. Nardi, and Y. Nir, *Leptogenesis*, Phys. Rept. **466** (2008) 105–177 [arXiv:0802.2962 [hep-ph]].

[DR08] G. Dvali and M. Redi, *Black Hole Bound on the Number of Species and Quantum Gravity at LHC*, Phys. Rev. D **77** (2008) 045027 [arXiv:0710.4344 [hep-th]].

[DS93] G. R. Dvali and G. Senjanovic, *Topologically stable electroweak flux tubes*, Phys. Rev. Lett. **71** (1993) 2376–2379 [arXiv:hep-ph/9305278].

[DS94]   G. R. Dvali and G. Senjanovic, *Topologically stable Z strings in the supersymmetric Standard Model*, Phys. Lett. B **331** (1994) 63–68 [arXiv:hep-ph/9403277].

[DSW87]   M. Dine, N. Seiberg, and E. Witten, *Fayet-Iliopoulos Terms in String Theory*, Nucl. Phys. B **289** (1987) 589–598.

[DW82]   A. Davidson and K. C. Wali, *MINIMAL FLAVOR UNIFICATION VIA MULTIGENERATIONAL PECCEI-QUINN SYMMETRY*, Phys. Rev. Lett. **48** (1982) 11.

[EGKO18]   S. A. R. Ellis, T. Gherghetta, K. Kaneta, and K. A. Olive, *New Weak-Scale Physics from SO(10) with High-Scale Supersymmetry*, Phys. Rev. D **98** no. 5, (2018) 055009 [arXiv:1807.06488 [hep-ph]].

[EHKN20a] M. Eto, Y. Hamada, M. Kurachi, and M. Nitta, *Dynamics of Nambu monopole in two Higgs doublet models. Cosmological Monopole Collider*, JHEP **07** (2020) 004 [arXiv:2003.08772 [hep-ph]].

[EHKN20b] M. Eto, Y. Hamada, M. Kurachi, and M. Nitta, *Topological Nambu monopole in two Higgs doublet models*, Phys. Lett. B **802** (2020) 135220 [arXiv:1904.09269 [hep-ph]].

[EHN20]   M. Eto, Y. Hamada, and M. Nitta, *Topological structure of a Nambu monopole in two-Higgs-doublet models: Fiber bundle, Dirac's quantization, and a dyon*, Phys. Rev. D **102** no. 10, (2020) 105018 [arXiv:2007.15587 [hep-th]].

[EKN18a]   M. Eto, M. Kurachi, and M. Nitta, *Constraints on two Higgs doublet models from domain walls*, Phys. Lett. B **785** (2018) 447–453 [arXiv:1803.04662 [hep-ph]].

[EKN18b]   M. Eto, M. Kurachi, and M. Nitta, *Non-Abelian strings and domain walls in two Higgs doublet models*, JHEP **08** (2018) 195 [arXiv:1805.07015 [hep-ph]].

[EKNO13]   M. Eto, K. Konishi, M. Nitta, and Y. Ookouchi, *Brane Realization of Nambu Monopoles and Electroweak Strings*, Phys. Rev. D **87** no. 4, (2013) 045006 [arXiv:1211.2971 [hep-th]].

[EKU15]   F. Elahi, C. Kolda, and J. Unwin, *UltraViolet Freeze-in*, JHEP **03** (2015) 048 [arXiv:1410.6157 [hep-ph]].

[ENTT14]   K. Enqvist, S. Nurmi, T. Tenkanen, and K. Tuominen, *Standard Model with a real singlet scalar and inflation*, JCAP **08** (2014) 035 [arXiv:1407.0659 [astro-ph.CO]].

[FGL15] A. Falkowski, C. Gross, and O. Lebedev, *A second Higgs from the Higgs portal*, JHEP **05** (2015) 057 [arXiv:1502.01361 [hep-ph]].

[FHHT19] S. Ferrari, T. Hambye, J. Heeck, and M. H. G. Tytgat, *SO(10) paths to dark matter*, Phys. Rev. D **99** no. 5, (2019) 055032 [arXiv:1811.07910 [hep-ph]].

[FIK⁺05] T. Fukuyama, A. Ilakovac, T. Kikuchi, S. Meljanac, and N. Okada, *SO(10) group theory for the unified model building*, J. Math. Phys. **46** (2005) 033505 [arXiv:hep-ph/0405300].

[FK15] R. Feger and T. W. Kephart, *LieART—A Mathematica application for Lie algebras and representation theory*, Comput. Phys. Commun. **192** (2015) 166–195 [arXiv:1206.6379 [math-ph]].

[FKS20] R. Feger, T. W. Kephart, and R. J. Saskowski, *LieART 2.0 – A Mathematica application for Lie Algebras and Representation Theory*, Comput. Phys. Commun. **257** (2020) 107490 [arXiv:1912.10969 [hep-th]].

[FL11] M. Freytsis and Z. Ligeti, *On dark matter models with uniquely spin-dependent detection possibilities*, Phys. Rev. D **83** (2011) 115009 [arXiv:1012.5317 [hep-ph]].

[FM75] H. Fritzsch and P. Minkowski, *Unified Interactions of Leptons and Hadrons*, Annals Phys. **93** (1975) 193–266.

[FN79] C. D. Froggatt and H. B. Nielsen, *Hierarchy of Quark Masses, Cabibbo Angles and CP Violation*, Nucl. Phys. B **147** (1979) 277–298.

[Fon12] R. M. Fonseca, *Calculating the renormalisation group equations of a SUSY model with Susyno*, Comput. Phys. Commun. **183** (2012) 2298–2306 [arXiv:1106.5016 [hep-ph]].

[Fon21] R. M. Fonseca, *GroupMath: A Mathematica package for group theory calculations*, Comput. Phys. Commun. **267** (2021) 108085 [arXiv:2011.01764 [hep-th]].

[Fuk13] T. Fukuyama, *SO(10) GUT in Four and Five Dimensions: A Review*, Int. J. Mod. Phys. A **28** (2013) 1330008 [arXiv:1212.3407 [hep-ph]].

[FY86] M. Fukugita and T. Yanagida, *Baryogenesis Without Grand Unification*, Phys. Lett. B **174** (1986) 45–47.

[FZFLLH15] N. Fonseca, R. Zukanovich Funchal, A. Lessa, and L. Lopez-Honorez, *Dark Matter Constraints on Composite Higgs Models*, JHEP **06** (2015) 154 [arXiv:1501.05957 [hep-ph]].

[GCH17]   C. Garcia-Cely and J. Heeck, *Neutrino Lines from Majoron Dark Matter*, JHEP **05** (2017) 102 [arXiv:1701.07209 [hep-ph]].

[GG74]   H. Georgi and S. L. Glashow, *Unity of All Elementary Particle Forces*, Phys. Rev. Lett. **32** (1974) 438–441.

[GGK89]   G. B. Gelmini, M. Gleiser, and E. W. Kolb, *Cosmology of Biased Discrete Symmetry Breaking*, Phys. Rev. D **39** (1989) 1558.

[GIn19]   E. Gonzalo and L. E. Ibáñez, *A Strong Scalar Weak Gravity Conjecture and Some Implications*, JHEP **08** (2019) 118 [arXiv:1903.08878 [hep-th]].

[GK19]   S. K. Garg and C. Krishnan, *Bounds on Slow Roll and the de Sitter Swampland*, JHEP **11** (2019) 075 [arXiv:1807.05193 [hep-th]].

[GL89]   N. Ganoulis and G. Lazarides, *Fermionic Zero Modes for Cosmic Strings*, Nucl. Phys. B **316** (1989) 443–455.

[GLT17]   C. Gross, O. Lebedev, and T. Toma, *Cancellation Mechanism for Dark-Matter–Nucleon Interaction*, Phys. Rev. Lett. **119** no. 19, (2017) 191801 [arXiv:1708.02253 [hep-ph]].

[GMP21]   A. Granelli, K. Moffat, and S. T. Petcov, *Aspects of high scale leptogenesis with low-energy leptonic CP violation*, JHEP **11** (2021) 149 [arXiv:2107.02079 [hep-ph]].

[GMRS79]   M. Gell-Mann, P. Ramond, and R. Slansky, *Complex Spinors and Unified Theories*, Conf. Proc. C **790927** (1979) 315–321 [arXiv:1306.4669 [hep-th]].

[GMS10]   P.-H. Gu, E. Ma, and U. Sarkar, *Pseudo-Majoron as Dark Matter*, Phys. Lett. B **690** (2010) 145–148 [arXiv:1004.1919 [hep-ph]].

[GMW11]   B. Grzadkowski, M. Maniatis, and J. Wudka, *The bilinear formalism and the custodial symmetry in the two-Higgs-doublet model*, JHEP **11** (2011) 030 [arXiv:1011.5228 [hep-ph]].

[GnH21]   M. Graña and A. Herráez, *The Swampland Conjectures: A Bridge from Quantum Gravity to Particle Physics*, Universe **7** no. 8, (2021) 273 [arXiv:2107.00087 [hep-th]].

[GP11]   D. S. Gorbunov and A. G. Panin, *Scalaron the mighty: producing dark matter and baryon asymmetry at reheating*, Phys. Lett. B **700** (2011) 157–162 [arXiv:1009.2448 [hep-ph]].

[GR81]   G. B. Gelmini and M. Roncadelli, *Left-Handed Neutrino Mass Scale and Spontaneously Broken Lepton Number*, Phys. Lett. B **99** (1981) 411–415.

[GRW98]   S. Gukov, M. Rangamani, and E. Witten, *Dibaryons, strings and branes in AdS orbifold models*, JHEP **12** (1998) 025 [arXiv:hep-th/9811048].

[GS84]   M. B. Green and J. H. Schwarz, *Anomaly Cancellation in Supersymmetric D=10 Gauge Theory and Superstring Theory*, Phys. Lett. B **149** (1984) 117–122.

[GVMU19]   E. Garćıa-Valdecasas, A. Mininno, and A. M. Uranga, *Discrete Symmetries in Dimer Diagrams*, JHEP **10** (2019) 091 [arXiv:1907.06938 [hep-th]].

[H⁺99]   P. G. Harris *et al.*, *New experimental limit on the electric dipole moment of the neutron*, Phys. Rev. Lett. **82** (1999) 904–907.

[Hal81]   L. J. Hall, *Grand Unification of Effective Gauge Theories*, Nucl. Phys. B **178** (1981) 75–124.

[Ham02]   T. Hambye, *Leptogenesis at the TeV scale*, Nucl. Phys. B **633** (2002) 171–192 [arXiv:hep-ph/0111089].

[HBL⁺20]   D.-Z. He, X.-J. Bi, S.-J. Lin, P.-F. Yin, and X. Zhang, *Expected LHAASO sensitivity to decaying dark matter signatures from dwarf galaxies gamma-ray emission*, Chin. Phys. C **44** no. 8, (2020) 085001 [arXiv:1910.05017 [astro-ph.HE]].

[HEK⁺14]   T. Hiramatsu, M. Eto, K. Kamada, T. Kobayashi, and Y. Ookouchi, *Instability of colliding metastable strings*, JHEP **01** (2014) 165 [arXiv:1304.0623 [hep-ph]].

[HJMRW10] L. J. Hall, K. Jedamzik, J. March-Russell, and S. M. West, *Freeze-In Production of FIMP Dark Matter*, JHEP **03** (2010) 080 [arXiv:0911.1120 [hep-ph]].

[HKL⁺19]   K. Huitu, N. Koivunen, O. Lebedev, S. Mondal, and T. Toma, *Probing pseudo-Goldstone dark matter at the LHC*, Phys. Rev. D **100** no. 1, (2019) 015009 [arXiv:1812.05952 [hep-ph]].

[HO21]   D. Harlow and H. Ooguri, *Symmetries in quantum field theory and quantum gravity*, Commun. Math. Phys. **383** no. 3, (2021) 1669–1804 [arXiv:1810.05338 [hep-th]].

[HRR19]   B. Heidenreich, M. Reece, and T. Rudelius, *Repulsive Forces and the Weak Gravity Conjecture*, JHEP **10** (2019) 055 [arXiv:1906.02206 [hep-th]].

[HST+13]   T. Hiramatsu, Y. Sendouda, K. Takahashi, D. Yamauchi, and C.-M. Yoo, *Type-I cosmic string network*, Phys. Rev. D **88** no. 8, (2013) 085021 [arXiv:1307.0308 [astro-ph.CO]].

[HT20]   J. Heeck and V. Takhistov, *Inclusive Nucleon Decay Searches as a Frontier of Baryon Number Violation*, Phys. Rev. D **101** no. 1, (2020) 015005 [arXiv:1910.07647 [hep-ph]].

[IMN14]   S. Ipek, D. McKeen, and A. E. Nelson, *A Renormalizable Model for the Galactic Center Gamma Ray Excess from Dark Matter Annihilation*, Phys. Rev. D **90** no. 5, (2014) 055021 [arXiv:1404.3716 [hep-ph]].

[IMR01]   L. E. Ibanez, F. Marchesano, and R. Rabadan, *Getting just the standard model at intersecting branes*, JHEP **11** (2001) 002 [arXiv:hep-th/0105155].

[IT18]   K. Ishiwata and T. Toma, *Probing pseudo Nambu-Goldstone boson dark matter at loop level*, JHEP **12** (2018) 089 [arXiv:1810.08139 [hep-ph]].

[Iva08]   I. P. Ivanov, *Minkowski space structure of the Higgs potential in 2HDM. II. Minima, symmetries, and topology*, Phys. Rev. D **77** (2008) 015017 [arXiv:0710.3490 [hep-ph]].

[Iwa97]   A. Iwazaki, *Spontaneous magnetization of axion domain wall and primordial magnetic field*, Phys. Rev. Lett. **79** (1997) 2927–2930 [arXiv:hep-ph/9705456].

[IYY]   R. Iwashima, M. Yamanaka, and K. Yoshioka, *to apear*,.

[JL05]   H. Jockers and J. Louis, *The Effective action of D7-branes in N = 1 Calabi-Yau orientifolds*, Nucl. Phys. B **705** (2005) 167–211 [arXiv:hep-th/0409098].

[Jon82]   D. R. T. Jones, *The Two Loop beta Function for a G(1) x G(2) Gauge Theory*, Phys. Rev. D **25** (1982) 581.

[JPV92]   M. James, L. Perivolaropoulos, and T. Vachaspati, *Stability of electroweak strings*, Phys. Rev. D **46** (1992) R5232–R5235.

[JPV93]   M. James, L. Perivolaropoulos, and T. Vachaspati, *Detailed stability analysis of electroweak strings*, Nucl. Phys. B **395** (1993) 534–546 [arXiv:hep-ph/9212301].

[JR81]   R. Jackiw and P. Rossi, *Zero Modes of the Vortex - Fermion System*, Nucl. Phys. B **190** (1981) 681–691.

211

[JS19]   K. Jedamzik and A. Saveliev, *Stringent Limit on Primordial Magnetic Fields from the Cosmic Microwave Background Radiation*, Phys. Rev. Lett. **123** no. 2, (2019) 021301 [arXiv:1804.06115 [astro-ph.CO]].

[KC10]   J. E. Kim and G. Carosi, *Axions and the Strong CP Problem*, Rev. Mod. Phys. **82** (2010) 557–602 [arXiv:0807.3125 [hep-ph]]. [Erratum: Rev.Mod.Phys. 91, 049902 (2019)].

[KDMQ10]   S. Krippendorf, M. J. Dolan, A. Maharana, and F. Quevedo, *D-branes at Toric Singularities: Model Building, Yukawa Couplings and Flavour Physics*, JHEP **06** (2010) 092 [arXiv:1002.1790 [hep-th]].

[Kib80]   T. W. B. Kibble, *Some Implications of a Cosmological Phase Transition*, Phys. Rept. **67** (1980) 183.

[Kim79]   J. E. Kim, *Weak Interaction Singlet and Strong CP Invariance*, Phys. Rev. Lett. **43** (1979) 103.

[KM84]   F. R. Klinkhamer and N. S. Manton, *A Saddle Point Solution in the Weinberg-Salam Theory*, Phys. Rev. D **30** (1984) 2212.

[KP14]   A. Katz and M. Perelstein, *Higgs Couplings and Electroweak Phase Transition*, JHEP **07** (2014) 108 [arXiv:1401.1827 [hep-ph]].

[KRS85]   V. A. Kuzmin, V. A. Rubakov, and M. E. Shaposhnikov, *On the Anomalous Electroweak Baryon Number Nonconservation in the Early Universe*, Phys. Lett. B **155** (1985) 36.

[KT90]   E. W. Kolb and M. S. Turner, *The Early Universe*, vol. 69. 1990.

[KTY16]   M. Kawasaki, F. Takahashi, and M. Yamada, *Suppressing the QCD Axion Abundance by Hidden Monopoles*, Phys. Lett. B **753** (2016) 677–681 [arXiv:1511.05030 [hep-ph]].

[Kum69]   R. Kumar, *Covariant phase-space calculations of n-body decay and production processes*, Phys. Rev. **185** (1969) 1865–1875.

[KW86]   L. M. Krauss and F. Wilczek, *A SHORTLIVED AXION VARIANT*, Phys. Lett. B **173** (1986) 189–192.

[La93]   H. La, *Vortex solutions in two Higgs systems and tan Beta*, arXiv:hep-ph/9302220.

[LDR14]   M. Le Dall and A. Ritz, *Leptogenesis and the Higgs Portal*, Phys. Rev. D **90** no. 9, (2014) 096002 [arXiv:1408.2498 [hep-ph]].

[LLW19a]   S.-J. Lee, W. Lerche, and T. Weigand, *A Stringy Test of the Scalar Weak Gravity Conjecture*, Nucl. Phys. B **938** (2019) 321–350 [arXiv:1810.05169 [hep-th]].

[LLW19b]   S.-J. Lee, W. Lerche, and T. Weigand, *Modular Fluxes, Elliptic Genera, and Weak Gravity Conjectures in Four Dimensions*, JHEP **08** (2019) 104 [arXiv:1901.08065 [hep-th]].

[LOSW99]   A. Lukas, B. A. Ovrut, K. S. Stelle, and D. Waldram, *Heterotic M theory in five-dimensions*, Nucl. Phys. B **552** (1999) 246–290 [arXiv:hep-th/9806051].

[LP18]   D. Lust and E. Palti, *Scalar Fields, Hierarchical UV/IR Mixing and The Weak Gravity Conjecture*, JHEP **02** (2018) 040 [arXiv:1709.01790 [hep-th]].

[LPS88]   G. Lazarides, C. Panagiotakopoulos, and Q. Shafi, *COSMIC SUPERCONDUCTING STRINGS AND COLLIDERS*, Nucl. Phys. B **296** (1988) 657–668.

[LS82]   G. Lazarides and Q. Shafi, *Axion Models with No Domain Wall Problem*, Phys. Lett. B **115** (1982) 21–25.

[LS85]   G. Lazarides and Q. Shafi, *Superconducting Strings in Axion Models*, Phys. Lett. B **151** (1985) 123–126.

[LSW97]   S. E. Larsson, S. Sarkar, and P. L. White, *Evading the cosmological domain wall problem*, Phys. Rev. D **55** (1997) 5129–5135 [arXiv:hep-ph/9608319].

[LT19]   O. Lebedev and T. Toma, *Relativistic Freeze-in*, Phys. Lett. B **798** (2019) 134961 [arXiv:1908.05491 [hep-ph]].

[Mar16]   D. J. E. Marsh, *Axion Cosmology*, Phys. Rept. **643** (2016) 1–79 [arXiv:1510.07633 [astro-ph.CO]].

[Min77]   P. Minkowski, $\mu \to e\gamma$ *at a Rate of One Out of* 10^9 *Muon Decays?*, Phys. Lett. B **67** (1977) 421–428.

[MKR10]   R. Massey, T. Kitching, and J. Richard, *The dark matter of gravitational lensing*, Rept. Prog. Phys. **73** (2010) 086901 [arXiv:1001.1739 [astro-ph.CO]].

[MLMP15]   V. Martín Lozano, J. M. Moreno, and C. B. Park, *Resonant Higgs boson pair production in the* $hh \to b\bar{b}\,WW \to b\bar{b}\ell^+\nu\ell^-\bar{\nu}$ *decay channel*, JHEP **08** (2015) 004 [arXiv:1501.03799 [hep-ph]].

213

[MNO+15]   Y. Mambrini, N. Nagata, K. A. Olive, J. Quevillon, and J. Zheng, *Dark matter and gauge coupling unification in nonsupersymmetric SO(10) grand unified models*, Phys. Rev. D **91** no. 9, (2015) 095010 [arXiv:1502.06929 [hep-ph]].

[Moh02]   R. N. Mohapatra, *Unification and Supersymmetry -The Frontiers of Quarks-Lepton Physics-*. Springer, 2002.

[MP75]   R. N. Mohapatra and J. C. Pati, *Left-Right Gauge Symmetry and an Isoconjugate Model of CP Violation*, Phys. Rev. D **11** (1975) 566–571.

[MP81]   W. G. McKay and J. Patera, *Tables of Dimensions, Indices, and Branching Rules for Representations of Simple Lie Algebras*. Marcel Dekker, Inc., New York, 1981.

[MS78]   R. N. Mohapatra and G. Senjanovic, *Natural Suppression of Strong p and t Noninvariance*, Phys. Lett. B **79** (1978) 283–286.

[MS10]   H. Murayama and J. Shu, *Topological Dark Matter*, Phys. Lett. B **686** (2010) 162–165 [arXiv:0905.1720 [hep-ph]].

[MS15]   E. Ma and R. Srivastava, *Dirac or inverse seesaw neutrino masses with $B - L$ gauge symmetry and S_3 flavor symmetry*, Phys. Lett. B **741** (2015) 217–222 [arXiv:1411.5042 [hep-ph]].

[MV83]   M. E. Machacek and M. T. Vaughn, *Two Loop Renormalization Group Equations in a General Quantum Field Theory. 1. Wave Function Renormalization*, Nucl. Phys. B **222** (1983) 83–103.

[MV84]   M. E. Machacek and M. T. Vaughn, *Two Loop Renormalization Group Equations in a General Quantum Field Theory. 2. Yukawa Couplings*, Nucl. Phys. B **236** (1984) 221–232.

[MV85]   M. E. Machacek and M. T. Vaughn, *Two Loop Renormalization Group Equations in a General Quantum Field Theory. 3. Scalar Quartic Couplings*, Nucl. Phys. B **249** (1985) 70–92.

[MY10]   S. Matsumoto and K. Yoshioka, *Deep Correlation Between Cosmic-Ray Anomaly and Neutrino Masses*, Phys. Rev. D **82** (2010) 053009 [arXiv:1006.1688 [hep-ph]].

[Nam77]   Y. Nambu, *String-Like Configurations in the Weinberg-Salam Theory*, Nucl. Phys. B **130** (1977) 505.

[NFP07]   P. Nath and P. Fileviez Perez, *Proton stability in grand unified theories, in strings and in branes*, Phys. Rept. **441** (2007) 191–317 [arXiv:hep-ph/0601023].

[NO73]   H. B. Nielsen and P. Olesen, *Vortex Line Models for Dual Strings*, Nucl. Phys. B **61** (1973) 45–61.

[NV10]   A. Neronov and I. Vovk, *Evidence for strong extragalactic magnetic fields from fermi observations of tev blazars*, Science **328** no. 5974, (2010) 73–75.

[OOSV18]   G. Obied, H. Ooguri, L. Spodyneiko, and C. Vafa, *De Sitter Space and the Swampland*, arXiv:1806.08362 [hep-th].

[OPSV19]   H. Ooguri, E. Palti, G. Shiu, and C. Vafa, *Distance and de Sitter Conjectures on the Swampland*, Phys. Lett. B **788** (2019) 180–184 [arXiv:1810.05506 [hep-th]].

[ORS21]   N. Okada, D. Raut, and Q. Shafi, *Pseudo-Goldstone dark matter in a gauged $B - L$ extended standard model*, Phys. Rev. D **103** no. 5, (2021) 055024 [arXiv:2001.05910 [hep-ph]].

[OV07]   H. Ooguri and C. Vafa, *On the Geometry of the String Landscape and the Swampland*, Nucl. Phys. B **766** (2007) 21–33 [arXiv:hep-th/0605264].

[Pal17]   E. Palti, *The Weak Gravity Conjecture and Scalar Fields*, JHEP **08** (2017) 034 [arXiv:1705.04328 [hep-th]].

[Pal19]   E. Palti, *The Swampland: Introduction and Review*, Fortsch. Phys. **67** no. 6, (2019) 1900037 [arXiv:1903.06239 [hep-th]].

[Par55]   E. N. Parker, *Hydromagnetic Dynamo Models*, Astrophys. J. **122** (1955) 293.

[Per93]   L. Perivolaropoulos, *Existence of double vortex solutions*, Phys. Lett. B **316** (1993) 528–533 [arXiv:hep-ph/9309261].

[Pol07]   J. Polchinski, *String theory. Vol. 1: An introduction to the bosonic string*. Cambridge Monographs on Mathematical Physics. Cambridge University Press, 12, 2007.

[PQ77a]   R. D. Peccei and H. R. Quinn, *Constraints Imposed by CP Conservation in the Presence of Instantons*, Phys. Rev. D **16** (1977) 1791–1797.

[PQ77b]   R. D. Peccei and H. R. Quinn, *CP Conservation in the Presence of Instantons*, Phys. Rev. Lett. **38** (1977) 1440–1443.

[PR08]   S. Palomares-Ruiz, *Model-independent bound on the dark matter lifetime*, Phys. Lett. B **665** (2008) 50–53 [arXiv:0712.1937 [astro-ph]].

[PS74]   J. C. Pati and A. Salam, *Lepton Number as the Fourth Color*, Phys. Rev. D **10** (1974) 275–289. [Erratum: Phys.Rev.D 11, 703–703 (1975)].

[PS95]   M. E. Peskin and D. V. Schroeder, *An Introduction to quantum field theory*. Addison-Wesley, Reading, USA, 1995.

[PSS75]   J. C. Pati, A. Salam, and J. A. Strathdee, *On Fermion number and its conservation*, Nuovo Cim. A **26** (1975) 72–83.

[PU04]   A. Pilaftsis and T. E. J. Underwood, *Resonant leptogenesis*, Nucl. Phys. B **692** (2004) 303–345 [arXiv:hep-ph/0309342].

[PV94]   A. Pomarol and R. Vega, *Constraints on CP violation in the Higgs sector from the rho parameter*, Nucl. Phys. B **413** (1994) 3–15 [arXiv:hep-ph/9305272].

[PWW83]   J. Preskill, M. B. Wise, and F. Wilczek, *Cosmology of the Invisible Axion*, Phys. Lett. B **120** (1983) 127–132.

[PWY86]   R. D. Peccei, T. T. Wu, and T. Yanagida, *A VIABLE AXION MODEL*, Phys. Lett. B **172** (1986) 435–440.

[QS14]   F. S. Queiroz and K. Sinha, *The Poker Face of the Majoron Dark Matter Model: LUX to keV Line*, Phys. Lett. B **735** (2014) 69–74 [arXiv:1404.1400 [hep-ph]].

[Ram20]   M. Ramos, *Composite dark matter phenomenology in the presence of lighter degrees of freedom*, JHEP **07** (2020) 128 [arXiv:1912.11061 [hep-ph]].

[Rin12]   A. Ringwald, *Exploring the Role of Axions and Other WISPs in the Dark Universe*, Phys. Dark Univ. **1** (2012) 116–135 [arXiv:1210.5081 [hep-ph]].

[RMC+08]   S. W. Randall, M. Markevitch, D. Clowe, A. H. Gonzalez, and M. Bradac, *Constraints on the Self-Interaction Cross-Section of Dark Matter from Numerical Simulations of the Merging Galaxy Cluster 1E 0657-56*, Astrophys. J. **679** (2008) 1173–1180 [arXiv:0704.0261 [astro-ph]].

[Rob06]   S. P. Robinson, *Normalization conventions for Newton's constant and the Planck scale in arbitrary spacetime dimension*, arXiv:gr-qc/0609060.

[RSW20]   M. Ruhdorfer, E. Salvioni, and A. Weiler, *A Global View of the Off-Shell Higgs Portal*, SciPost Phys. **8** (2020) 027 [arXiv:1910.04170 [hep-ph]].

[S+19]   **CMS** Collaboration, A. M. Sirunyan *et al.*, *Search for invisible decays of a Higgs boson produced through vector boson fusion in proton-proton collisions at $\sqrt{s}$ = 13 TeV*, Phys. Lett. B **793** (2019) 520–551 [arXiv:1809.05937 [hep-ex]].

[SAC+08]   P. Salmi, A. Achucarro, E. J. Copeland, T. W. B. Kibble, R. de Putter, and D. A. Steer, *Kinematic constraints on formation of bound states of cosmic strings: Field theoretical approach*, Phys. Rev. D **77** (2008) 041701 [arXiv:0712.1204 [hep-th]].

[Sar17]   P. Saraswat, *Weak gravity conjecture and effective field theory*, Phys. Rev. D **95** no. 2, (2017) 025013 [arXiv:1608.06951 [hep-th]].

[Sem16]   A. Semenov, *LanHEP — A package for automatic generation of Feynman rules from the Lagrangian. Version 3.2*, Comput. Phys. Commun. **201** (2016) 167–170 [arXiv:1412.5016 [physics.comp-ph]].

[She87]   E. P. S. Shellard, *Cosmic String Interactions*, Nucl. Phys. B **283** (1987) 624–656.

[She88]   E. P. S. Shellard, *UNDERSTANDING INTERCOMMUTING*, in Workshop on Current Status of Cosmic String Scenarios. 7, 1988.

[Sik82]   P. Sikivie, *Of Axions, Domain Walls and the Early Universe*, Phys. Rev. Lett. **48** (1982) 1156–1159.

[Sik08]   P. Sikivie, *Axion Cosmology*, Lect. Notes Phys. **741** (2008) 19–50 [arXiv:astro-ph/0610440].

[Sla81]   R. Slansky, *Group Theory for Unified Model Building*, Phys. Rept. **79** (1981) 1–128.

[SM75]   G. Senjanovic and R. N. Mohapatra, *Exact Left-Right Symmetry and Spontaneous Violation of Parity*, Phys. Rev. D **12** (1975) 1502.

[SR01]   Y. Sofue and V. Rubin, *Rotation curves of spiral galaxies*, Ann. Rev. Astron. Astrophys. **39** (2001) 137–174 [arXiv:astro-ph/0010594].

[STY18]   R. Sato, F. Takahashi, and M. Yamada, *Unified Origin of Axion and Monopole Dark Matter, and Solution to the Domain-wall Problem*, Phys. Rev. D **98** no. 4, (2018) 043535 [arXiv:1805.10533 [hep-ph]].

[SVZ80]   M. A. Shifman, A. I. Vainshtein, and V. I. Zakharov, *Can Confinement Ensure Natural CP Invariance of Strong Interactions?*, Nucl. Phys. B **166** (1980) 493–506.

[T+20] **Super-Kamiokande** Collaboration, A. Takenaka *et al.*, *Search for proton decay via $p \to e^+ \pi^0$ and $p \to \mu^+ \pi^0$ with an enlarged fiducial volume in Super-Kamiokande I-IV*, Phys. Rev. D **102** no. 11, (2020) 112011 [arXiv:2010.16098 [hep-ex]].

[Tak08] F. Takahashi, *Gravitino dark matter from inflaton decay*, Phys. Lett. B **660** (2008) 100–106 [arXiv:0705.0579 [hep-ph]].

[Ura00] A. M. Uranga, *From quiver diagrams to particle physics*, in 3rd European Congress of Mathematics: Shaping the 21st Century. 7, 2000. arXiv:hep-th/0007173.

[Vac92] T. Vachaspati, *Vortex solutions in the Weinberg-Salam model*, Phys. Rev. Lett. **68** (1992) 1977–1980. [Erratum: Phys.Rev.Lett. 69, 216 (1992)].

[Vac93] T. Vachaspati, *Electroweak strings*, Nucl. Phys. B **397** (1993) 648–671.

[Vaf05] C. Vafa, *The String landscape and the swampland*, arXiv:hep-th/0509212.

[vBCIMV21] M. van Beest, J. Calderón-Infante, D. Mirfendereski, and I. Valenzuela, *Lectures on the Swampland Program in String Compactifications*, arXiv:2102.01111 [hep-th].

[VF94] T. Vachaspati and G. B. Field, *Electroweak string configurations with baryon number*, Phys. Rev. Lett. **73** (1994) 373–376 [arXiv:hep-ph/9401220].

[Vil81] A. Vilenkin, *Gravitational Field of Vacuum Domain Walls and Strings*, Phys. Rev. D **23** (1981) 852–857.

[VS00] A. Vilenkin and E. P. S. Shellard, *Cosmic Strings and Other Topological Defects.* Cambridge University Press, 7, 2000.

[VW07] H. Verlinde and M. Wijnholt, *Building the standard model on a D3-brane*, JHEP **01** (2007) 106 [arXiv:hep-th/0508089].

[Wei74] S. Weinberg, *Gauge and Global Symmetries at High Temperature*, Phys. Rev. D **9** (1974) 3357–3378.

[Wei78] S. Weinberg, *A New Light Boson?*, Phys. Rev. Lett. **40** (1978) 223–226.

[Wei05] S. Weinberg, *The Quantum theory of fields. Vol. 1: Foundations.* Cambridge University Press, 6, 2005.

[Wei13a] S. Weinberg, *The quantum theory of fields. Vol. 2: Modern applications.* Cambridge University Press, 8, 2013.

[Wei13b]   S. Weinberg, *The quantum theory of fields. Vol. 3: Supersymmetry.* Cambridge University Press, 6, 2013.

[Wil78]   F. Wilczek, *Problem of Strong P and T Invariance in the Presence of Instantons*, Phys. Rev. Lett. **40** (1978) 279–282.

[Wil82]   F. Wilczek, *Axions and Family Symmetry Breaking*, Phys. Rev. Lett. **49** (1982) 1549–1552.

[Wit85]   E. Witten, *Superconducting Strings*, Nucl. Phys. B **249** (1985) 557–592.

[WS10]   O. Wantz and E. P. S. Shellard, *Axion Cosmology Revisited*, Phys. Rev. D **82** (2010) 123508 [arXiv:0910.1066 [astro-ph.CO]].

[Yam08]   M. Yamazaki, *Brane Tilings and Their Applications*, Fortsch. Phys. **56** (2008) 555–686 [arXiv:0803.4474 [hep-th]].

[Yam15]   N. Yamatsu, *Finite-Dimensional Lie Algebras and Their Representations for Unified Model Building*, arXiv:1511.08771 [hep-ph].

[Yan79]   T. Yanagida, *Horizontal gauge symmetry and masses of neutrinos*, Conf. Proc. C **7902131** (1979) 95–99.

[Z⁺20]   **Particle Data Group** Collaboration, P. A. Zyla *et al.*, *Review of Particle Physics*, PTEP **2020** no. 8, (2020) 083C01.

[Zhi80]   A. R. Zhitnitsky, *On Possible Suppression of the Axion Hadron Interactions. (In Russian)*, Sov. J. Nucl. Phys. **31** (1980) 260.

[Zur85]   W. H. Zurek, *Cosmological Experiments in Superfluid Helium?*, Nature **317** (1985) 505–508.